EVALUATION OF GEOTECHNICAL PARAMETERS OF SOIL USING ELECTRICAL

RESISTIVITY IMAGING

by

MD ASIF AKHTAR

Presented to the Faculty of the Graduate School of

The University of Texas at Arlington

in Partial Fulfillment of the

requirements for the Degree of

DOCTOR OF PHILOSOPHY IN CIVIL ENGINEERING

THE UNIVERSITY OF TEXAS AT ARLINGTON

December 2021

ACKNOWLEDGEMENTS

I want to express my gratitude to my supervising professor, Dr. MD Sahadat Hossain, for all his contributions toward the completion of my journey. His constant guidance, suggestions, and inspiration made this possible. Having the chance to work on this research project under his supervision is an honor I will always be grateful for. Your constructive feedback strengthened the final product of my research.

I would also like to thank my other committee members: Dr. Mohsen Shahandashti, Dr. Xinbao Yu, Dr. Muhammad N. Huda, for their precious time. I really appreciate your valuable suggestions and advice. I would also like to acknowledge the Texas Department of Transportation for funding this study.

My heartfelt thanks go to all the SWIS members who supported me unconditionally. Without your assistance, it would not be possible to cope with the mental stress during this pandemic. A very special thanks go to Sabrina Mahjabin and Kranti Kumar for their invaluable support and help during the sample collection and laboratory testing. It was a great experience to be a part of this team.

And lastly, but most importantly, it would never have been possible for me to get here without my family. It is with great gratitude that I acknowledge my mother; I will always treasure memories of our first day at school together. Thank you for everything Ma, you will always be with me. Through the journey, I am grateful for the unconditional love, support, and encouragement of my lovely wife, Nipa. Maya, you are the most precious thing I have. Please accept my apology for not being with you all the time. My friends here in Arlington made my journey worthwhile, and I am very grateful for them.

ABSTRACT

EVALUATION OF GEOTECHNICAL PARAMETERS OF SOIL USING

ELECTRICAL RESISTIVITY IMAGING

Md Asif Akhtar

The University of Texas at Arlington, 2021

Supervising Professor: Dr. MD Sahadat Hossain

Electric resistivity imaging (ERI) is an effective non-destructive and rapid measuring way of obtaining continuous soil subsurface resistivity profiles. An ERI technique can be used to identify moisture variations and soil heterogeneities in an area. Thus, ERI is becoming a popular tool in geotechnical (FHWA, 2015)engineering; however, it only provides qualitative information at the current time. Using qualitative images, it is challenging to extract quantitative geotechnical information, such as the type of soil, moisture content, degree of saturation, and atterberg limit, of the subsurface. Several studies have described the electrical resistance of soil as a function of pore fluid conductivity and surface conductance. Additionally, electrical resistivity measurements have also been made on commercial soils in order to determine the influence of geotechnical properties. Since a conventional geotechnical investigation may not perform characterization tests of pore water or surface charge, electrical resistivity must be correlated with geotechnical properties that can be tested in the laboratory. The objective of this experimental study is to investigate the relationship between the electrical properties of soil and geotechnical parameters of locally available soil and determine correlations between geotechnical parameters and electrical resistivity that can be used by geotechnical engineers.

A study was conducted to study the electrical properties of soils obtained from 22 boreholes of four different locations, namely Fort-Worth, Beaumont, Corpus Christi, and El-Paso, selected based on their geological formation. Besides collecting soil samples through soil borings using the Texas Cone Penetration (TCP) method, a field, electrical resistivity survey was also conducted using 28 and 56 electrodes at the same locations to obtain a subsurface resistivity map. Field resistivity values were correlated with soil TCP values, and the correlation was compared to previous literature. In this study, 44 soil samples classified as low plastic clay (CL), 15 samples as high plastic clay (CH), and four samples as elastic silt (MH) were used to measure the resistivity of compacted clay soils. Furthermore, soil samples were categorized into six categories based on their liquid limit higher than 50, between 35 and 50, and lower than 35, and plastic limit higher than 25 and lower than 25 to investigate the changes in geoelectrical properties of soil. Various geotechnical conditions were used in laboratory tests to determine the influence of soil parameters on electrical resistivity. In both clayey soils and sandy soils, electrical resistivity measurements were found strongly influenced by the moisture content and degree of saturation. Soil resistivity was found to be averagely decreased by 80%, 43%, and 21% of initial value when the soil moisture content was increased from 10% to 20%, 20% to 30%, and 30% to 40% except for the soil samples contains liquid limit less than 50 and plasticity index higher than 25 for unit weight of 11.8 KN/m^3. Soil resistivity was found to be decreased by 42%, 25%, and 41% for the above-mentioned water content due to the high activity of soil. Moreover, soil resistivity decreases 45% and 49% of the initial values when the unit weight increases from 11.8 KN/m^3 to 13.4 KN/m^3 and 13.4 KN/m^3 to 14.9 KN/m^3. Soil resistivity decreases as much as 57-fold for normal clay and 7.5 fold for active clay from the initial value when the degree of saturation increased from 17% to 100%. However, the rate of change of resistivity is low when the degree of saturation of compacted clay is more

than 50%. Furthermore, clay properties such as liquid limit and plasticity index also affect electrical resistance at different saturation levels. However, at a higher level of saturation, geotechnical parameters have less impact on electrical resistivity.

The soil engineering properties of both sandy and clayey soils were correlated with electrical resistance using different multiple linear regression (MLR) models developed with R-studio. In developing a multiple linear regression equation for clayey soil, the degree of saturation and plasticity index were selected as independent parameters, while for sandy soil, moisture and sand content were used. Validation of the MLR models was based on field data, and therefore these models can be used for estimating engineering properties.

TABLE OF CONTENTS

LIST OF FIGURES

LIST OF TABLES

CHAPTER 1 INTRODUCTION

1.1 Introduction

The subsurface investigation is one of the most critical and challenging phases of any civil engineering construction or development activity. The successful performance of a construction project depends on determining the ground conditions accurately. An insufficient investigation is often cited as a significant cause of geotechnical failures of a project and can be considered as one of the main reasons behind substantial cost and time overruns of about 20% to 50% of the infrastructural projects (Baynes, 2010; Tonks et al., 2017). Lack of subsurface exploration before construction will eventually lead to geotechnical-related problems during construction. According to (Boeckmann & Loehr, 2016), about $10 million per state DOT was annually spent on geotechnical-related change orders, which occurred due to a lack of geotechnical investigation prior to the project. A detailed site investigation should be conducted to reduce geotechnical-related change orders, thus reducing the project's over-run cost (Shrestha & Neupane, 2020). Geotechnical risk during the construction and serving period can be reduced substantially if the subsurface investigation is carried out properly. Moreover, improved site characterization directly reduces the likelihood of encountering unforeseen ground conditions during construction. Amadi & Omotayo (2017) showed that due to unforeseen ground conditions, costs increased by 63% in seven big-budgeted projects. Uncertainty related to ground conditions often leads to claims, change orders, and cost overruns during construction and may lead to unacceptable performance following construction (Loehr et al., 2016).

Limited knowledge about the subsurface condition can also lead to geo-hazards which is a major threat to the transportation infrastructure system. Transportation networks are the backbone

of critical infrastructures because they provide access to other systems (Argyroudis et al., 2018). Each year geohazard causes significant damage to the transportation infrastructure and environment. Hence, high cost needs to be borne by transportation agencies due to repairing (Creedy, 2006). Geohazard potential can be reduced substantially by performing an accurate subsoil investigation prior to the construction.

Slopes constructed on high plastic clay are very susceptible to rainfall-induced slope failure, which is a common type of geohazard (J. Hossain, 2012). During rainfall events, water is infiltrated into the soil, which causes an increase in pore water pressure and results in a reduction of shear strength. Moreover, the presence of crack and fissure in the soil top layer due to the wetting and drying cycles allows rainwater to infiltrate and increase the moisture content. Due to increasing moisture in the soil bodies, the degree of saturation increases, which affects the stability of the slope to a great deal (Chen & Lee, 2004). Therefore, it is important to know the degree of saturation at shallow depths in slopes to determine the geohazard potential. Moreover, collapse occurs in slopes constructed with certain types of soil with high void ratios and relatively low densities (Bell & Culshaw, 1998). Thus, proper investigation of the subsurface condition is mandatory for any infrastructural construction to avoid such kinds of geohazard potential.

Although conventional site investigation incorporating borehole sampling produced the most reliable values of the relevant soil parameters, which are required for the calculations of the factor of safety, it is very time consuming, very expensive, and can provide information of only one specific point (Ameratunga et al., 2016). According to conventional industry practices, linear or curvilinear interpolations are used to determine the subsurface profile. Such interpolation of soil properties between two boreholes often leads to wrong interpretation and may incur increased project costs (Leung et al., 2018). Thus, the use of geophysical testing is increasingly becoming a

very popular tool for geotechnical engineers to collect continuous subsurface data prior to construction. Assessment of soil properties using an electrical resistivity survey is a very impressive tool for describing the subsurface profiles without disrupting the soil structure. The method is less costly, and subsurface investigation of a wide area can be conducted in a short time frame (Amato et al., 2012). Electrical Resistivity Imaging (ERI) can provide an image of the subsurface condition of a large survey area within a very short period, which is also inexpensive, and the survey data can be processed very quickly. In addition to geotechnical site investigations, RI is also being considered as an effective technique in geoenvironmental applications. Application of resistivity imaging in landfill bottom liner, cover, and leachate recirculation in a bioreactor landfill was studied by many researchers (Alam, 2017; M. I. Hossain, 2017; Manzur, 2013). Due to these advantages of ERI over the conventional subsurface exploration techniques, it has become a considerably popular method for preliminary subsurface investigations, geo-environmental research, and geohazard studies.

1.2 Problem Statement

An accurate determination of the engineering properties of the soil at the site is essential for proper designing and successful construction of any project. Available traditional field-testing methods that are used to investigate the geotechnical properties of subsurface soil only provide information at the site-specific points (Cosenza et al., 2006). As a result, geotechnical engineers sometimes perform linear interpolation to collect the missing data, which can be misleading. Field and laboratory tests are performed on both disturbed and undisturbed soil samples to obtain the necessary design parameters. Although laboratory experiments provide accurate results, it is an expensive and time-consuming procedure to collect soil samples and conduct tests in a controlled environment. Therefore, to obtain a continuous profile of subsurface conditions before

3

construction and to evaluate the geotechnical properties of the underlying soil, a geophysical test method is required. A continuous image of the subsurface will also assists geotechnical engineers in finding out the anomalies and eliminating them during the designing phase.

The use of geophysical methods for site investigations offers the opportunity to overcome the limitations and inherent problems of conventional site investigation methods. Applications of Electrical Resistivity Imaging (ERI) for soil profile investigation is a promising approach to obtain a continuous profile of the subsurface (Hossain et al., 2019). The resistivity Imaging (RI) method employs the fundamental physics principles of Ohm's law to measure the horizontal and vertical discontinuities in the electrical properties of the ground (A. Samouëlian et al., 2005). Moisture variation and heterogeneity of the investigated area can be identified using this technique (S. Hossain et al., 2010). Resistivity response measurement equipment was developed significantly over the last decade, yet the usage of Electrical Resistivity Imaging (ERI) in the field of geotechnical engineering is limited because of the lack of knowledge of resistivity responses of different soil conditions (Kibria, 2014). Moreover, there is a lack of transformation equation to obtain the quantitative value from the qualitative soil electrical resistivity image to link up between this geophysical test and geotechnical engineering.

Several studies have been conducted to find out an electrical mixing model for soil as a function of pore fluid and surface conductivity (Alsharari et al., 2020; Bryson & Bathe, 2009; Datsios et al., 2017; Shah & Singh, 2005). However, finding out the pore water conductivity requires the extraction of pore fluid from the soil, which is very difficult to conduct in a regular subsurface investigation. Though soil properties that affect the electrical resistivity response were studied by many, a general model for a wide range of soil to explain the variation of soil resistivity with geotechnical parameters is not available. Therefore, correlations are required to understand

the effect of geotechnical properties on the electrical resistivity of soil. Moreover, these correlations will also be helpful to quantify moisture content, unit weight, void ratio, and degree of saturation from the Electrical Resistivity Image during the subsurface investigations.

1.3 Objective of this Study

The objective of this study is to evaluate geotechnical parameters of soil from electrical resistivity response. Based on the field and experimental data, correlations will be developed to determine the geotechnical properties of soil using the electrical resistivity of soils. The specific tasks of this study to achieve the objective are:

- Identification of sites in different locations of Texas to study variable site soil profile.

- Field investigations and collection of soil samples from different locations.

- Electrical resistivity imaging at different sites during sample collection.

- Physical and advanced characterization of soil samples.

- Evaluation of effects of water content, void ratio, and degree of saturation on the resistivity of soil specimen.

- Evaluation of variation of electrical resistivity as a function of soil properties.

- Development of a mathematical model to predict moisture content, void ratio, unit weight, plasticity index, and degree of saturation from resistivity imaging results.
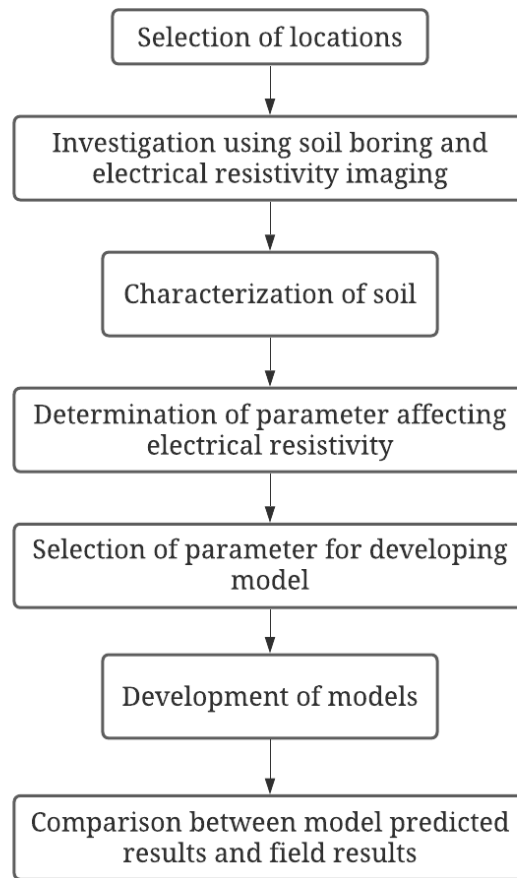
Figure 1-1 Flow chart of research activities in the current study

1.4 Organization of Dissertation

Chapter 1 presented the problem statement and objective of the current study

Chapter 2 described a literature review on soil characterization, effects of geotechnical properties on the electrical resistivity of soils.

Chapter 3 describes the research methodology of the current study. This chapter included the soil sample collection method, test methodologies.

Chapter 4 described the soil characterization of tested samples.

Chapter 5 presented the electrical resistivity properties of the soil and the impact of different geotechnical properties on them.

Chapter 6 described the development of multiple linear regression models using both disturbed and undisturbed samples for clayey soils and sandy soils. Validation of the models was also conducted using the laboratory and field results.

Chapter 7 summarized the conclusion of the study and proposed recommendations for future works.

CHAPTER 2 LITERATURE REVIEW

2.1 Introduction

Variations in ground and water conditions can be observed from place to place and within depths. Subsurface investigations are, therefore, the most critical and challenging phase of any infrastructure project. Both conventional and geophysical methods can be used for geotechnical subsurface investigation. Rather than using conventional methods, geophysical methods can provide comprehensive information about the entire site area. The electrical resistivity imaging (ERI) survey is one of the most promising geophysical approaches to obtain comprehensive subsurface profiles. In 1912, Schlumberger introduced the concept of measuring electrical resistance in rock bodies. This concept was initially used to discover petroleum reservoirs by oil companies. The use of electrical measurements to determine soil properties beneath the surface has become increasingly popular since then. Data processing techniques and measuring techniques have both improved greatly over the past two decades. Although resistivity imaging techniques are still evolving in the geotechnical engineering field, agricultural resistivity is widely used to measure soil salinity. To use resistivity imaging techniques in geotechnical engineering effectively, the geoelectric properties of soil need to be correlated with engineering parameters.

2.2 Subsurface Investigation Techniques

It is common to use soil tests in situ for geotechnical analyses and designs. The geological environment must be characterized in geotechnical investigations in order to build infrastructure over it with sufficient stability (Hunt, 2005). Soil and rock formations can also be studied for their engineering properties and physical properties.

2.2.1 Geotechnical Subsurface Investigation

A geological subsurface investigation consists of a preliminary subsurface investigation and a detailed subsurface investigation (Sew et al., 2000). Among the preliminary investigation's objectives is confirming the area's layout and formation. Drilling a borehole, collecting soil samples, conducting laboratory tests, and measuring engineering properties would comprise a detailed subsurface investigation. Based on its penetration resistance, subsoils are classified and characterized.

2.2.1.1 Conventional Subsurface Investigation

A standard penetration test (SPT) is the common method to measure the in situ soil conditions. Additionally, in situ soil properties can be obtained effectively by devices like cone penetration test (CPT) as well as dilatometer, pressure meter, and vane shears (Bowles, 1988). Texas Department of Transportation uses TCP for determining soil parameters in situ similar to SPTs and CPTs. The driving methods of a TCP test are similar to those employed in SPT, as are the cone shapes, albeit larger in diameter. In this respect, TCP can be compared to SPT and CPT. TCP can be used in both soil and rock.

2.2.1.1.1 <u>Standard Penetration Test (SPT)</u>

The SPT has been in widespread use for the last 80 years. Obtaining subsurface information has become easier and more cost-effective in recent years with this method. In North America, 75 to 90 percent of conventional designs utilize SPTs (Mayne et al., 2002; Vipulanandan et al., 2008). As part of the procedure, a split-barrel sampler is driven into the soil and counted how many blows (N) are required to drive it into 150 mm depths each, resulting in 300 mm of depth in total.

Refusals result in early termination of the test. There are three reasons for refusal: increments of 150 mm require 50 blows, drives of 300 mm require 100 blows, and no penetration occurs after ten consecutive blows.

2.2.1.1.2 <u>Cone Penetration Test (CPT)</u>

The cone penetration test (CPT) was developed in the year 1932. The test is sometimes referred to as a static penetration test as well as a quasi-static penetration test or a Dutch sounding test (Meigh, 2013). When clays or soft silts are present, instead of SPT, the CPT is used (Kulhawy & Mayne, 1990). Resistances are measured between the tip and cone sleeve of an average cone penetrometer with a 60-degree apex angle. CPT tests are conducted in accordance with ASTM D 5778, the standard of the American Society of Testing and Materials.

2.2.1.1.3 <u>Texas Cone Penetration Test (TCP)</u>

Texas cone penetrometers are mostly used in Texas Department of Transportation site investigations. An embedded hardened conical point embedded in hard rock and soil is hit by a 170 lb (77 kg) hammer dropped from 2 feet (0.6 m) (Tex-132-E). For the soil test, the penetration resistance is equal to the number of blows of the hammer used for the first and second 6 inches (150 mm), so the number of blows is equal to TCP N. Both TCP and SPT use the same energy/blow. SPT and TCP determine the blow count using penetrations of 12 inches. The refusal conditions in both are the same.

2.2.2 Geophysical Subsurface Investigation

In the conventional site characterization process, boreholes are drilled at selected intervals, and models of soil layers are generated. Budget constraints, limited access to drilling equipment or, conservational regulations often prevent the drilling of sufficient boreholes from establishing

an adequate subsurface image. Recent advancements in equipment and systems of data processing have, however, resulted in significant improvements in the accuracy and resolution of geophysical testing techniques. Thus, due to the above reasons, geophysical methods have become increasingly practical when it comes to shallow geotechnical investigations. In terms of Geophysics, the processes most commonly used are electrical resistivity imaging (ERI), seismic refractions (SR), multiple-channel analysis of surface waves (MASW) as well as ground-penetrating radars (GPR). Despite their relatively low costs, fast speeds, and environmentally friendly nature (Groves et al., 2011), it is possible to conduct these tests from the surface of the ground.

An investigation of a retaining wall foundation near Atlanta, Georgia, was conducted by Tomeh et al. (2006), using seismic refractions and multi-channel surface wave analysis. As a result of an SR survey, bedrock profiles were delineated, and an MASW survey was used to further characterize shallow beds (up to 12 meters). Hirsch et al. (2008) studied the Bow River near Calgary, Alberta using ERI, SR, and GPR. A thick layer of gravel and fine-grained lacustrine deposits were found as deep as 8.5 meters overlying mudstone bedrock. In locating boundaries and detecting sediment type changes, the ERI method was the most effective. Using resistivity, electromagnetic, seismic, and GPR methods to evaluate a test site in eastern Germany, Niederleithinger et al. (2013) presents evaluation results. The author suggested ERT as the best method out of three.

2.2.2.1 Electrical Resistivity Imaging (ERI)

Despite the fact that laboratory results showed excellent correlations between physical properties and geophysical measurements, there are several issues involved with the application of these methods at a larger scale. It must be noted that in contrast to laboratory-scale studies, the majority of studies on the ground utilize qualitative rather than quantitative methods. The first

difference is that many laboratory studies focus on relatively few soil textures tested over a relatively narrow range of soil moisture contents, whereas in the field, there can be many soil textures studied over a relatively wide range of soil moisture contents. Furthermore, these studies at small scales cannot easily take into account the heterogeneous nature of large-scale natural systems or the variable resolution applied to geophysical measurements in heterogeneous systems of interest at different scales (Singha & Gorelick, 2006). Furthermore, the relationship between soil moisture and resistivity can be complicated based on mineralogy, soil structure, hydraulic properties, and soil chemistry (Abu-Hassanein et al., 1996; Rinaldi & Cuestas, 2002). This can be challenging to replicate in the controlled environment since such characteristics frequently differ between fields.

In various geological conditions, electrical resistivity imaging (ERI) has been used successfully as a way to monitor soil moisture trends over time (Binley et al., 2002; Zhou et al., 2001). To measure temporal soil moisture variation, ERI was used, and it was assumed that changes in soil moistures affect the soil resistivity and that soils that have been wet or dry will have decreased or increased resistivity values.

2.3 Electrical Conduction in Geomaterials

The soil is a medium for fluids, chemicals, heat, and electricity to flow through. Electrical current is the flow of electricity through the soil. As long as the flow process does not change the state of materials, the current flow rate or flux will correlate linearly with the corresponding driving force. Generally, metals act as good conductors of current, meaning they allow current to flow easily, while insulators prevent current from flowing easily. There is a general rule that the electrical resistance of a device is inversely proportional to the density of the carriers and the mobility of those carriers. By understanding how electrical current flows through materials, it is

12

possible to separate conductor materials, such as metals or electrolytes, where conductivity is high, from insulating materials, such as air, ice, or plastic, where conductivity is low. As one of the latter, soil materials possess intermediate electrical properties based on their physical and chemical characteristics, such as thickness, salinity, or moisture content. The first use of electrical resistivity measurement to study subsurface rock bodies was introduced by Schlumberger in 1912 (Samouëlian et al., 2005). An electrical resistivity survey, also known as an electrical ERI survey, is a method of determining the resistance distribution of the soil volume around it. The electric field is critical for the transportation of water and ground stabilization by electroosmosis, insulation, corrosion, and subsurface investigations (Mitchell & Soga, 2005b).

In soil profiles, three types of potentials are found: diffusion-adsorption, electrode, and temporal fields (Semenov, 1980). Natural electrical fields are grouped into two main groups based on the mechanisms and nature of their occurrence: electrical fields arising in saturated and unsaturated soils due to the movement of soil solutions and electrical fields associated with stationary processes. Soil electrical fields are mainly attributed to diffusion-adsorption potentials, where sorption plays a more important role than diffusion. Electrode potentials, which are artificially created at the contact points between electrodes and the soil, are measured along with the natural electrical fields. Potentials of soil are defined as diffusion-adsorption between soil aggregates, horizons, and pedons in topographic sequences (Pozdnyakova, 1999). In the following sections, it will be explained how electrical conduction takes place through geomaterials.

2.3.1 Conduction of Electricity

There is a fundamental law of physics that is used in the measurement of the electrical resistivity of soils, known as Ohm's law. This law states that the voltage can be calculated by

13

multiplying the current by the resistance of the material. How current propagates through a cross-sectional area of the cylindrical shape of the material is shown here.
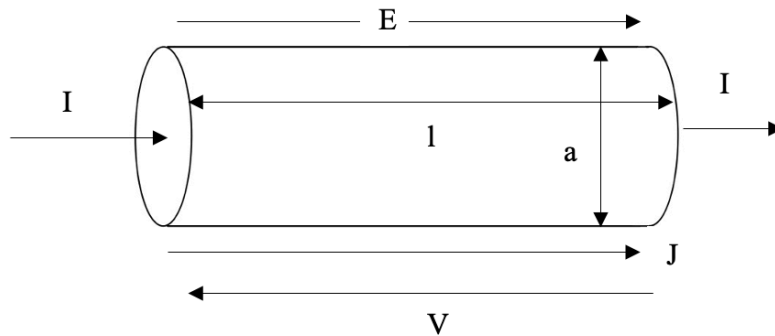
Figure 2-1 Current flow through a cylindrical area

In microscopy, the current density (J) represents the electricity flowing through a given area of a cross-section. The current can be calculated by taking the product of the dot of the current and the area, which is calculated as.

$$I = \int J.dA$$

Assuming that the E is electric field vector, then DV is the difference of potential, which can be expressed:

$$\Delta V = -\int E.dl$$

The element dl represents the integration element of the vector E of an electric field. If the field of electricity is uniform, it is possible to substitute the equations above into Ohm's law:

$$V = IR.$$

$$E.l = J.A.\frac{\rho.l}{A}$$

$$E = J.\rho, or, \qquad E = \frac{J}{\sigma}$$

Where resistivity of the materials is represented as r, which varies as a resistance function, conduction path length, and the cross-section area of the conductive material, also, σ is the reciprocal of resistivity and referred to as the conductivity of the material.

In addition to DC resistivity, alternative current (AC) signals can also be retarded by DC resistivity. At low frequency, the material's magnetic properties can be ignored, and the equation of Maxwell can be written as:

$$\nabla . E = \frac{1}{\varepsilon_o} q$$

$$\nabla \times E = 0$$

In the equation, the electric field is denoted as E and ε_o are dielectric permittivity (8.854×10-12 F/m). The charge density is designated as q. In this case, E can be seen as the electric poetical (V) gradient as:

$$E = -\nabla V$$

Three-dimensionally (x, y, z)

$$\nabla . E = \frac{1}{\varepsilon_o} q(x, y, z)$$

$$E = -\nabla V(x, y, z)$$

The expression can be presented as below by substituting the E vector:

$$\nabla^2 U(x, y, z) = -\frac{1}{\varepsilon_0} q(x, y, z)$$

The continuity equation of a point can be described by employing the Dirac delta function in 3D space (Loke, 2004).

$$\nabla . J(x, y, z, t) = -\frac{\partial q(x, y, z, t)}{\partial t} \partial(x) \partial(y) \partial(z)$$

The above equation can be rearranged as below:

$$-\nabla[\sigma(x,y,z)\nabla V(x,y,z)] = \frac{\partial q(x,y,z,t)}{\partial t}\partial(x-x_s)\partial(y-y_s)\partial(z-z_s)$$

Where xs, ys, and zs are the injected current source coordinates. The current source considering an elemental volume ΔV can be represented as follows:

$$\frac{\partial q(x,y,z,t)}{\partial t}\partial(x-x_s)\partial(y-y_s)\partial(z-z_s) = \frac{1}{\Delta V}\partial(x-x_s)\partial(y-y_s)\partial(z-z_s)$$

In the field condition, through a source of point, it is possible to inject the current I, i.e., electrodes. An isotropic non-uniform 3D medium can develop the partial differential equation of electric potential. The equation was developed by substituting a partial differential equation for the previous equation.

$$-\nabla.\,[\sigma(x,y,z)\nabla U(x,y,z)] = \frac{1}{\Delta V}\partial(x-x_s)\partial(y-y_s)\partial(z-z_s)$$

In order to find the distribution of potentials in the subsurface when current is applied from a point source, this is the basic equation that is used to determine the potential distribution. The electrical conduction phenomena, however, differ according to the types of soil. Depending on the geotechnical properties of clayey and sandy soils, the propagation method for electrons varies.

2.3.2 Electrical Conduction in Clay

A media that conducts electricity may do so with the aid of electrolytic pore water, which is present in the void, as well as through the movement of ions at the surface (Bryson, 2005). Another significant parameter that influences the electrical conductivity of clayey soils is the surface charge. Particles of clay possess electrical charge insufficiencies due to ions substitution at crystal structures and acid-base reactions between the water and silanol-aluminol (Si-O-H and Al-O-H) groups. It is thought that adjacent cations are attracted to the clay particles in order to counterbalance the net negative charge. There is an extremely high concentration of cations around

the solid surface; however, the concentrated cations try to diffuse across the structure to equalize concentration. As a result of the negative electrical field created by the clay particles, the effects of diffusion are restricted, and the anions are also able to migrate away due to the negative force created by the particles. This results in the presence of relatively mobile ions consisting of both positive and negative charges located adjacent to the adsorption layer. Together, the electrical double layer is constructed by the adsorption layer and the charged surface. It is called the Stern layer because it is the plane along which the counterions are strongly absorbed by the particles with the negative charge. There is evidence for charge separation in the diffuse double layer when an external electrical field is applied along a Z-potential plane (Revil et al., 2017; Rinaldi & Cuestas, 2002). Thus, in clayey soil, electrical conductivity is determined by two factors, bulk fluid, and surface conductivity. Figure 2-2 shows a simplified schematic of the location of the diffuse double layer (DDL), the stern layer, and the precipitated ions in clays.

A pivotal role, as well, is played with clayey soil by the water interaction in the electrical conductivity of the soil. The adsorption of cations by clay particles when dry is tightly held together by their negative charges. During neutralization, excess cations are precipitated as salts as a result of the net negative charges in clay particles. In the presence of moisture, precipitated salts go into the soil-water solution, forming a water-salt solution. In a previous study, Holtz & Kovacs (1981) suggested that the electrical and thermodynamic properties of adsorbed water differ from that of free water. The authors of Revil et al. (1996) have also emphasized the role of chemical reactions on clay surfaces in the presence of water. Based on the results of the study, a particle surface with silanol group appears to be capable of dissociating to positive and negative charges ($SiO-+H+/SiOH*H+*SiOH2+$) based on the chemical reaction that occurs when water is added.

17
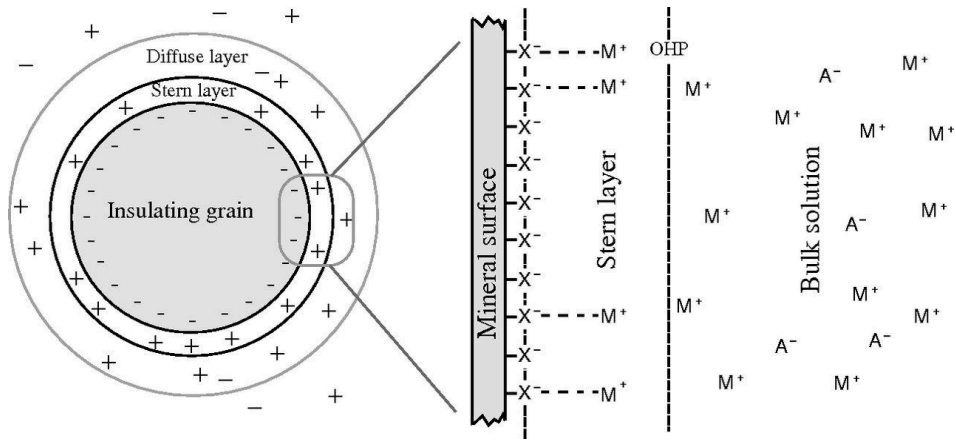
Figure 2-2 Diffusive double layer (DDL) in clay (Mitchell & Soga, 2005b)

2.3.2.1 Clay Minerals

Hydrous aluminosilicates and metallic ions make up the crystalline structure of clay minerals. Clay minerals are classified into two types of crystal units, namely tetrahedra and octahedra. In the tetrahedron, there is four oxygen surrounded by silicon. At the same time, the octahedron is composed of six oxygens or hydroxyls in the corners. The ions are being surrounded by aluminum, magnesium, iron, or other ions. A simple diagram of a tetrahedral unit and an octahedral unit is shown in Figure 2-3.

A variety of clay minerals are composed depending on the orientation and bonding of stacks, as well as the presence of metallic ions and isomorphous substitutions. In addition to kaolinite, montmorillonite, illite, muscovite, nontronite, we can also see maggots and spirules in clay minerals (Mitchell & Soga, 2005). As a matter of fact, in terms of engineering purposes, the minerals kaolinite, montmorillonite, and illite come into focus in engineering practices (Holtz & Kovacs, 1981).
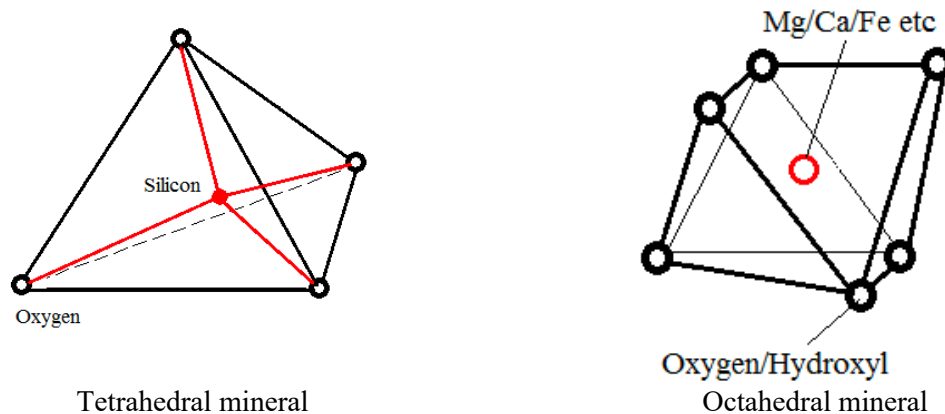
Figure 2-3 Different minerals (Mitchell & Soga, 2005b)

A 1:1 mineral is referred to as Kaolinite because the inherent crystal structure consists of two sheets; one is tetrahedral while the other is octahedral. Montmorillonite is composed of two silica sheets and one alumina sheet, which are the basic components. This particular type of mineral is known as 2:1 mineral, where the distance between unit cells is about 0.96 nanometers. However, the illite mineral, also known as 2:1 mineral, is composed of two silica layers and one alumina layer. It is exactly the same unit configuration as montmorillonite; however, it is bonded together by potassium so that the basic layers can be separated. The typical chemical formula of the clay minerals is presented in Table 2-1.

Table 2-1 Clay minerals chemical formulations (Yang, 2002)

Clay Mineral	Layer type	Typical Chemical Formula
Kaolinite	1:1	$[Si_4]Al_4O_{10}(OH)_8.nH_2O$ (n= 0 or 4)
Montmorillonite	2:1	$M_x[Si_8]Al_3.2Fe_{0-2}Mg_{0-6}O_{20}(OH)_4$
Illite	2:1	$M_x[Si_{6-8}Al_{1-2}]Al_3Fe_{0-25}Mg_{0-75}O_{20}(OH)_4$

2.3.2.2 Clay Water Interaction

A significant amount of water is adsorbed by clay minerals in soils, and this has significant effects on almost all aspects of soil behavior. Soil water or pore water is defined as water present in pore spaces or pockets of soil. In order to analyze the physical, chemical, and engineering

properties of the pores, it is necessary to determine how much water is present in each of them. This interaction between soil and held water is complex and is influenced by a variety of factors such as soil type, mineralogy, current, and past environmental conditions, stress history, etc. The physical and chemical properties of clay are largely influenced by the moisture content, which is evident from the engineering and physico-chemistry of clay. Therefore, it is important to understand the mechanism by which clay and water interact with each other. The mechanism of clay water interaction is briefly discussed below.

At dry conditions, the clay particles contain counterions and excess ions as precipitated salts, both of which are adsorbed onto the surface. As a result of the addition of water, the counterions adsorb to the surface of the particle and become hydrated. When the counterions undergo hydration, some of them lose their primary hydration shell (wholly or partly) and develop an inner sphere complex. It is also possible to find these ions as outer-sphere complexes when they possess primary hydration shells. There is a surface charge present on the particles, which enables the hydrated counterions to attach to them. Water separates the remaining counterions from the surface of the particles by bringing them back into the solution.

Among the causes of clay water interaction, Mitchell & Soga (2005) identified hydrogen bonding, osmosis, hydration of exchangeable cations, charged surface dipoles, and London dispersion forces, as illustrated in Figure 2-4.
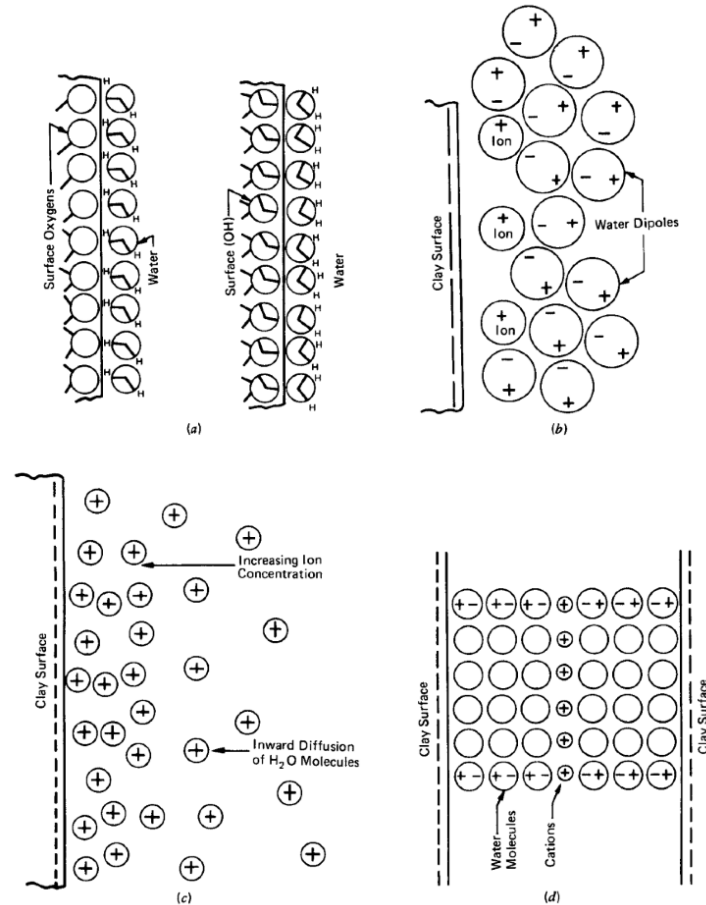
Figure 2-4 Interaction of clay-water (a) hydrogen bonding (b) ion hydration (c) attraction by osmosis (d) dipole attraction (Mitchell and Soga, 2005)

2.3.2.3 Clay Minerals Characterization

2.3.2.3.1 Soil Index Properties

It is necessary to characterize clay minerals in order to identify the engineering and physico-chemical properties of fine-grained soils. Further, for the development of stabilizers, it is essential to determine the specific mineral composition of clay. For the purpose of determining the qualitative mineral content of the soil, Casagrande used Atterberg limits. In Mitchell & Soga (2005), it was demonstrated that clay minerals had different ranges of activities depending on the mineral, which they identified as the dominant mineral in the soil sample. The experimental results were used to develop a chart for identifying the dominant minerals in the samples. Despite the fact

21

that the chart provides means for assessing the mineral in a preliminary manner, the information provided can be of great use from an engineering viewpoint. The following table gives an indication of the typical ranges of LL, PI, and activity for several minerals.

Table 2-2 Typical ranges of Atterberg limits and activity (Mitchell and Soga, 2005)

Mineral Name	Liquid limits	Plastic limits	Activity
Montmorillonite	100-900	50-100	1-7
Illite	60-120	35-60	0.5-1
Kaolinite	30-110	25-400	0.5

2.3.2.3.2 Scanning Electron Microscope

Electron beams are used in scanning electron microscopes (SEM) to analyze very fine objects. SEM can reveal topography (surface details), morphology (size, shape, and composition of a particle), and crystallographic information (arrangement of the elements). In a review, Voutou et al. (2008) explained SEM's mechanism. Below is a brief description.

With a point source called an electron gun, monochromatic electrons are created in a series. A conventional gun and a field emission electron gun are two types of guns. Two electron guns differ primarily in the mechanism that produces electrons and in the potentials of the vacuum tubes. Yet, the guns' primary purpose is to generate highly energetic electron beams.

Electrons can scatter both elastically and inelastically when they strike the atoms of the target material. This results in backscattered electrons, secondary electrons, and auger electrons. SEM uses secondary electrons to visualize soil fabric. A substantial amount of energy is lost when an incident electron excites an electron in the specimen. After being excited, the electrons are subjected to elastic and inelastic collisions until they reach the surface of a specimen. They can escape from the surface if that surface is energetic enough.

A specimen's topography is one of the most important factors in the development of secondary electrons. Due to their low energy (5eV), these electrons can escape from the surface (located close to 10 nm). For targets with high atomic numbers and angles of incidence, the number of secondary electrons is generally higher. Additionally, it indicates the strongest electron energy spectrum region. Consequently, secondary electrons can show the topography of the surface.

Backscattered electrons can differentiate specimen constituents. A specimen's atomic number affects how many backscattered electrons it has. Emitted electrons appear brighter from elements with a higher atomic number. As shown in Figure 2-5, SEM tests produce a certain type of radiation.
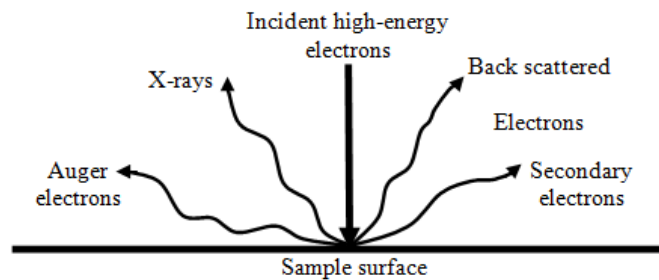
Figure 2-5 Electron bombardment effects

2.3.2.3.3 Energy Dispersive X-ray Spectroscopy (EDS)

In EDS, the constituent elements of a specimen are identified by energy-dispersive X-ray spectroscopy. Under X-ray excitation, this technique analyzes how the specific atomic structure interacts. Nuclei maintain discrete electron energy levels at rest. An electron may escape from an existing shell after being excited by the strike of an incident high-energy beam. A void is created in the parent shell as the excited electrons jump to the next energy level. X-rays are released when electrons from a higher energy shell fill the void space. Energy-dispersive spectrometers measure X-ray energy and number emitted by a specimen, as well as the elemental makeup of the sample.

Inelastic scattering is attributed to electron excitation by Voutou et al. (2008). Electrons in the ground state gravitate towards unstable or excited states. As a result, the electrons radiate more energy due to atomic relaxation. Each element has its own relaxation energy. EDS X-ray detectors can determine elemental composition based on relaxation energy.

2.3.3 Electrical Conduction in Sand

Conduction occurs mostly electrolytically in coarse-grained soil. Santamarina et al. (2001) refer to both granular structure and electrolyte conductivity as determining factors. The resistivity of marine sands was measured by Jackson et al. (1978). The findings indicated that the resistivity of sand was primarily determined by pore fluid resistance and porosity. Additionally, the shape and size distribution of particles affected the resistivity of sands. While clay may have more complicated electrical properties, sand's resistivity may be more influenced by the microstructure, porosity, and resistance of the pore fluid (Fukue et al., 1999). It has also been demonstrated by Kalinski (1992) that the electrical resistivity of sandy soil depends on pore water conductivity, apparent particle conductivity, as well as material constants depending on the distribution of pores. As Yoon et al. (2002) and Sreedeep et al. (2004) also concluded, sand electrical resistivity is influenced more by water content, unit weight, and pore fluid than any other soil property.

the following empirical equations were suggested by Archie (1942) based on lab measurements:

For saturated sands, $\frac{\rho_o}{\rho_w} = (n)^{-c}$

For unsaturated sands, $\frac{\rho'}{\rho_o} = (s_r)^{-d}$

Where, Sr = degree of saturation, ρ' = unsaturated soil electrical resistivity, ρ_o=soil resistivity, ρ_w= free water resistivity, n= porosity of the soil, c and d = parameters of soil

2.4 Geotechnical Properties Affecting Resistivity

Porosity, pore size distribution, and connectivity play a role in electronic conductivity in the soil (particle size distribution, mineralogy). These properties are influenced by the distribution of mobile electrical charges in soil, mostly inorganic ions, and are determined by the natural and artificial electrical fields in soil. The electrical resistivity of the soil can also be affected by water content and temperature. There are two major factors that can alter soil resistivity: moisture content and saturation (Abu-Hassanein et al., 1996; Kibria, 2014; McCarter, 1984) . Earlier studies were conducted on pore water composition and geologic formation and found they had a strong impact on soil electrical resistivity (Giao et al., 2003; R. Kalinski & Kelly, 1993). A clayey soil's ion content and its interaction with moisture have major effects on its electrical conductivity (Fukue et al., 1999; Yang, 2002). In a continuous medium, the air media is an insulator (i.e., infinitely resistive); in a water solution, the ionic concentration determines the resistance, and in solid grains, the electrical charge density determines the resistance. Electrical resistivity is affected by these parameters, but in different ways and to different degrees. An electrical resistivity experiment has been conducted to determine the relationship between these soil characteristics and electrical resistivity. The following subsections discuss the factors that influence electrical resistivity:

2.4.1 Moisture Content

In soils, electrical current is mainly electrolytic, i.e., based on ion displacements in pore-water and is consequently greater in soils with dissolved salt. Water quality and amount determine the electrical current in soil. The electrical conductivity of the solution is considered relatively constant in most studies regarding the water content, to be neglected as a result of water content variation. Moisture affects clayey soils' engineering behavior. Several layers of moisture films

surround clay particles because of their high surface activity. Clayey soil adsorbs water from the crystal structure. This water plays a major role in clayey soil physico-chemical behavior. A soil's moisture content is a basic parameter to understand its behavior. A soil's moisture content is usually determined by weight (gravimetry) or volume (volumetry). Gravimetric moisture content is the amount of water within the void compared to the soil solids. Volumetric water content, on the other hand, measures moisture in terms of volume. It is calculated by comparing water volume to total soil volume.

A change in ion concentration in the pore water results in changes in electrical conductivity. Adsorbed ions in solid particles are precipitated in the pore water when moisture content increases. Electrical resistivity is reduced by free electrical charges. This causes electrical resistivity to decrease as moisture increases. Samouëlian et al. (2005) report a significant reduction in resistivity below 15% moisture content.

Based on the natural logarithm of moisture content vs. electrical resistivity curve, Pozdnyakov et al. (2006) divided the curve into several segments. Adsorption water, film water, film capillary water, capillary water, and gravitational water were the segments of the curve. As moisture increased in the adsorption moisture zone, electrical resistivity rapidly decreased despite the immobility of water molecules in adsorbed water, a conductive path created by dipolar water for electrical currents. As moisture increased in the adsorption zone, electrical resistance decreased. As Van der Waals' force increased in the film moisture zone, the reduction rate decreased. Pore water flows from film to fissure when water film reaches maximum thickness. In the film capillary water zone, molecular attraction is stronger than capillary attraction. In the film capillary and capillary water zone, electrical resistance decreased less dramatically. Electrical

charges move without being affected by the movement of water molecules, and electrical resistivity becomes almost independent of water content in the gravitational water zone.
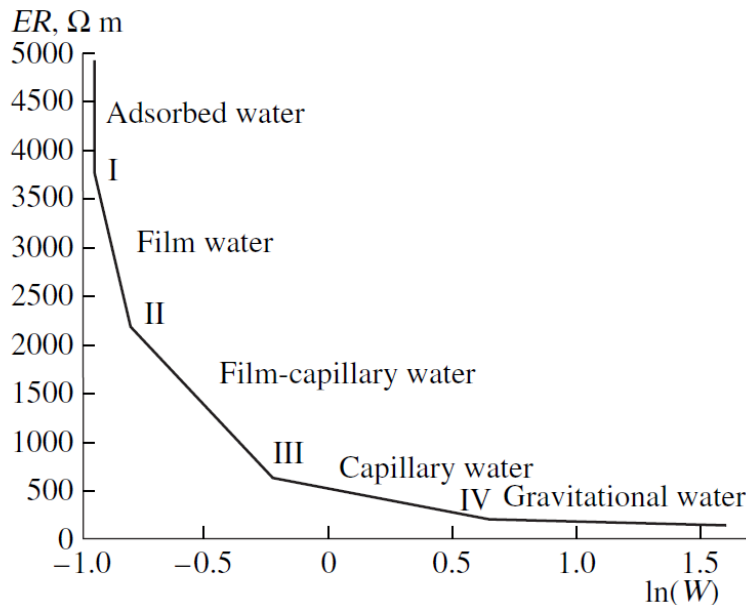
Figure 2-6 Changes of resistivity with moisture (Pozdnyakov et al., 2006)

2.4.2 Degree of Saturation

Reduced soil resistivity is caused by increasing saturation, but the relationship is highly influenced by the critical saturation level. In order for continuous water film to develop around soil particles, critical saturation requires a minimum amount of water. Under critical saturation, soil resistivity increases abruptly (Bryson & Bathe, 2009).

Rinaldi & Cuestas (2002) found a concave upward relationship between conductivity and saturation. High saturation may lead to pore space reduction and enhanced particle contact. In the figure, the effect of different electrolyte concentrations on conductivity is shown.

According to Matsui et al. (2000), rock properties are correlated with electrical resistivity. For the study, granites and sedimentary rocks from Japan were used. At different stages of natural drying and artificial desiccation, the samples were saturated with tap water. Up to a certain level,

resistivity decreased with increasing saturation, but the variation was insignificant above that point.
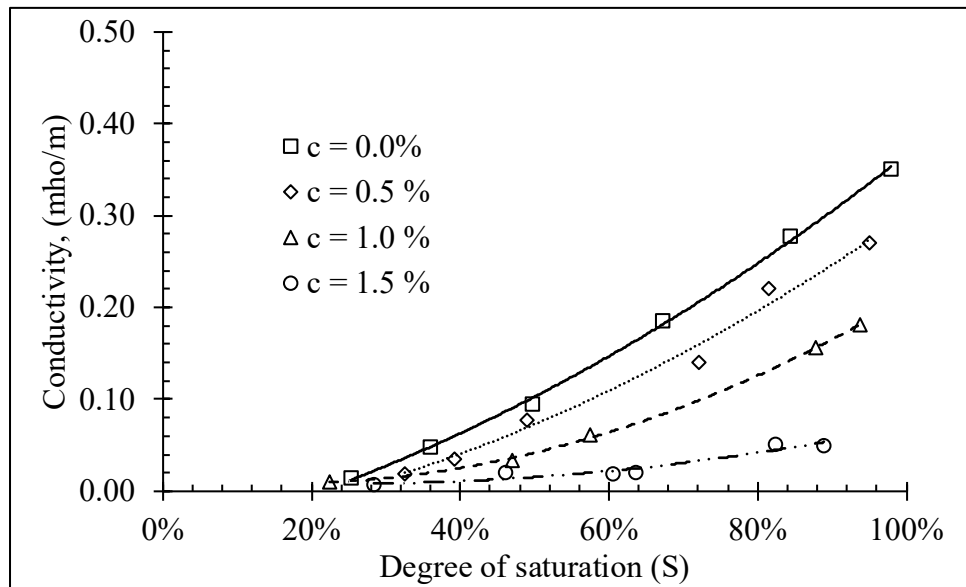
Figure 2-7 Effects of conductivity on degree of saturation (Rinaldi and Cuestas, 2002)

2.4.3 Clay Fraction

The clay fraction also indicates a soil's surface charge. As the clay fraction increases, so does the soil's affinity for water. Thus, the soil's electrical resistance varies with it. Clay content and field resistivity of Norwegian clay were studied by Long et al. (2012). From the results, the author concluded that soil samples with clay content greater than 40% have low resistivity. There was a 0.59 correlation between resistivity and clay content.
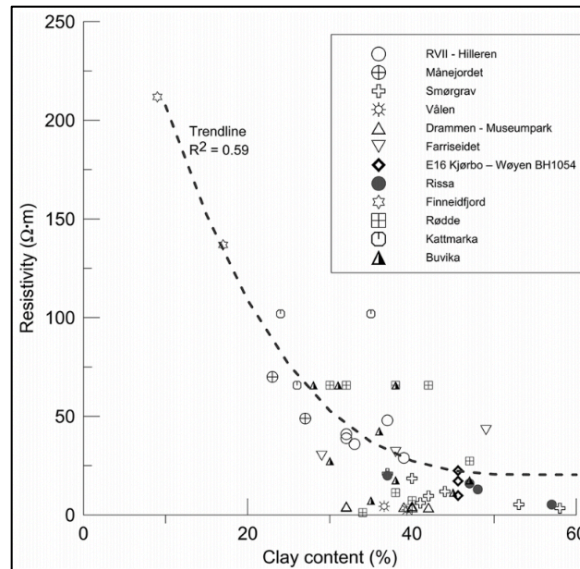
Figure 2-8 Resistivity and clay content (Long et al., 2012)

2.4.4 Atterberg Limit

As the soil sample passed number 40 sieve after being tested in the laboratory, the Atterberg limit of any soil sample changes with its fine and clay content. Using the proctor method, Abu-Hassanein et al. (1996) estimated the electrical resistivity variation in soil samples with Atterberg limits. LL and PI with higher values had lower resistivity.

Mineralogy of the samples was used to explain the variation of resistivity with LL and PI. Surface conductivity is higher in clay samples with high levels of LL and PI. Nevertheless, clay samples' sensitivity makes comparing resistivity with the Atterberg limit difficult (Long et al., 2012).

2.4.5 CEC & SSA

Under a given set of environmental conditions such as temperature, pressure, pH, and pore water chemistry, clay adsorbs specific types of cations. A change in the environment can partially or fully replace the adsorbed ions with ions of another type. Soils may change physicochemically.

29

Na+, K+, Ca+, and Mg+ are the most common cations in soil. Electrical resistance is determined by cations adsorbed on the soil. The literature indicates that the physico-chemical properties are correlated with the cation exchange capacity of the soils (Friedman, 2005; Schwartz et al., 2008).

2.4.6 Pore Water Conductivity

Conductivity is related to ion mobility in the fluid filling the pores. -For water, conductivity depends on the concentration and viscosity. Resistivity measurements require knowledge of dissolved ions. Rhoades et al. (1999) faced the problem of estimating soil salinity variation in their studies determining soil water content. Salts are ionized to conduct current, and soil water determines the available paths. Electrical resistance and salinity are closely correlated for soil water contents ranging from saturation to -3 kPa. Electrical resistance requires the same water content for estimating soil salinity. As a standard condition, soil salinity is usually measured at saturation. The mobility of ions in a porous medium determines its electrical conductivity. Clayey soil forms electrolytes through the hydration of precipitated salts. Hydrated cations and anions move towards cathode and anode. Santamarina et al. (2001) say that when electric fields and charge interactions combine, ions achieve a terminal velocity. The einsten-Nernst equation describes the terminal velocity of an ion subjected to a unit electric field:

$$u = \frac{v_{(ion)}}{E} = \frac{ze}{6\Pi \eta R_h}$$

here, $v_{(ion)}$ is ion velocity (m/s), E is electric field (V/m), z is ion valence, η is solution viscosity (Pa.s), e is electron charge (1.602×10^{-19} C) and R_h is hydrated ions Stokes' radius.

Due to the varied mobility of ions in the soil, electrical conductivity is affected. The soil contains different ions such as H^+, OH^-, SO_4^{2-}, Na^+, Cl^-. Their ion mobility differs, so they do not affect conductivity similarly. The electrical resistance of soil decreases with increasing pore

water conductivity, according to Kalinski & Kelly (1993). For estimating pore water conductivity, the following equation was developed:

$$EC_w = EC_0 - \frac{EC_s}{\Theta(a\Theta + b)}$$

Where ECw = electrical conductivity of pore water, ECs= soil particle surface apparent conductivity, ECo= electrical conductivity of bulk soil, Θ = volumetric moisture content, a and b= constant.

In their study, Rinaldi and Cuestas (2002) focused on the sodium chloride influences on loess soil in Argentina. Electrolytes were added to compacted soil samples. Different electrolyte concentrations were measured. As shown in Figure 2-9, the conductivity of soil and electrolyte have a linear relationship. The study found sodium samples to have the highest conductivity. Conductivity differed due to ion mobility, soil structure, and adsorption.
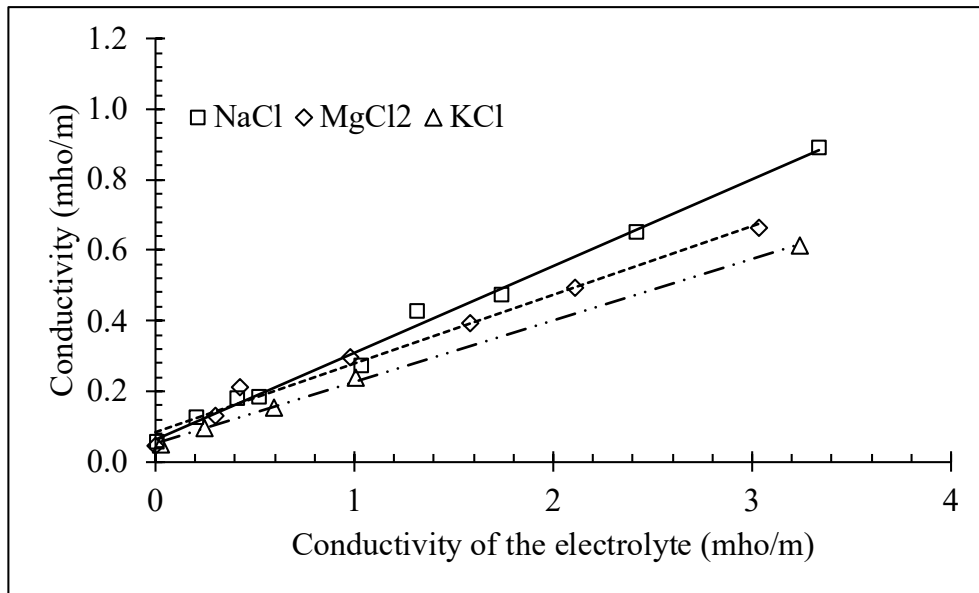
Figure 2-9 Saturated sample conductivity relationship with different electrolytes (Rinaldi and Cuestas, 2002)

Despite the increase in electrical conductivity in pore water, the mobility of charge is limited by the high concentration of ions present. It is possible for the conductivity to be reduced under that condition (Santamarina et al., 2001).

A study by Oh et al. (2014) examined the effects of pore-fluids on the electrical resistivity of soil-water mixtures. Sand and clay with various porosities and electrical resistivities were used for the experiments. In cases of low specific surface soil (e.g., the Ottawa 20-30 sand), a formation factor (or Archie's law constant) was shown independent of pore fluid electrical resistivity. As a result, Archie's law constants can provide pore information. An electrical resistivity-dependent soil with a high specific surface (e.g., kaolinite) has different Archie's law constants. In lower ionic concentration fluids, surface conduction in soil particles seems to contribute to this.

2.4.7 Temperature

With the increase of temperature, the resistivity starts to decrease because of the agitation of the ions. Electrical resistivity measurements at a standardized temperature are compared. According to Campbell et al. (1949), if the temperature changes one degree Celsius the resistivity of soil decreases by 2.02%. Electrical resistivity and soil temperature have an exponential relationship, according to Abu Hassanein et al. (1996). To understand the changes of electrical resistivity with different soil properties, experiment measurements need to be corrected for a reference temperature.

2.4.8 Structure and Packing of Soil

Charge density at the surface of solid constituents determines electrical conductivity. Clay particles with electrical charges on their surfaces provide higher electrical conductivity than coarse-textured soils (Fukue et al., 1999). Giao et al. (2003) measured the electrical resistivity on

25 clay samples collected worldwide. The electrical resistivity of two cultivated sandy soils of very similar composition was found to differ significantly by Lamotte et al. (1994). The most resistive soil is sandy, with very few micro-aggregates of clay juxtaposed with sand grains. The sand in the other soil was coated and bridged by clay, leading to an extremely continuous clay phase.

According to the water potential, pores are shaped (void distribution and form). In 1996, Robinson et al. (2003) identified that high and low resistivity values were related to macro-and Meso-porousness, respectively. As a result, badger burrows and their network were detected and studied. In addition, Samouëlian et al. (2003) were able to study the crack opening at the centimetric scale.

For a saturated soil with no clay, Archie's law gives the porosity as:

$F = \rho/\rho_w = a\emptyset^{-m}$

The formation factor F is the proportionality factor. These are the constants a and m, which are related, respectively, to the coefficient of saturation and the cementation factor. ρ and ρw are, respectively, the resistance of the formation and the resistance of the pore water, and f is the porosity. The factor F is then dependent on the pore geometry. In order to calculate the porosity using a resistivity value, the pore-water resistivity is known, as well as the a and m constants. Porosity calculated by Archie's law implies that all void space is filled with water, excluding gas presence in the void space.

Using electrical resistivity measurements, Zha et al. (2007) evaluated the expansive soil structure. With increasing swell percentages, the formation factor linearly increases with the shape factor. Further, the relationship between log-time, formation factor, and shape factor was used to determine the initial, primary, and secondary swellings. Researchers found decreased average

formation factors to be related to changes in microstructure, destruction of formations, an increase

in moisture content, and decreased strength, cementation, and stability of soils.

Electrical resistivity varies widely in soil mapping, from 1 ohm-m for saline soil to several

105 ohm-m for dry soil overlying crystalline rocks. The Figure 2-10 below shows the change in

electrical resistivity for different soil types.
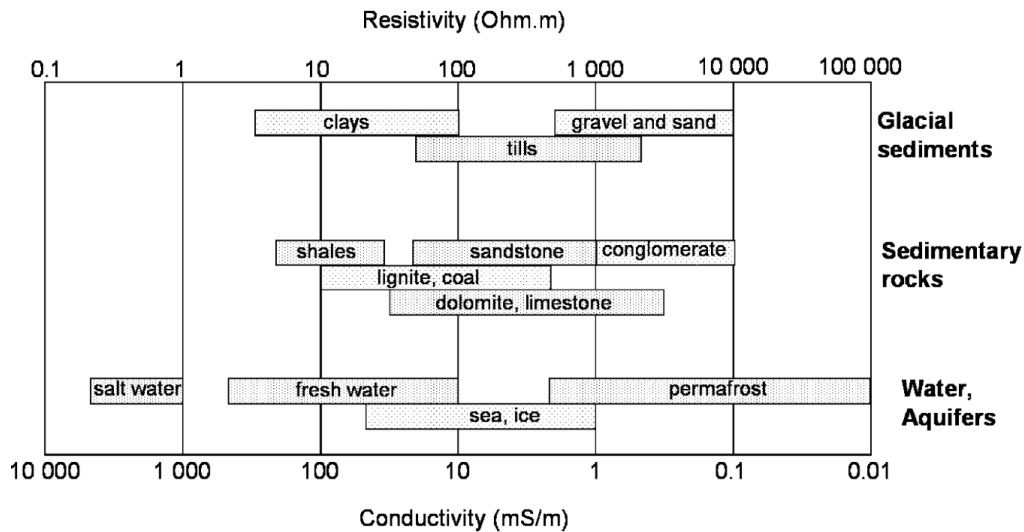
Figure 2-10 Variation of electrical resistivities ranges (after modified Palacky, 1987)

2.5 Evaluation of Geotechnical Properties through Electrical Resistivity

When it comes to ground engineering, the most important consideration is the soil

properties. The most important aspects that should be taken into account in a geotechnical

engineering design are the soil moisture content, cohesion, friction angle, unit weight, saturation

degree, porosity, plasticity index, and size distribution (Abidin et al., 2017; Bery & Saad, 2012;

Gunn et al., 2015; Hisyam & Osman, 2017; Kim et al., 2011; Zha et al., 2010). Especially in

determining slope stability and bearing capacity, these properties are important. Geotechnical

design is better performed with soil investigation (SI) through borehole drilling and soil sampling,

but it is laborious, costly, and invasive. So, it is very important to find a non-destructive, quick,

and environmentally friendly method of assessing soil properties to enable quick and widespread

calculations of ground engineering design under varying soil conditions in the event of soil failures or landslides. A geophysical method can be used to describe the subsurface profiles without disturbing soil structure. Geotechnical engineers will be able to use electrical resistivity data to estimate geotechnical parameters, bridging the gap between geotechnical and geophysical engineering. Below are previous studies relating soil parameters to resistance values:

2.5.1 Moisture Content

Kalinski and Kelly (1993) used a four-probe circular cell to measure the volumetric water content of soil from resistivity responses Figure 2-11. As the extracted water is more representative than soaking water from soil specimen using porous plates, pore water was extracted. As the volumetric water content increased, the ratio of soil conductivity to pore water conductivity increased. In addition, an equation was developed to determine the volumetric moisture content based on the apparent conductivity (ECs) of soil particles. Validation of the predicted results was done by using measured moisture content values.

$$EC_o = EC_s + EC_w \theta \ (1.04\theta - 0.09)$$
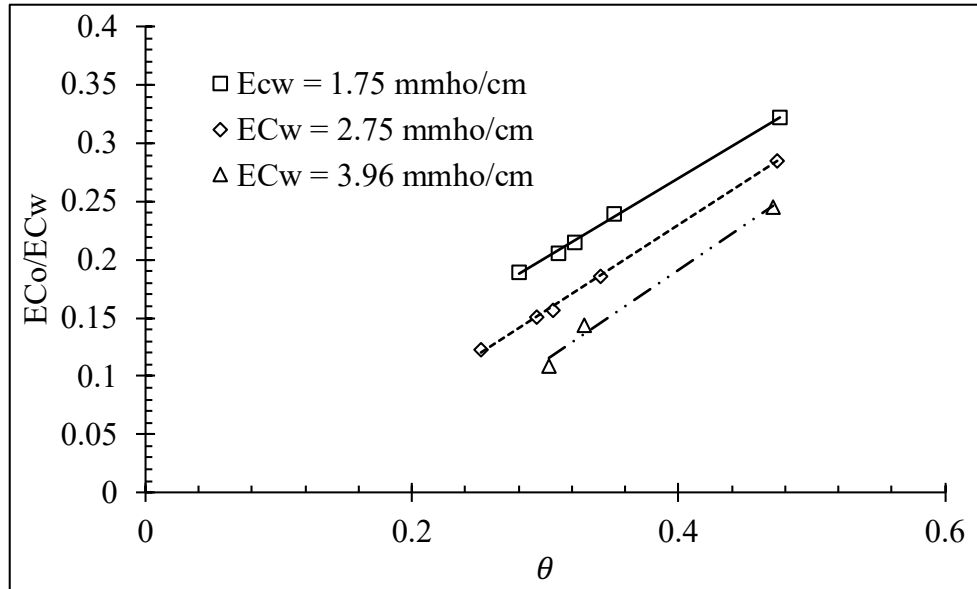
Figure 2-11 Relationship of ECo/ECw for θ laboratory-measured specimens Kalinski and Kelly (1993)

Schwartz et al. (2008) quantified field scale moisture content by using ERI. Kentland experimental farm at Virginia Tech in Montgomery County, VA, served as a study site for this project. Moisture content and electrical resistivity data were measured using TDR and ERI. From the two-dimensional Electrical Resistivity Image, a one-dimensional resistivity profile was determined by EarthImager 2D software. Numerical optimization of Archie's law coefficients was used to quantify water content. Archie's law coefficient was developed by using extractable cations rather than pore water resistivity. In the experiment, the model was able to predict heterogeneous settings and meter-scale soil moisture variations.
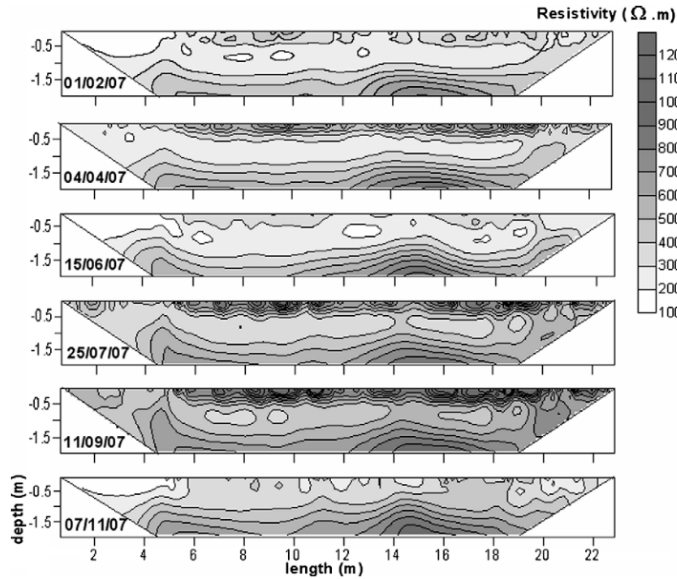
Figure 2-12 ERT resistivities (Corrected to 25 °C) in space and over time, during the year 2007 (Brunet et al., 2010)
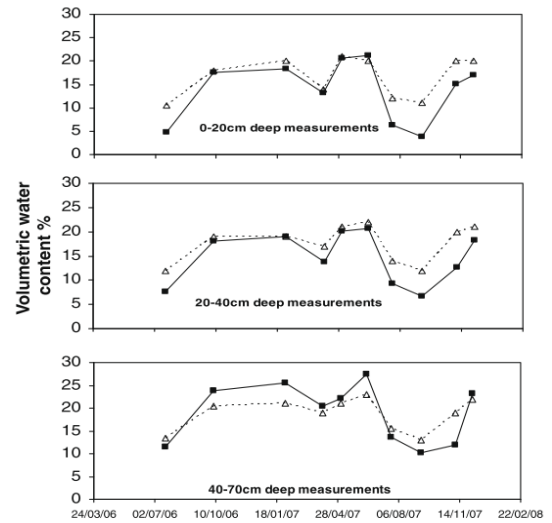
Figure 2-13 Comparison of TDR and ERT water content at depths: 0–20 cm, 20–40 cm, 40–70 cm (Brunet et al., 2010)

An ERT-based estimate of moisture deficit was carried out in Southern Cevennes, France, by Brunet et al. (2010). In the study area, more than 10 ERTs were performed between February 2006 and December 2007, and volumetric moisture was determined by means of Time Domain Reflectometry.

A cementation coefficient (m) and coefficient of saturation (n) of 1.25 and 1.65 were calculated depending on results obtained in the laboratory. Temperature, water solution resistance, porosity, and the inversion algorithm were all factors influencing water content measurements from resistivity. Figure 2-12 and Figure 2-13compare predicted and observed water content and the ERT profiles at different depths. ERT predicted moisture contents are indicated by solid lines in the figure.

Using two sites in Istanbul and Golcuk, Turkey, Ozcep et al. (2009) investigated the relationship between soil resistivity and moisture content. These two sites' resistivity was obtained by means of VES. A soil sample was also taken for lab testing. VES measures soil moisture and

soil resistivity. For two different study areas, two different exponential equations were developed to correlate moisture content with electrical conductivity.

$$W = 51.074 \, e^{-0.0199R}, R^2 = 0.76 \, (Istanbul \, Area)$$

$$W = 47.579 \, e^{-0.0158 \, R}, R^2 = 0.75 \, (Golcuk \, Area)$$

Based on laboratory testing, Kibria (2014) measured both compacted and undisturbed clay soil moisture content and electrical resistivity. A soil sample containing high plastic clay (CH) and a soil sample containing low plastic clay (CL) was collected from two different sites. For compacted and undisturbed soil samples, two different equations, one with two parameters, the other with a single parameter, was developed and validated. The field and laboratory resistivity tests were performed using the Super Sting R8/IP multichannel system from Advance Geoscience Inc (AGI). By translating apparent electrical resistivity into actual resistivity measured in the field, EarthImager 2D software developed a resistivity image profile. According to ASTM G187-05, field resistivity values were corrected to 15.5.

A preliminary study was conducted by Miracapillo & Morel-Seytoux (2015) in a protected area in Basel in order to investigate variations in soil resistivity and soil water content. Data accuracy was assessed. Water content has an inverse relationship with resistivity, meaning the results are easily interpreted.

2.5.2 Atterberg Limit

Soils' liquid limits (LL) and plastic limits (PL) are also affected by surface activity. Therefore, there is a correlation between electrical resistivity and index properties. Bryson (2005) correlated LL and PI with conductivity which shows as:

$$LL = (BQ)^{b1}a_1$$

$$PI = (BQ)^{b2}a_2$$

Where BQ= conductivity of surface in siemens/m. The coefficient α and β coefficients are clay mineralogy functions.

Mineralogy of clay affects soil electrical resistance and index properties (Abu Hassanein et al., 1996). Smectite-rich soils had increased LL, PI. Moreover, the electrical conductivity is higher in these soils. Therefore, the resistivity of the soil mixture decreases.

2.5.3 Clay Content

The Atterberg limit increases with soil clay content, and similar trends can be observed in changes in resistivity. Shevnin et al. (2007) used electrical resistivity to estimate clay content in soils. The resistivity model considered soil micropore electrochemical processes. 0.6-100 gm/L of NaCl were used for the experiments on brine saturated soil samples. Using resistivity measurements at concentrations of salinity between 0.6 and 100 gm/L, different soil properties can be discovered. In comparison to sand-clay mixtures, an overall 20% error proposed method showed. To determine the clay content, CEC, and porosity of the soil in Mexico, the proposed method was used. A boundary electrical resistivity was found, which separates the clean soil from oil-contaminated soil; hence, the model could identify the oil-contaminated zone.

2.5.4 Compaction Condition

To determine the impact of molding moisture as well as compaction energy on soil resistivity, Abu Hassanein et al. (1996) directed extensive research. A CL-CH, two CH with different plasticity indexes, and one CL soil sample were used in the study. Three different compaction methods were used to compact the soil samples; standard, modified, and reduced proctor methods were employed. Electrical resistivity was measured using the four-electrode

method for all soil samples. When the soil was compacted at wet optimum, the resistivity was low, and when it was compacted at dry optimum, it was high. The results also indicated that molding moisture content affected resistivity. According to the author, a soil sample's electrical resistivity is sensitive to moisture content when the molding water content is below optimum. The electrical resistance of clay compacted at the wetter of optimum is almost independent of the water content of the molding. Figure 2-14 shows the results of the study.
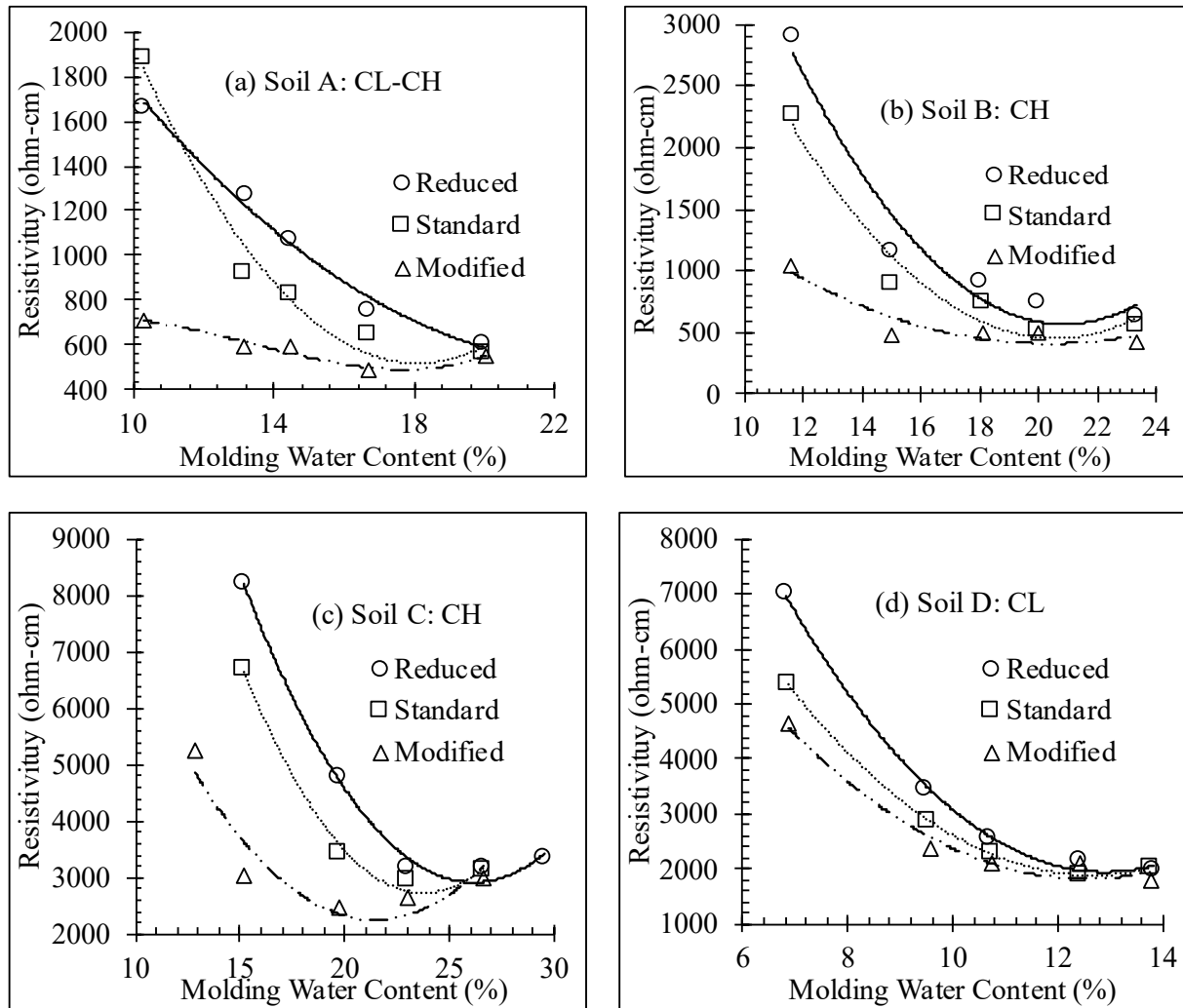
Figure 2-14 Correlation between resistivity with molding moisture and compaction energy for (a) CL-CH (b) CH (c) CH (d) CL (Abu Hassanein et al. 1996)

Changes in resistivity with molding moisture are caused by soil structural changes during compaction (Gingine et al., 2016). As the soil structure flocculates at low compactive effort and optimum water content, the electron flow mechanism occurs primarily through water in macropores, like in granular soil. Furthermore, it is difficult to remold clay clods when they are dry. Moreover, pores in the interclods are relatively large, dielectric air fills the pores, and DDL is partially formed. Clay clods, however, easily can be remolded with optimal and high compactive efforts, increasing saturation. By improving particle-to-particle contact and forming a bridge between particles, soil conducts electrically (Abu Hassanein et al. 1996). The soil structure is dispersive on the wet side of the compaction curve. Therefore, even if macropores are small, micropores and adsorbed water contribute to growing conductivity (Gingine et al., 2016).

2.6 Field Condition and Electrical Resistivity

Various relationships were developed by researchers between soil SPT-N and the resistivity of soil for a particular region. A nonlinear correlation was found between the SPT-N and the soil electrical resistivity values by Braga et al. (1999). In Gang City, Jiangsu province, China, Liu et al. (2008) found a linear relationship between standard penetration values and electrical resistivity of soil. In Malaysia, Hatta & Syed Osman (2015) employed the Wenner array arrangement to develop SPT-resistivity correlations. They found that the parameters are linearly correlated. Soil electrical resistivity and SPT-N were reported to be exponentially correlated by Rezaei et al. (2018) for Iran. For one location in South Korea, Oh & Sun (2008) established a linear relationship between soil electrical resistivity and SPT-N value. A study conducted in Aligarh and Jhansi, India, reported that SPT-N and resistivity of the soil must be correlated to each other (Sudha et al., 2009). Researchers found linear correlations between these two parameters for both places.

2.7 Measurement of Resistivity

It is important to understand that the electrical resistivity test is based on Ohm's law. As a result of a resistivity test, there are many measurements to be made, each involving four electrodes. Two electrodes are used to measure the potential electrical changes (DV) in the ground due to the imposed current flow (I), while two additional electrodes are used to measure the flow of current (I) from the electrodes into the ground. A number of factors, including the length of the line running through the electrode array, the position of the current dipole relative to the potential dipole, and the spacing of the electrodes, are correlated to the depth of penetration desired (Barker, 1989).

2.7.1 Laboratory Resistivity Tests

It is possible to study the electrical properties of materials in the laboratory by using either direct current (DC) or alternative current (AC). DC method operates based on the principle of Ohm's law, in which voltage is calculated when current is applied. Two- and four-electrode configurations are available for resistivity tests. Both are described herein.

2.7.1.1 Two Electrode Method

ASTM G187-05 is the standard method for measuring soil electrical resistivity with two electrodes. Figure 2-15 illustrates the methods of testing the resistivity of the soil in the laboratory using two-electrode methods along with the current source and measuring device. Using the same electrodes, voltage and current measurements can be made. An insulated and durable soil box should protect the two electrodes from the short circuit during experiments. A pair of polished, corrosion-resistant end plates for measuring current flow or voltage. This method recommends correcting the measured resistivity according to the following equation:

$$\rho_{15.5} = \frac{(24.5 + T)}{40} \rho_T$$

here, $\rho 15.5$ = resistivity at 15.5 deg. C, ρT= measured resistivity, T = temperature.
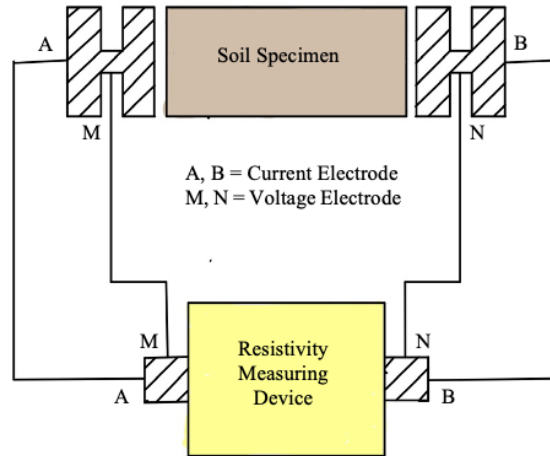
Figure 2-15 System for two-electrode measurement

2.7.1.2 Four Electrode Method

In the end, two current electrodes are connected, and a potential drop is measured between two points (ASTM G57-20). In the four-electrode method, potential can be determined within the sample; thus, current electrodes' charge transfer processes can be avoided. In this way, polarization can be avoided. The method can also measure the voltage of the sample within; thus, actual electric fields can be encountered during tests. Electrical resistivity measurement is not affected by a chemical reaction in this case because the electrodes are different. Figure 2-16 presents the setup for four-electrode experimental measurements.
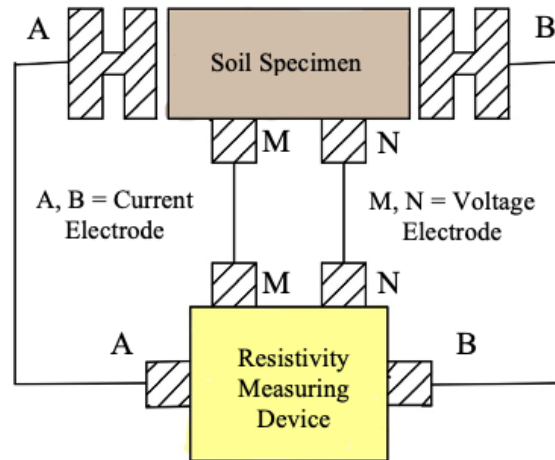
Figure 2-16 System for four-electrode measurement

2.7.2 Field Resistivity Measurement

Throughout history, electrical resistivity measurements have been used in geological investigations near the surface since the early 20th century. Recent improvements in test methods and data processing have made this method very popular. In a number of fields, geo-electrical measurements are useful (Aizebeokhai, 2010; Hossain et al., 2019).

In the isotropic homogeneous semi-circular space of the Earth, current (I) is introduced through the current electrode C1 (Figure 2-17). There is an inverse relationship between the electric potential and the distance from the source of current. According to the current distribution, the outward radial direction is perpendicular to the equipotential lines. One electrode's potential is:

$$\Theta = \frac{\rho I}{2 p r}$$
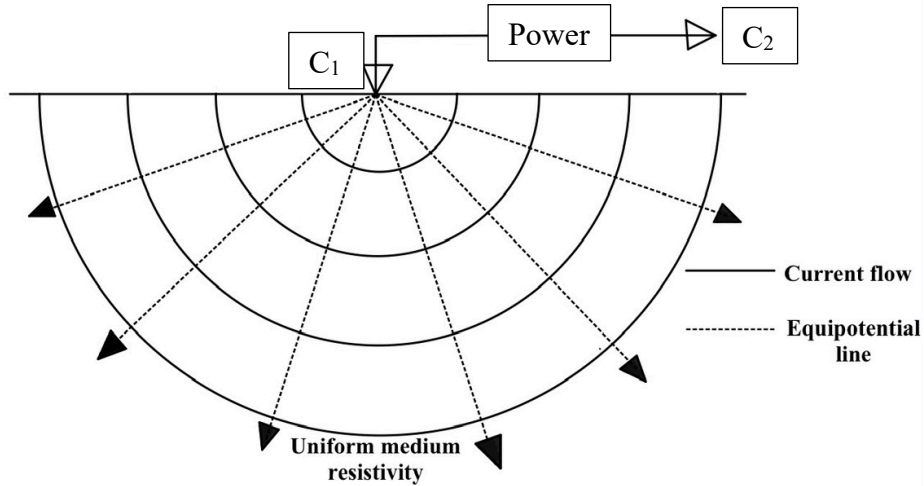
Figure 2-17 Representation of current flow and equipotential lines

In a conventional resistivity survey, two current electrodes are generally used as the positive and negative ends of the survey. There is a symmetry to the potential distribution around a vertical plane that is centered on the electrodes. It can be expressed as follows:

$$\theta = \frac{\rho I}{2p}\left(\frac{1}{r_1} - \frac{1}{r_2}\right)$$

rc1 and rc2 are the distances of the measured point from the first and second current electrodes.

As per Figure 2-18, for a four-electrode system, the equation can be extended as

$$\theta = \frac{\rho I}{2p}\left(\frac{1}{r_1} - \frac{1}{r_2} - \frac{1}{r_3} + \frac{1}{r_4}\right)$$
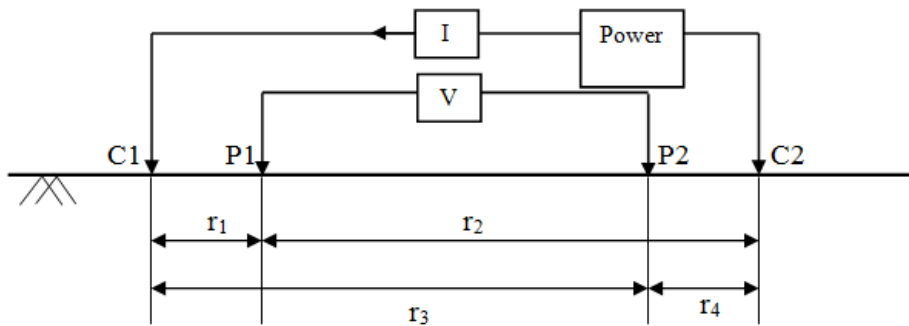
Figure 2-18 Resistivity measurement in the field using four electrodes

45

Despite the fact that these equations can be applied to isotropic medium, which is homogeneous, actual surveys investigation in the site deals with inhomogeneous and anisotropic subsurface. In order to calculate apparent resistivity, measured current and potential are combined as follows:

$$p_a = \frac{k\Delta\Theta}{I}$$

where geometric factor was designated as k. the geometric factor can be expressed as:

$$K = \frac{2p}{(\frac{1}{r_{c1p1}} - \frac{1}{r_{c2p1}} - \frac{1}{r_{c1p2}} + \frac{1}{r_{c2p2}})}$$

Under the four electrodes, it can be viewed as a weighted average of resistivity. For true resistivity from apparent measurements, inversion modeling is needed (Aizebeokhai, 2010; Loke, 2015). In one-, two- and three-dimensional resistivity surveys, Wenner, Dipole-Dipole, Schlumberger, pole pole, and pole-dipole arrays are used. They are briefly described below.

2.7.2.1 Array Types

There are several types of arrays available to measure the resistivity in the laboratory as well as for the field measurement. Few array types are discussed in this section. Depending on the requirements and necessity of the survey, the array types were chosen for the survey.

2.7.2.1.1 <u>Wenner Array</u>

Research conducted at the University of Birmingham has led to the widespread use of Wenner arrays. Resistivity variation vertically is more sensitive than horizontally. Wenner arrays are typically good at evaluating horizontal structures but struggle with narrow vertical structures. Additionally, Wenner arrays are best suited to surveys where substantial noise is likely to occur. Figure 2-19 shows the configuration of the electrode of the Wenner alpha array.
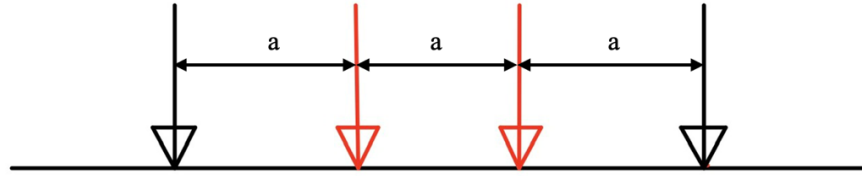
Figure 2-19 Wenner array

2.7.2.1.2 Dipole-dipole Array

Low electromagnetic coupling makes Dipole-Dipole arrays an effective method for conducting the survey in the field (Loke, 2004). In this array, potential electrodes spacing and current electrodes spacing is the same. The horizontal resistance variation is more sensitive than the vertical variation. Dipole-dipole arrays are popular for imaging vertical structures (Figure 2-20).

$$K = \pi n(n + 1)(n + 2)a$$
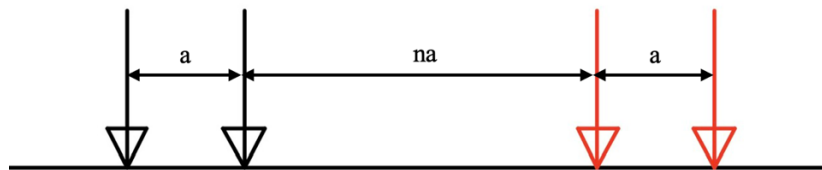
Figure 2-20 Dipole-dipole array

2.7.2.1.3 Schlumberger

The Figure 2-21 below shows the schematic of the Schlumberger array. Vertical resistivity is a more important factor in this array than horizontal variations in resistivity. As the electrode spacing increases, it is possible to decrease the horizontal coverage of the electrodes (Aizebeokhai, 2010).

$$K = \pi n(n + 1)a$$
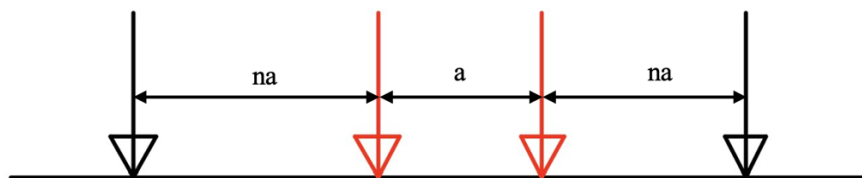
Figure 2-21 Schlumberger array

47

2.7.2.1.4 <u>Pole Pole</u>

This array is conventionally comprised of one electrode which contains current and one electrode for potential measurement (C1 and P1). Compared to other types of arrays, the pole pole method is never usually utilized in electrical resistivity sounding. Vertically and horizontally, it covers large areas. Because of the large spacing between electrodes, the obtained image is not satisfactory in resolution. Figure 2-22 shows the electrode configuration of the pole pole array.

$$K = 2\pi a$$
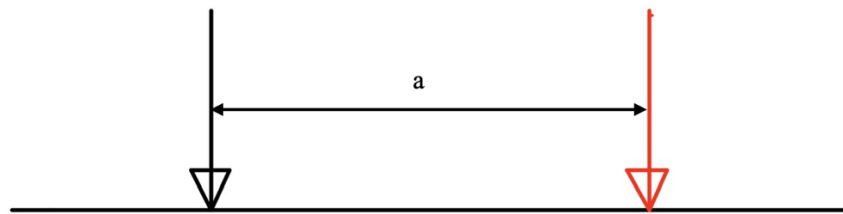
Figure 2-22 Pole-pole array

2.7.2.1.5 <u>Pole dipole</u>

Telluric currents are insensitive to the Pole-Dipole method because it produces high signal strength. Asymmetric coverage is provided by this method. As Pole-dipole is asymmetrically configured, it can be divided into reverse and forward pole-dipole arrays (Figure 2-23). Pole-dipole array diagram electrode configuration is shown below.

$$K = 2\pi n(n + 1)a$$
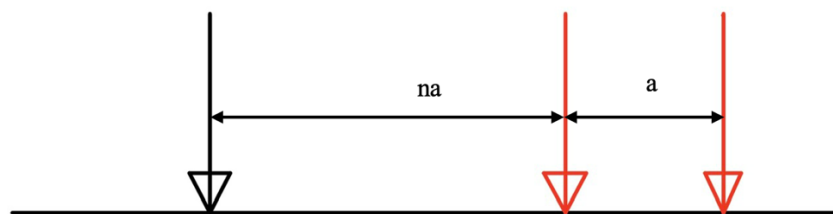
Figure 2-23 Pole-dipole array

Different survey characteristics based on the array types are summarized in Table 2-3.

Table 2-3 Different arrays characteristics (Rungroj Arjwech & Everett, 2015)

Array Types	Wenner	Wenner Schlumberger	Dipole-Dipole	Pole-Pole	Pole-Dipole
Horizontal structures sensitivity	4	2	1	2	2
Vertical structures sensitivity	1	2	4	2	1
Depth of investigation sensitivity	1	2	3	4	3
Horizontal Data Coverage sensitivity	1	2	3	4	3
Strength sensitivity	4	3	1	1	2

Weak sensitivity = 1 and high sensitivity = 4

2.7.2.2 Survey Dimension

2.7.2.2.1 <u>One-dimensional survey</u>

The laboratory commonly uses four electrode arrays containing cells A, B, M, N for the calibration of electrical resistivity and vertical electrical sounding (Rhoades & van Schilfgaarde, 1976). The latter involves increasing the distance between electrodes during electrical measurements. Loke (2004) shows the variation in soil resistivity with depth without taking into account the horizontal variation of soil depth (at each step). Landviser (2001) assumes that the subsurface is composed of several horizontal layers. According to Bottraud et al. (1986), soil sciences are interested in recording information about vertical discontinuities in soil horizons.

2.7.2.2.2 <u>Two-Dimensional Survey</u>

An array of multi-electrodes in two dimensions provides a two-dimensional vertical profile of the sounding medium. Using a regular fixed distance between electrodes, the current and potential electrodes are gradually moved along a surface line, as shown in Figure 2-24. Every step is measured. This first interelectrode spacing gives a resistivity profile. Since the distribution of the current also depends on the resistivity contrasts of the medium, they are called "pseudo-depths" because they are derived from the spacing. A pseudo-section plot displays both horizontal and vertical variations in resistivity simultaneously. This is then inverted for a continuous subsurface

image (Samouëlian et al., 2005). The most commonly used array configurations are Wenner and Wenner-Schlumberger, dipole-dipole, pole–pole, and pole–dipole arrays. Based on the type of heterogeneity to be mapped and the background noise level, the array configuration will be chosen. Using multiple configurations may improve the chances of capturing different subsoil features and lead to a better interpretation in specific cases, as Hesse et al. (1986) pointed out.
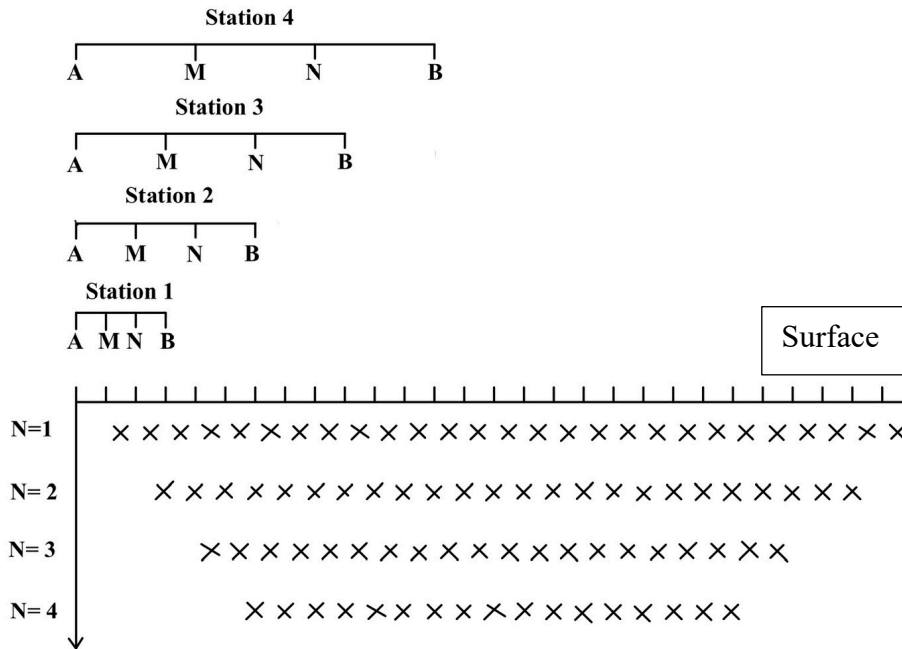
Figure 2-24 Two-dimensional electrical resistivity survey (Samoulien et al. 2005)

2.7.2.2.3 Three-Dimensional Survey

Resistivity surveys in three dimensions could provide accurate knowledge about the ground surface. There are two types of 3D resistivity profiles that can be established based on subsurface resistivity data: one is, quasi 3D and the other one is actual 3D resistivity surveys. By combining pseudo-sections of 2D parallel lines, it is possible to determine a 3D contour of the examined area in a quasi-3D resistivity survey. However, in order to obtain an accurate 3D resistivity profile, the measurements should be made in X and Y directions (Arjwech, 2011).

2.7.2.2.4 <u>Electrical Resistivity Inversion Modeling</u>

For determining the distribution of potential in the soil, the basic equation could be expressed as:

$$-\nabla[\sigma(x,y,z)\nabla U(x,y,z)] = \frac{1}{\Delta V}\partial(x-x_s)\partial(y-y_s)\partial(z-z_s)$$

It is possible to solve the equation using a forward modeling approach. In 2D and 3D resistivity measurements, finite difference and finite element methods are employed, while analytical methods can be applied for 1D resistivity surveys.

A model is developed to provide a similar response to actual resistance measurements during the inversion process. Based on the observed data, a set of parameters was estimated (Loke, 2004). Using forward modeling, theoretical values of apparent resistivity can be calculated for subsurface resistivity distributions. Calculating theoretical apparent resistivity is commonly done using finite element and finite difference modeling. Under certain conditions, inversion results in a subsurface model whose responses match those measured. Arjwech (2011) & Loke (2015) present mathematical procedures for inversion modeling. The Figure 2-25 shows an inversion flow diagram.
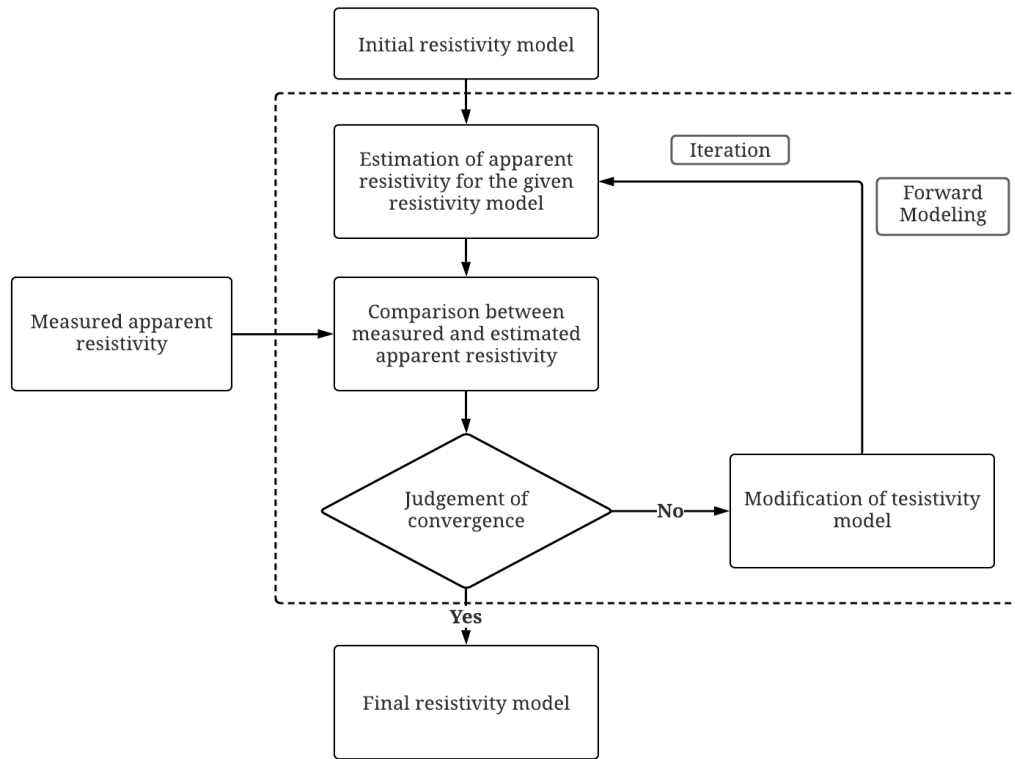
Figure 2-25 Inversion modeling algorithm (Arjwech, 2011)

2.8 Limitation of Previous Studies

The complex nature of soil-water systems and the difficulty in characterizing the wide range of particle size, shape, and composition has precluded the development of electrical resistivity equations that are generally applicable. Various soil properties must be taken into account to make a fully functional practical equation to evaluate the resistivity of soil. Laboratory results must be incorporated with the results of the field test. The purpose of this research is to bridge the gap between laboratory-based testing results and field results. Previously soil electrical resistivity model tried to include pore water conductivity and different clay properties, which is difficult and time-consuming to measure in the laboratory. However, soils that are commercially available were used for the identification of the geotechnical engineering properties that are

affecting the electrical resistivity responses of the soil. To generate a comprehensive equation to explain the electrical resistivity changes of the soil with changing geotechnical properties of soils, wide ranges of soils need to be examined with varying geotechnical conditions. Through the collaboration of a wide range of soil properties, this study attempted to integrate geotechnical properties with electrical resistivity, which can be measured in the laboratory.

CHAPTER 3 MATERIALS AND METHODS

3.1 Introduction

According to their geological formation, four separate locations were selected for sampling soil with different geotechnical properties. Soil samples were collected during the investigation, and a subsurface geotechnical investigation was carried out. As part of the subsurface investigation, an electrical resistivity imaging survey was performed at the exact location of the drilling. The changes in electrical resistivity for different soil engineering properties were investigated through experiments. Both clayey and sandy soil samples were collected during the soil boring. The experiments were conducted with both disturbed and undisturbed clayey samples. Both conventional geotechnical tests and advanced methods were used to determine the geotechnical properties of the soil samples. Various geotechnical conditions were used to conduct electrical resistivity tests after soil characterization. A summary of the methodology of studies is provided below:
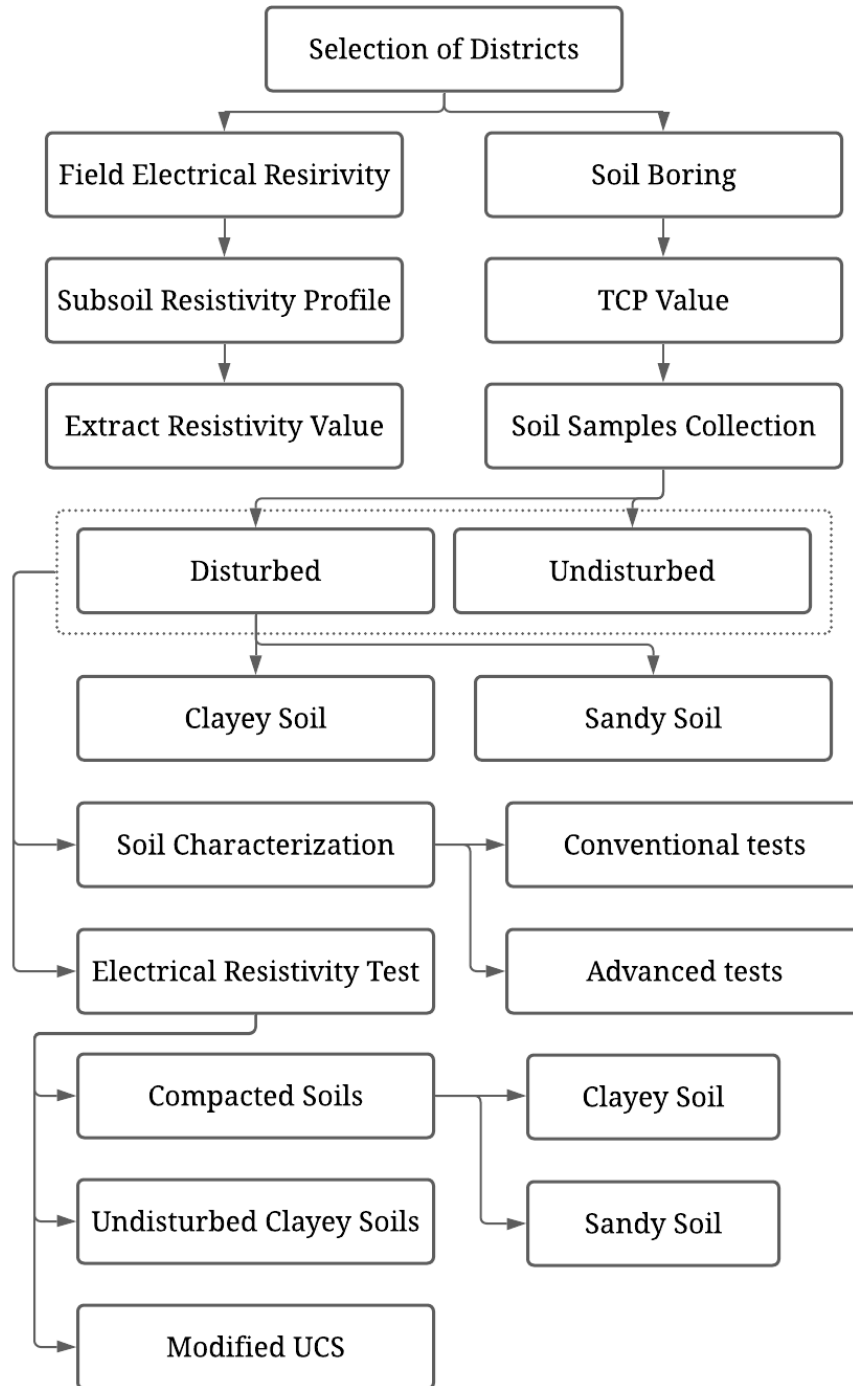
Figure 3-1 Laboratory tests methodologies

3.2 Selection of Different Locations

Across Texas, the geology varies drastically from northwest part to southeast part. The formation of the northwest part of Texas occurred in the Cenozoic era primarily, which began to form 65 million years ago. At the same time, the central part of Texas was formed in the mostly cretaceous period of the Mesozoic era. The formation of North Texas mainly is from the Mesozoic, and Paleozoic ages occurred ~66 million years to ~320 million years ago. It consists of Virgilian series, Desmoinesian series, and Missourian series of Pennsylvanian period (formed ~320 million years ago), Leonardian series and Guadalupian series of the Permian period (formed ~286 million years ago) and Trinity group, Fredericksburg and L. Washita groups, Austin, Eagle ford, woodbine, and U. Washita groups and Navarro and Taylor groups from the Cretaceous period which formed 144 million years ago. The Southeast part of Texas mainly formed in the Tertiary and Quaternary period of the Cenozoic era, which occurred 58 million years to 2 million years ago; this is the newest formation of all.

Four different locations were selected, formed in a different era, based on their geographical areas with various soil properties for this experimental program. From the Southeast part of Texas, the Beaumont district was selected from Alluvium, Beaumont, and Willis formations. Fort Worth was selected from north Texas, situated on Austin, Eagle ford, Woodbine, U. Washita, Fredericksburg, and Trinity groups. Corpus Christi, located in south Texas upon Alluvium and Lissie formations, was also selected. Finally, El-Paso from the Northwest part of Texas was determined, situated on Quaternary undivided formation from the Pleistocene period. The locations are summarized below and shown in Figure 3-2.
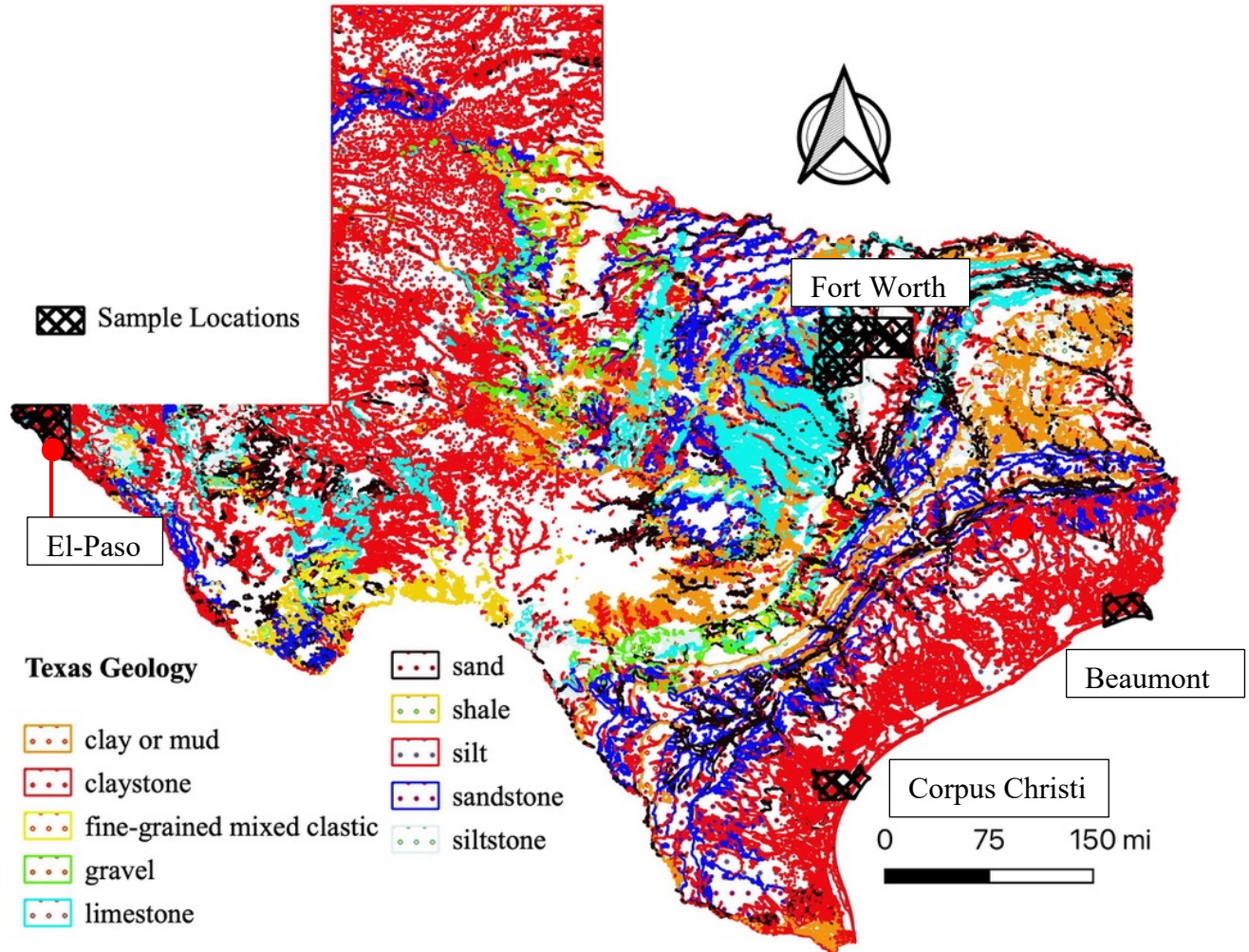
Figure 3-2 Geology of Texas and sample collection locations

1. Beaumont

2. Fort-Worth

3. Corpus Christi

4. El-Paso

3.2.1 Beaumont District

Soil samples were collected from the intersection of SH73 and US96 of the city of Port Arthur in Jefferson County (Figure 3-3). Specimens from six boreholes were collected during the investigation procedure. The six boreholes were sampled for disturbed and undisturbed soil.

Figure 3-3 Location of sample collection in Beaumont

Locations and depths of sample collection for both disturbed and undisturbed samples are provided in Table 3-1 and Table 3-2. Total of 17 nos of disturbed soil samples and 8eightundisturbed soil samples were collected from the Beaumont district.

Table 3-1 Depth of collected disturbed samples in Beaumont

Locations	Samples Depth (ft)	Total Samples
B-P1	2, 5, 10	3
B-P4	2, 10	2
B-P6	5,10	2
B-P17	5,10	2
BR-6A	5, 20, 30,40, 50, 60, 70, 80	8

All the undisturbed soil samples were collected with a Shelby tube. After collecting the soil samples, all the samples were taken to the laboratory; those measurements and weights were taken to calculate the degree of saturation and other soil parameters. After that, the soil samples were wrapped in plastic and taken to a temperature-controlled room to preserve the soil samples.

Table 3-2 Depth of collected undisturbed samples in Beaumont

Locations	Samples Depth (ft)	Total Samples
P4	5, 10	2
P6	5, 10	2
P17	5, 10	2
BR-10A	30, 40, 50, 60	4

3.2.2 Fort-Worth District

Soil samples were collected from eight different locations of the Fort-Worth district. All the locations are shown in Figure 3-4. Two of the locations were located on the south and north side of the I-30 and fielder road intersection. Several boreholes and depth of collected samples are also shown in Table 3-3. Other locations of sample collections are in I-20 and park spring intersection of Arlington city, I-820 and Sun valley intersection, and I-820 and Rosedale intersection of Fort-Worth city.
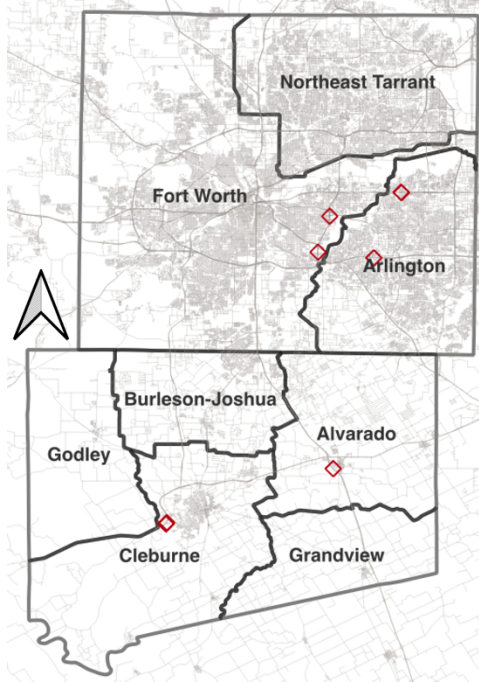
Figure 3-4 Locations of sample collection in Fort-Worth

Two locations were selected on the south and north side of U.S. 67 and W Henderson st of

Cleburne city. Lastly, one location situated in Alvarado city was selected to collect the soil sample

from the Fort-Worth district. In total, 40 soil samples from different locations and different depths

were collected for this research.

Table 3-3 Depth of collected disturbed samples in Fort-Worth

Locations	Samples Depth (ft)	Total Samples
North Fielder	Borehole 1: 5, 10 Borehole 2: 5, 10, 15	5
South Fielder	Borehole 1: 5, 10, 15	3
Park Spring	Borehole 1: 5, 20 Borehole 2: 5, 10, 15	5
Rosedale	Borehole 1: 5, 10, 15, 20, 25	5
Sun Valley	Borehole 1: 5, 10, 13, 15, 20, 25	6

3.2.3 Corpus Christi District

A total of 15 soil specimens from four different locations was collected from Corpus Christi District. The location of sample collection is shown in Figure 3-5 and the number of samples and depth of collected samples are shown in Table 3-4. The site was located near the intersection of Interstate 37 and US77 highway. The site was located near the Nueces River in the city of Sinton-Odem.
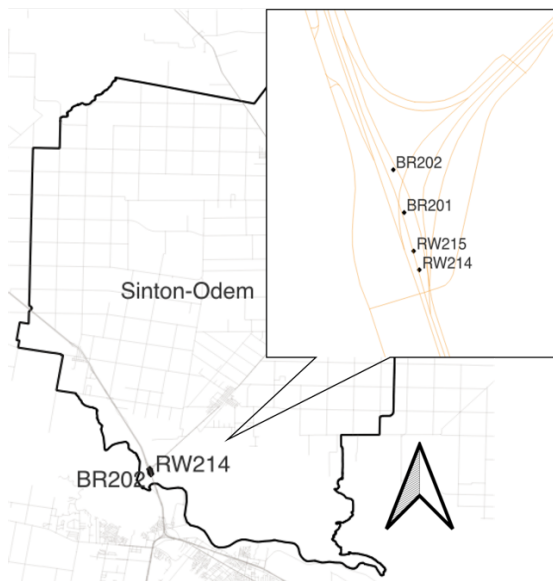
Figure 3-5 Locations of sample collection in Corpus-Christi

Table 3-4 Depth of collected disturbed samples in Corpus Christi

Locations	Samples Depth (ft)	Total Samples
BR201	2, 5, 7, 10, 50, 60	6
BR202	10, 15, 60	3
RW214	5, 10, 15	3
RW215	5, 10, 15	3

3.2.4 El-Paso District

Soil samples were also collected from different locations of El-Paso, shown in Figure 3-6. Total two different locations were selected to collect the soil sample from the El-Paso district.
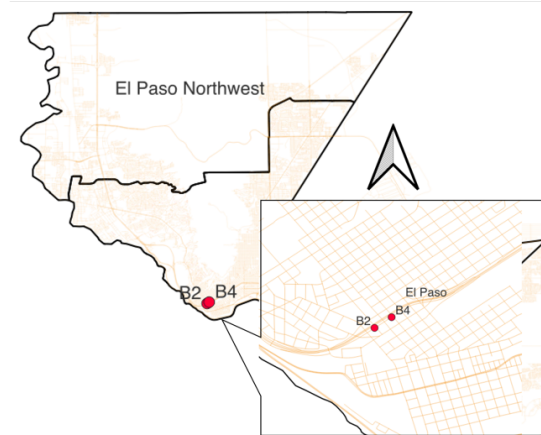
Figure 3-6 Locations of sample collection in El-Paso

A total of 14 soil samples was collected from a different depth of two boreholes. B-2 location was located at Wyoming Ave. and north el-Paso road intersection, whereas B-4 was located near Wyoming Ave. and N. Oregon road intersection. Sample number and depth are shown in Table 3-5.

Table 3-5 Depth of collected disturbed samples in El-Paso

Locations	Samples Depth (ft)	Total Samples
B-2	5, 10, 15, 20, 30, 40, 50	7
B-4	5, 10, 15, 20, 30, 50	6

3.3 Soil Sampling in the Field

The drilling locations were determined following the determination of the districts to be sampled. A total of thirty boreholes were drilled for the collection of subsurface samples, as shown in Figure 3-7. A truck-mounted drilling rig was used with hollow stem augers for drilling. The augers have a length of 5 feet, so as the drilling progressed, each additional section was attached.

A certain number of soil samples, both disturbed and undisturbed, were collected at various intervals.
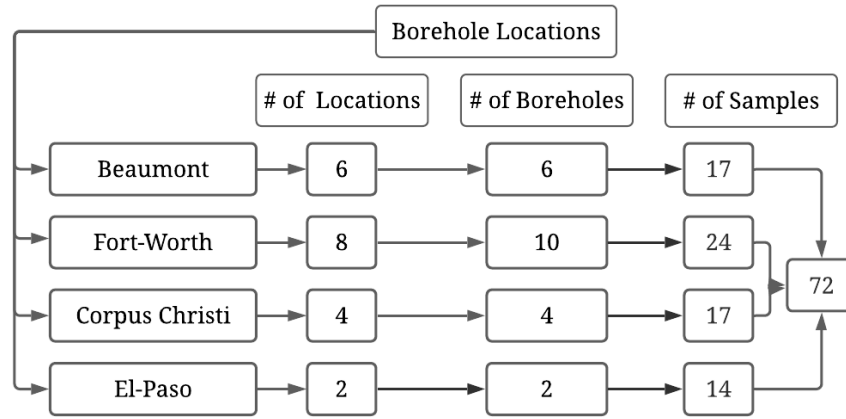
Figure 3-7 Location and number of sample collection

A number of undisturbed samples have been obtained from boreholes conducted in the Beaumont district of the area. A total of ten samples have been collected from four boreholes. In order to collect the samples, Shelby tubes with a diameter of three inches were used. It was necessary to measure the depth of the hole in order to confirm the depth of the sampling hole. In an effort to recover the Shelby tube from the bottom, the tube was carefully lifted to the with the assistance of an extruder; the sample was extruded from As soon as the sample was extruded, it was packed in a moisture bag and placed in a storage box before being transported for testing to It was important that the soil samples be preserved and transported according to ASTM Standard D4220 (2014) in order to maintain their in-situ characteristics. Each sample was labeled according to the location and depth at which it was collected. For storing the samples at the University of Texas at Arlington, a humidity-controlled room was used until the samples were taken to the lab for testing. It was decided to name each sample according to the district, borehole, and sampling order in which it was taken. As mentioned earlier, a sample was designated B-P1-5 when it was

taken from the Beaumont district, a borehole named P1 was used, and the depth of the sample was 5 feet.

Each borehole was sampled at a different depth interval to obtain disturbed samples. To measure soil resistance, the Texas Cone Penetrometer (TCP) was used to determine soil's compactness. For each borehole, TCPs were performed at every 10 feet depth. In accordance with Tex-132-E, the TCP test has been conducted. Test equipment includes a 170 lb hammer, a drill stem with a 24 x 0.5 in drop, an anvil threaded to fit the drill stem and slotted to accept the hammer, and a TCP cone was measuring 3 inches in diameter and 2.5 inches in length. During the test, the penetrometer cone attached to the stem was initially driven with a hammer by dropping it on the ground. There were 12 blows or 6 inches of driving before the cone was seated in the soil or 6 inches if it was 6 inches. Following this, a reference was taken as the point of reference in the test. It has been noted that N values (number of blows) were recorded for the first and second 6 inches for a total of 12 inches for relatively soft materials, while penetration depths were recorded for the first and second 50 blows for a total of 100 blows in relatively hard materials. An example of a drill setup and sample collection can be seen in the Figure 3-8.

(a) Soil boring   (b) Sample collection

Figure 3-8 Soil boring and sample collection

3.4 Field Electrical Resistivity

A typical electrical resistivity imaging device (ERI) usually uses four electrodes: two current electrodes and two voltage electrodes. It is the current electrodes (A, B) that create an electric field within the subsurface in a direct current form from an external direct current source, whereas the voltage electrodes (P, Q) determine the voltage potential between two subsurface points. The apparent electrical resistivity (E.R.) can be obtained using the following equation-

$$\rho_a = \frac{2\pi V_{PQ}}{I}[\frac{1}{r_{AP}} - \frac{1}{r_{AQ}} - \frac{1}{r_{BP}} + \frac{1}{r_{BQ}}]^{-1}$$

Here, r is the lateral distance between electrodes (m), I is the electric current (amperes), and V is the voltage potential (volts), and A, B, P, Q represent the electrodes used to measure current or voltage. Since ERT assumes the subsurface as a whole is homogenous, the term "apparent" is used when describing ERT measurements (Everett, 2013). In order to collect data more quickly and cover a larger area, a greater number of electrodes can be used simultaneously.

Taking advantage of both vertical sounding and lateral profiling, dipole-dipole arrays offer the best of both worlds.

Dipole-dipole arrays also reduce data acquisition time because multiple voltage measurements can be made in multi-electrode systems. Compared to other arrays, the dipole-dipole array minimizes coupling effects as well (Binley & Kemna, 2005) . It was therefore selected for this study that a dipole-dipole array is used.

Dipole-dipole arrays maintain constant spacings between current electrodes (A, B) and voltage electrodes (P, Q); however, the spacing between the current electrode pair and the voltage electrode pair differs (Figure 3-9). It should be noted that the depth to the measured apparent resistivity point increases with increasing n.
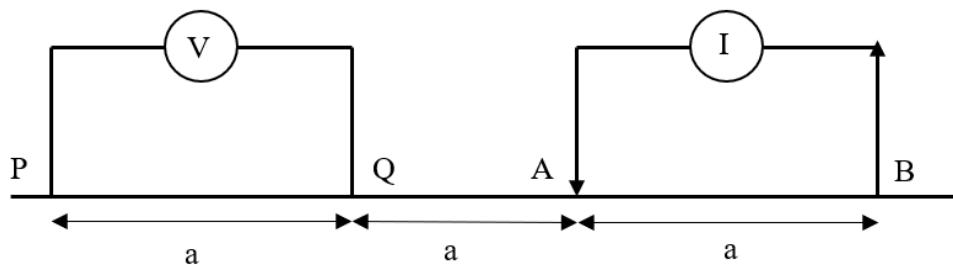
Figure 3-9 Schematic demonstration of dipole-dipole array

Depending on the site conditions, a total of 28 electrodes or 56 electrodes were used. The electrodes were spaced uniformly according to the desired depth of the borehole. While conducting the resistivity survey, the borehole was kept in the middle of the survey line in order to obtain a high-resolution image of the borehole location. Prior to collecting resistivity data at each site, a contact resistance test was conducted with the resistivity meter to ensure that all electrodes were installed and connected properly. Depending on the number of electrodes and distance between electrodes, each ERT survey took about 10 minutes to 27 minutes to complete. Using Google Earth, the relative elevation of each electrode was measured and accounted for in the resistivity

measurement. The Table 3-6 is provided below that summarizes the number of electrodes, the spacing between electrodes, and the length of the electrical survey lines for every location.

Table 3-6 Summary of Resistivity Survey Lines

Locations	Borehole Name	Number of Electrodes	Spacing Between Electrodes (ft)	Length of Survey Lines (ft)
Beaumont	P1, P4, P6, P17	28	3	81
	BR-6A, BR-10A	56	10	550
Corpus Christi	BR201, BR202	56	10	550
	RW214, RW215	28	6	162
Fort-Worth	North Fielder, South Fielder, Park Spring, Sun Valley	28	3	81
	Rosedale	28	4	108

Data collection equipment for resistivity measurements was manufactured by Advanced Geoscience Institute (AGI) and used in the field for data collection at different sites. With the help of the programmable eight-channel option, the testing can be completed in a much shorter period of time. All resistivity data collected was processed with AGI EarthImager 2D software (AGI, 2009). The raw data set was filtered to remove erroneous data (e.g., apparent negative resistivities or extreme outliers) before inversion. As a result of using an iterative resistivity inversion algorithm, the apparent resistivity values were then converted into inverted resistivity values. The relative data misfit, which is limited to 20%, was tested after the initial inversion of all the electrical resistivity profiles. As far as the inversion modeling is concerned, a smooth inversion model as well as terrain correction, together with damped mash transformation, have been used. In the analysis of the data, a starting model with average chargeability and a horizontal-vertical ratio of 0.2 was used. Using the RMS error reduction technique, the RMS error reduction was kept under 5%, and the L2 value was kept below 1. With the help of the finite element method with the

Cholesky decomposition as the forward equation solver, two mesh divisions, an incremental thickness factor of 1.1, and an incremental depth factor of 0.7, the forward modeling of the boreholes was carried out. The value of the resistivity of the boreholes along the drilled path was determined. Electrical resistivity survey procedures implemented in the field are shown in Figure 3-10.

| Step-1 | Step-2 | Step-3 | Step-4 |
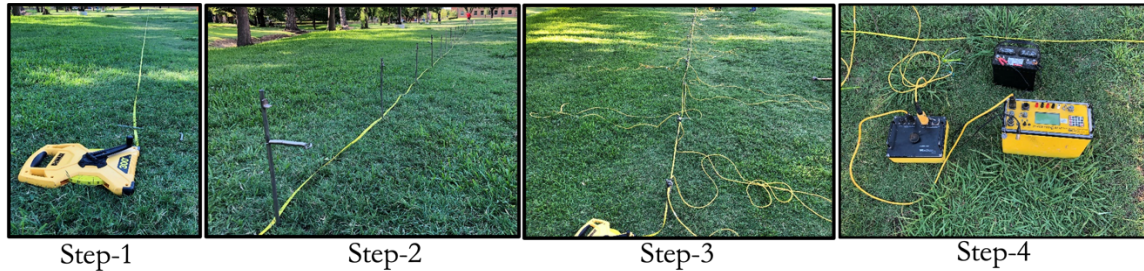
Figure 3-10 Steps of electrical resistivity measurements

3.5 Determination of Geotechnical Properties

Various geotechnical properties of test specimens were determined in the laboratory. An experimental program was developed to determine the soil properties. The experiments included in this laboratory study include a) specific gravity, b) grain size distribution, c) Atterberg limits, d) pore water conductivity, e) soluble sulfate content, and f) water content and unit weight. Using Farrar & Coleman (1967) correlations, the specific surface areas (SSA) and cation exchange capacity (CEC) of the samples were determined. The Table 3-7 below summarizes the tests conducted on the soil specimens.

Table 3-7 Geotechnical tests summary

Name of Test	Test Method
Grain size distribution	ASTM D422-63
Atterberg limits	ASTM D431
Specific gravity	ASTM D854-00
Moisture content	ASTM D2216-90
Soluble Sulfate content	Tex-145E
Unit weight	ASTM D2937-00

3.5.1 Grain Size Distribution

ASTM D422-63 is the standard test method for determining the particle size of the soil sample. Grain size distributions of the specimens were determined by using the mentioned method. During the 24-hour drying process, the specimens were dried in an oven at a temperature of 100-110 degrees Celsius. Approximately 600 gm of the oven-dried sample was considered for sieve analysis after aggregation was broken with a mortar and rubber-covered pestle. Flowing water was used to wash the soil sample using the #200 sieve until the leached water was clean. Drying of the retained and leached samples took place in an oven at 100-110 degrees Celsius over a period of 24 hours. In the following steps, the retained soils were sieved using US standard sieves #4, #10, #30, #40, #50, #60, #100, and #200. Upon the conclusion of the experiment, each sieve was weighed to determine the mass of the retained sample. Soil samples were used for the hydrometer test, which was passed through the #200 sieve during the wash sieving. For the hydrometer test, sodium hexametaphosphate was used as a dispersive agent (Figure 3-11).

Figure 3-11 Grain size distribution (ASTM 422-63)

3.5.2 Atterberg Limits

In accordance with ASTM D4318, tests for determining the Atterberg limit were conducted for the collected soil samples. Test samples were first processed through a sieve of No. 40. In the following step, water was added to the soil samples, and those were chopped, stimulated, and kneaded repeatedly. In the Cassagrande liquid limit device, a portion of the soil was put into the cup, and a groove was cut down the center of the cup by a grooving tool (Figure 3-12). In this experiment, two drops per second were applied until the groove was closed around 13 mm after lifting the cup of the device. The number of blows was plotted against the moisture content after three repetitions of the test. As a liquid limit for the specimen, moisture content associated with 25 blows was used.
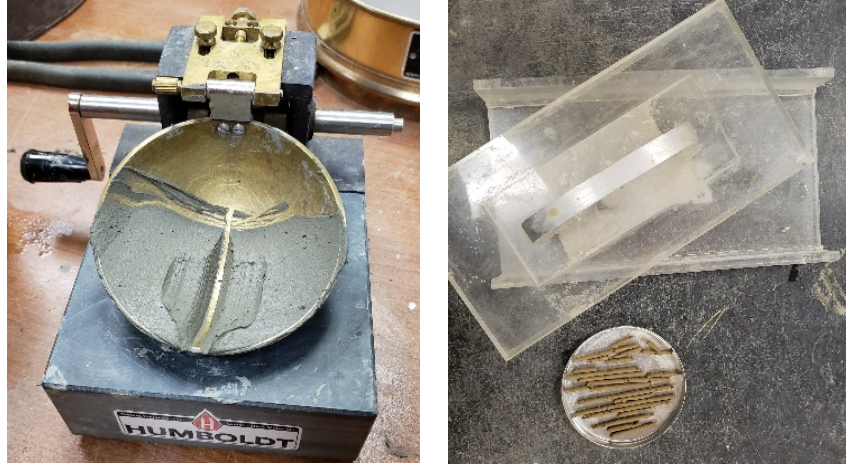
Figure 3-12 Atterberg limit tests (ASTM D-4318)

During the determination of the plastic limit in the soil, water was added into the soil, and the soil was repeatedly kneaded. After the soil masses were rolled in a glass plate, they were stranded into threads about 3 mm long. When the thread was about to break at 3 mm diameter, during that time, the soil thread was taken into the moisture can to measure the moisture content of soil during that condition. After drying in an oven at around 100-110 degrees C overnight, the samples were weighed. Water content was considered as a measurement of the plastic limit of specimens.

From the Atterberg limits value, the plasticity index and activity of any soil samples can be calculated. The activity was calculated using Skempton (1984) method, which considers particles smaller than 2μm to be clay fractions. SSA and cation exchange capacity (CEC) was determined based on the liquid limits of soil samples (Farrar and Coleman, 1967):

$$CEC = 0.55LL - 12.2 \ (cmol +/kg)$$

$$LL = 19 + 0.56 \ SSA \ (SSA = \frac{m^2}{gm})$$

3.5.3 Specific Gravity

According to ASTM D854-00 standard test method, the specific gravity of the soil samples was measured using a water pycnometer. In the test, a soil mass of 50 gm passing through sieve number 10 was considered. A pycnometer with an empty specimen and a pycnometer with a specimen was weighed. A 24-hour soak in distilled water under partial vacuum was conducted on the soil sample (Figure 3-13). The pycnometer was filled with water up to the designated mark; then, the weight was taken. In the next step, the pycnometer was filled with distilled water up to the mark, and the total weight was measured.

Figure 3-13 Specific gravity test (ASTM D854-14

3.6 Characterization of Clay Minerals

3.6.1 Scanning Electron Microscope (SEM)

Using scanning electron microscopes (SEMs), the powdered samples were used to study fabric morphology. A high-energy electron beam was used to scan the sample to produce the images. Secondary electrons were reflected by the induced electrons when they interacted with the atom's inherent electrons. Secondary electrons could provide data regarding the topography of sample surfaces. The electrons induced had the energy of acceleration which is less than 25 keV. Observations have shown that electrons induced by the clay particles accumulate on the surface

after interacting with them. When the voltage of the electrons is increased, the tendency of charge accumulation increases as well. Silver coatings can reduce charge accumulation, but they change the composition of elements. As a result, the silver coating was not used, and low voltage electrons were used instead. Figure 3-14 illustrates the SEM used for fabric imaging.
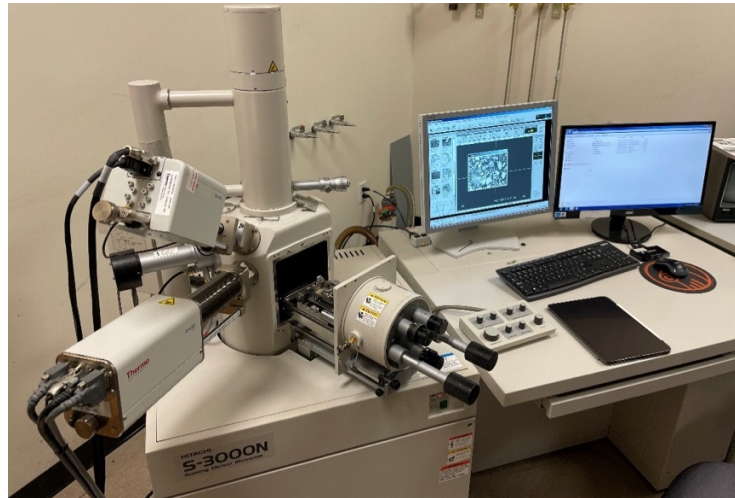
Figure 3-14 Scanning electron microscope

3.6.2 Energy Dispersive X-Ray Spectroscopy (EDS)

For the determination of compositional elements, EDS is common. An induced X-ray beam was used during the tests in order to stimulate and excite the atomic electrons of the specimens. It has been determined that based on the characteristics of X-rays that were emitted from the soil surface, the specimen elements can be determined. These tests were conducted at similar magnification and working distance configuration as the SEM test. During EDS, however, the electrons' energy was increased to increase the efficiency of the measurement and shorten the time it takes to collect the information.

3.6.3 Pore Water Conductivity Measurement

The ion content present in the pore water of the collected soil specimens was measured for all soil samples. Pore water conductivity was measured for all the collected soil samples. The soil samples were mixed properly with deionized water (1:1), and the mixture was stored in an airtight can for 24 hours. After the slurry had been placed in the centrifuge, the soil particles were separated from the pore water. The separated pore water was collected from the can by using filter paper in order to collect the pore water. Once the pore water was collected, a bench-top conductivity/P.H. meter was used to measure the conductivity of collected water.

3.6.4 Determination of Soluble Sulfate Content

The soluble sulfate of the soil samples was determined by using a turbidity-based technique. Tex-145E was followed to determine the sulfate content of the soil samples. Using this technique, 400 g field samples are dried at 60°C. Once dry, the soil is pulverized to pass the U.S. No. 40 sieve. In order to obtain a final sulfate value, duplicates must be run on this method. Then,

200 mL of DI water is added to 10g of sample. Stoppered flasks are vigorously shaken for around one minute by hand. Samples are then allowed to sit for a minimum of 12 hours before analyzing them. The sample is placed in a sealed glass tube for 12 hours, agitated by shaking for 1 minute, and then filtered through Whatman 42® (fine porosity) filter paper or an equivalent filter paper. A pipette is used to carefully transfer a volume of the filtrate of 10 ml into the glass vile used for the colorimetric device with which it is being used (Figure 3-15). Once the glass vile is in the colorimetric device, it is zeroed so that the device is calibrated, ensuring that the calibration is done.

One sulfate tablet is then added and crushed with a plastic rod. Solutions with sulfates become milky or hazy. After that, the vile is tested in a colorimeter. The method requires a minimum of three readings and then averages them. In order to determine the ppm of your sample, multiply the average reading number by the dilution ratio.

a) transferring 10 gm of soil to bottle

b) Sample after adding 200 ml of Deionized (DI) Water

c) Centrifugation of Soil Solids from dissolved Solids

d) Filtration of Remaining Soil Particles

e) Clear Filtrate

f) Filtrate transferred to Vial

g) Resulting solution after adding Sulfate Tablet

h) Measuring Sulfate Content in mg/L

Figure 3-15 Determination of soluble sulfate of soil sample

3.7 Laboratory Investigation of Electrical Resistivity of Soils

Both disturbed and undisturbed specimens were tested for electrical resistivity. D.C. current was applied, and soil resistance was measured with Super Sting IP equipment. A high-strength plexiglass soil resistivity box was used (Miller resistivity box). Additionally, two round-shaped stainless-steel was used as an electrode for the resistance measurement of undisturbed soil samples, which was manufactured in the workshop. Moreover, two electrodes were used on two ends of remolded samples in a uniaxial compression machine to measure the changes in resistivity with the increasing compressive load.

3.7.1 Electrical Resistivity Tests on Compacted Clays

Different moisture contents and dry weights were tested for soil resistivity. Resistance tests were performed with deionized water. The electrical resistivity of soil is measured at different moisture content and dry weight in the resistivity box, which was determined prior to the test. ASTM G57-20 instrumentation using four electrodes of the Wenner array method was followed to conduct the experiment. Through two current electrodes, a current was applied to the soil, and the voltage drop between two points was measured. The Figure 3-16 presented below shows the circuit diagram and the test procedures for electrical resistivity measurements for compacted clays.
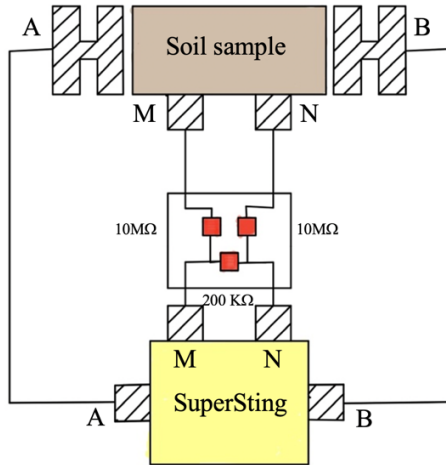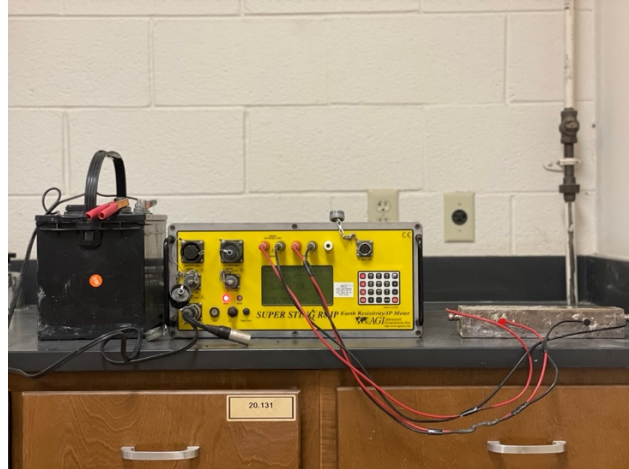
(a)   (b)

Figure 3-16 Electrical resistivity measurement procedures for compacted soils (a) circuit diagram (b) laboratory measurement procedures

The resistivity of soil samples in this configuration can be measured using the following equation:

$$\rho = \frac{RA}{l}$$

Where ρ is the resistivity of soil sample (Ohm-m), R is the resistance measure by Super Sting R8/IP resistivity meter (Ohm), A is the cross-sectional area of the specimen (cm^2), and l is the length between two voltage electrodes (cm). The length of the soil box used to compact soil samples is 12.8 cm, and the cross-sectional area is 12.8 cm^2. Therefore, the ratio of cross-sectional area to length (A/l) is 1 cm. The magnitude of the measured electrical resistance (R) in this setup is the same as its equivalent resistance (E.R.) in Ω.m. The sample preparation and measurement procedures were kept the same for all soil samples to maintain consistency among the soil samples.

In the beginning, the moisture and soil samples were weighed accurately to 0.01 g by using a weighing scale and mixed thoroughly. The soil moisture mix was then kept in a sealed container and kept at room temperature for 24 hours. For the soil box to be as uniform as possible, it was very important to place the specimen as evenly as possible. A total of 3 equal layers of soil were placed in the box to achieve the target densities. After the soil box was filled, the total weight of

the soil box was recorded; the E.R. of the specimen was then measured, and the temperature was measured three times in the specimen and averaged. Summary of different test conditions for resistivity of compacted soil samples shown in Figure 3-17.
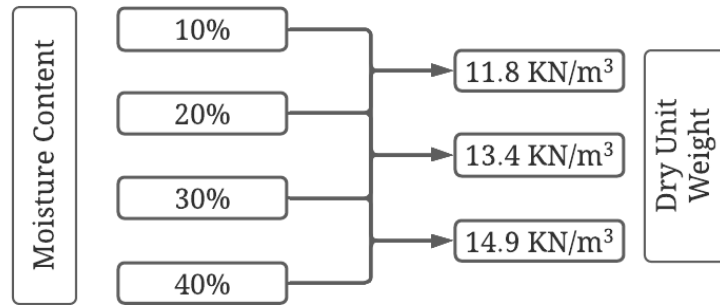
Figure 3-17 Different geotechnical conditions under consideration

3.7.2 Electrical Resistivity Tests on Undisturbed Specimens

Currently, there is no standard method available for determining resistivity for undisturbed specimens. Therefore, a simple method to measure the electrical resistivity of the undisturbed soil samples was developed in the laboratory (similar to Kibria, 2014). The resistivity of the undisturbed soil samples was taken throughout the drying process of the sample. Instrumentation methods of ASTM G187-18 were followed to measure the resistivity.

During the drying phase, the undisturbed soil samples were weighed at a regular interval, and the electrical resistivity measurement was taken with the help of a resistivity meter. Final water content was measured when the sample was dried completely. From the final water content, the moisture present at different drying processes was calculated. All the resistivity measurements that were taken was calibrated for 15.5 degree Celsius temperature as per ASTM G187-05. The laboratory measurement setup for electrical resistivity of undisturbed soil samples is shown in Figure 3-18.
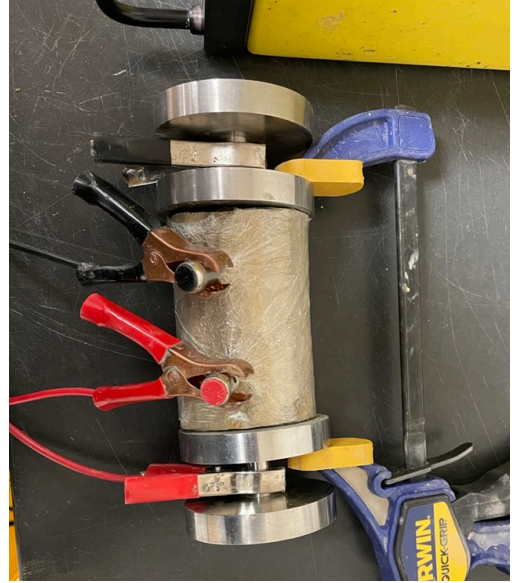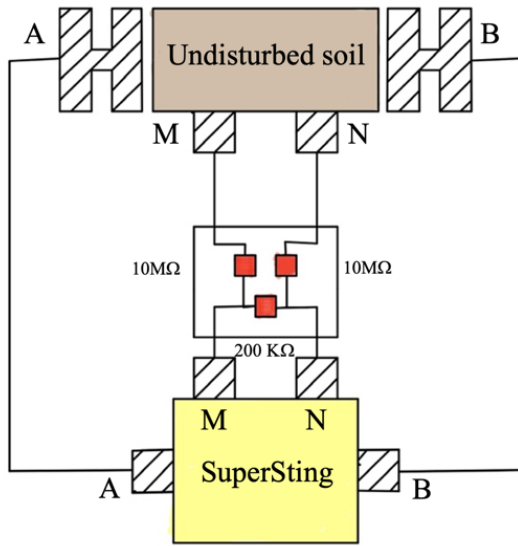
Figure 3-18 resistivity measurements techniques for undisturbed samples

3.7.3 Electrical Resistivity Tests on Modified Uniaxial Test Machine

The electrical resistivity of the remolded soil specimens was measured using the two-electrode method by following the ASTM G187-18 standard. The soil specimens were compacted in a compaction mold at different moisture content with three different compaction energies, and then they were extracted and trimmed. Two rounded prefabricated stainless steel were used as electrodes at two ends of the remolded sample to measure the resistivity.
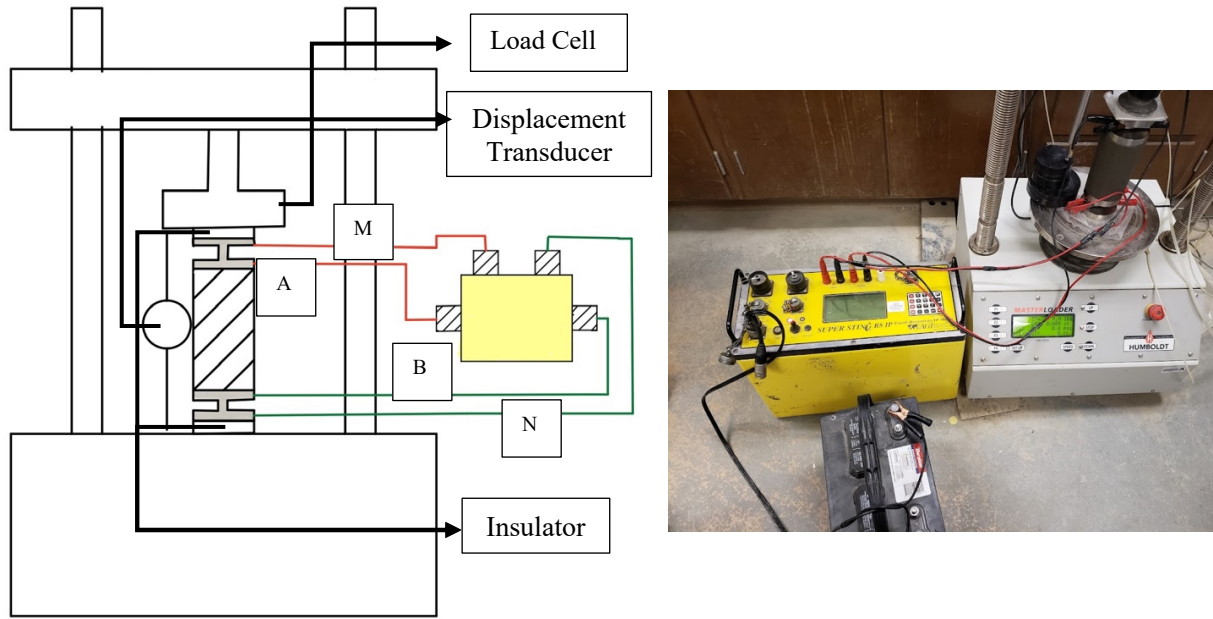
Figure 3-19 Electrical resistivity measurement of remolded sample in a modified uniaxial test

The electrical resistivity of the soil specimen was also measured during the unconfined compressive strength test using the Humboldt HM-3000 loading frame. Two prefabricated S.S. plates have used an electrode, as shown in Figure 3-19. The pedestal and load cell of the loading frame were covered using plastic wrap so that the current flow was discontinued between the electrode and loading frame. The stain was applied to soil samples at a rate of 0.127 cm/min during the test. Electrical resistivity measurements were taken continuously throughout the test using the super sting I.P. equipment. The measured resistivity was corrected using equation 2 to the standard temperature of 15.5 °C.

3.7.4 Calibration for Temperature

The changes of resistivity with the changing temperature were observed for clayey and sandy soil separately (Figure 3-20). The changes were observed at different degrees of saturation levels. Clayey soils exhibit greater changes in electrical resistivity at lower saturation levels than sandy soils. As saturation increases, changes become less pronounced. Compared to lower

saturation levels, there was less change in resistivity at higher saturation levels. As the higher temperature increases the mobility of the ions, thus the resistivity value decreases. Moreover, the effect of temperature on the resistivity value for clayey soil was found more complex. (Clavier et al., 2013). All the resistivity value measured in the current study was corrected using the following equation:

$$\rho = \rho_T \frac{(24.5 + T)}{40}$$

Here, ρ is the calibrated resistivity and ρ_T is the measured resistivity at T (degree Celcius).

(a) Clayey Soil
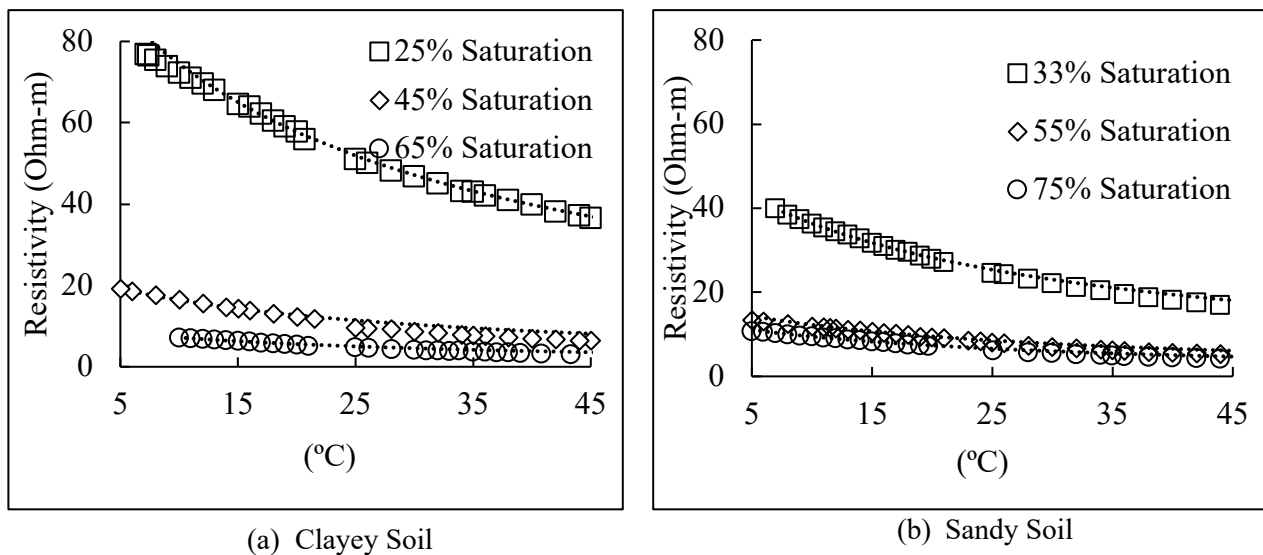
(b) Sandy Soil

Figure 3-20 Variation of resistivity with temperature for (a) clayey soil and (b) sandy soil

3.7.5 Repeatability of Electrical Resistivity Measurements

Experimental repeatability refers to the variation in results whilst the exact equipment, the exact conditions, and the exact operator are used for tests on different samples. ASTM G187-05, which describes soil resistivity using two electrodes, suggests that the coefficient of variation be used to verify the repeatability. In the current study, both clayey soil and sandy soil specimens were used to determine the repeatability of soil resistivity (Table 3-8).

Table 3-8 Statistics of repeatability tests

	Moisture Content	Degree of Saturation	Mean Resistivity	Standard Deviation	COV
Clayey sample	8.8%	20%	109.13	2.76	2.53%
	33.6%	91%	3.09	0.16	5.30%
Sandy sample	10.5%	21%	102.51	4.84	4.72%
	19.2%	100%	23.46	0.62	2.63%

3.8 Statistical Modeling

To associate the experimental resistivity value with the soil geotechnical engineering properties, multiple linear regression (MLR) analyses were used. The statistical analysis software R Studio was utilized for the multiple linear regression modeling. Results from the experimental program were utilized to develop the statistical model. Separate MLR models were developed for compacted soil specimens and sandy soils. Influential parameters related to soil properties were determined beforehand. After performing the initial analysis, the following MLR assumptions were verified for the modeling.

- Constant variance

- Normality

- Independent error terms

- Presence of outlier

- Multicollinearity, and

- Applicability of regression on the current data set

Transformation of the parameter was conducted where it was necessary.

3.9 Model Validation

The developed models were applied to predict the geotechnical properties of soil for the field condition. A field resistivity survey was conducted in different areas, and the resistivity results were utilized in the model to verify the calculated and obtained geotechnical conditions of the soils. Soil electrical resistivity survey conducted in Beaumont district for borehole BR-10A was utilized for the verification purpose. Moreover, undisturbed soil samples were also collected from boreholes P1, P4, P6, and P17 from the Beaumont district. The resistivity survey line was conducted 7 ft to 15 ft far from the boreholes due to roadway conditions for these boreholes. These undisturbed soil characteristics were also utilized to validate the model.

CHAPTER 4 FIELD AND LABORATORY TESTS RESULTS

4.1 Geotechnical Properties

4.1.1 Grain Size Distribution

Grain Size distribution was conducted for all collected soil specimens, and the percent of sand examined from the test is presented in Figure 4-1. It was observed from the histogram of sample size with the percent of sand that a total of 63 soil samples among 88 samples were found containing sand percentage lower than 50. The rest of the soil samples can be classified as sandy samples according to the USCS.
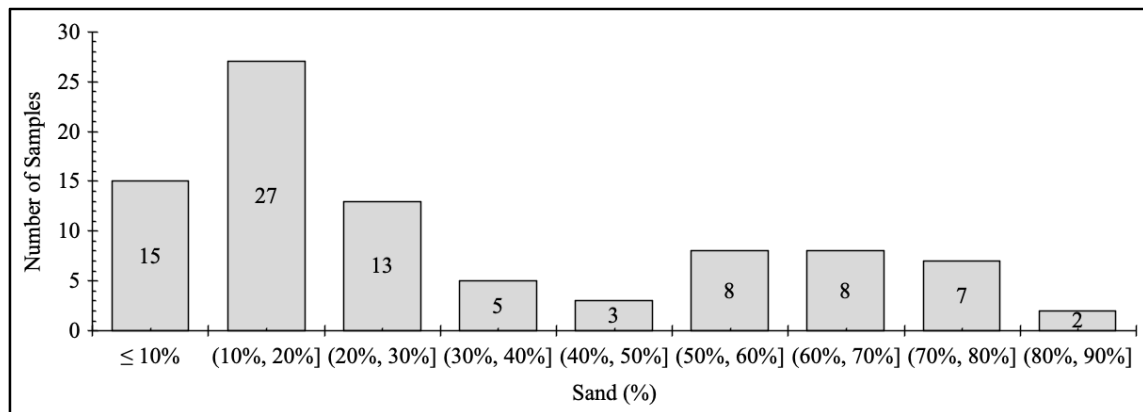
Figure 4-1 Number of Samples vs. Percent of Sand

Clay content in the soil samples was determined by conducting a hydrometer test. The results of hydrometer tests are shown in Figure 4-2. In sandy soil samples, the clay content was found between 3.2% to 23.2%, whereas clay contents varied from 9.4% to 62.2% in finer soil samples. Finer soil samples can be classified further into lean clay and fat clay from the Atterberg limit tests.

(a)   (b)
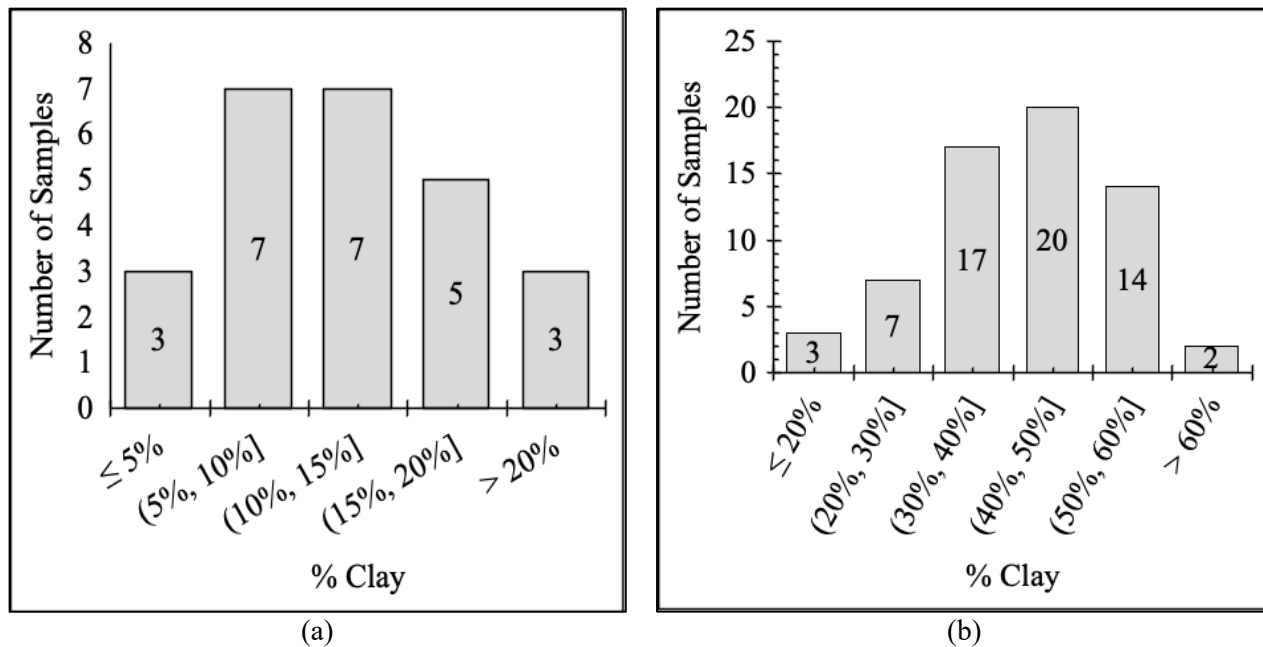
Figure 4-2 Number of sample and percent of clay for (a) sand and (b) clay

4.1.2 Atterberg Limit

Atterberg tests were conducted to find out the liquid limit and plastic limit of the soil sample. The plasticity index was determined by subtracting the plastic limit from the liquid limit. Total 63 samples were tested, and the results are shown in Figure 4-3 and Figure 4-4. The liquid limit of 44 samples was found to be less than 50. The rest of the soil samples, i.e., 19 samples, contain a liquid limit higher than 50. Therefore, a total of 44 soil samples can be considered as low plastic clay whereas, 19 clay samples that are considered in this study will be considered as high plastic clay. The lowest liquid limit for all soil samples was found as 27.3%, and the highest liquid limit was found as 73.2%.
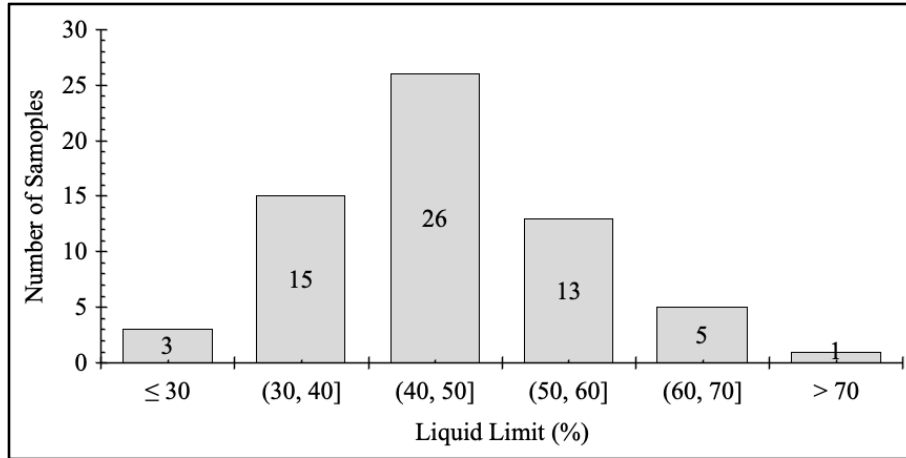
Figure 4-3 Distribution of liquid limit of collected samples

Figure 4-4 shows the distribution of the plasticity index. A plasticity index between 20% and 30% was found in 34 soil samples. All the soil samples had a plasticity index between medium and high. The higher plasticity index was found as 49.5%, and the lowest plasticity index was found as 10.4%.
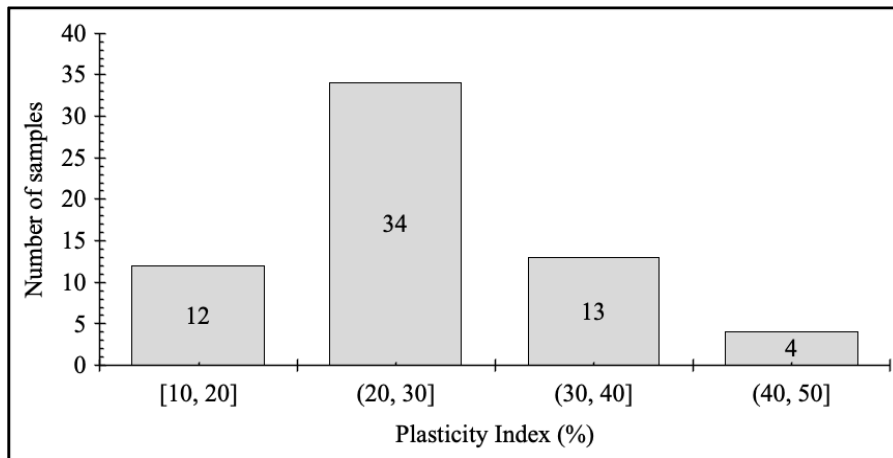
Figure 4-4 Distribution of plasticity indices of testes samples

All soil samples are plotted in a plasticity chart to determine the soil classification according to the USCS classification system. Four of 19 samples of high plastic clay were found to be silty clay. The four samples were collected from El-Paso district B2 boreholes from depths of 20 ft, 30 ft, 40 ft, and 50 ft. Soil samples used for the investigation are shown in a flow chart in Figure 4-5.
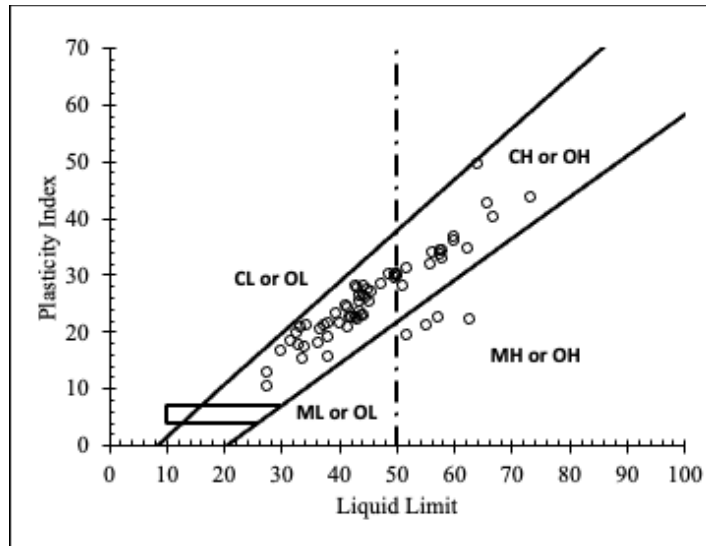
Figure 4-5 Plasticity chart
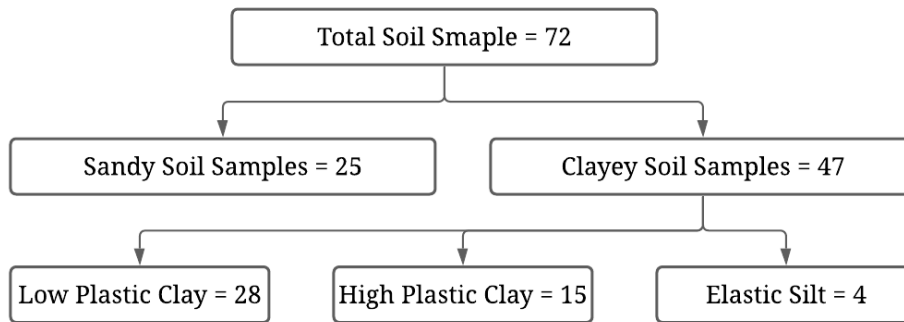
Figure 4-6 Distribution of soil samples

4.1.3 Specific Gravity

A water pycnometer was used to measure the specific gravity of the soil samples according to the ASTM D854-00 standard test method. The specific gravity of all the collected soil specimens was determined in the laboratory. Among the soil samples, specific gravities ranged from 2.62 to 2.78.

4.1.4 Activity of Soil

Physicochemical characteristics of the constituent clay and non-clay minerals and their relative proportions also influence the soil properties and engineering behavior. It is possible to distinguish between fine-grained soils that have differing mineral-chemical properties by measuring the soil activity. An indicator of soil activity is the ratio of the plasticity index to the fraction of clay in the soil sample. The results obtained from the calculations are shown in Figure 4-7. There is a correlation between activity levels and clay fractions since clay fractions become more influential as activity levels increase. Therefore, clay fraction properties are more sensitive to the type and composition of exchangeable cations and pore fluids. The results indicate that 47 soil samples were classified as inactive clay, 15 samples as normal clay, and one sample as active clay (Skempton, 1984). The activity of soil samples changes with the variation of clay content. Sixteen soil samples with higher than 50% clay content obtained from hydrometer tests have an average activity of 0.50. The number of soil samples with clay content from 40% to 50% have an average activity of 0.64. Soil sample contains clay content from 30% to 40% considered in this study was 17, and average activity value was calculated as 0.64, whereas ten soil samples with less than 30% clay content contain an average activity of 0.94. Thus, it was observed from the results that soil samples containing more than 50% clay particles had lower activity values than soil samples containing a lower percentage of clay particles.
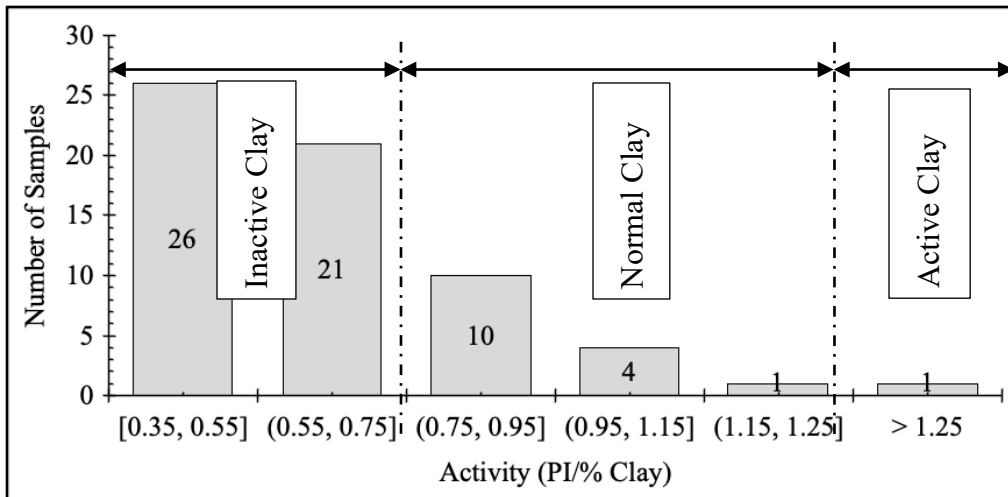
Figure 4-7 Distribution of activity of soil samples

4.1.5 Cation Exchange Capacity (CEC) and Specific Surface Area (SSA)

The cation exchange capacity (CEC) and specific surface area (SSA) results obtained from Farrar and Coleman (1967) correlation equation are summarized in Figure 4-8 and Figure 4-9. There are a number of exchangeable charges associated with the cation exchange capacity. In contrast, this number represents the number of exchangeable cations which have a higher exchangeability than cations adsorbing to small surface areas and can be easily replaced by leaching with a solution containing other dissolved cations of higher exchangeability.
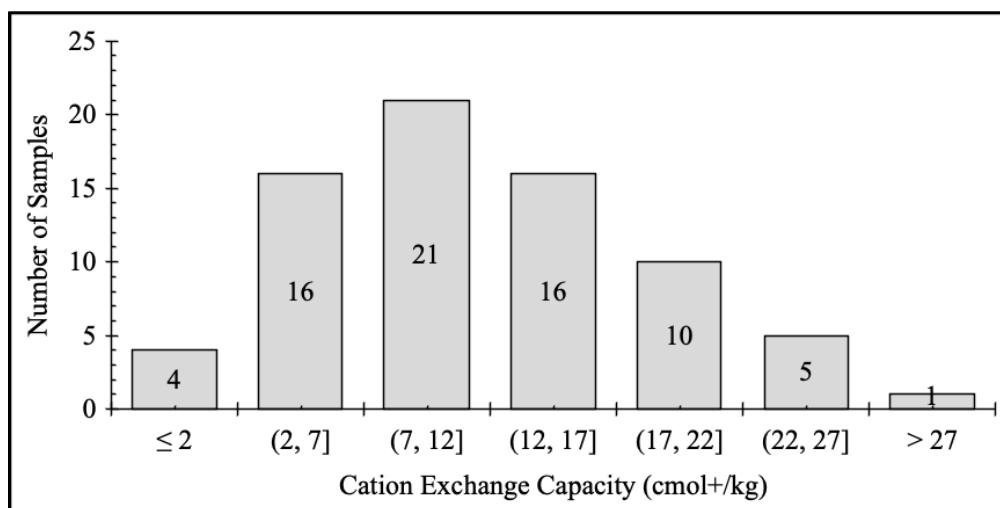
Figure 4-8 Distribution of cation exchange capacity of soils

In any given soil, the total SSA varies considerably due to different mineralogy, organic composition, and particle size distributions. As a mineral constituent of soil, clays contribute the greatest amount of soil surface area but may also vary greatly depending on the specific soil type. It has been reported that swelling clays, like montmorillonites, can have specific surface areas of up to 810 m2/g. For non-expanding soils such as kaolinites, the SSA typically ranges from 10 to 40 m2/g (Mitchell & Soga, 2005). Consequently, when it comes to determining the effects of specific surface area on the properties of a soil, the type of clay mineral present in the soil has an important role to play. Because the grain-size distribution and clay mineralogy govern the surface area of soil, this property can be considered part of the soil's "inherent" characteristics.
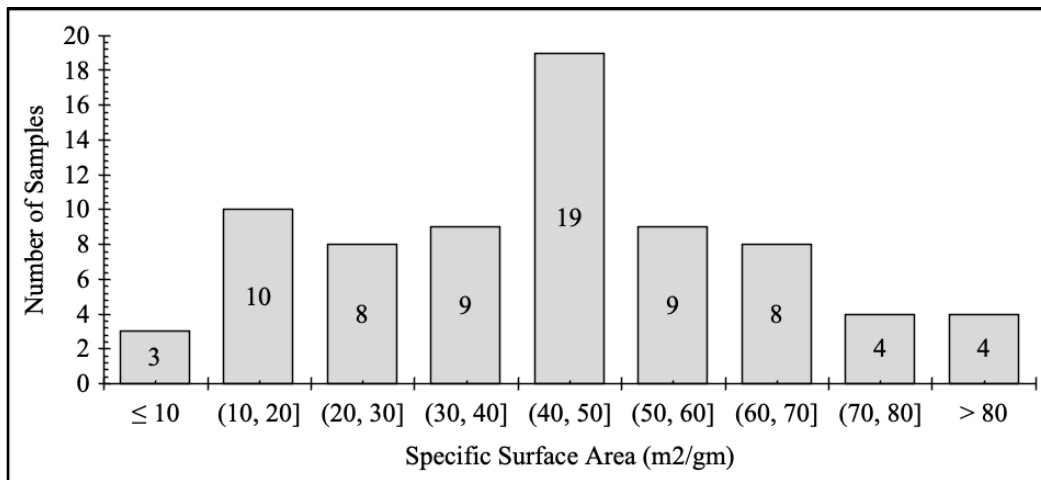
Figure 4-9 Distribution of specific surface area of soil

4.2 Study of Composition and Fabric

4.2.1 Scanning Electron Microscope (SEM)

It is very important from a geotechnical engineering perspective to assess the microstructure of the soil because its behavior is heavily dependent on the fabric structure. Using a scanning electron microscope (SEM) at various magnifications, fabric structure has been analyzed in the current study. An example of an SEM image of a mineral can be seen inFigure

4-10. A major problem associated with SEM study is preparing surface replicas, which, according to Mitchell and Soga (2005), is the most difficult part of the study. For this reason, it is extremely important to ensure that the samples are undisturbed before SEM analysis is conducted. A sedimentation method was used in the current study to prepare the samples for SEM analysis.
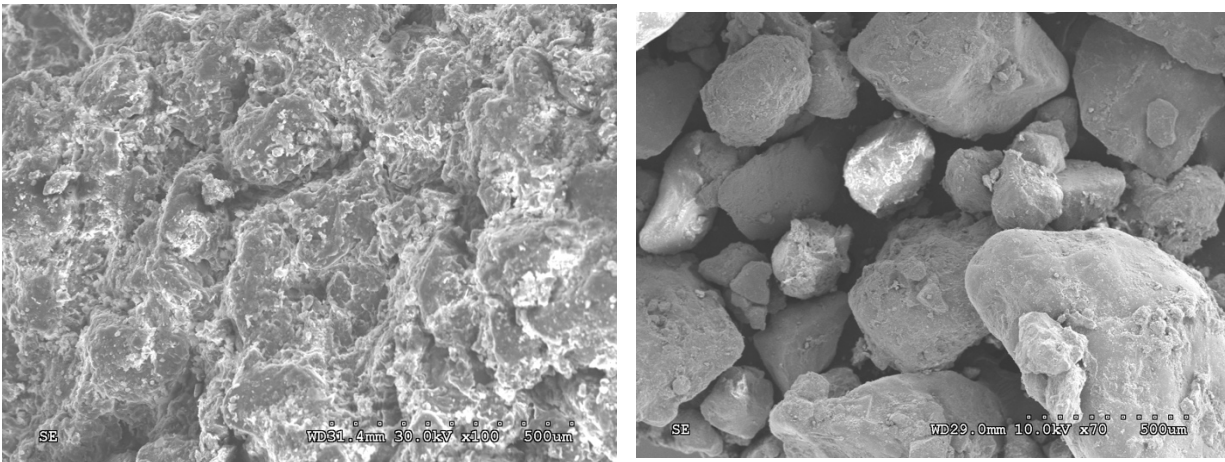
(a) Clayey Soil   (b) Sandy Soil

Figure 4-10 Scanning electron microscopic image of clayey and sandy soil

On the basis of the surface study of microscopic images of sandy and clayey soil, it can be concluded that clay particles are more closely interlocked than particles in sandy soil. Clayey soils feature a peeling surface and have a smaller pore space than sandy soils. Based on the analysis conducted on the SEM images of the sample, it was found that the fabrics in the sample did not consist of flaky structures. Despite the fact that the soil samples did not acquire a very distinct hexagonal shape, there was evidence of a hexagonal fabric structure which was evident. In light of this, it can be assumed that poorly crystallized kaolinite is likely to occur to be found in the samples. However, based only on SEM images, it was difficult to make specific conclusions about this clay mineral. The pore space between soil samples of sandy soil was also assessed in this study. It has been found that sandy particles have a rounder shape and have a larger pore space between them.

4.2.2 Energy Dispersive Spectroscopy (EDS)

The results of EDS analyses are shown in the Figure 4-11 and summarized in Table 4-1. According to these findings, clay is a very reactive material composed of oxygen (58.84%), carbon (10.50%), and silicon (20.05%). Further, an insignificant amount of aluminum (4.67%), iron (1.54%), sodium (1%), and potassium (1.02%) were also detected in the clay. It is calculated that the percentage of silicon, oxygen, and carbon in the sample being considered in this study is 89.4%.

Additionally, the energy dispersive spectroscopy results for sandy soil samples are also presented. In general, silica (SiO2) constitutes much of the sand sample. The oxygen concentration in the sample is found to be high according to the testing. Additionally, laboratory tests also confirm the presence of aluminum in the sample.

Clay   Sand
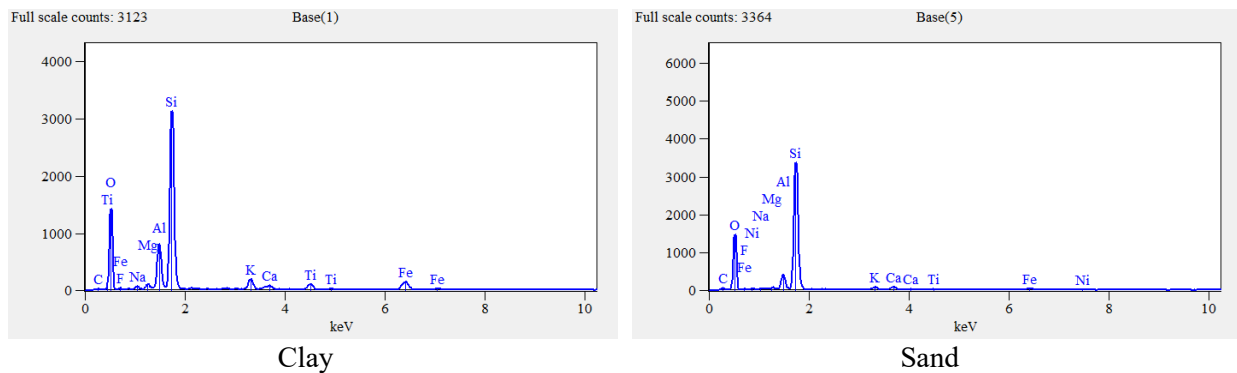
Figure 4-11 EDS results analysis for clayey and sandy soils

Table 4-1 Summary of EDS results

Sample	C	O	Si	Al	Mg	K	Fe	Na	F	Ca	Ti
Clay	10.50	58.84	20.05	4.67	.55	1.02	1.54	1	.81	.33	.69
Sand	3.62	66.50	26.83	1.87	.35	.19	.28	-	-	.32	.04

4.3 Pore-Water Conductivity

Pore water conductivity was also measured using a benchtop conductivity meter. The results are shown in Figure 4-12. From the results, it is evident that most of the soil samples have conductivity less than 3600 microS/cm. Around 42 soil samples have conductivity between 200 microS/cm to 1050 microS/cm.

All soil samples were also measured for pH using a benchtop PH meter. PH The pH range was found to be 7.05 to 7.31, meaning no acidic samples were discovered.
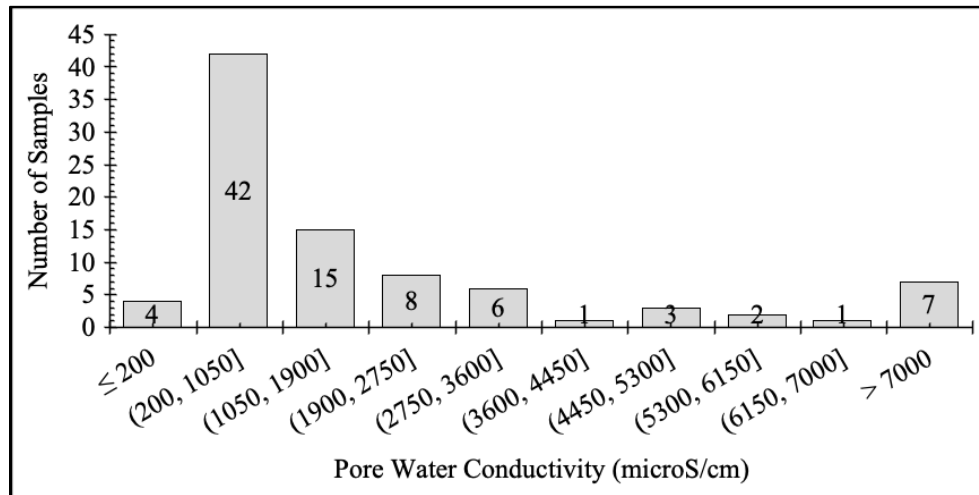
Figure 4-12 Pore water conductivity distribution of soil samples

4.4 Sulfate Content

Sulfate content in each soil sample was also measured using the colorimetric method. The distribution of sulfate in content in the soil samples is given in Figure 4-13. Most of the soil contains sulfate content less than 3000 ppm, which does not harm the structure built above it due to any expansion. Five soil samples were found containing sulfate content between 3000 ppm to 8000 ppm.
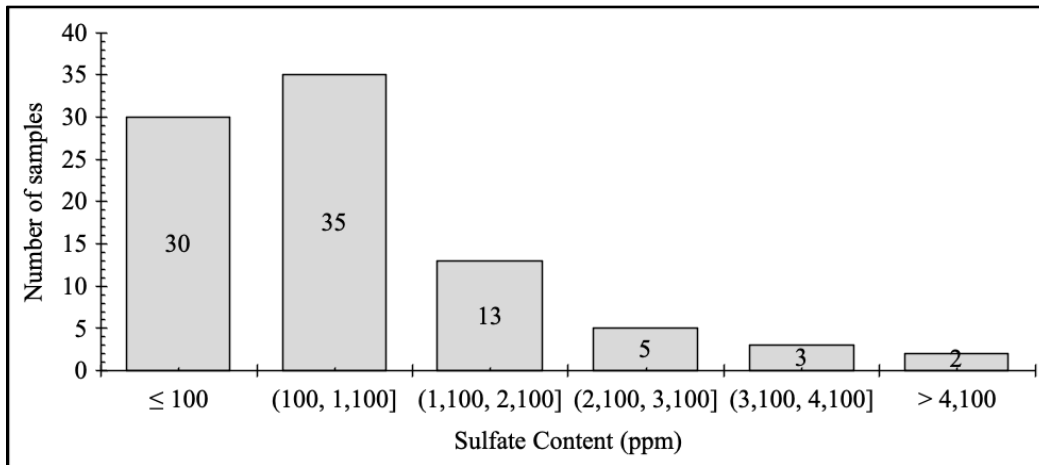
Figure 4-13 Soluble sulfate content of soils

4.5 Soil Boring

Soil boring and blow counts were measured using the Texas cone penetration (TCP) method. Soil boring was conducted in 18 different locations in four three districts. Total TCP blows were counted while performing the drilling. Bore logs are provided in the appendix chapter. Total blow counts were measured from 1 to 100 on different locations. Soil samples were collected, and after visual inspection and laboratory testing, the soil types were determined. Blow counts were separated for clayey and sandy soils.

The conversion factor was used to convert the value of TCP to find out the SPT value. For clayey soil, the factor was used as 0.7 whereas, for sandy soil, 0.5 conversion value was used.

4.6 Field Electrical Resistivity Test Results

An electrical resistivity survey was conducted to determine the resistivity value of soil at any depth. The survey was conducted on the same day of soil boring. The resistivity survey was conducted on top of the boring point. When it was not possible to conduct the resistivity survey on top of a boring location, the survey line was carried away not far than 5 feet from the point. The resistivity image and boring location are shown in Figure 4-14 for BR6A locations of Beaumont.

The drilling depth was 100 feet, and the resistivity survey was conducted with 56 electrodes with 10 feet spacing to cover the depth. The total survey line length was 550 feet. The resistivity value was extracted from the resistivity imaging using Earth Imager software.
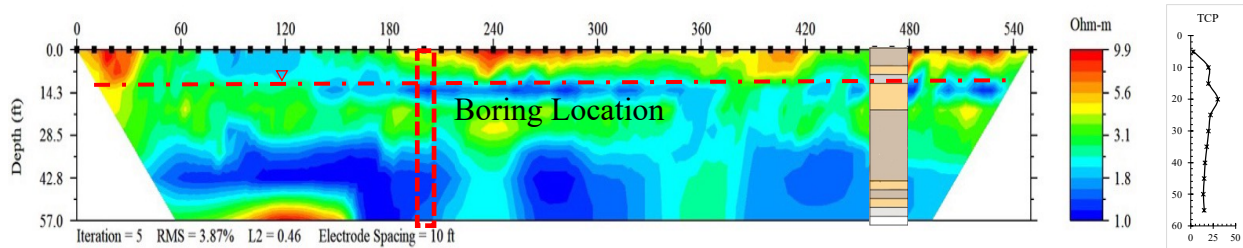
Figure 4-14 Boring location and soil resistivity image (Beaumont)

Five different types of soil, according to USCS, were found in the field during the investigation. Soil samples can be classified as high plastic clay (CH), low plastic clay (CL), clayey sand (SC), silty sand (SM), and sandy samples with silt (SW-SM). Soil samples were tested in the laboratory to classify. Field electrical resistivity was measured from three districts, namely Fort-worth, Beaumont, and Corpus-Christi. A field electrical resistivity survey was not conducted in the El-Paso district. All types of samples except SW-SM were found in all three districts, whereas sandy sample with silt (SW-SM) was found only in the Corpus-Christi district. Soil field resistivity value obtained from the Earth Imager 2D software was plotted for different types of soil in Figure 4-15.
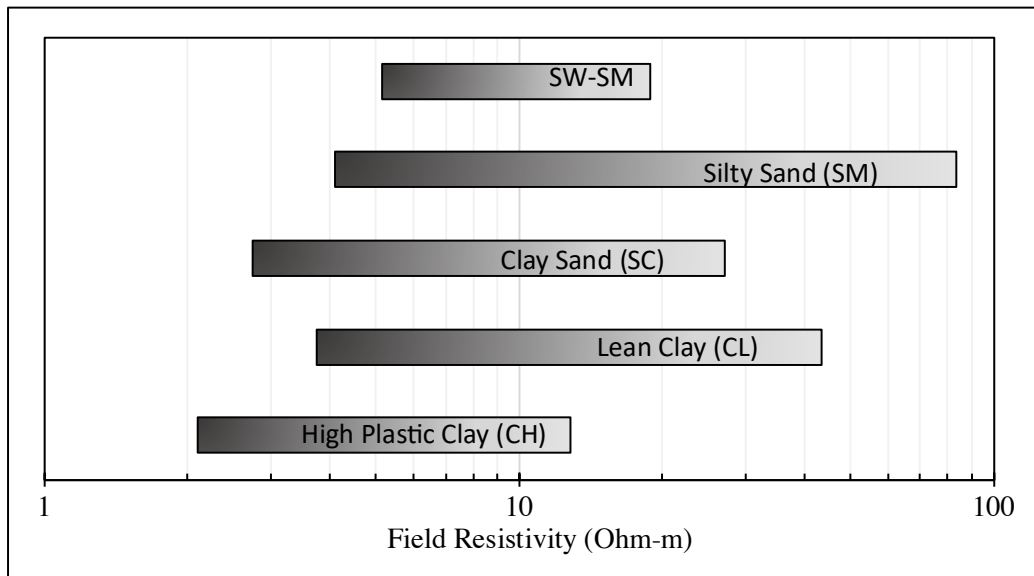
Figure 4-15 Field resistivity value for different soil types

Figure 4-15 shows the resistivity ranges found in the field for different types of soil samples. Minimum resistivity for high plastic clay was found at 2.1 ohm-m, and maximum resistivity was found at 14.1 ohm-m for the same types of soil samples. Moreover, minimum resistivity of lean clay, clayey sand, silty clay, and sandy soil with silt was found at 3.7 ohm-m, 2.7 ohm-m, 4.1 ohm-m, and 5.1 ohm-m, respectively, whereas maximum resistivity was found at 10.7 ohm-m, 39.8 ohm-m, 24.3 ohm-m, 79.3 ohm-m, and 13.8 ohm-m respectively.

Soil resistivity for different types of soil was found by researchers are shown in Table 4-2. Minimum soil resistivity was found at the saturated condition in the current research. Field pore water conductivity of the soil sample was also measured in the laboratory. The electrical resistivity of different soil samples was measured by Kouchaki et al. (2019)using the deionized water. Field resistivity for different soil found by Kaufman & Hoekstra (2001) was also shown in table. The minimum resistivity found by both researchers was for high plasticity clayey soil.

Table 4-2 Electrical resistivity ranges for different soils

Soil Type	Soil Classification	Reistivity (Kaufman and Hoekstra 2001)	Resistivity (Kouchaki et al., 2019)
Silts & Clays	CH	10-50	5.5-9
	CL	24-60	26-90
Sands	SC	46-178	13-28
	SM	95-450	52-110

The blow counts value and resistivity value were separated based on the soil types, i.e., clayey and sandy. At any given depth, soil resistivity and TCP-N value show a similar trend. Figure 4-16 shows the variation of the resistivity and TCP-N of the soil. With the increasing TCP value, the resistivity value was also found to increase. A linear relationship was observed between the parameters as mentioned below:

$$\text{For clayey soil, } Resistivity = 0.20 \times TCP + 5.08$$
$$\text{For sandy soil, } Resistivity = 0.85 \times TCP + 3.41$$

The correlation coefficient was found 0.59 for clayey soil and 0.8 for sandy soil, meaning there is a strong correlation between resistivity and TCP counts. The coefficients in the linear relations are sensitive to the clay content and lithology of the soil. Researchers found that electrical resistivity depends on the porosity and pore structure of the soil, which also affects the blow counts of the penetration test. Thus, these two parameters of soil can be correlated. While developing the relationship between TCP blow counts with electrical resistivity, blow counts below two and above 99 was omitted. All the resistivity responses obtained from the field ERI were separated into two categories, namely clayey soil, and sandy soils. After that, the resistivity was plotted against the blow counts monitored during the field investigation. Figure 4-16 shows the correlations between clayey soil and sandy soils.

(a) Clayey Soil   (b) Sandy Soil
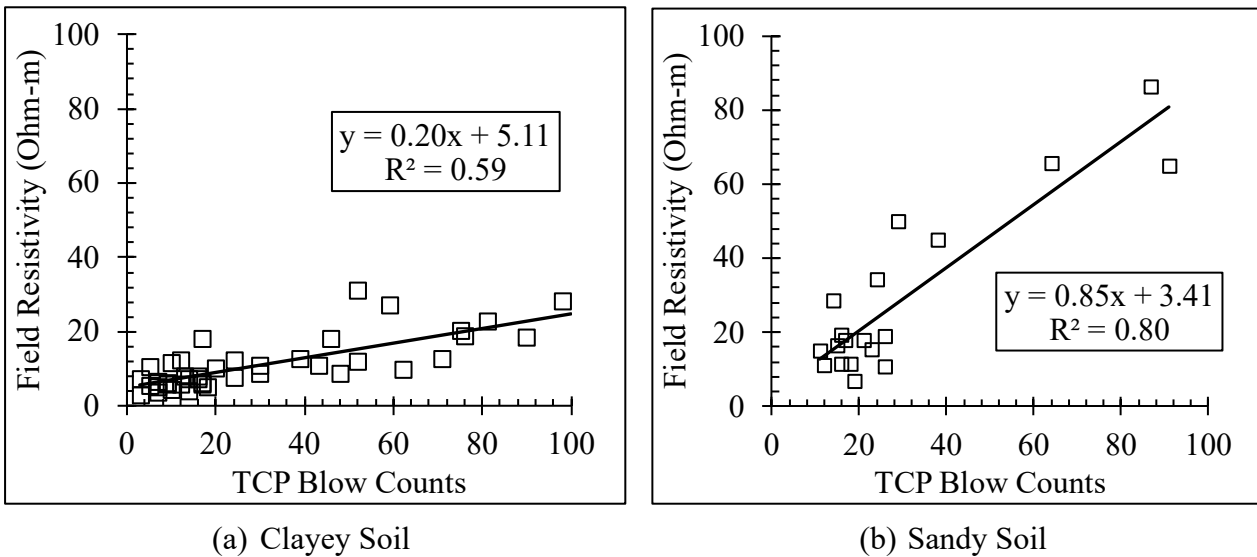
Figure 4-16 Relationship between field electrical resistivity and blow count

Soil TCP blow counts can be converted to SPT values using the correlations. Correlations between SPT and electrical resistivity were also determined for sandy soils and compared with the previous results obtained by researchers (Figure 4-17). Because of the different types of soil formation, the resistivity was found different.
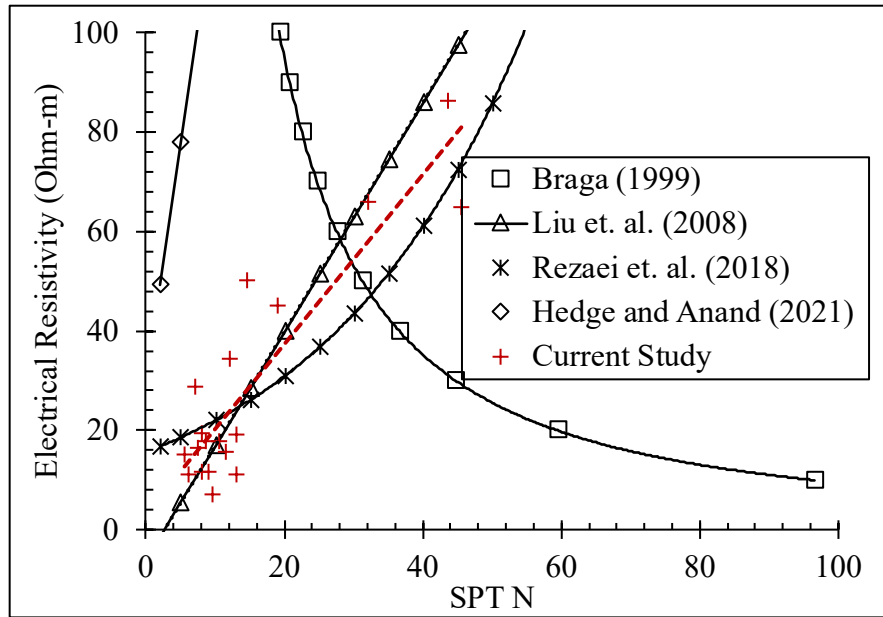
Figure 4-17 Correlation between SPT and electrical resistivity

CHAPTER 5 LABORATORY ELECTRICAL RESISTIVITY RESULTS

5.1 Introduction

During this section, the effect of influential parameters related to soil properties and phase

relationships on the electrical resistivity of soil is investigated. A laboratory test was conducted in

order to determine how the particle size, moisture content, void ratio, and degree of saturation of

soils are affecting the electrical resistivity response properties of soils. Furthermore, soil samples

collected from different locations have different inherent mineral properties. It was also

determined in the laboratory tests that different clay properties have an influence on the electrical

resistance of clays. Soil samples obtained from both clayey and sandy soils were used for testing.

It was decided to test both disturbed and undisturbed soil samples in laboratory settings in the case

of clayey soil samples. With respect to undisturbed soil samples, gravimetric moisture content and

volumetric moisture content, as well as the degree of saturation, were selected as independent

variables. There are differences in electrical resistance in clayey soils and sandy soils due to

different soil properties, which will be discussed in the following section.

5.2 Resistivity Results for Clayey Soil

5.2.1 Influential Parameters Related to Soil Properties

In an attempt to assess the effects of soil properties on electrical resistivity results,

compacted clays were used to evaluate these effects. In order to minimize the influence of the

degree of saturation on the resistivity results the degree of saturation was kept constant throughout

the analysis (Kibria & Hossain, 2015). Various fixed degrees of saturation were chosen, and then

the effect of fine content, clay content, Atterberg limit, activity, pore water conductivity, sulfate content, CEC & SSA on the resistivity response were determined.

5.2.1.1 Effects of Fine Content

The samples were passed through a #200 sieve, which is 75 mm in size, to determine its fine content. For clayey soil samples, a maximum of 95.7% fine content was determined, and a minimum of 54.2% of fine content was determined. As the degree of saturation is a prominent parameter controlling the resistivity value, the relationship between electrical resistivity value with fine content of clayey soil is determined at 100% degree of saturation which is shown in Figure 5-1. From the experimental laboratory results, the maximum resistivity at 100% degree of saturation was found at 11.92 Ohm-m whereas, the minimum resistivity at the same degree of saturation was observed as 1.83. Therefore, resistivity decreases 6.5 times from the initial value when the fine content increases from 54.2% to 95.7%. The coefficient of correlation was determined as 0.65, i.e., 65% of the variation in electrical resistivity value at 100% degree of saturation can be explained with the change of fine content of the soil with the help of below mentioned polynomial equation.
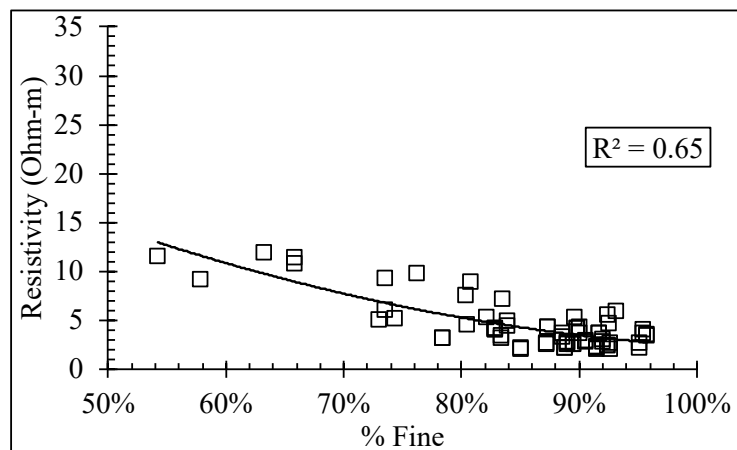
Figure 5-1 The relationship between resistivity and fine content at 100% degree of saturation

$$Resistivity = 33.51 \times (Fine\ Content)^2 - 74.82 \times (Fine\ Content) + 43.67$$

The equation provided below was generated to explain the decreasing resistivity value with increasing fine content.

The equation shown above was generated to explain the decreasing resistivity value with increasing fine content. Similarly, the sand content percentage was also determined during the sieve analysis. The relationship between the sand content percentage of clayey soil and laboratory resistivity will follow an overall upward trend which will be reciprocal to this relationship.

Change of resistivity with fine content was also examined at 50% degree of saturation. A downward trend similar to the 100% saturation level was observed; however, the correlation between fine content and degree of saturation was found not significant as the fine content increases the surface conductance increases resulting in the increase in conductivity of the soil (Kwader, 1985). Therefore, soil with more fines content generally has lower electrical resistivity responses. Moreover, pore space decreases when a soil sample with more fines is compacted in a higher degree of saturation. Decreasing pores in a compacted soil sample also help the electrical current to pass easily through the compacted sample. Abu-Hassanein et al. (1996) showed that the relationship between fine content and resistivity at optimum moisture content, which is shown in Figure 5-2 and compared with the current study.
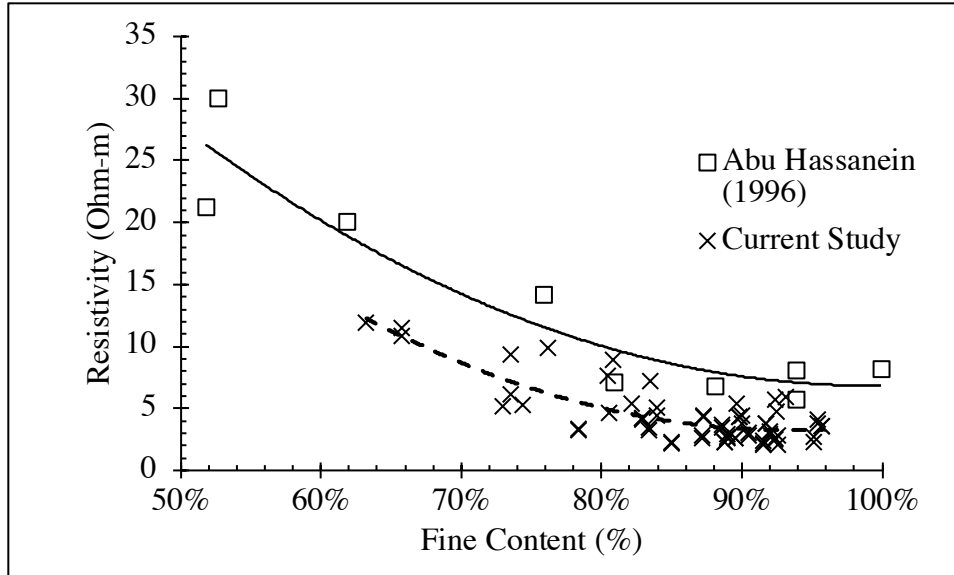
Figure 5-2 Comparison between the current study and previous study results

Current study results follow a similar trend as the previous study; however, the overall resistivity value dropped. Since the resistivity test was conducted at 100% saturation rather than at optimum moisture content, similar to previous studies, the resistivity results were lower.

5.2.1.2 Effect of Clay Content

The clay content of the soil sample was determined in the laboratory with the help of a hydrometer test. Clay and silt content of collected soil sample was determined. Figure 5-3 illustrates the change in electrical resistivity as a function of the amount of clay in the soil at 100% saturation. From the figure, it is evident that when the clay content is increasing in any soil, the electrical resistivity decreases. The relationship between resistivity and clay content is not linear. Polynomial functions best describe changes in resistivity, and the equation is provided below:

$$Resistivity = 61.08 \times (Clay\ Content)^2 - 60.84 \times (clay\ content) + 18.34$$
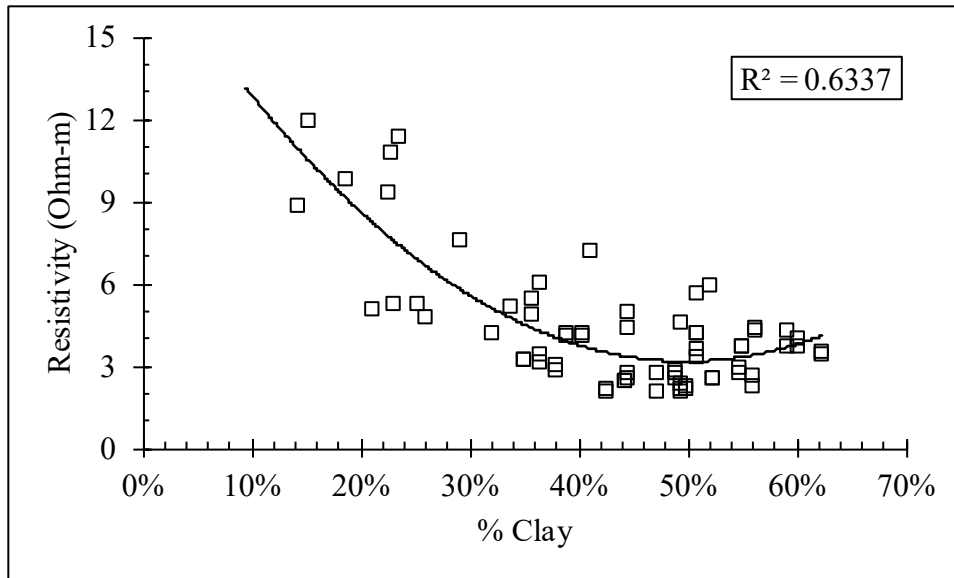
Figure 5-3 The relationship between electrical resistivity and clay content

The coefficient of correlation was found as 0.634, which means 63.4% of changes in electrical resistivity can be described with this equation. From the experimental results, soil clay percentages found decreased 6.62 times from the initial value of 62.2%, and the minimum resistivity value was found to decrease 6.5 times from the initial value of 11.92 Ohm-m. Therefore, soil resistivity was found to decrease with a slope of 1:1 with the increasing clay content initially. Afterward, the slope between resistivity and clay content becomes mild and changes with the rate of decrease. Clay particles facilitate the conductivity of electrical current on their surfaces, as expected. In their study, Long et al. (2012) determined that the coefficient of correlation between resistivity and clay content was 0.59. The author found Soil samples with relatively low clay content show high resistivity values. Changes in resistivity value decrease sharply up to 40% mass of clay content in a soil sample. The resistivity values are generally low for clay content greater than 40% by weight.
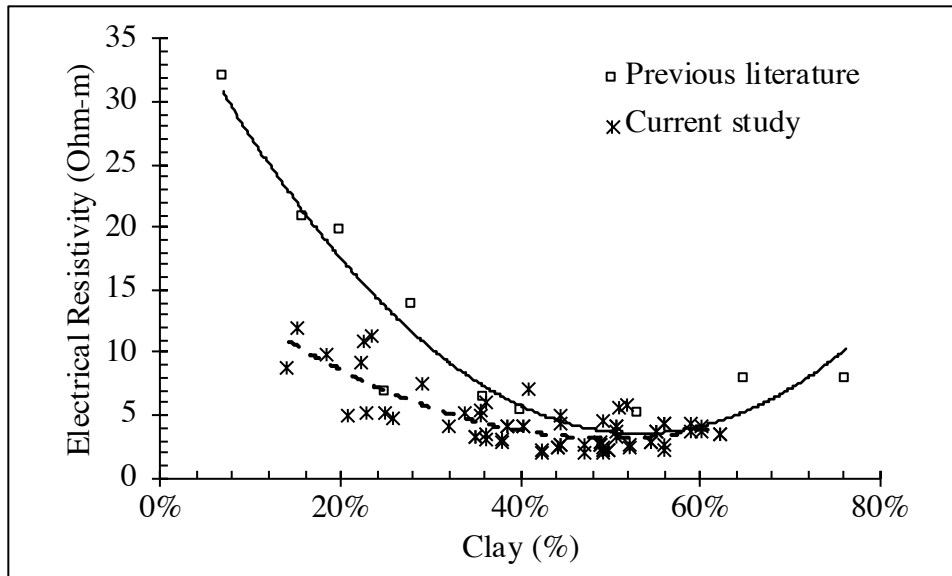
Figure 5-4 Comparison of changes in resistivity with clay content with the previous study

However, the soil resistivity trend also indicated that the resistivity value was increasing once the clay content in a soil sample increased beyond 50%. Abu-Hassanein et al. (1996) found a similar trend using tap water for moistening the compacted soil samples. The conductivity of deionized water, which was used in this current study, was very low; therefore, when the soil is saturated, and clay content reaches beyond 50%, the resistivity starts to show an upward trend (Figure 5-4). Due to the deionized water filling the pores between particles, the electrical conduction path is interrupted, resulting in an increase in resistivity. Since the conductivity of deionized water used in this study was very low, once the soil is saturated and the clay content reaches 50% or more, the resistivity begins to rise. As the deionized water fills in the pores between particles, the electrical conduction paths become interrupted, increasing the resistivity

5.2.1.3 Effects of Liquid Limit

There is a direct correlation between the surface activity of soil and the particle size and proportion of fine fractions in the soil. The index properties of soils are also affected by specific surface areas, electrolyte concentrations, cation valences, and the dielectric constant when they are

mixed. In light of this, liquid limits, as well as plasticity indexes, can be regarded as two important indicators of physicochemical characteristics of soils (Mitchell and Soga, 2005).

Figure 5-5 shows the variation in resistivity at different degrees of saturation with liquid limits. Experimental data points showed overall downward trends, and correlation coefficients were also measured. In order to measure resistivity, saturation played an important role in evaluating the relationship between liquid limit and electrical resistivity. Different saturation levels of resistance resulted in different rates of decrease of resistivity. This was to be expected. The relationship between the resistivity and liquid limit is not linear. The electrical resistivity of the soil samples decreases 14.3, 10.3, 6.3, and 11.4 times the initial value for increasing the liquid limit value of 23 to 73.2 for the degree of saturation of 44%, 66%, 88%, and 100%, respectively. However, the resistivity value of F-PS-1-5 was found unusually higher (23.40 Ohm-m) at 100% degree of saturation; if the resistivity value was not considered, then resistivity value was found to be decreased 6.9 times the initial value. Therefore, it can be concluded that the decreasing rate of resistivity with the increasing liquid limit is similar at a higher degree of saturation.
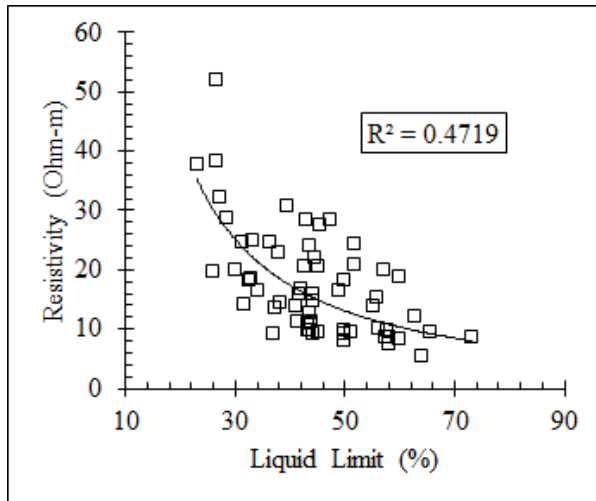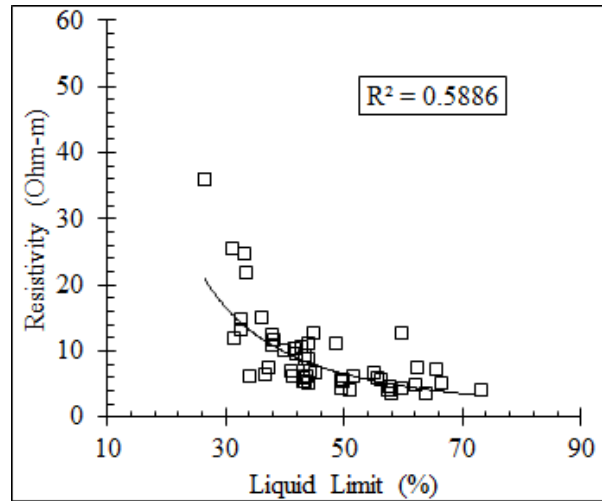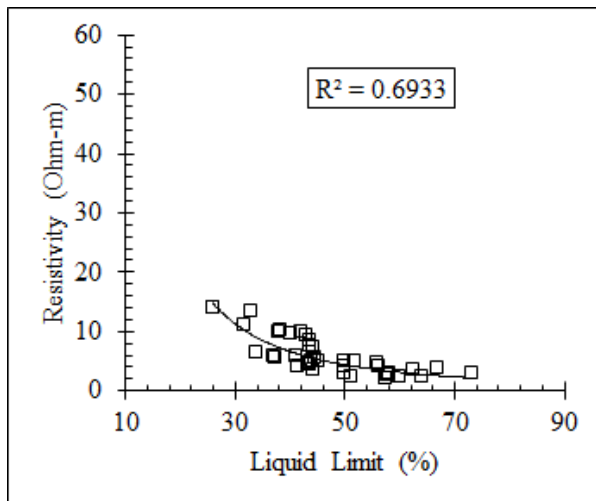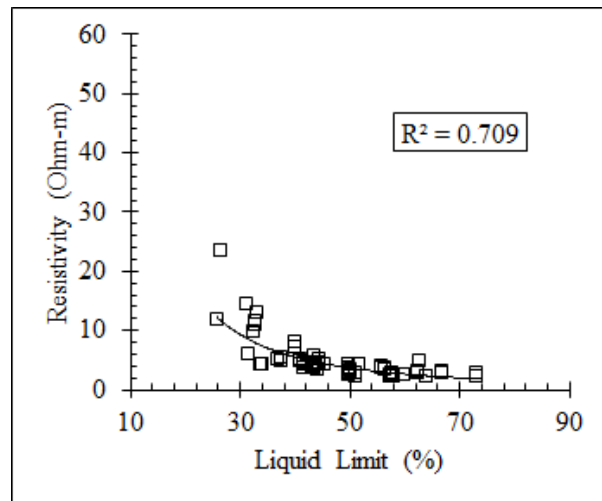
Figure 5-5 Relationship between electrical resistivity and liquid limit at different degrees of saturation

From the experimental value, it can be observed that high plastic clay that contains a liquid limit greater than or equal to 50 seemed to have a low impact on resistivity value with the changing liquid limit at 66% degree of saturation. The resistivity value decreases 11.4, 4.6, 6.3, and 2.3 times from the initial value for the high plastic soil samples at the degree of saturation of 44%, 66%, 88%, and 100%, respectively, with an increasing liquid limit from 50 to 73.2. However, the changes in electrical resistivity for low plastic clays are not similar. When the degree of saturation

is 44%, 66%, 88%, and 100% for low plastic clays, the resistivity value decreases 9.7, 8.9, 4.7, and 5.5 times from the initial value. It can be concluded that the impact of the liquid limit is higher for low plastic clays at a higher degree of saturation.

There can be an explanation for the observed variations in resistivity found among the samples due to clay-water interaction. Clay structure has a net negative charge in the surrounding area, which attracts a positive area of water ions and binds them to clay. As surface charges increase, it becomes more likely that water can adsorb on the surface. As a result, moisture can overcome the barrier between particles with an increased affinity for water. By Abu-Hassanein et al. (1996), they were able to find a similar result when measuring changes in resistance as a function of the liquid limit at optimum moisture content.

5.2.1.4 Effects of Plasticity Index

Changes in electrical resistivity with plasticity index are also evaluated from the laboratory test results (Figure 5-6). The rate of changes is different for different resistivity at different saturation levels. The maximum measured resistivity value is also decreased with the increasing degree of saturation. The coefficient of correlation measured at each degree of saturation level was found at acceptable ranges. However, the r^2 value was found to be increasing with the degree of saturation; at 100% degree of saturation, the value was calculated as 0.76. Thus, 76% of the changes in electrical resistance at 100% saturation can be explained by the plasticity index.

In all four cases, the resistivity value decreases with the increasing plasticity index. In addition, as saturation increases, the effect of plasticity index on resistivity value decreases. Resistivity value decreased 9.5, 10.3, 6.3, and 6.9 folds from the initial value when the degree of saturation was 44%, 66%, 88%, and 100%, respectively, for plasticity index from 11 to 49.5.
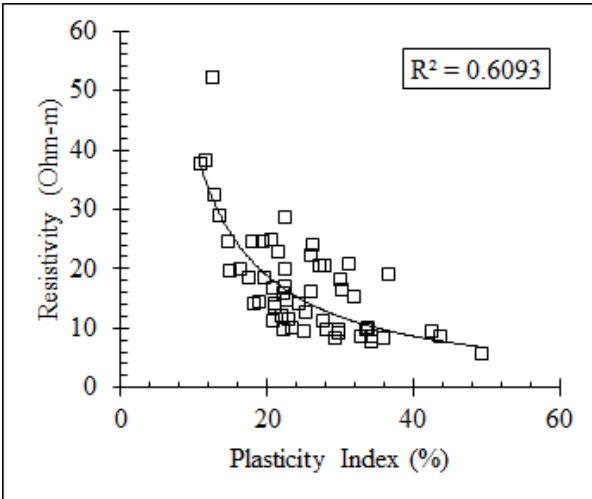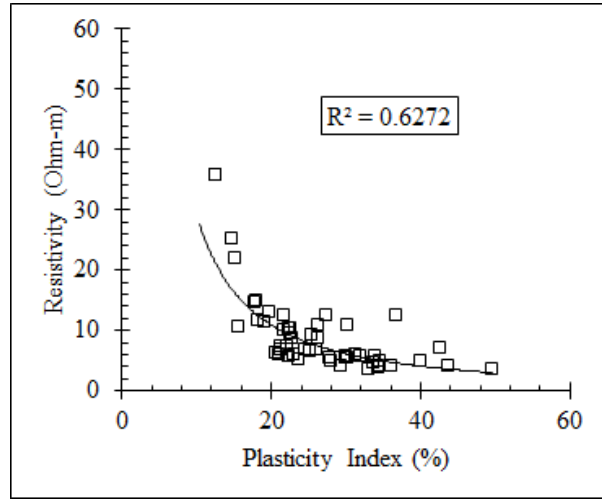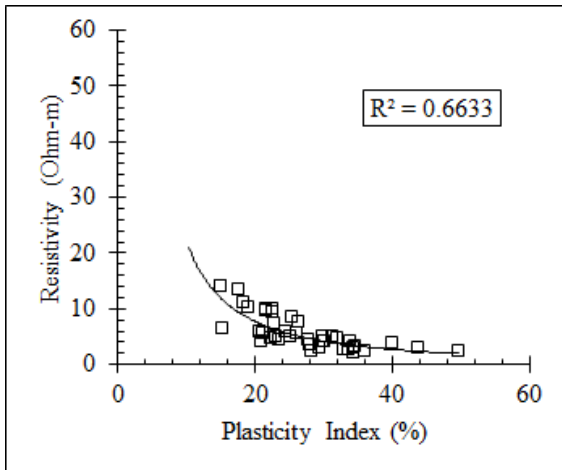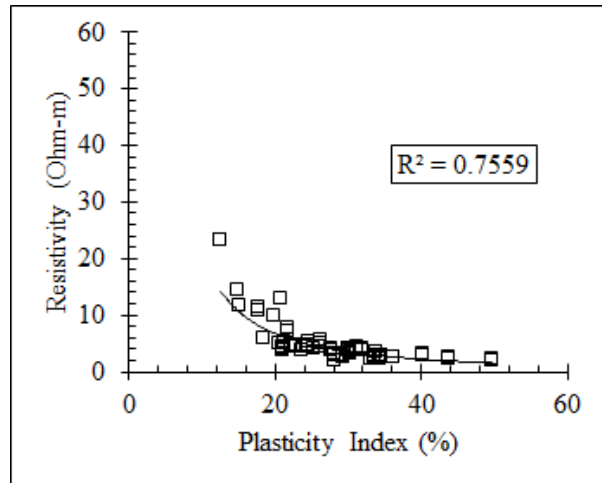
Sr = 44%	Sr = 66%
Sr = 88%	Sr = 100%

Figure 5-6 Relationship between electrical resistivity and plasticity indices at different degrees of saturation

When the PI of soil crosses 40, the impact of PI on the resistivity value is minimal when the degree of saturation reaches 44%, whereas when the percentage of saturation is 100%, the impact of PI on the resistivity value is minimal when the percentage of saturation reaches 20. As the degree of saturation increases, so do the correlations, which get stronger as the level of saturation increases. It has been found that as the clay content in any soil increases, the plasticity index will also increase. When clay content is increased, it decreases resistivity value at higher

saturation levels, which leads to very low resistivity values at higher saturation levels. It is concluded, in this case, that the minimum resistivity is found at 100% saturation.

5.2.1.5 Effects of Activity

In fine-grained soils, activity is defined as the ratio between the plasticity index and the percent fine, and it allows distinguishing mineralogical differences between them. The Figure 5-7 shows the relationship between activity and the changes in electrical resistance at 100% saturation at 100% degree of saturation. Based on the calculated values, it is evident that the soil electrical resistivity value is decreasing with increased activity in the soil. On the other hand, the activity of any soil is directly related to the plasticity index of that soil. The change in resistivity with activity, therefore, follows a similar pattern to the change in resistivity with the plasticity index. Despite the fact that the pattern is similar to the previous one, the equation used to correlate resistivity with activity is different. Using the equation and experimental results as inputs, the correlation coefficient was found to be 0.7131.

$$Resistivity = 2.2491 \times Activity^{-1.383}$$
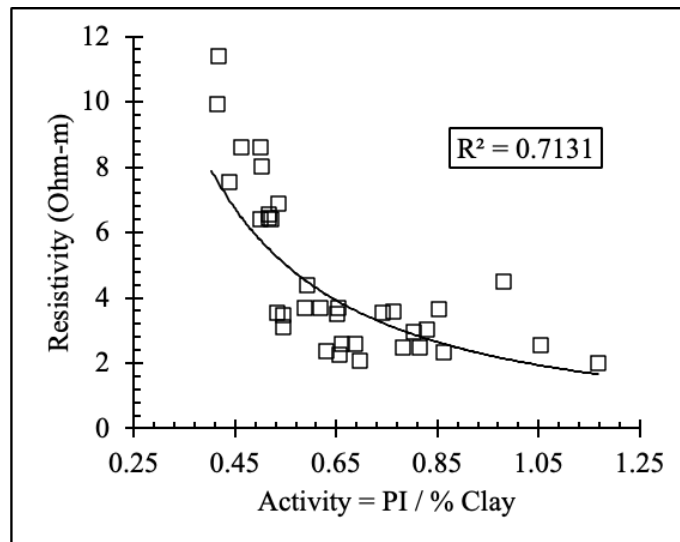
Figure 5-7 Changes of resistivity with the activity of soil

The impact of activity also depends on the degree of saturation. The relationship between activity and resistivity at a lower degree of saturation was not significant. From the graph, it can be concluded that the impact of activity decreased when the activity of the soil was found higher than 1.25.

5.2.1.6 Effects of Pore Water Conductivity

It was examined how the electrical resistivity of soil samples relates to pore water conductivity in the laboratory (Figure 5-8). Three levels of saturation were used to determine the changes in resistivity: 50%, 75%, & 100%. The coefficient correlation was found to be significant in all three cases and is greater than 0.70. In addition, the relationship was found to follow a power function with changes in pore water conductivity. From this figure, the following relationships can be observed.

For Sr = 50%, $Resistivity = 425 \times (Pore\ water\ conductivity)^{-0.487}$

For Sr = 75%, $Resistivity = 476.62 \times (Pore\ water\ conductivity)^{-0.546}$

For Sr = 100%, $Resistivity = 216.45 \times (Pore\ water\ conductivity)^{-0.494}$

The presence of precipitated ions from the clay structure is indicated by the conductivity of the porous water. It was found that the pH of the pore water extracted from the natural soil sample was slightly basic (7.06 to 7.38 in nature), which induced a favorable environment for the precipitation of surface ions. Under current application, the highly precipitated ions in pore water may enhance the conductivity in clays, which will result in a low value of resistivity in the pore water.

111
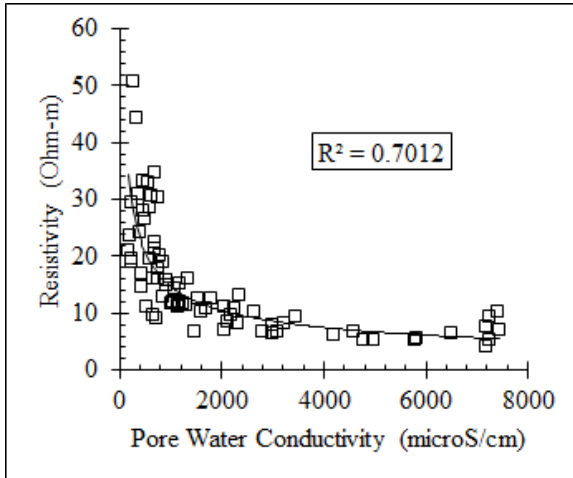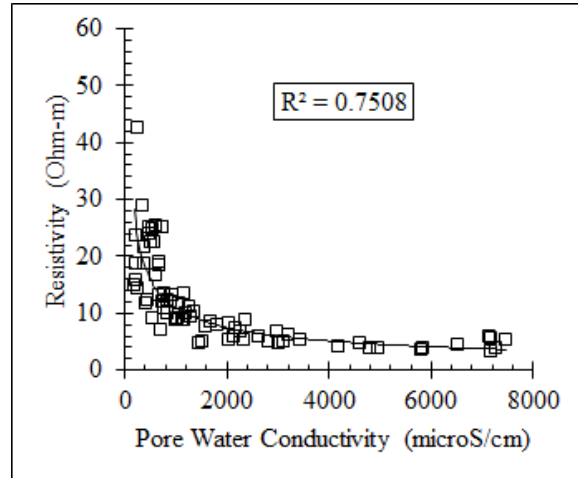
Sr = 50%   Sr = 75%
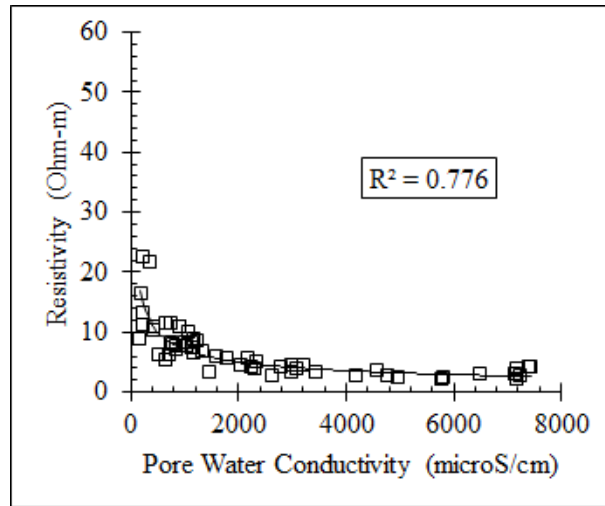
Sr = 100%

Figure 5-8 Relationship between electrical resistivity and pore water conductivity at different degrees of saturation level

5.2.1.7 Effects of Sulfate Content

The concentrations of sulfates in extracted pore water varied significantly among samples based on conductivity tests. As a result, the sulfate ions in the pore water were correlated with resistivity at various saturation levels. The soil samples will have a higher pore water conductivity when sulfate ions are present. The Figure 5-9 illustrates the relationship between these two

parameters. According to the figure, as the sulfate content increases, so does the conductivity of the pore water.
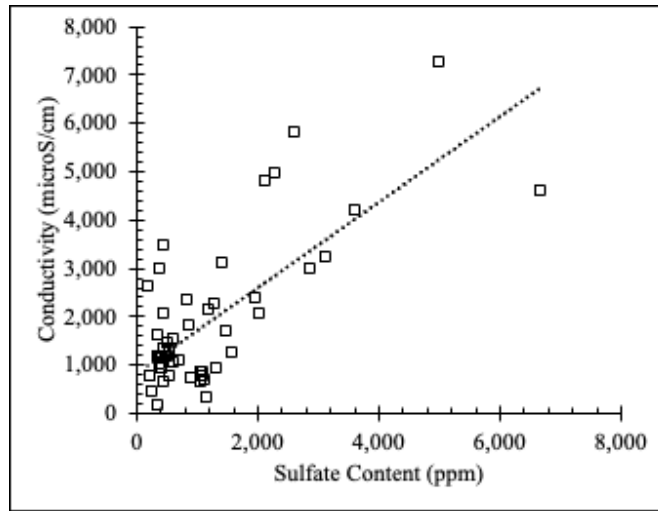
Figure 5-9 Relationship between sulfate content and pore water conductivity

A relationship was observed between sulfate content and resistivity in the Figure 5-10. There is significant evidence that an increase in sulfate ions results in a substantial reduction in resistivity. This change in the resistivity of the material was not similar in all levels of saturation. Increasing saturation leads to a declining impact of sulfate content on resistivity values as a function of sulfate content. At high concentrations of sulfate, the observed variations may be caused by ionic conduction enhanced by the high concentration of sulfate.
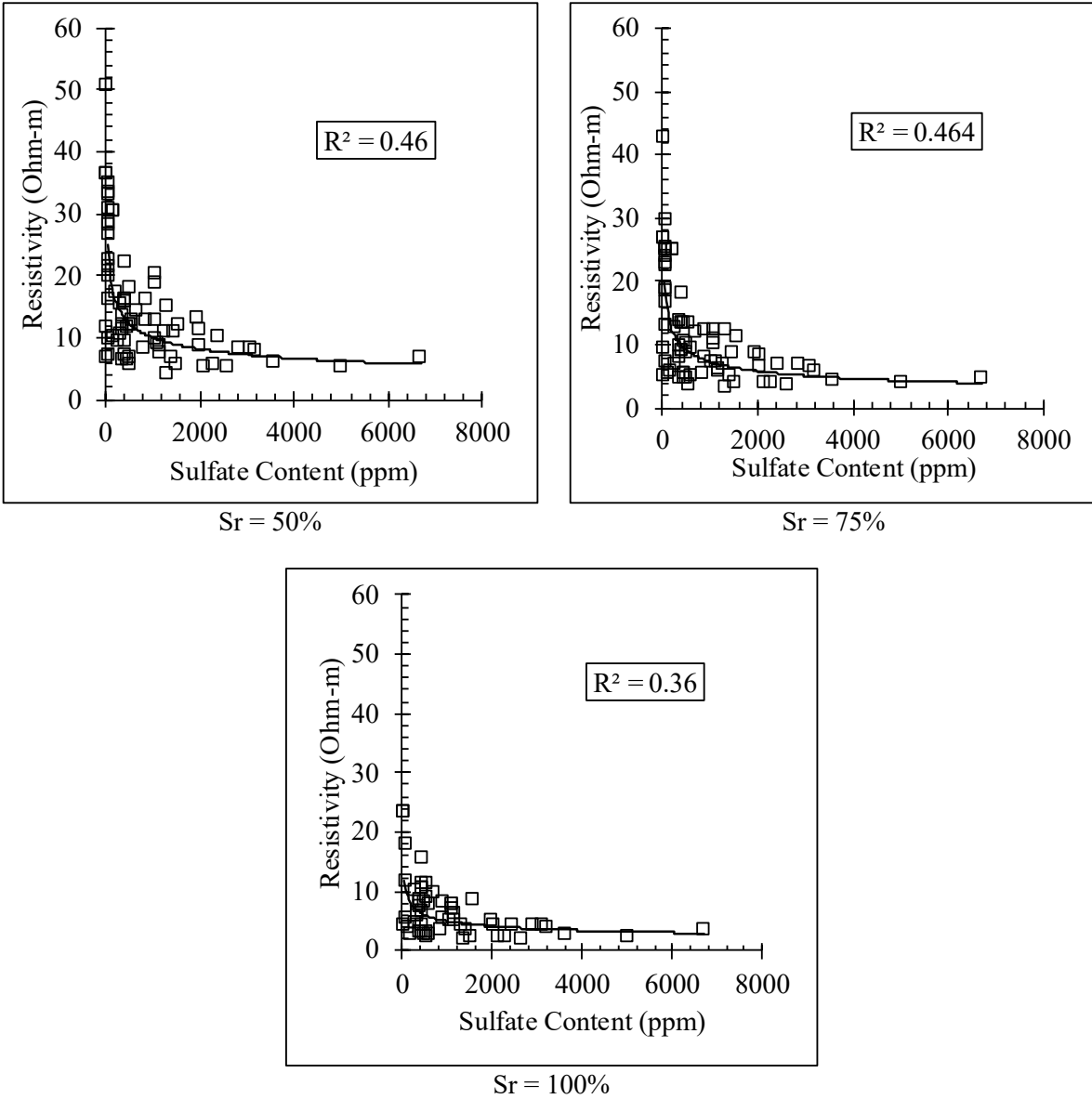
Figure 5-10 Relationship between resistivity and sulfate content at various saturation level

5.2.1.8 Effects of CEC

A study of the resistivity values at variable cation exchange capacities was carried out for compacted clay samples, as shown in Figure 5-11. In order to calculate the CEC, the correlation provided by Farrar was used. Different researchers have evaluated the validity of the equation. It has been observed that the results of resistivity measurements for the specimens at a specific degree of saturation and temperature are different. Depending on the type of isomorphous substitution

carried out on the clay particles, variation may occur. On the basis of the experiments in the scatter plots, it could be seen that the regression coefficients were the highest in power fitted trend lines. Thus, a power function fitting model was used to try and fit the experimental results.
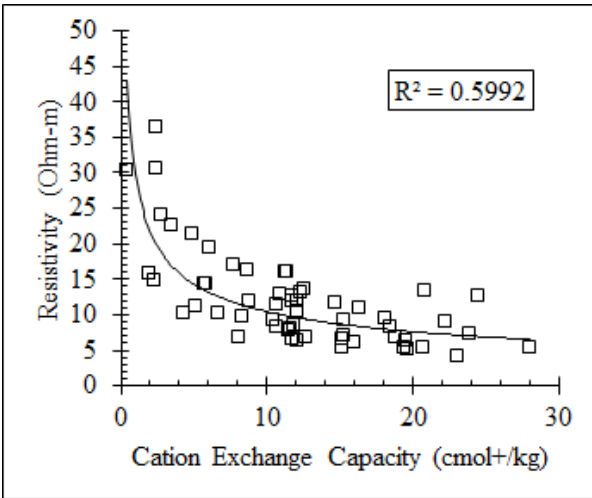
Sr = 50%
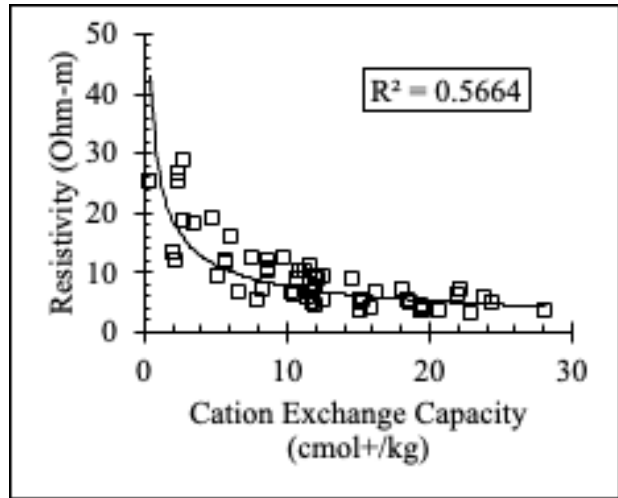
Sr = 75%
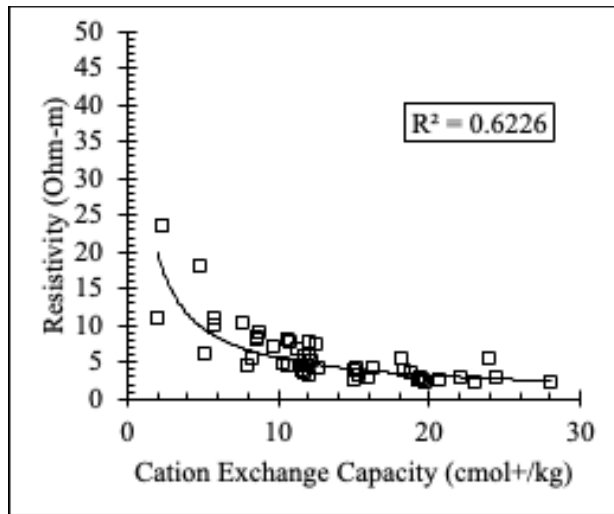
Sr = 100%

Figure 5-11 Relationship between electrical resistivity and cation exchange capacity at different degrees of saturation level

With increasing moveable ions in the pore water of the soil, the electrical conductivity of the soil increases. Because of the presence of conductive ions in the soil, a decrease in soil resistivity was observed with an increase in CEC. It was reported by Mitchell and Soga (2005) that cation exchange reactions had not been found to induce structural changes in clays. There may, however, be a significant variation in physical and physicochemical properties due to the change in CEC. However, a high degree of saturation (e.g., S = 100%) resulted in a lower sensitivity of resistivity to the effect of CEC.

With the increase in the amount of CEC, there was a decreased rate of reduction in electrical resistivity. When a specific level of saturation is reached, the mobility of precipitated ions has a tendency to decrease as the CEC increases. As a result, at high CEC compared to low ion exchange conditions, the response curve was flatter.

5.2.1.9 Effects of SSA

In this study, the specific surface area (SSA) of compacted clays was determined by using the Farrar and Coleman (1967) correlation. As shown in the Figure 5-12, the observed SSAs were plotted against electrical resistivity at different levels of saturation. As the SSA of the specimens increased, the overall resistivity of the specimens was observed to decrease. In fact, as the SSA of the specimens increased, the reduction rate of the specimens varied. Due to the increase in surface saturation due to SSA changes, the conductivity due to changes in SSA will decrease as the degree of saturation increases. Additionally, at any given degree of saturation, the effect of SSA on resistivity decreases with the increase of SSA. Therefore, the greater the SSA, the lower was the resistivity. Although the SSA can have a significant effect on resistivity, there is a cutoff point after which SSA does not have any effect at all. This is the point where the electrical connectivity's

of the conductors are already established. Once the electrical connection is established, an increase in SSA will not affect the resistivity value.

Sr = 50%

Sr = 75%

Sr= 100%
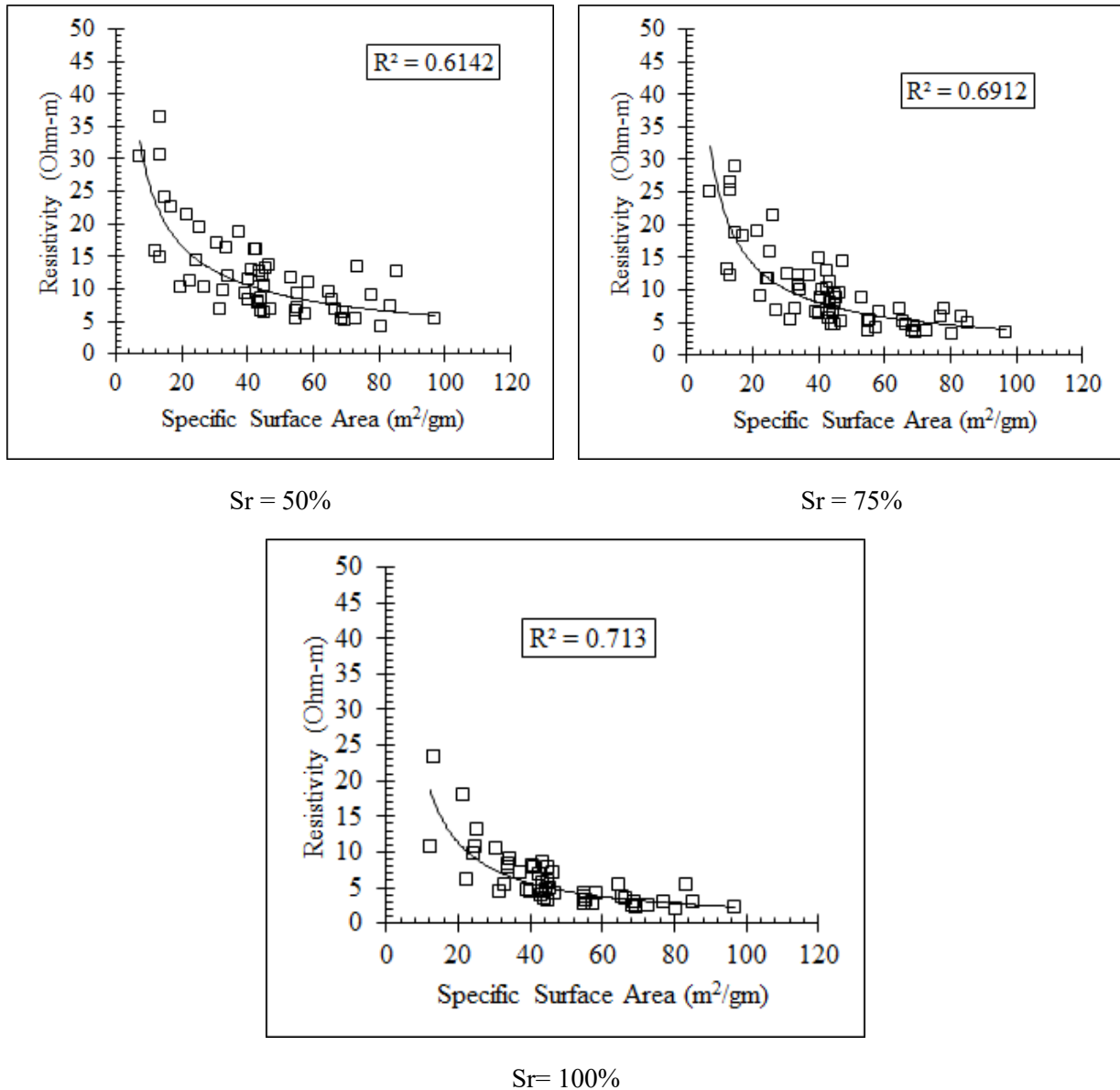
Figure 5-12 Relationship between electrical resistivity and specific surface area at different degrees of saturation level

5.2.2 Influential Parameters Related to Phase Relationship

In compacted clays, the influence of gravimetric moisture content, void ratio, unit weight, volumetric moisture content, and degree of saturation was examined individually. However,

117

volumetric moisture content and degree of saturation are determined by gravimetric moisture content, dry unit weight, void ratio, and specific gravity. The electrical resistivity responses of compacted clay are studied under a variety of conditions, including gravimetric moisture content, dry unit mass, void ratio, volumetric moisture content, and saturation degree.
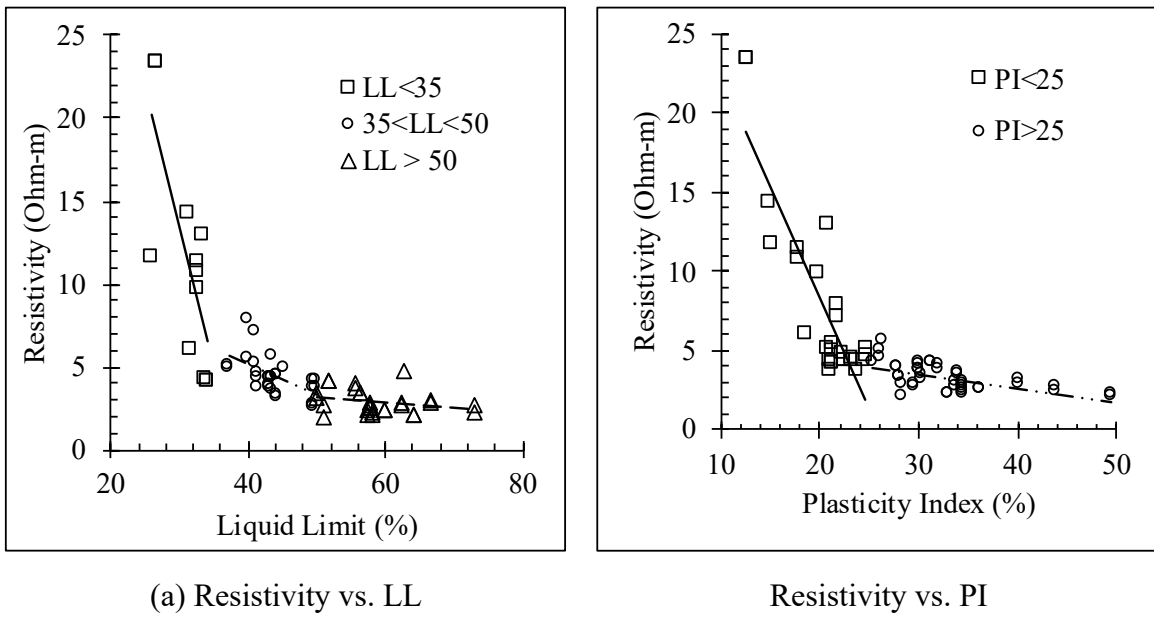
(a) Resistivity vs. LL   Resistivity vs. PI

Figure 5-13 Changes of resistivity with liquid limit and plasticity index

The influences of the Atterberg limit on the electrical resistivity properties of clayey soil samples are shown in the Figure 5-13. All the clayey soils can be separated into three categories based on the changes of resistivity with the liquid limit of individual soils. The changes in resistivity were observed very steep when the liquid limit of the soil sample was found to be 35%. From liquid limit observed greater than or equal to 35 to less than 50, the changes of resistivity were not found as steep as the previous one. When the liquid limit is greater than 50, the changes of resistivity with the liquid limit were not very impactful. A similar observation was made when the changes of resistivity were examined with the changes of plasticity index. When the plasticity index was lower than 25, the changes in resistivity were steep. But the slope changes when the plasticity index value was found greater than 25.

Based on the observations in Table 5-1, all clayey soil samples are divided into six different categories below-

Table 5-1 Soil Categories

Category (i)	Category (iii)	Category (v)
LL>50, PI>25; 209	35<LL<50, PI>25; 185	LL>35, PI>25
Category (ii)	**Category (iv)**	**Category (vi)**
LL>50, PI<25; 59	35<LL<50, PI<25; 158	LL>50, PI>25; 71

5.2.2.1 Effects of Gravimetric Moisture Content

This Figure 5-14 represents the variation of electrical resistivity of a clayey soil with different gravimetric moisture contents at variable dry unit weights. It was found that moisture is a significant factor affecting the electrical resistance of the soil. In this study, the average resistivity value was found to be 82.69 Ohm-m with a standard deviation of 32.51 Ohm-m, 8.91 Ohm-m with a standard deviation of 0.83 Ohm-m, 4.57 Ohm-m with a standard deviation of 0.84 Ohm-m, and 3.01 Ohm-m with a standard deviation of 0.69 Ohm-m for moist content 10%, 20%, 30%, and

40% respectively. However, resistivity responses are different for different soil samples. In the case of the type (i) sample, average soil resistivity decreases 89% of the initial value of 82.69 Ohm-m when the moisture content increases from 10% to 20% at a unit constant unit weight of 11.8 KN/m^3. At the same time, the resistivity value decreases 48% of the initial value of 8.91 Ohm-m and 34% of the initial value of 4.57 Ohm-m when the moisture content increases from 20% to 30% and 30% to 40%, respectively. A similar pattern was observed for other types of soil too.

However, the changes of resistivity were similar for other types of samples except for type (ii). For type (ii) soil, resistivity value decreased 42%, 25%, and 41% of the initial value when the moisture content was increased from 10% to 20%, 20% to 30%, and 30% to 40%, respectively at the unit weight of 11.8 KN/m^3. Activity charts of the soil samples from different categories are plotted in Figure 5-15. From the chart, it is shown that the type (ii) samples are plotted in high activity zone, which enables the soil from this group to possess more surface charges compared to other soil samples.

A substantial reduction in electrical conductivity was observed between 10 and 30% moisture content; however, the rate of reduction stepped down after 30% water content. It is possible to explain the observed phenomenon through the explanation of Pozdnyakov (2006). A graph of electrical resistance versus the natural logarithm of moisture content was divided by Pozdnyakov (2006) into various segments. The curve is divided into segments labeled adsorbed water, film water, film capillary water, capillary water, and gravitational water. The electrical resistivity in the adsorption water zone decreases rapidly with increasing moisture content, according to the author. In the adsorbed water zone, the dipolar water creates a conductive path for electrical current even though the molecules of water are immobile.
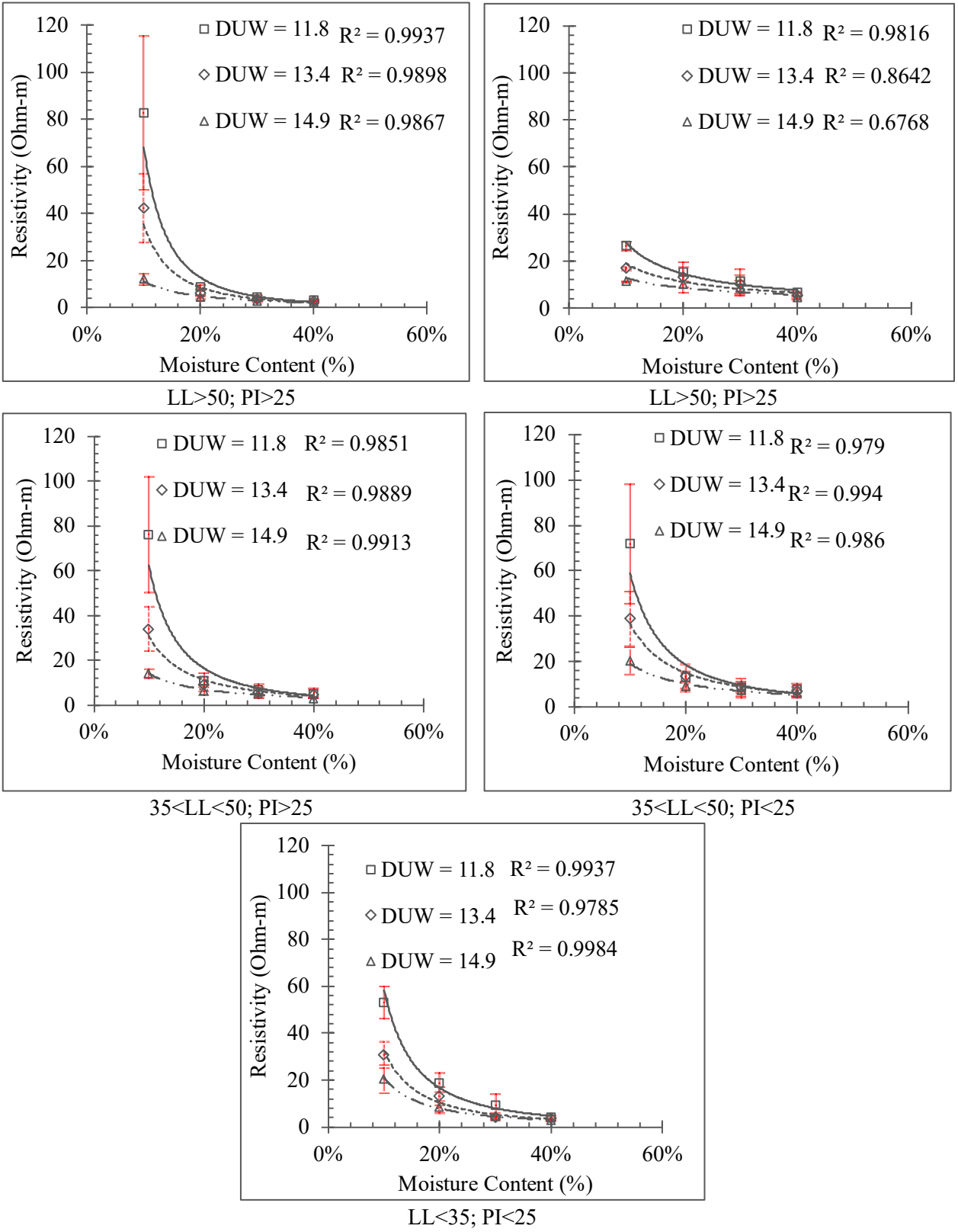
Figure 5-14 Relationship between electrical resistivity and moisture content of the soil

As moisture in the adsorption zone increases, electrical resistivity decreases dramatically. As the Van der Waals force increases in the film water zone, the rate of reduction decreases. Pore water moves from the film to the fissure when the maximum thickness of the water film has been achieved. In the film capillary water zone, molecular attraction is greater than capillary attraction—the film capillary zone and the capillary water zone experience a step-down in the rate of reduction. Water molecules ions move independently of electrical charges in gravitational water zones, so electrical resistance is almost independent of water content.

Changes in resistivity with changing moisture content were also observed at 13.4 KN/m^3 and 14.9 KN/m^3 dry unit weight. A similar downward pattern was observed for all other types of samples. However, the average resistivity value was decreased gradually from type (iii) to type (vi) categories sample. Because the liquid limit and plasticity index are changing and these properties are directly related to sample size so, the clay content is decreasing with the changing category types. As the fine contents decrease, the connectivity between the pore improves, which leads to a decrease in the resistivity value of soils.

Changes in resistivity responses with the changes of moisture content at different unit weights are shown in tabular form in Table 5-2, Table 5-3 and Table 5-4. For category (i), average soil resistivity was observed 82.69 Ohm-m at 10% gravimetric moisture content when the unit weight is observed as 11.8 KN/m3. For category ii samples, the resistivity was observed as 26.43 Ohm-m at the same moisture content and unit weight. At the same time, the resistivity value was observed increased in category (iii), (iv) & (vi) compared to category (ii) in the same condition.

Table 5-2 Resistivity value for unit weight 11.8 KN/m3

Moisture Content	10%		20%		30%		40%	
	Average	SD	Average	SD	Average	SD	Average	SD
I	82.69	32.51	8.91	0.83	4.57	0.84	3.01	0.69
ii	26.43	1.94	15.28	4.13	11.43	5.11	6.73	0.28
iii	76.21	25.82	11.27	3.07	7.19	2.40	5.58	2.03
iv	71.75	26.48	13.13	2.50	8.63	2.37	7.61	2.50
v	53.20	6.92	18.75	4.04	9.13	4.99	7.77	4.27

Table 5-3 Resistivity value for unit weight 13.4 KN/m^3

MC	10%		20%		30%		40%	
	Average	SD	Average	SD	Average	SD	Average	SD
I	42.25	14.73	6.25	1.47	3.57	0.71	2.68	0.49
ii	16.83	0.73	13.08	4.44	9.83	4.05	5.30	0.76
iii	34.12	9.72	9.57	3.13	6.02	2.20	4.84	1.75
iv	38.89	12.06	13.52	5.23	8.65	3.68	6.67	2.18
v	30.77	5.57	13.10	4.01	8.76	5.30	6.38	3.77

Table 5-4 Resistivity value for unit weight 14.9 KN/m^3

MC	10%		20%		30%		40%	
	Average	SD	Average	SD	Average	SD	Average	SD
I	12.14	2.39	4.42	0.91	2.77	0.50	2.57	0.58
ii	11.27	0.20	10.12	3.64	8.61	3.32	4.33	0.96
iii	14.25	2.02	6.68	2.12	5.34	2.08	3.33	0.40
iv	20.22	5.92	9.11	2.26	7.21	3.05	5.67	1.82
v	20.41	5.88	11.37	4.68	7.80	4.05	5.33	3.43

On the contrary, the resistivity value was increased from category (i) to category (vi) at the moisture content 20%, 30%, and 40%. Resistivity value increased 71% from category (i) to category (ii), whereas it increased 26%, 47%, and 110% for category (iii), (iv), and (vi), respectively. A similar pattern was observed when the moisture content of the soil sample was increased to 30% and 40%. For category (ii) samples, the resistivity value was increased 150% and 124% from the initial value when the moisture content was increased to 30% and 40%, respectively. For category (iii) samples, the resistivity value was increased 57% and 85% from the initial value when the moisture content was increased to 30% and 40%, respectively. For category

(iv) samples, the resistivity value was increased 89% and 153% from the initial value when the moisture content was increased to 30% and 40%, respectively. For category (vi) samples, the resistivity value was increased 100% and 158% from the initial value when the moisture content was increased to 30% and 40%, respectively.
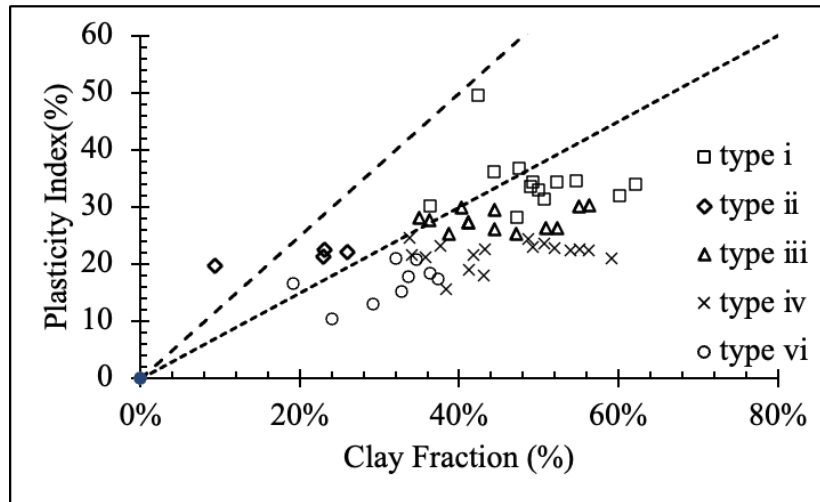
Figure 5-15 Activity chart of tested soils

The relationship between electrical resistivity and moisture content is shown in Figure 5-16 for all soil samples at every moisture content. The resistivity value obtained at each measurement was plotted in the logarithmic scale. The best fitted line was drawn, and the relationship equation was determined. Results obtained by previous researchers are also incorporated in the graph.
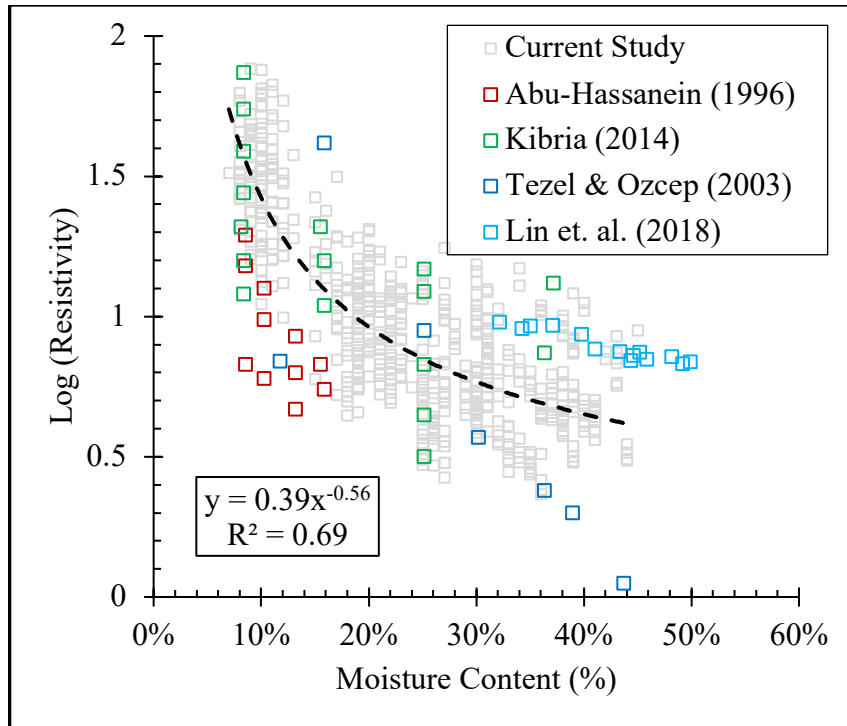
Figure 5-16 Relationship between electrical resistivity and moisture content

5.2.2.2 Effects of Dry Unit Weight

In the Figure 5-17, the resistivity is shown as a function of dry unit weight for different moisture contents. It can be seen from the graph that resistivity decreases with increasing unit weight. The rate of change, however, differs for different samples of the same type. For category (ii) samples, the rate of changes in resistivity was found very less compared to other soil samples. A corresponding decrease in resistivity is predicted for all other types of samples except those mentioned above. It appears that PI, resistivity, and bulk density correlate, despite some soils overlapping in some locations.

Despite being expected (McCarter 1984), the trend suggests that density should be monitored during laboratory resistivity tests. It could possibly be used to measure compaction or improve the ground. Among the moistened samples, there was no significant change in resistivity value with increasing unit weight at 20% moisture content. With the use of an activity chart, it can

be explained the different rates at which resistivity changes for different types of soils. Due to their high activity, type (ii) soils have lower resistance changes than other types of soil, so their activity is less than other types of soil. By having a higher level of activity, the soil sample is able to absorb a greater volume of moisture into the outer layer of the sample and is thus able to establish electron connectivity at a much lower moisture content. This is due to the fact that, as a result, the resistance changes at a relatively low rate for soils of this kind.
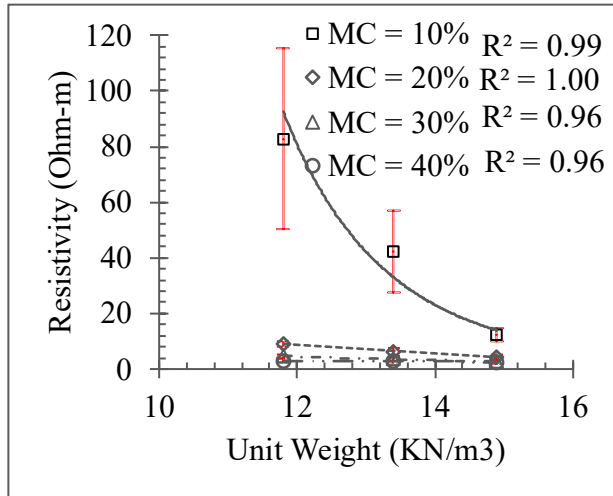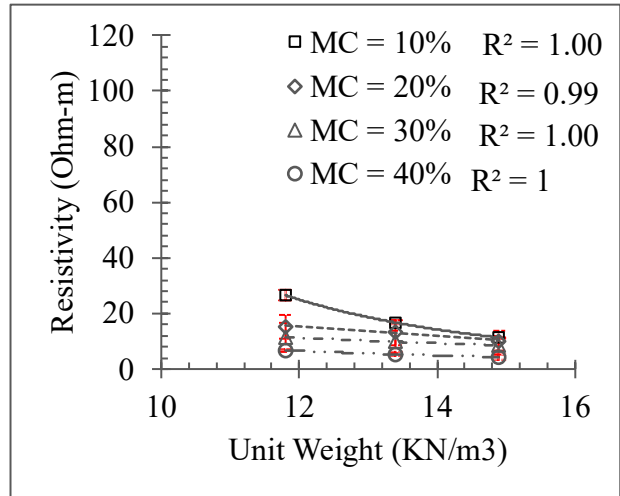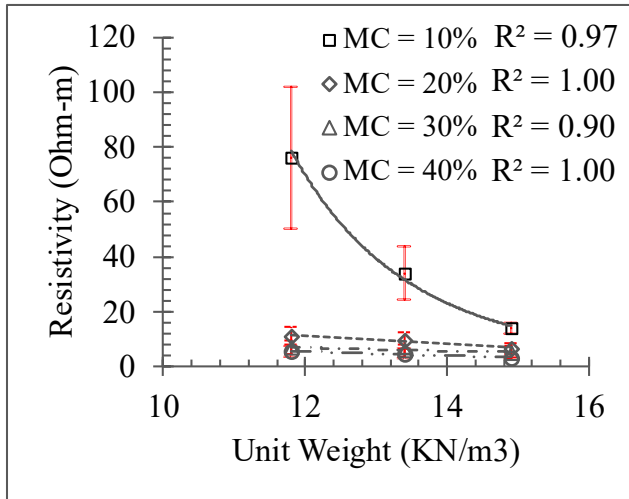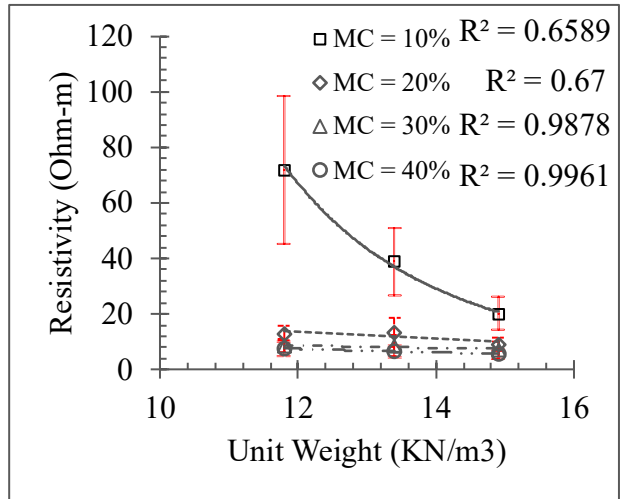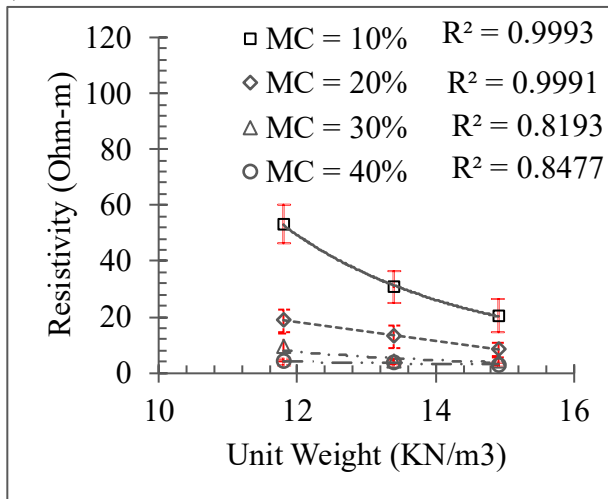
Figure 5-17 Relationship between resistivity and unit weight of compacted soil

5.2.2.3 Effects of Void Ratio

The changes of resistivity with the void ratio at different moisture level was plotted in Figure 5-18 for all types of soil samples. The general trend of the void ratio was observed as the void ratio is increasing, the resistivity value is increasing. Although, the rate of increase is different based on the moisture content and soil type. At lower moisture content, the soil with a higher liquid limit, meaning the fine content is high, tends to show a higher increasing rate. The presence of air voids reduces the interconnectivity of moisture film in the soil grains, which results in a reduction in resistivity. However, the interconnectivity of moisture with soil particles increased with the increase in moisture content and caused a substantial reduction in resistivity.
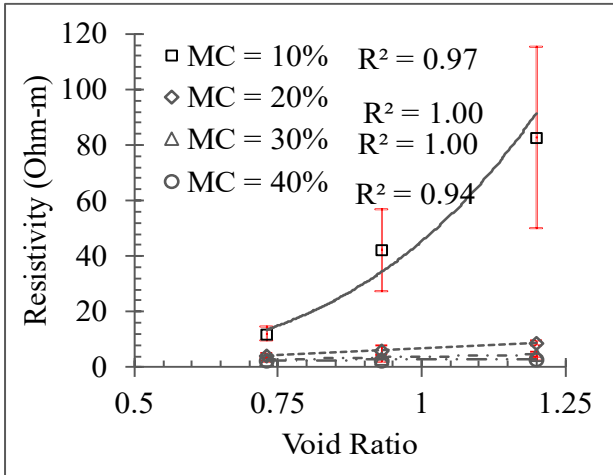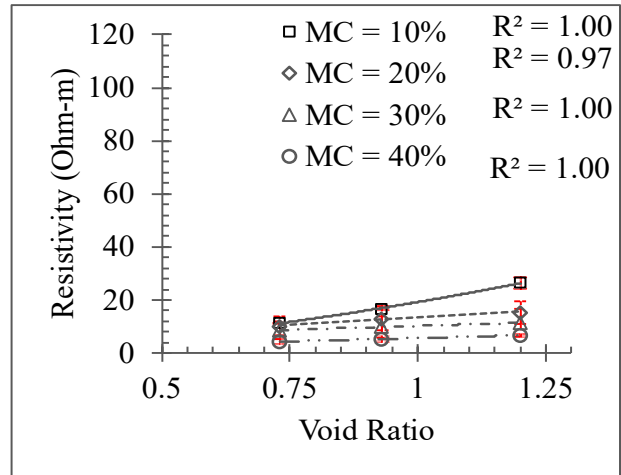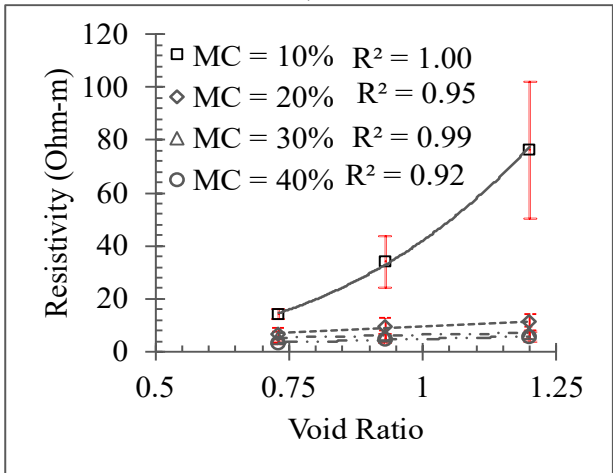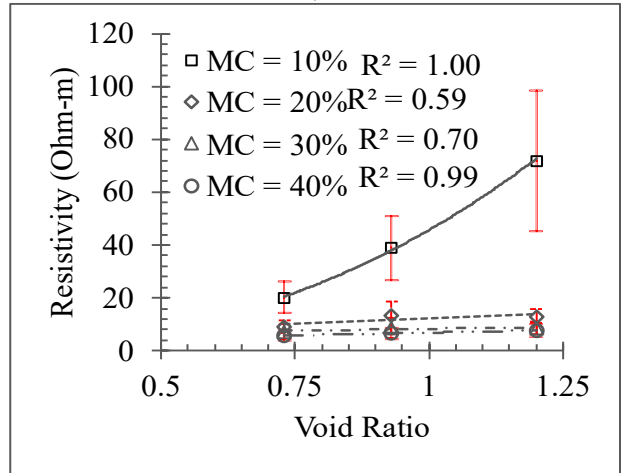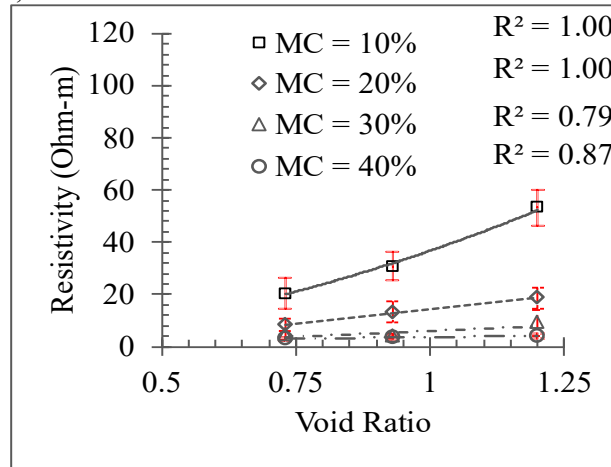
Figure 5-18 Relationship between electrical resistivity and void ratioEffects of Volumetric Moisture Content

The volumetric water content of soils is correlated with the dry weight and gravimetric moisture content. A plot of electrical resistivity results observed in this study was plotted against the volumetric water content of soil samples. Figure 5-19 illustrates how resistance varies with volumetric water content in compacted clay samples. The resistivity changes significantly when the volumetric moisture content changes. The change in resistivity is not linear, but it can be explained using a power function curve. At lower moisture content, the rate of change of resistivity is higher than at higher moisture content. It became evident that moisture began to accumulate on the surface of the particles when the soil sample changed from a dry state to a wet state. When the moisture content ranges were taken into account, the total reduction in resistivity was as much as 44 Ohm-m. According to the study of Mojid & Cho (2006), the observed difference in resistivity in relation to moisture content can be explained. There is evidence that the thickness of the diffuse double layer (DDL) on clay surfaces increases with the increase of moisture, which together with the increase of moisture provides quality bridging among the particles. Furthermore, the precipitated ions in clay surfaces are exposed to moisture and thus increase electrical conductivity when in contact with it.
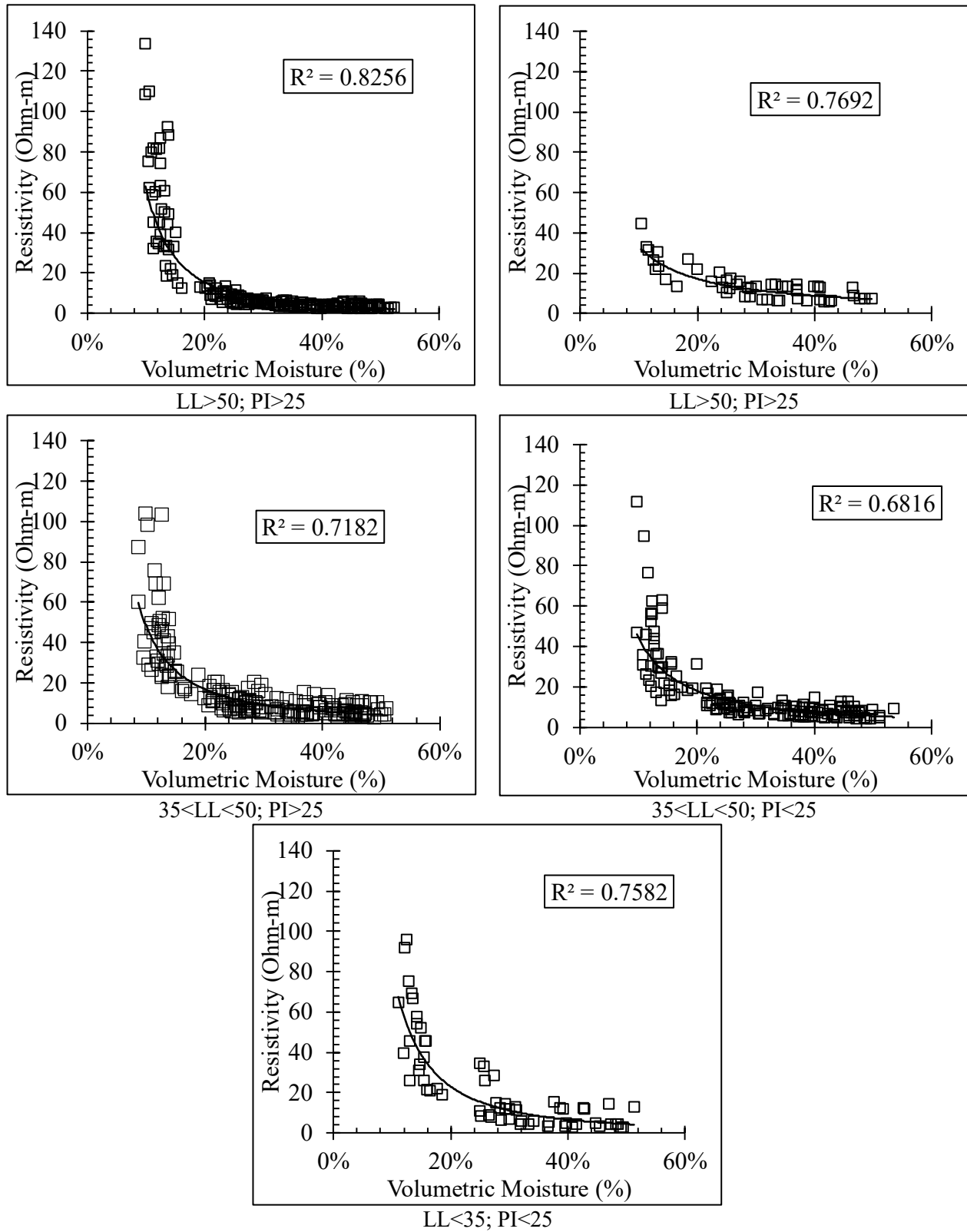
Figure 5-19 Relationship between resistivity and volumetric moisture content

The relationship between electrical resistivity and volumetric moisture content was determined and shown in Figure 5-20. The resistivity values were plotted in the logarithmic scale and the equation for the best fitted line is shown in the graph. Results from previous studies are incorporated in the graph.
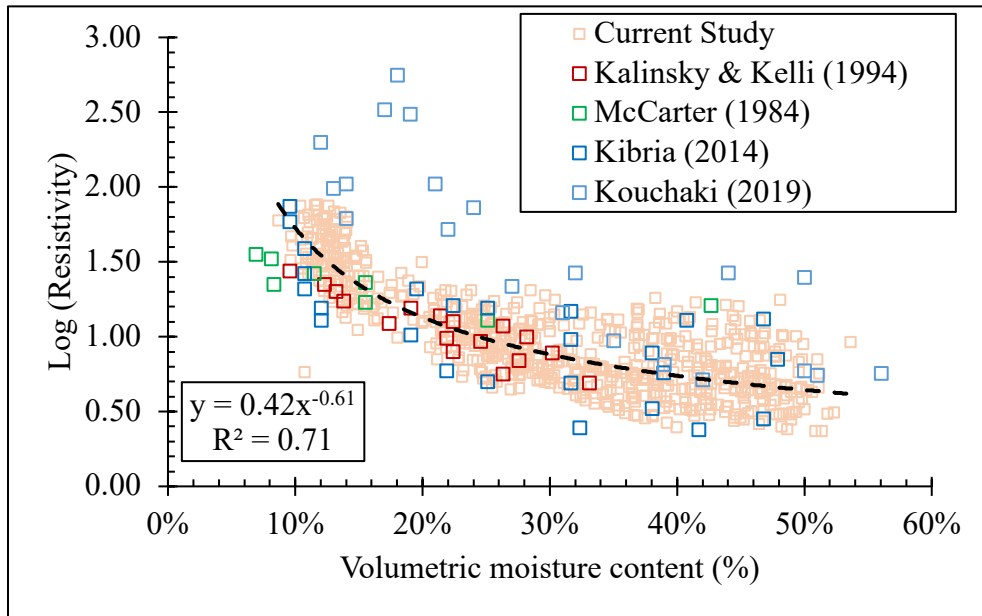
Figure 5-20 Relationship between electrical resistivity and volumetric moisture content

The liquidity index of the soil samples was determined based on the moisture content during the electrical resistivity tests. The liquidity index was plotted against the volumetric moisture content and shown in Figure 5-21. It is evident from the graph that, when the volumetric moisture content crosses 25% barrier, the soil liquidity index value reaches to 0. Therefore, the soil sample enters from solid state to semi-solid state. Thus, the connection between the pore has been established. As a results, the resistivity value decreases very slowly.
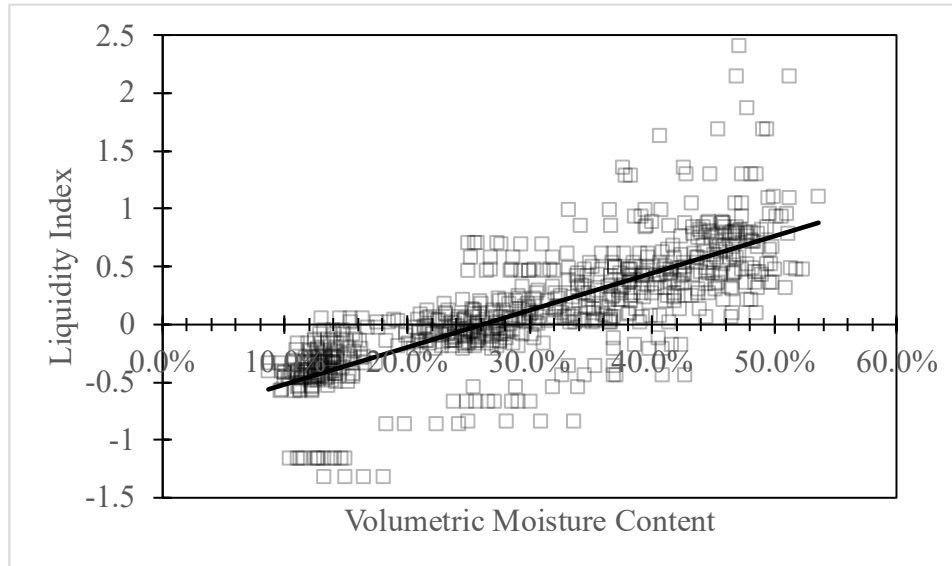
Figure 5-21 Liquidity index vs. volumetric moisture content

5.2.2.4 Effects of Degree of Saturation

The relationship between the degree of saturation and resistivity of various soil types is shown in Figure 5-22. A change in resistivity is similar to a change in volumetric moisture content. This causes the total resistance in these moisture ranges to decrease by 44 Ohm-m. Using the study by Mojid and Cho (2006), it is possible to explain the observed variability in resistivity as a function of moisture content. According to the authors, the double diffusion layer (DDL) thickness increasing as moisture is added to the clay surface provides a bonding mechanism between the particles. Also, the precipitated ions on clay surfaces become more visible when they are exposed to moisture, and this enhances electrical conductivity. It is well known that an increase in saturation is accompanied by a greater degree of particle bridge formation. There is an increase in the connectivity of the pore network at higher saturation levels because the dielectric air voids are reduced. As a result, moisture bridges result in an increased flow of current through a soil mass, resulting in a low level of resistance. In the investigation, the results indicated that resistance decreased with an increase in the degree of saturation.

133
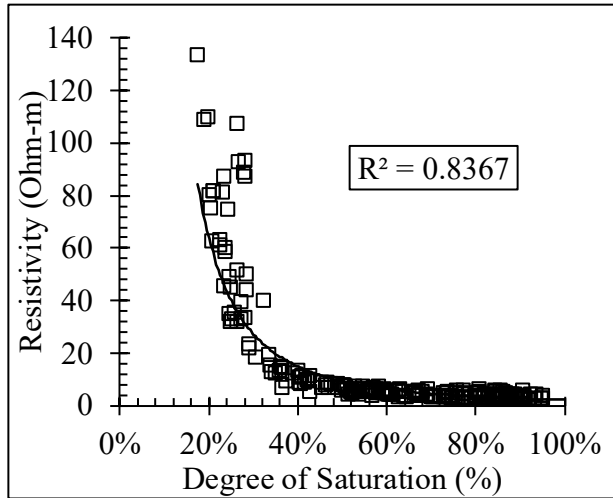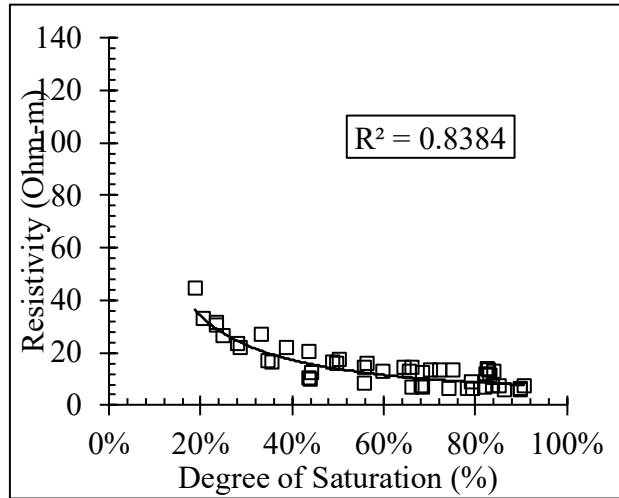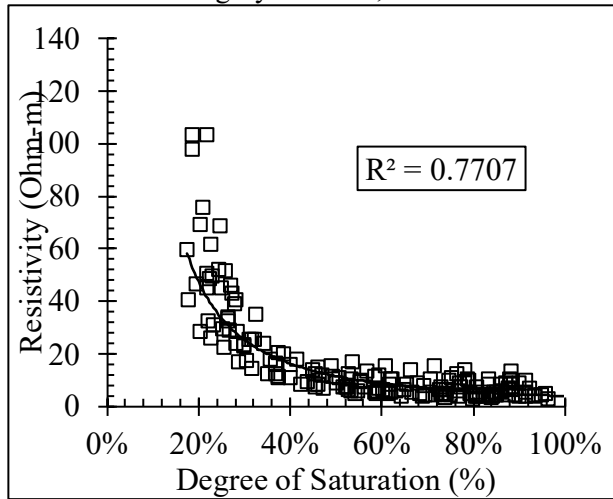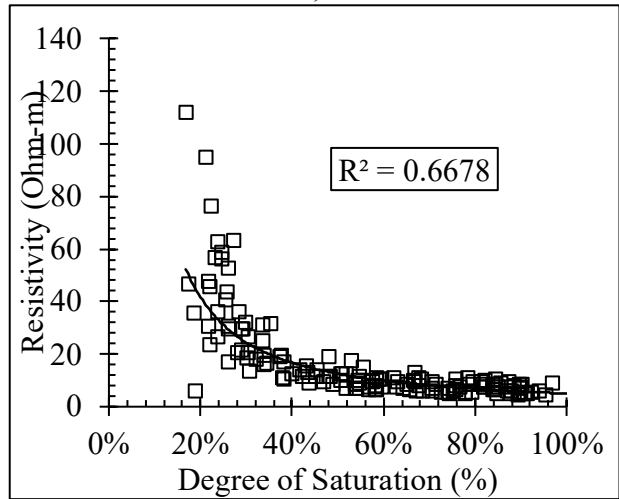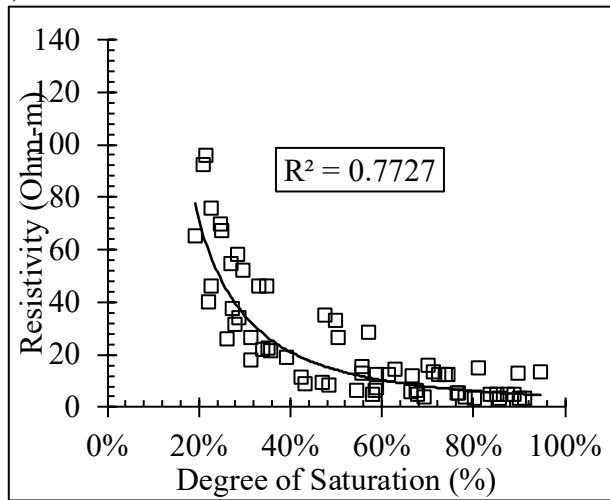
Figure 5-22 Relationship between electrical resistivity and degree of saturation of compacted soil samples

The relationship between electrical resistivity and degree of saturation is shown in Figure 5-23. The results from previous studies are incorporated in the graph shown here. The relationship between the resistivity and degree of saturation can be expressed using the equation obtained from the best fitted line.
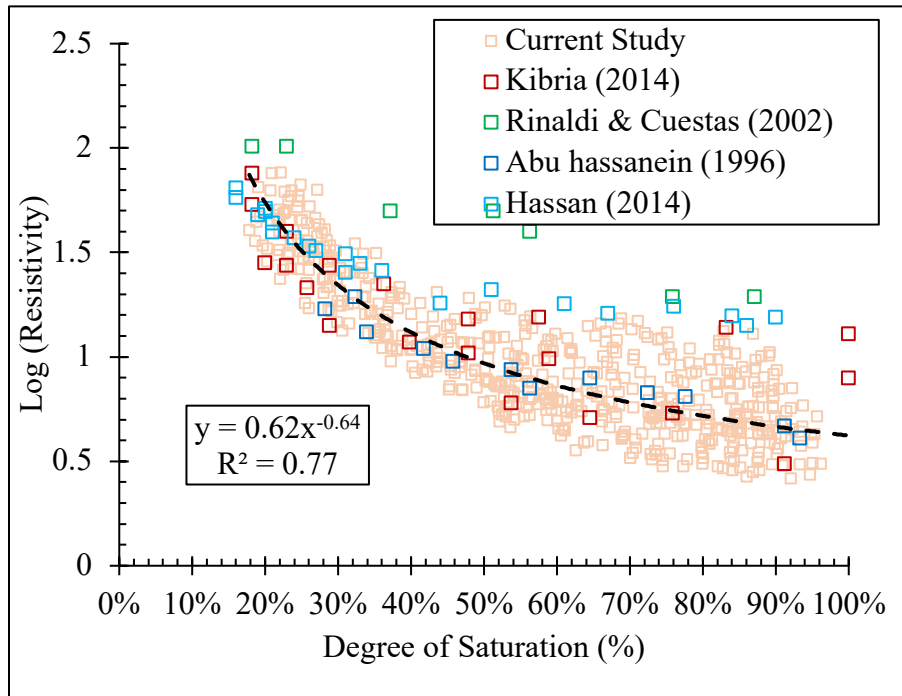
Figure 5-23 The relationship between electrical resistivity and degree of saturation

From the plot of liquidity index vs degree of saturation graph shown in Figure 5-24. It is evident that the soil samples enter the semi solid states when the degree of saturation crosses 50%. The soil samples can no longer be considered as in solid state. Therefore, the connectivity between pore is established in this semi solid state. Thus, the reduction in resistivity value slows down significantly in this stage.
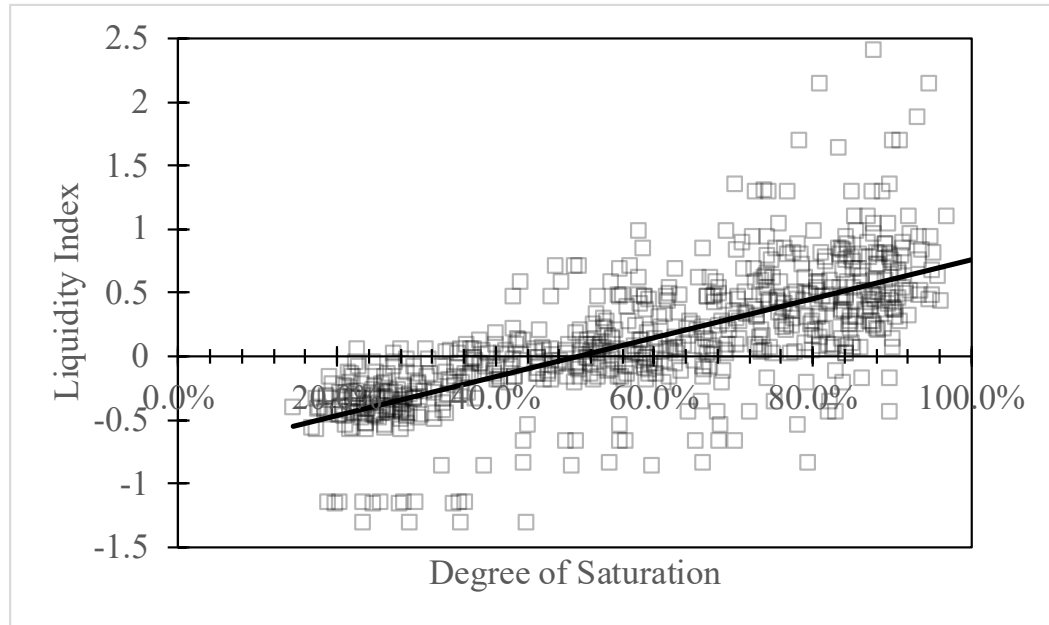
Figure 5-24 Liquidity index vs. degree of saturation

5.3 Resistivity Results for Sandy Soil

5.3.1 Effects of Sand Contents

Changes in electrical resistivity responses with the changes of sand content at various degrees of saturation are shown in Figure 5-25. As high as 78% and as low as 52% sand was examined in the soil samples. The soil sample was categorized into four different degrees of saturation of 44%, 60%, 75%, and 100%. The highest resistivity was observed 61.9 ohm-m at 44% degree of saturation, whereas the maximum observed resistivity was 50.7 ohm-m, 42.7 ohm-m, and 18.7 ohm-m at 60%, 75%, and 100% degree of saturation. Moreover, the Lowest resistivity was observed 13.2, 8.6, 5.9, and 7.9 Ohm-m for the degree of saturation of 44%, 60%, 75%, and 100%, respectively. The reason is deionized water was used to conduct the testing. It was not conducive at all. When the sample is fully saturated, the extra water content resists conducting the electricity as deionized water is used in the experiments. Density increased with the higher fines content, but the sand particles were able to move easily around each other due to their low plasticity

136

(Phan et al., 2016). Consequently, the fine sand mixture will behave similarly to loosen sand in similar conditions. Contrary to the fines content of over 20%, the structure was primarily dominated by fine particles when the fines content exceeded 20%. The relative density of the mixture improved significantly as the fineness content increased, and the stiffness of the mixture was encouraged by the low plasticity of the fines; thus, the mixture behaved as if it were sand.
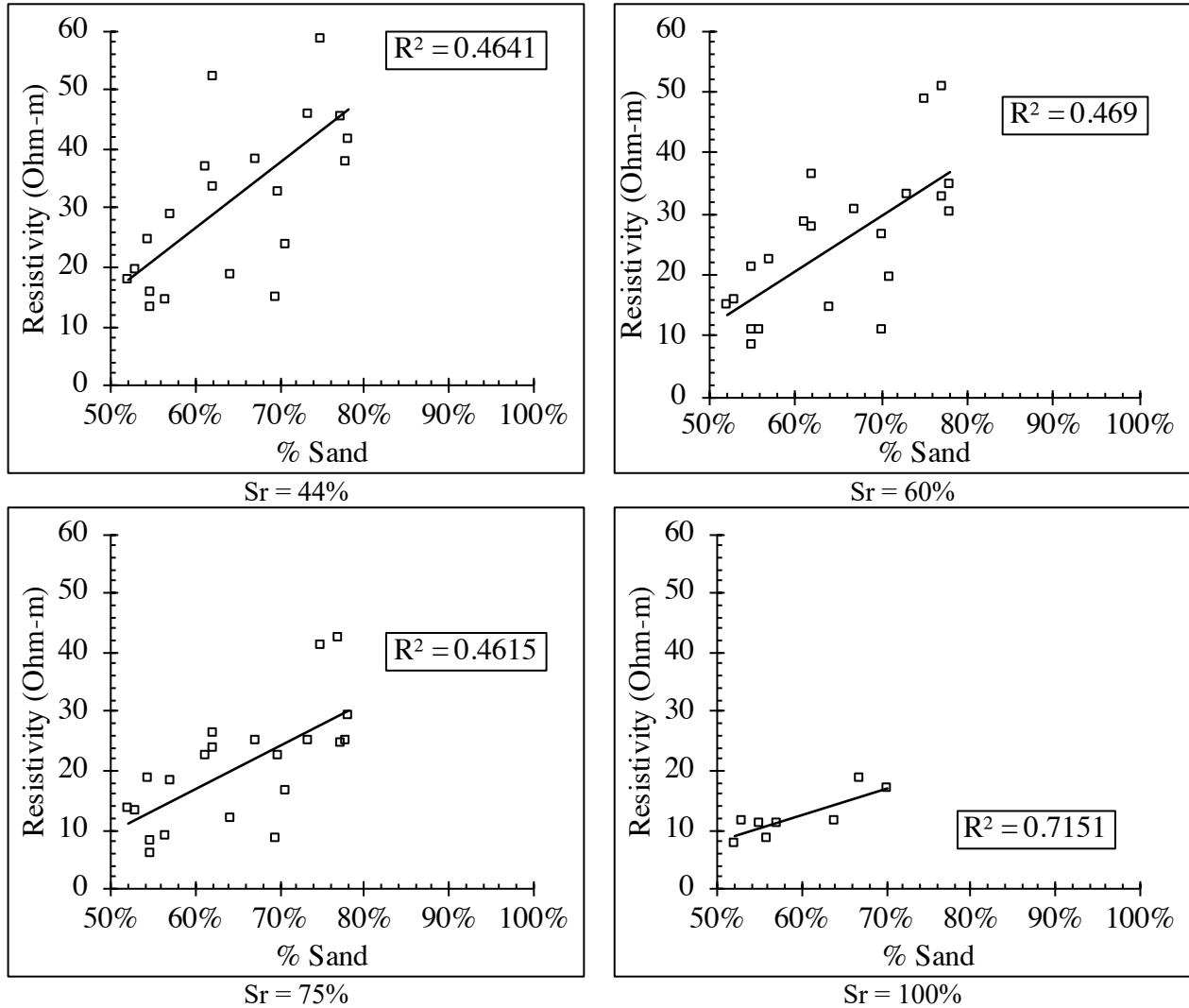
Figure 5-25 Relationship between resistivity and sand percentage

5.3.2 Effects of Moisture Content

Figure 5-26 illustrates how resistivity measurements change when water content changes when employing a resistivity box fitted with electrodes. Similar trends were observed for different unit weights of samples. The best-fitted power function was used to connect the points. The coefficient of correlation was not found significant except at a unit weight of 11.8 KN/m³. Thus, the sandy soil samples are separated into two categories, i.e., silty sand and clayey sand, based on their physical properties.
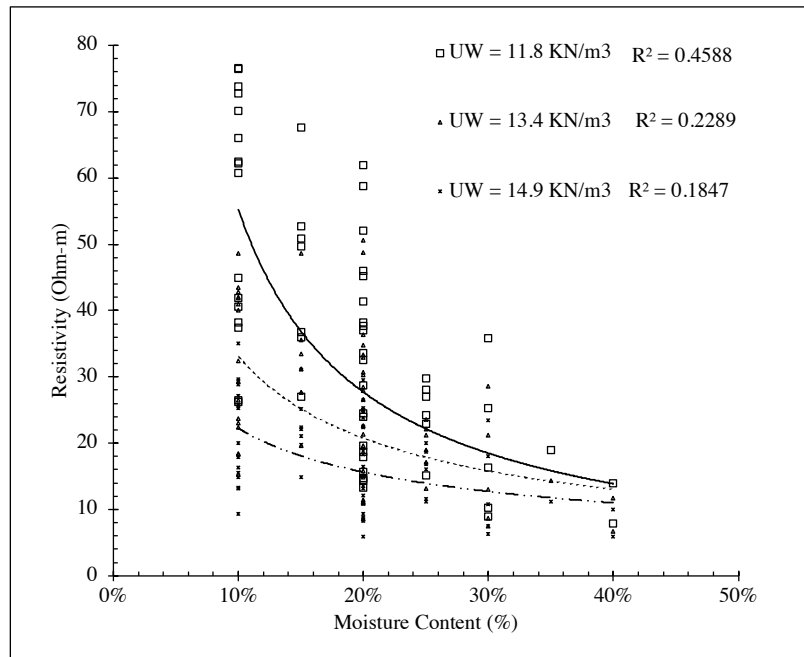
Figure 5-26 Relationship between resistivity and moisture content

The relationship was then further plotted in Figure 5-27, a similar trend was observed here; however, the coefficient correlation was increased. The average and standard deviation in resistivity values is given in Table 5-5, Table 5-6 & Table 5-7 for different unit weights.

The resistivity tends to become nearly constant when the soil water content exceeds about 16%, which corresponds to the onset of saturation in the soil. Dry sand has a high electrical resistivity, and therefore these observations can be explained by that fact (Fukue et al., 1999;

Munoz-Castelblanco et al., 2012). Sand is an amorphous material, so its electrical resistivity is determined primarily by the amount of permeating fluid, porosity, and pore continuity (Gil Lim Yoon & Park, 2001). It follows, therefore, that even when the water content is slightly increased, the resistivity shows a sharp decrease.

| Silty Sand | Clayey Sand |
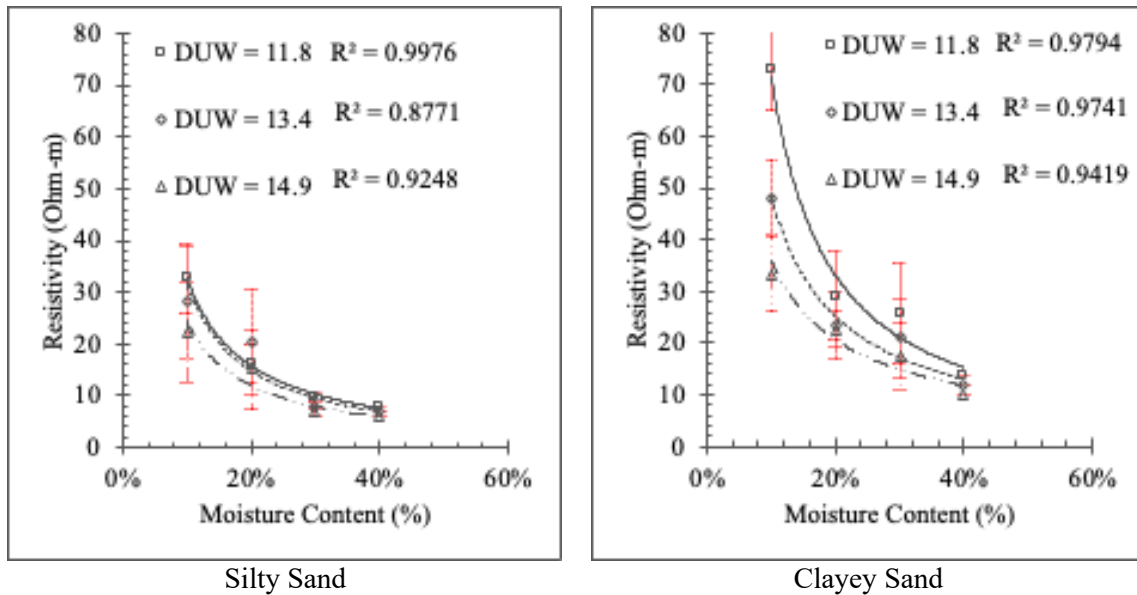
Figure 5-27 Changes of resistivity with moisture for different types of sand

Table 5-5 Resistivity values for unit weight 11.8 KN/m^3

	10%		20%		30%		40%	
	Average	SD	Average	SD	Average	SD	Average	SD
SM	32.61	6.60	16.31	3.65	9.55	.91	7.88	-
SC	73.08	8.07	29.21	8.55	25.83	9.80	13.93	0.28

Table 5-6 Resistivity values for unit weight 13.4 KN/m^3

	10%		20%		30%		40%	
	Average	SD	Average	SD	Average	SD	Average	SD
SM	27.99	10.78	20.29	10.13	8.03	.85	6.75	-
SC	48.09	7.23	23.43	6.62	20.95	7.76	11.69	-

Table 5-7 Resistivity values for unit weight 14.9 KN/m^3

	10%		20%		30%		40%	
	Average	SD	Average	SD	Average	SD	Average	SD
SM	22.22	9.55	15.16	7.56	6.89	0.79	5.87	-
SC	33.29	7.24	22.74	3.49	17.40	6.34	10	-

5.3.3 Effects of Dry Unit Weight

Silty Sand   Clayey Sand
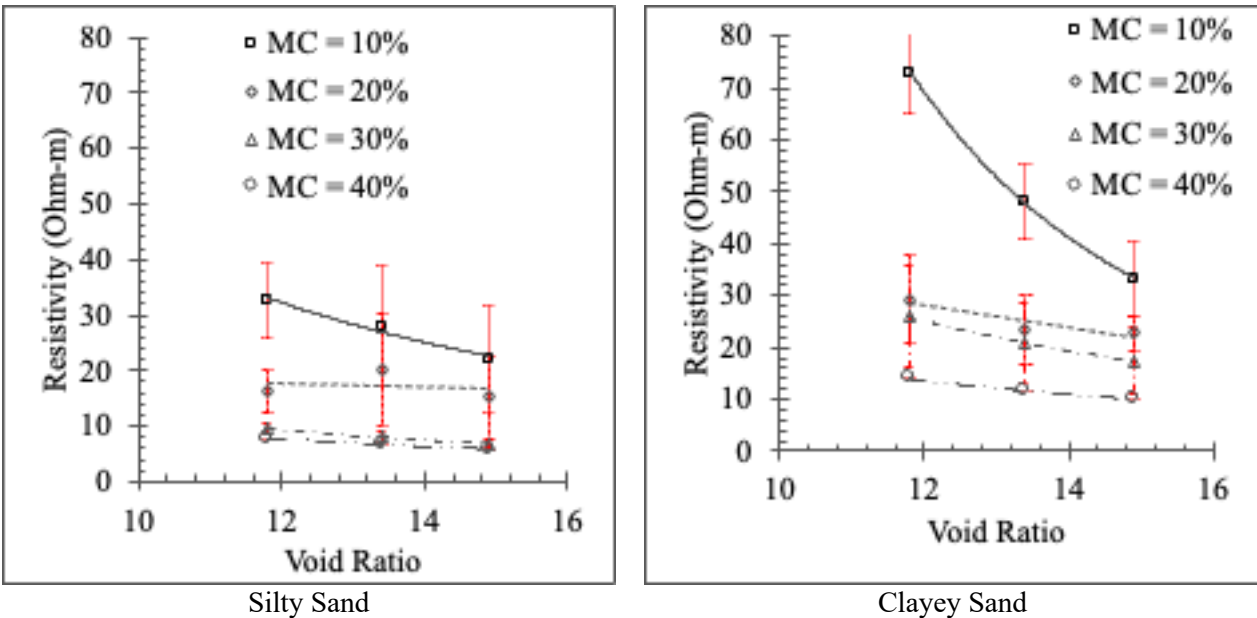
Figure 5-28 Changes of resistivity with unit weight for different types of sand

The relationship between resistivity and unit weight is shown in Figure 5-28. The changes in electrical resistivity for clayey sand are more significant compared to silty sand. Because the presence of fines increases the relative density of the samples; as a result, clayey sand behaved as fines. The presence of more fines restricts the pathway for flowing the electron freely in the soil water mixture resulting high resistivity value at lower moisture content.

The probability distribution function for sandy soil samples was determined for different moisture content. Depending on the probability distribution function of resistivity Figure 5-29 it can be concluded that at lower moisture content, the resistivity varied within a wider range whereas, at higher moisture content, the resistivity does not vary with the sand properties because the sandy samples used in the current study was mixed with clayey and silty particles which contain surface charges.
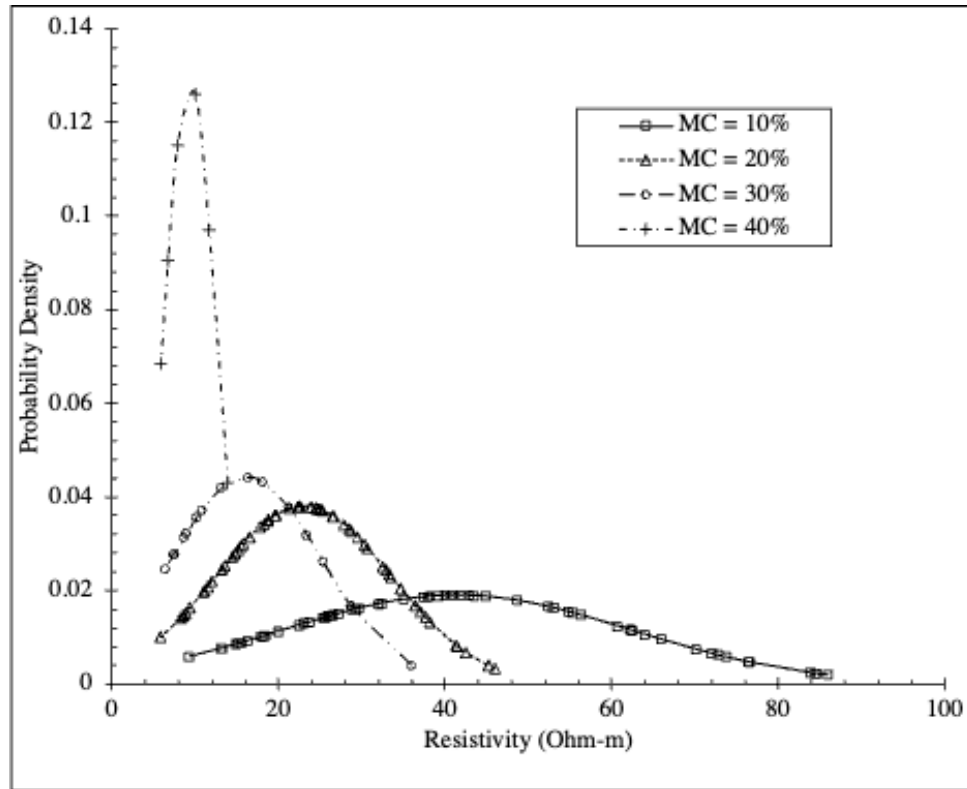
Figure 5-29 Probability density function for resistivity

5.3.4 Void Ratio

The relationship between resistivity and void ratio for both clayey sand and sandy sand is shown in Figure 5-30. The changes are not similar for these two types of sand. The changes in resistivity varied based on the sand contents of the soil. Higher the sand content, higher the resistivity found at lower moisture content. The results obtained for clayey sand are similar to clayey soil because at higher fines contained sand, the behavior of sandy soil is similar to dense sand.

141
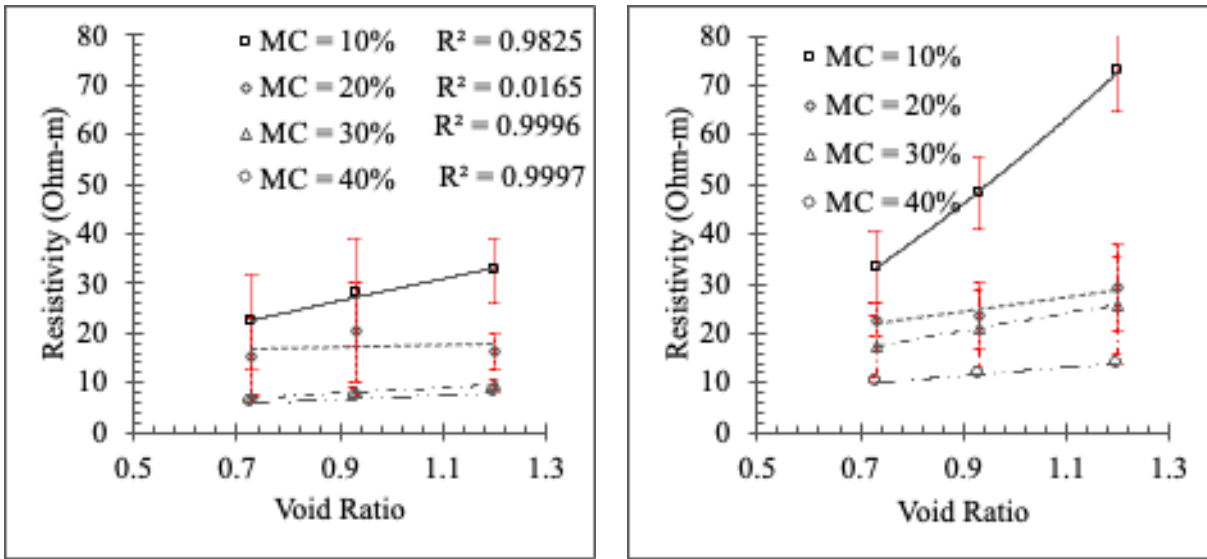
Silty Sand   Clayey Sand

Figure 5-30 Changes of resistivity with the void ratio for sandy soils

5.3.5 Effects of Volumetric Moisture Content

The effect of volumetric moisture content for sandy soil is shown in Figure 5-31. The coefficient of correlation was also measured and found 0.58 and 0.61 for silty sand and clayey sand, respectively. The changes in resistivity rate are different for these two sets of samples because the sand contents are different. Soil electrical resistivity of silty sand decreases 17.8 fold, whereas clayey sand decreases 5.8 fold of the initial resistivity value when the degree of saturation increases from 19% to 93% and 25% to 88%, respectively. Resistivity in silty sand decreases rapidly up to 40% degree of saturation; however, the rate of changes decreases after that.

a) Silty Sand   b) Clayey Sand
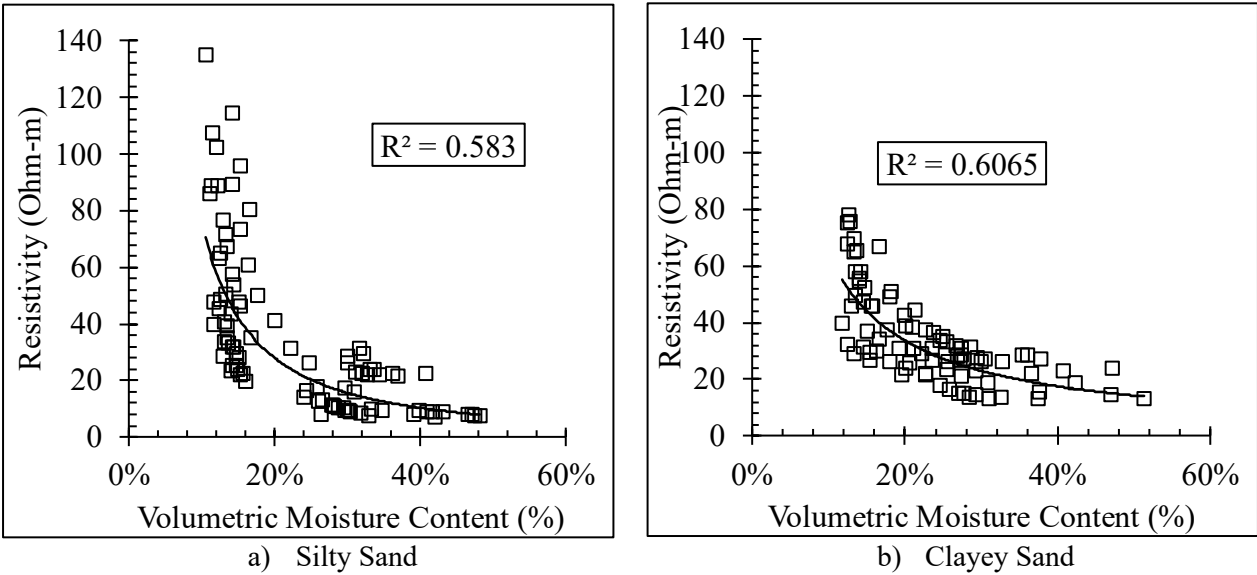
Figure 5-31 Relationship between volumetric moisture content and resistivity

5.3.6 Effects of Degree of Saturation

A decrease in resistivity was observed for all soil types with an increase in saturation, similar to the trend observed for volumetric water content (Figure 5-32). Since sand is saturated at a much lower volumetric water content than clay, using the degree of saturation yields a plot with much easier noticeability between soil types, particularly for high saturation values. The resistivity appears to remain relatively constant above a certain saturation level. It is also not affected by dry density above this level.
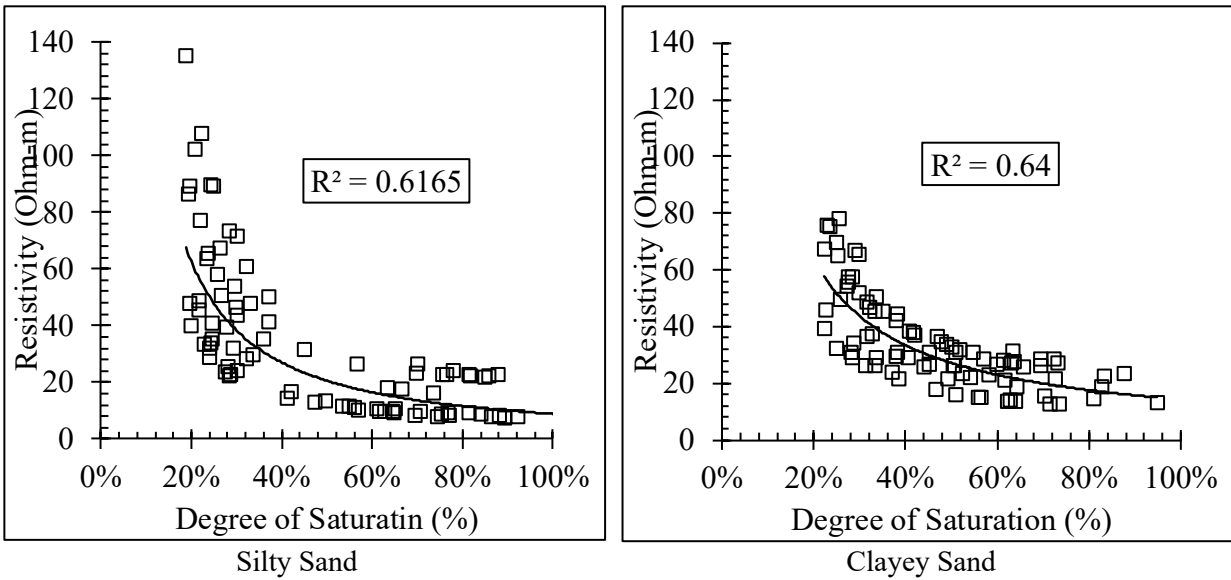
Figure 5-32 Relationship between resistivity and degree of saturation

5.4 Resistivity Results for Undisturbed Soil

Soil resistivity tests were also conducted for undisturbed soil samples. Total eight soil samples collected from the Beaumont district were used for the evaluation. The results are discussed below.

5.4.1 Effects of Moisture Content

Similar to the compacted soil samples, undisturbed soil samples are plotted in Figure 5-33. To evaluate the relationship between resistivity and moisture content. The coefficient of correlation was found to be 0.75. the obtained results were compared with previous research conducted by Kibria (2014). A similar pattern was observed. As the moisture content increases, the resistivity decreases up to a certain level very sharply, then the rate of reduction decreases. When the moisture content exceeds 30%, the resistivity decreases very minimally with the increasing moisture further.
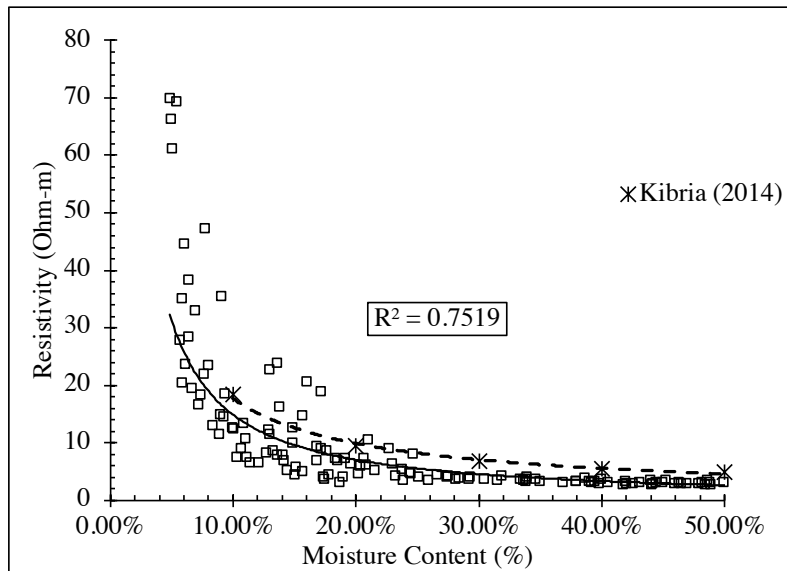
Figure 5-33 Resistivity vs. moisture content for undisturbed soil samples

5.4.2 Effects of Degree of Saturation

Soil electrical resistivity for undisturbed samples was also correlated with the degree of saturation; as the degree of saturation increases, the resistivity decreases (Figure 5-34). After 50% saturation, the changes in the degree of saturation are not significant. The results were also compared with the results tested by Kibria (2014). Though at a higher degree of saturation, the resistivity results were the same, at a lower degree of saturation, the results differ from the equation. Because of the difference in the sample's physical properties, the results are different. Moreover, the degree of saturation is an inherent property of the soil; as a result, the changes of resistivity will be different for any given soil.
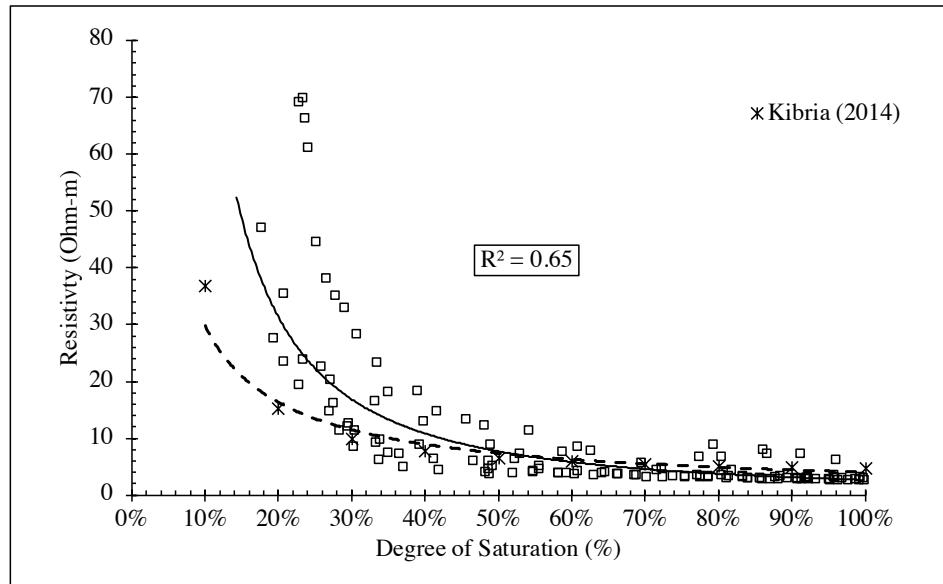
Figure 5-34 Relationship between resistivity and degree of saturation for undisturbed soil samples

5.5 Resistivity Results for Modified Uniaxial Compressive Test

The collected eagle ford shale sample from the City of Irving landfill, TX, was found medium to dark gray, flaky, and very stiff soil. Physical properties were tested in the laboratory for the soil sample and summarized in Table 5-8. The soil sample can be classified as high plastic clay (CH) according to the plasticity chart. Optimum moisture content and maximum dry density were also measured using the standard proctor compaction test for the collected soil samples.

Table 5-8. Physical properties of eagle ford shale

Properties	Values
Specific Gravity (G_S)	2.72
Soil Type (USCS)	CH
Sand (%)	8.5
Fines (%)	91.5
Silt (%)	48.4
Clay (%)	43.1
Liquid Limit	68
Plasticity Index	37
Optimum Moisture Content	21.81%
Maximum Dry Density	15.58 KN/m^3

Soil resistivity was also measured for the soil sample compacted with different compaction efforts. Reduced, standard, and modified proctor compaction efforts were followed to prepare the soil sample and examine the change of optimum moisture content for various compaction efforts. OMC and MDD of the soil sample obtained from different compaction efforts are shown in Table 5-9.

Figure 5-35 illustrates the change in laboratory electrical resistance measurements when soil specimens were compacted with different energy levels. The laboratory test results demonstrated that the electrical resistivity decreases for the compacted eagle ford shale with increasing water content and unit weight. Resistivity decreases rapidly up to optimum moisture content and maximum dry density point in all three cases.

Table 5-9 Compaction properties with different compaction effort

Compaction Effort	Optimum Moisture Content (%)	Maximum Dry Density (KN/m^3)
Reduced proctor (356 KN-m/m^3)	26.51	14.40
Standard proctor (600 KN-m/m^3)	21.81	15.58
Modified proctor (2700 KN-m/m^3)	12.81	17.27

When the moisture content reaches the optimum moisture content or more, the resistivity is independent of unit weight in all three cases. Experimental results show that resistivity measured at optimum moisture content point for the sample compacted with standard proctor energy was 18.03% lower than the resistivity found for sample compacted with reduced proctor energy. However, resistivity at OMC for the sample compacted with modified proctor energy was found 1.4 Ohm-m higher than the sample prepared with standard proctor energy. Since moisture content has more impact on resistivity compared to unit weight, the resistivity was found higher.

Despite the lower optimum moisture content when the sample was compacted in standard proctor conditions, less resistivity was measured for this sample than the sample prepared with reduced proctor energy. This phenomenon happened because, at higher energy levels, the

maximum dry density is also higher. Mitchell & Soga (2005) found that clay soil remolding reduces the size of large pores and breaks down the flocculated open fabric. Therefore, the electron conduction path is reduced in the remolded soil at a higher unit weight. Hence, the level of compaction energy in the soil also plays a significant role, which affects resistivity changes in compacted samples.
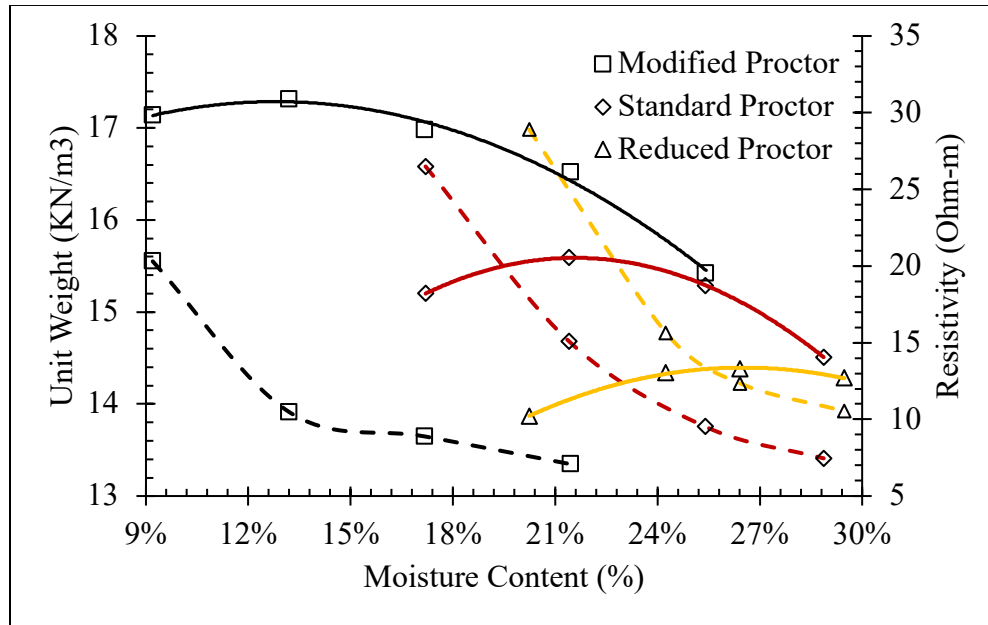
Figure 5-35 Relationship between compaction effort and electrical resistivity

The electrical resistivity data collected during the unconfined compressive strength tests of the remolded soil samples at different moisture contents are shown in Figure 5-36. As the axial strain increases, the resistivity starts to decrease from the initial value. For the soil sample prepared with a moisture content of 17.3%, the soil resistivity value decreased 65.5% from the initial value. With the increasing axial strain, air void within the soil specimen decreased, decreasing resistivity value. Resistivity value decreased 56.5%, 44.8%, and 38.5% of the initial value at failure for the soil sample prepared with moisture content 21.4%, 25.7%, and 29.3%, respectively, as illustrated in Figure 5-36. However, an increase in moisture content indicates high moist unit weight, which associates with the remolding of clay clods, eliminating inter-clod voids and reorientating the

particle (Abu-Hassanein et al. 1996). Consequently, the resistivity decreases with the increase in moisture content, and therefore, the reduction of resistivity value is also lower for later cases.
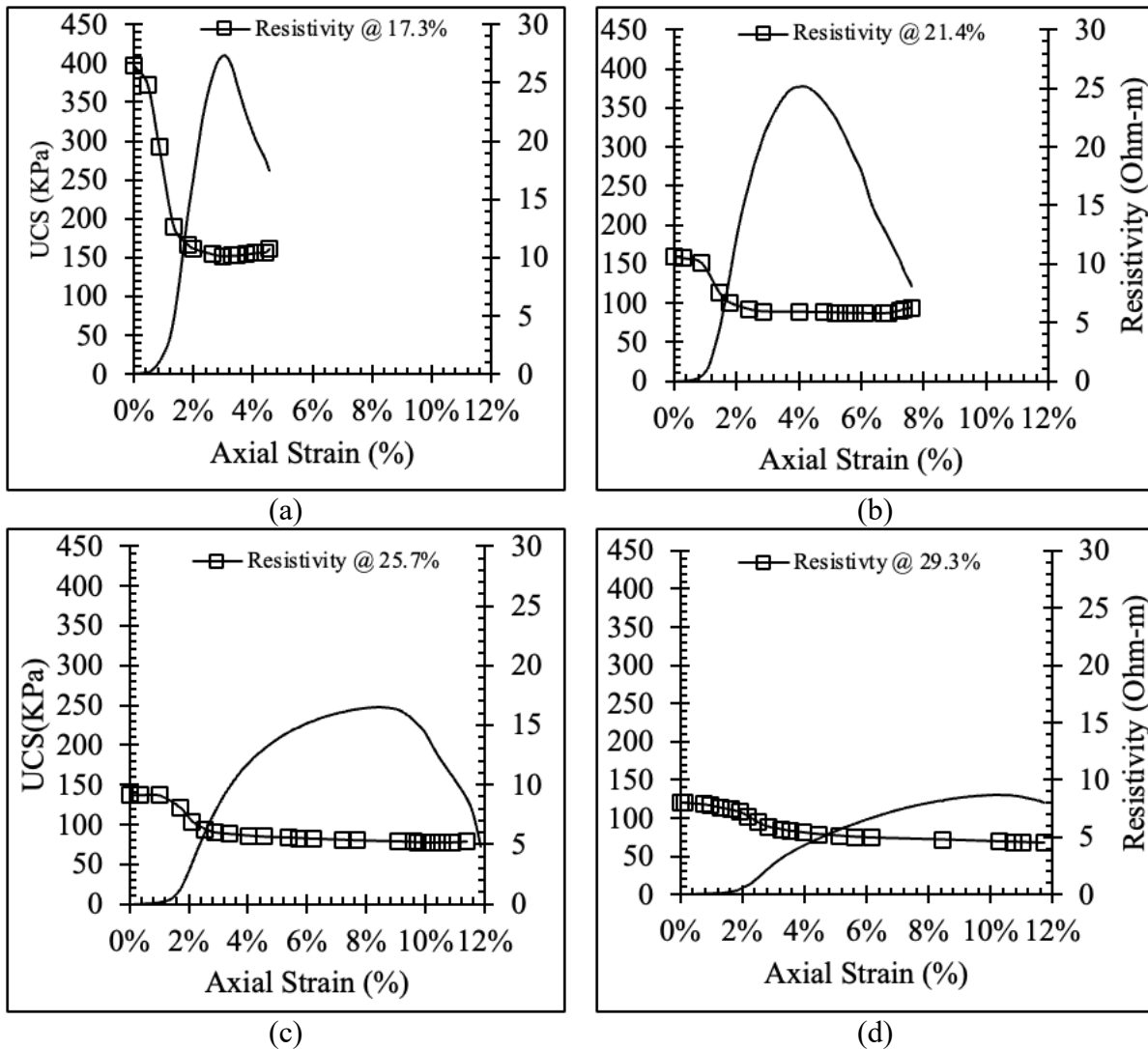
Figure 5-36 Electrical resistivity measurement at various stages of UCS tests of soil specimens with moisture content of (a) 17.3% (b) 21.4% (c) 25.7% (d) 29.3%

The Figure 5-37 shows how electrical resistivity correlates with unconfined compressive strength when these properties are compared. Similarly, when all compaction energy is considered, the relationship shows the same pattern. This relationship can be understood by the fact that the unconfined compressive strength increases as the resistivity increases. It should be noted that after reaching the maximum value, the value decreases with increasing resistivity. Using the compaction

curve, the moisture content corresponding to the resistivity value can be calculated. A resistivity value can be used as a predictor of moisture content for maximum unconfined compressive strength; however, the value overestimates the compressive strength.
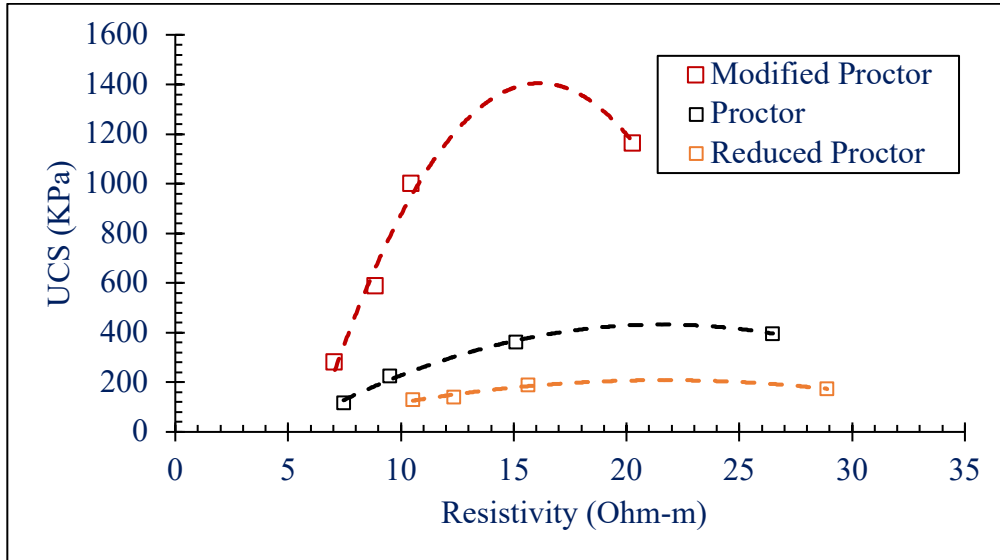
Figure 5-37 Relationship between UCS and resistivity

CHAPTER 6 STATISTICAL MODELING

6.1 Introduction

For soils, there are a few electrical mixing models to describe the soil's resistance. However, most of the models model electrical resistance as being determined by complex properties of soil. To estimate resistivity from pore water conductivity, the moisture must be extracted from the soil to measure pore water conductivity. However, it is difficult to perform on a regular basis. Moreover, to correlate with surface conductivity, measuring surface conductance is time-consuming. A model that can be applied practically to estimate soil geotechnical parameters based on electrical resistance is therefore needed.

The purpose of the study to develop a statistical model to correlate the electrical resistivity with the geotechnical engineering properties of the soil. This analysis can be used to associate the resistivity of soil samples collected from compacted soils to their geotechnical properties. As part of this study, multiple linear regression (MLR) analyses were performed using R-Studio, a statistical analysis program, and model assumptions were explored. A summary of the steps included in the development of the MLR model is shown in Figure 6-1.
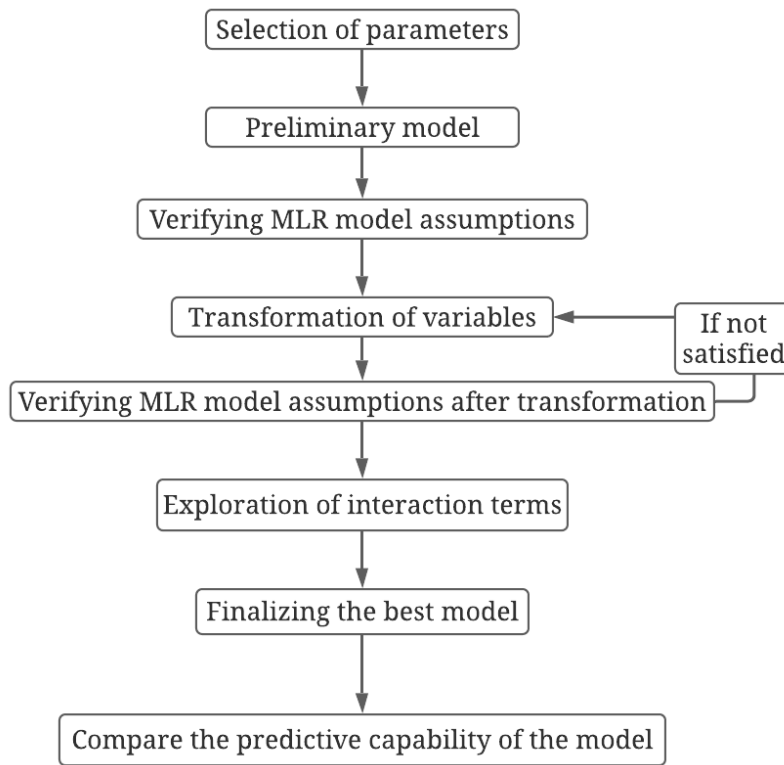
Figure 6-1 Model development steps

6.2 Parameters Selections for Model

The predictor variables should not be correlated with each other (Kutner et al., 2005). Even so, in practice, the predictor variables are often closely related to one another under certain conditions. The occurrence of interrelations between the independent variables is known as multicollinearity. Useful interpretation in such cases of regression parameters may not be obtained.

Moisture content, saturation level, and unit weight all relate to geotechnical parameters. However, soils that have higher fine content and higher liquid limit will have a higher plasticity index. It can be stated that these soil properties are correlated with one another. In this study, the aim was to investigate the relationship between soil electrical resistivity and the geotechnical properties of soil using the intended models.

6.2.1 Parameter: Related to Phase Relationship

A study of the influence of influential physical properties on electrical resistivity of soil determined that moist content and dry weight significantly affected electrical resistance responses. Additionally, the effect of void ratio and volumetric moisture content on electrical resistance was determined. According to the phase relation of soil, the amount of soil per unit weight of soil is negatively proportional to the amount of voids that it contains (Figure 6-2).
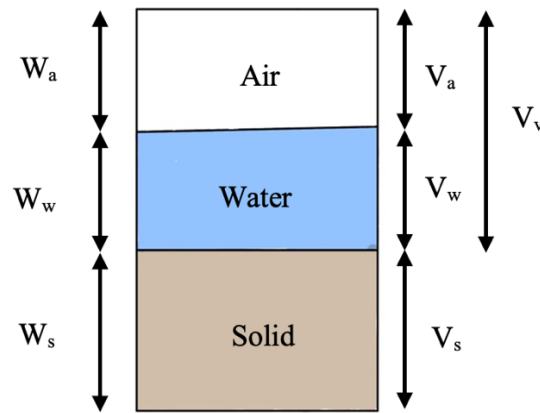
Figure 6-2 Soil phase relationship

Using the following equation, the degree of saturation of any soil specimen based on its dry unit weight, gravimetric moisture content, and void ratio can be estimated:

$$\gamma_d = \frac{\gamma_w G_s}{1 + e}$$

$$S = \frac{w.G_s}{e}$$

Here, γ_d = dry unit weight, G_s = specific gravity, w = gravimetric moisture content, e = void ratio and S = degree of saturation. A single parameter - the degree of saturation - can represent the combined effects of other three parameters mentioned earlier. Also, the following equation can help explain the relationship between volumetric moisture content and saturation degree:

$$\theta_d = \frac{S.e}{1+e}$$

Moisture content, however, has a significant impact on sandy soil resistivity. It is also not easy in practice to collect undisturbed sandy soil so that the test can be done to determine the degree of saturation of the samples of sandy soil. Therefore, for sandy soil moisture content was selected as the predictor variable related to phase relationship.

6.2.2 Selection of Parameter Related to Clay Properties

Plasticity indices of soil were plotted against the tested liquid limit, conductivity and soluble sulfate content of the soil samples which is shown in Figure 6-3. The correlations among PI, LL, conductivity, and soluble sulfate were determined. The relationship between PI and LL is linear and correlation coefficient was determined above 0.7. PI and conductivity, however, are also related, the higher the conductivity, the higher the PI. Similar relationship was found when Pi was plotted against the soluble sulfate content. Therefore, multicollinearity may occur if all these parameters were chosen to determine the multiple linear regression model response variable.

(a)
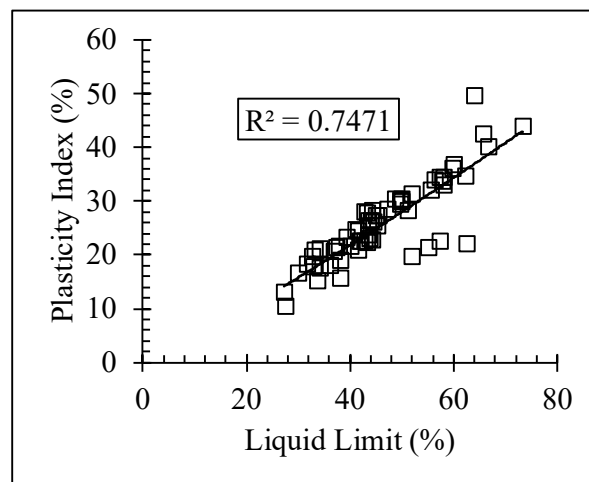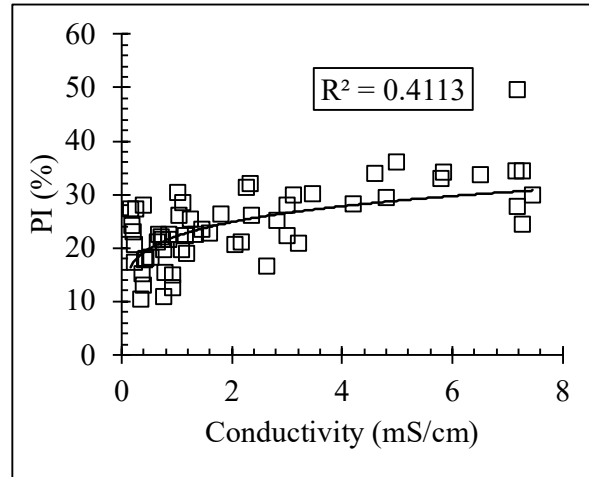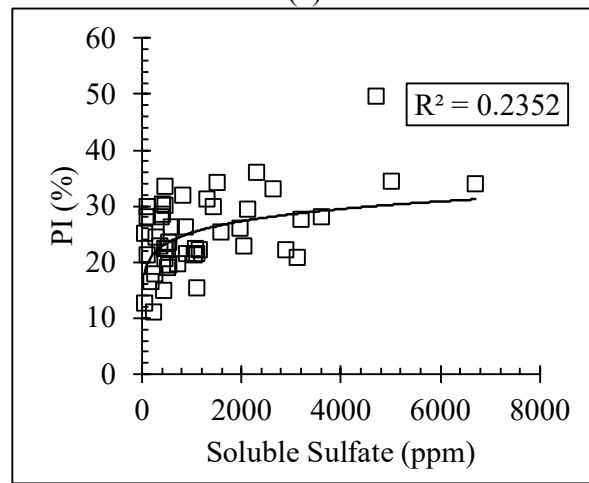
Figure 6-3 Correlation between PI and (a) LL, (b) conductivity and (c) soluble sulfate content of soil

According to Kibria (2014), cation exchange capacity which is a function of liquid limit is linearly related to PI and mineral percentages and the coefficient of correlation was found higher. Moreover, specific surface area is also related to LL. Consequently, among all these parameters, a single parameter can be selected as a predictor variable to avoid the problem of multicollinearity. Most clayey samples exhibit an increase in Atterberg limits due to fine content; therefore, CEC correlates with both LL and PI.

According to the analysis, PI was selected for modeling as a predictor variable to represent the clay properties.

155

6.2.3 Selection of Parameter Related to Sand Properties

Multiple linear regression equation was also generated to explain the electrical resistivity properties of sandy soil. The relationship between sand content, clay content and conductivity of pore water is plotted Figure 6-4. Coefficient of correlation is also determined for those relationship and the value was found significant. It is found that sand content is linearly related to the fine soil content, while clay content is related to sand fraction as a power function.

The correlation was also determined between sand fraction and pore water conductivity of sandy soils. Pore water conductivity was considered as one of the major parameters related to electrical resistivity of the soil. Therefore, to avoid any multicollinearity among the predictor variables sand fraction was chosen to develop the multiple linear regression equation to predict the resistivity with soil parameters for sandy soils.
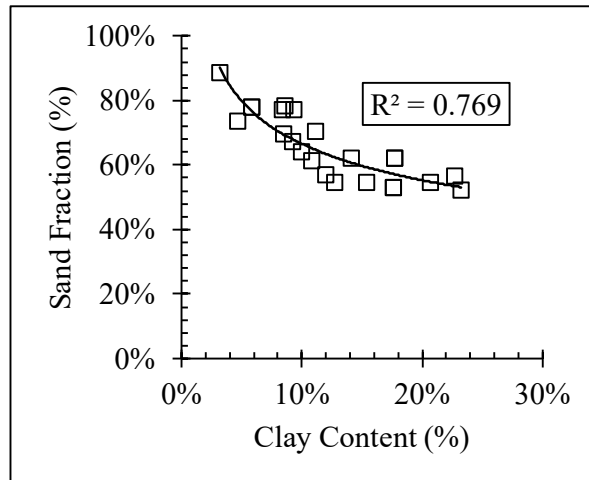
(a)
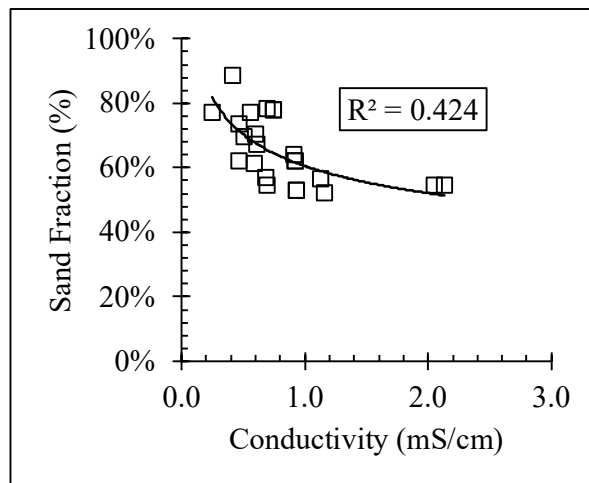
(b)

Figure 6-4 Relationship between sand fraction and (a) clay content and (b) pore water conductivity

6.3 MLR Model of Compacted Clays

All compacted soil samples were taken into consideration for the modeling.

6.3.1 Scatter plot and correlations among variables

All values of the different parameters are scatter plotted against each other in Figure 6-5 depicts that the degree of saturation clearly has an exponential relationship with the electrical resistivity of the soil. Scatter plotted values of two prediction variables shown that there is no certain relationship between the degree of saturation and plasticity indices.
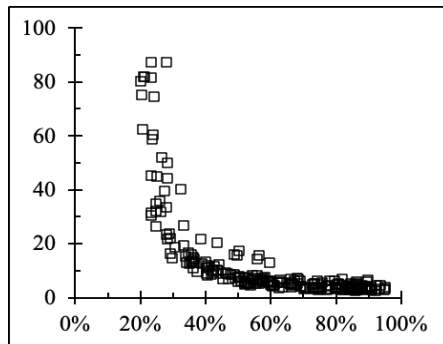
Resistivity

Degree of Saturation
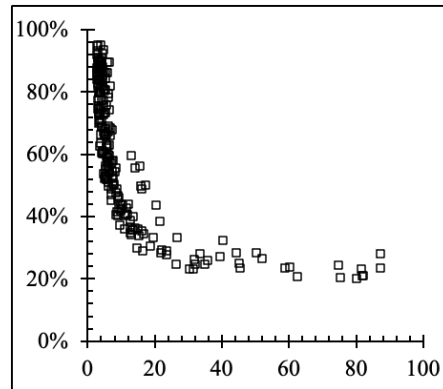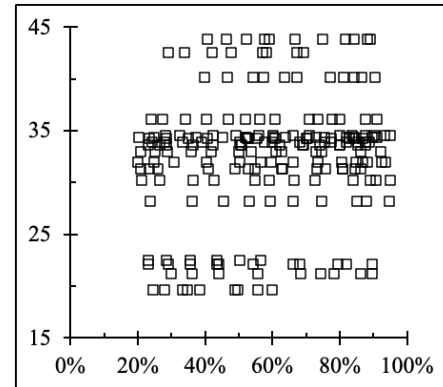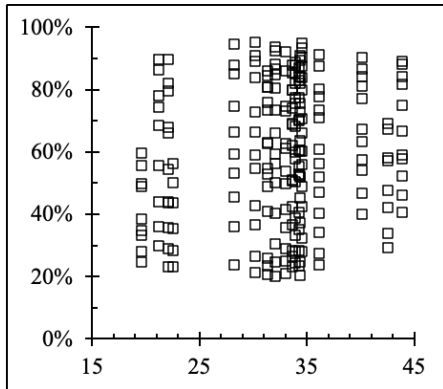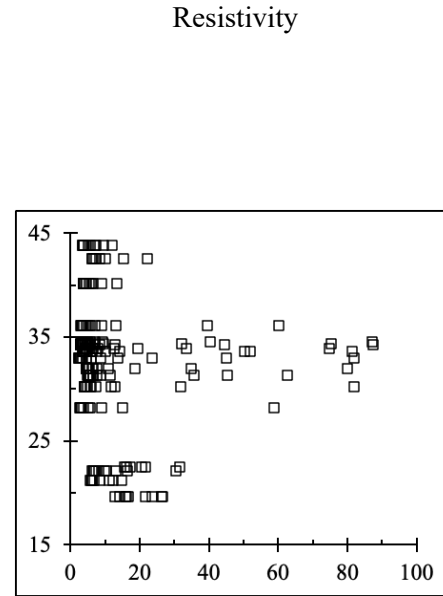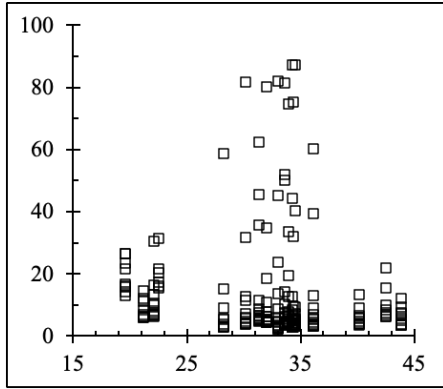
Figure 6-5 Scatterplot among parameters

159

Apart from scattering plotted graphs, correlation analysis was also conducted among the variables to understand the effect of each parameter on the response variable. Correlation analysis showed that the degree of saturation and resistivity is strongly correlated (r = -0.656). The relationship between electrical resistivity and plasticity index was not found strong enough. The relationship between the two predictor variables was also determined. The coefficient was found as 0.015, which indicated that there is no multicollinearity among the predictor variables. the correlations among the variables are shown in Table 6-1.

Table 6-1 Correlations among predictor and response variables

	Resistivity	Degree of Saturation	Plasticity Index
Resistivity	1.00	-0.65	-0.0302
Degree of Saturation	-0.65	1.00	0.03
Plasticity Index	-0.0302	0.03	1.00

6.3.2 Development of Preliminary Model

A preliminary multiple linear regression model was developed to correlate electrical resistivity of soil with degree of saturation and plasticity index. The model can be presented as:

$$(Resistivity)_i = \beta_0 + \beta_1 (DoS)_i + \beta_2 (PI)_i + \varepsilon_i$$

Where, $\beta_0, \beta_1, \beta_2$ are regression parameters, ε_i is random error, and i = 1, 2, 3, ……. n observations. When all other independent variables in the regression model remain constant, then regression parameters are explained by a variation in the mean response per unit increase in a predictor variable. Using least squares, regression parameters were estimated in this study. Predictor variables in the current study are quantitative.

In order to observe the relationship between the variables, an analysis was conducted. Correlation coefficients were also used to measure the linear relationship between the response and the predictor variables. Table 6-2 summarizes the results from R-studio that relate to parameter

estimations and ANOVA summary. Degree of saturation has a negative impact on the resistivity measurement of the soil whereas, the plasticity index has positive coefficient in the measurement of resistivity, i.e., an increase in plasticity index of the soil will increase the resistivity response value. The preliminary fitted multiple linear regression equation can therefore be presented as below. The ANOVA summary showed that the R^2 and adjusted R^2 was found ~0.46, which means the preliminary model can explain 46% of the variation of resistivity. P-values for the residuals were found to be very low.

$$Resistivity = 36.254 - 40.472 \times (DoS) - 0.005445 \times (PI)$$

Table 6-2 Preliminary model parameters (clayey soil)

	Coefficient	Std. Error	t Value	Pr(>|t|)	VIF
Intercept	46.07	3.35518	13.731	< 2e-16	
Saturation	-48.48	2.82940	-17.135	< 2e-16	1.0008
PI	-0.03	0.09971	-0.292	0.77	1.0008

Preliminary model ANOVA (clayey soil)

Residual Standard Error	R^2	Adjusted R^2	F-Statistics	p-Value
14.96	0.4196	.4167	147.1	<2.2e-16

6.3.2.1 Verification of Preliminary model

The next step would be to check if the assumptions of the multiple linear regression model were verified. A good statistical model should satisfy the following criteria: constant error variance, normality of variance, outliers and multicollinearity among predictor variables (Huda, 2011; Kutner et al., 2005; Stevens, 2012). During the present study, graphical plots and statistical tests were used to diagnose the model assumptions.

6.3.2.1.1 <u>Constant Error variance</u>

The Figure 6-6 shows the residuals and fitted values of the preliminary model, an indicator of heteroscedasticity. Whenever the residuals are plotted against fitted values, they should be randomly distributed without any trend. In the same way, when plotting residuals against fitted values, there should not be any trend in the values. As long as the constant error variance is met in a multiple linear regression model, the criterion is considered fulfilled. It was evident in the plotting that the absence of any shape indicated that the variance was not constant. There is the possibility in such cases that the regression may not be able to predict correctly the response variable. These conditions can be resolved by transforming the variables. There was a possibility that the preliminary model might have some heteroscedasticity present, as can be seen from the figure shown above. As can be seen, here is a curve that seems to be curving. In addition to this, the studentized Breusch-Pagan test has been performed in R-Studio as well. The p-value was observed from the test as 6.41e-13 which is much lower than a = 0.01. Therefore, it appears that the residuals are not homoscedastic at a = 0.01, indicating that homoscedasticity has been rejected.
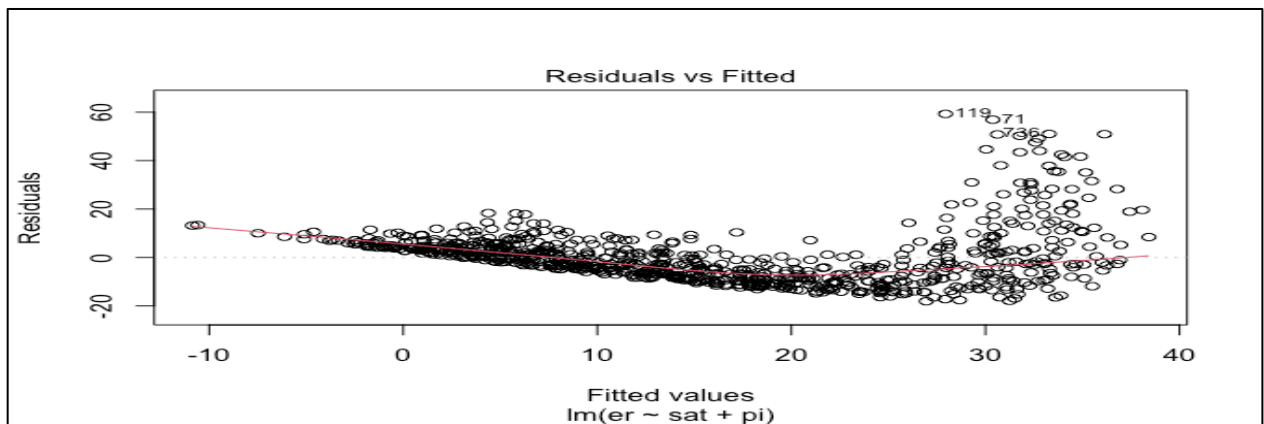
Figure 6-6 Preliminary model residuals vs fitted values (clayey soil)

6.3.2.1.2 <u>Normality</u>

The residuals or errors of a multiple linear regression should have a normal distribution. A normal probability plot can be used to determine whether the residuals are normal or not. For

instance, a moderately linear plot is a sign that the residuals are normally distributed. The Figure 6-7 depicts a plot showing the normal probability distribution for the preliminary multiple linear regression model.
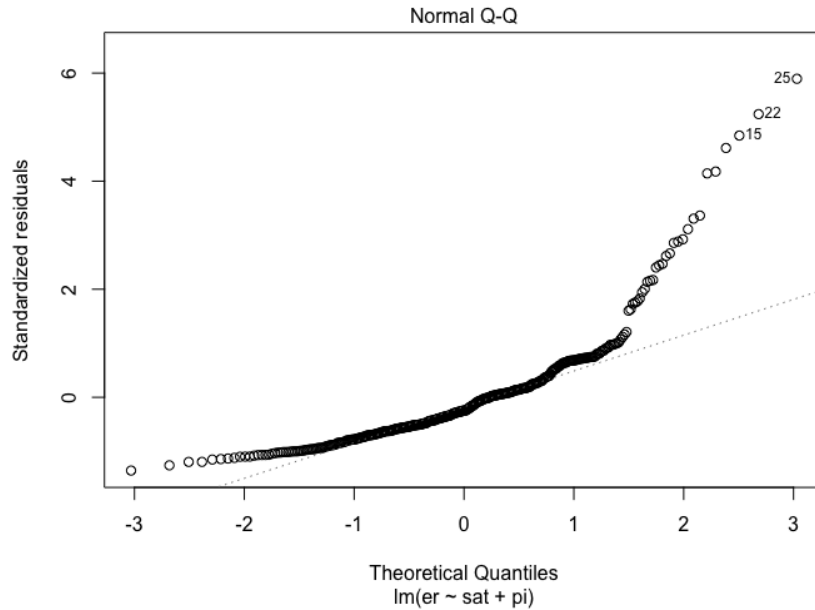
Figure 6-7 Preliminary model normal probability plot (clayey soil)

From the plot, it is evident that there is a long tail on the right side and a short tail on the left side. It is therefore believed that the distribution of the residuals may not be normal. In order to further verify the validity of the normality assumption, R-Studio was used to perform the Shapiro-Wilk normality test. In this case, the P value was estimated to be 2.2e-16, which is much smaller than the p-value for a = 0.01. This means that the null hypothesis was rejected since residuals at a = 0.01 were not normally distributed.

6.3.3 Transformation of Variables

In order to satisfy the assumptions of constant error variance and normality, a transformation of the response variable was required since the preliminary model did not meet these assumptions. As shown in the Figure 6-8, the Box-Cox plot method was used in R-Studio to

determine the optimum transformation variable for the response. The figure shows that the optimal value for the transformation, i.e., the power of the variable, was -0.75. The power of the response variable, however, was assumed to be -0.5 for final model development. The residual distribution also led to a transformation of the predictor variable degree of saturation in the final model. As a result, the final model appeared to be as follows:

$$(Resistivity')_i = \beta_0 + \beta_1 \times \log(DoS)_i + \beta_2(PI)_i + \varepsilon_i$$

Where, Resistivity$' = \dfrac{1}{\sqrt{Resistivity}}$
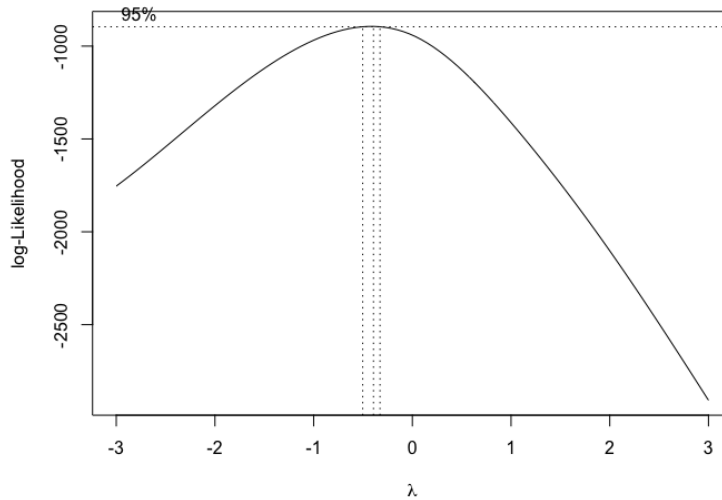
Figure 6-8 Box-Cox plot (clayey soil) response variable

The transformed model was used in multiple linear regression. ANOVA (analysis of variance) results and parameter estimates for the final model are shown in Table 6-3. The correlation coefficients follow the expected sign convention. The summary of the ANOVA showed that the adjusted R^2 was acceptable and satisfactory. Furthermore, the residual p-values were also quite low as well. Based on this, the final fitted MLR equation appears to be as follows:

$$\frac{1}{\sqrt{Resistivity}} = 0.3936782 + 0.5572772 \times \log(\text{Dos}) + 0.0036228 \times \text{PI}$$

Table 6-3 Final model parameters (clayey soil)

	Coefficient	Std. Error	T Value	Pr(>|t|)	VIF
Intercept	0.3936782	0.0132041	29.815	< 2e-16	
Saturation	0.5572772	0.0151602	36.759	< 2e-16	1.001
PI^{-1}	0.0036228	0.0004254	8.517	3.22e-16	1.001

Final model ANOVA (clayey soil)

Residual Standard Error	R^2	Adjusted R^2	F-Statistics	p-Value
0.0638	0.7806	0.7795	724	<2.2e-16

The next step is to verify that the assumptions underlying the MLR model are valid.

6.3.3.1 Verification of Final Model

6.3.3.1.1 <u>Constant Error variance</u>

The residuals vs fitted values plot for the final MLR model is shown in Figure 6-9.
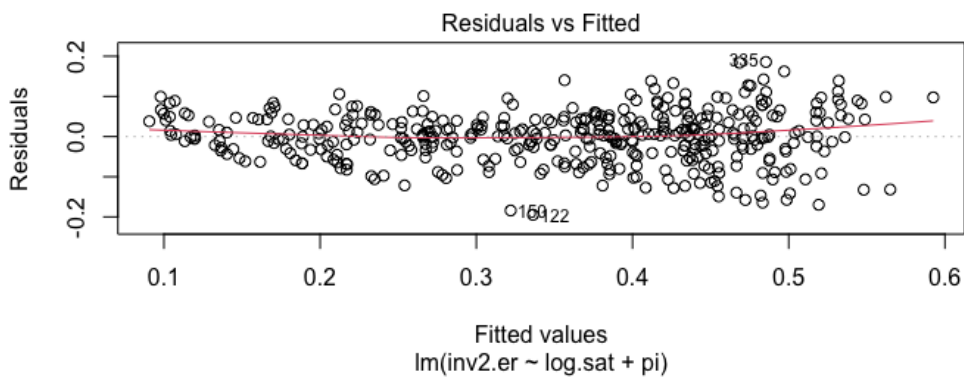
Figure 6-9 Final model residuals vs. fitted values plot (clayey soil)

The plot results did not indicate a curvilinear trend or funnel shape. It appears that residuals are randomly strewn across the plot. The next step was to conduct a studentized Breusch-Pagan test in RStudio, and the results were then analyzed. In the analysis that was conducted, the p-value

was greater than our hypothesis that a = 0.01. Based on these results, the null hypothesis was allowed to go, meaning the residuals are homoscedastic at a = 0.05. It was ensured that the constant error variance assumption was met for the model that was used.

6.3.3.1.2 Normality

Normal probability plot is shown in Figure 6-10 for the final MLR model.
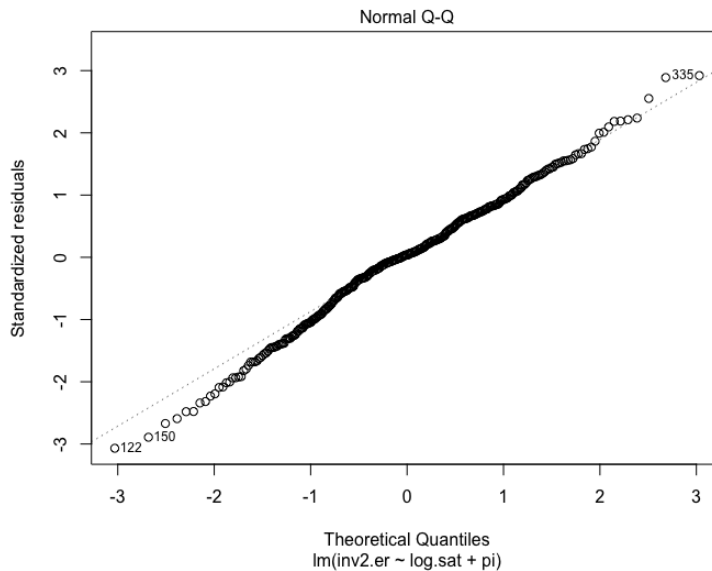
Figure 6-10 Final model normal probability (clayey soil)

On the plot, it can be seen that there are short tails on both sides. RStudio was used to perform a Shapiro-Wilk normality test, which further verified the assumption of normality. Using the test, a p-value of 0.0561 was estimated, which is greater than the level of 0.05. Thus, the null hypothesis failed to be rejected, which indicates that the residuals are normally distributed at an a-value of 0.05.

6.3.3.1.3 Outlier Test

In RStudio, the outliers were checked using several standard tests, if any were found. For detecting outliers, the Bonferroni outlier test was used. In order to determine the influence of the outliers on the final model, DFITS, DFBETAS, and Cook's Distance were used. In this set, the F-

statistic for comparing Cook's Distance is calculated as 3 for the a = 0.05. Furthermore, it is suggested to also investigate Di values greater than 0.5, as this may also be influential (Faysal, 2017).

The Bonferroni outlier test did not flag any of the observations as outliers. According to DFFITS, DFBETAS, and Cook's Distance Tests as well, all observations were consistent with the assumptions made in the study.

6.3.3.1.4 Multicollinearity

According to the VIF in figure, it appears that all of the VIFs in the figure are within the suggested range. It follows that there is no significant multicollinearity between the predictor variables.

6.3.3.1.5 Backward Elimination

It is important to note that the backward elimination method starts with all the variables in the model that will act as predictors. Subsequently, it removes insignificant variables incrementally from the model. When none of the insignificant variables remain in the model at the end of the analysis, the analysis is completed. By using this method, all predictor variables were significant at a significance level of 0.05 and nothing was removed from the model.

6.3.3.1.6 Stepwise Regression

The stepwise regression method makes use of both forward selection and backward selection algorithms. First, it is determined which predictor variable is most significant. After that, a regression analysis is carried out in order to calculate the relevant parameters. Once the parameters are calculated, additional variables are added incrementally based on their significance. Once one model has been developed with the optimal criteria parameters, the process is repeated. In order to conduct the statistical significance tests (Kutner et al., 2005), the F-statistic is used. It

was found that the inclusion of two predictor variables provided the best model, based on this method.

6.3.4 Validation of the Final Model

In order to evaluate the predictive power of the resistivity model for compacted soil samples, the experimental results of soil samples designated as B.BR6A.20, B.BR6A.40 and B.P4.10 were analyzed. By comparing new data sets with the existing model, the objective was to assess the applicability of the model to various types of clayey soils. Tests of electrical resistance were carried out at various saturation levels and the results observed were corrected for a temperature difference of 15.5 degrees Celsius. C temperature. It can be seen that the value of the experimental resistance was the same as the predicted value shown on Figure 6-11.
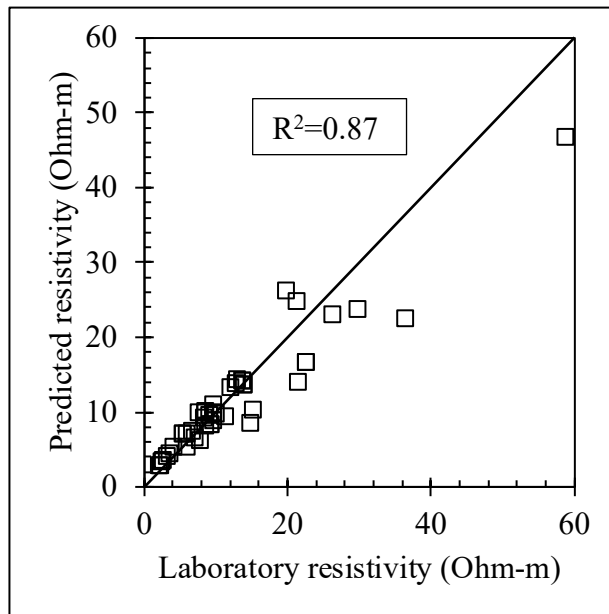
Figure 6-11 Comparison between experimental and estimated observations (clayey soil)

6.3.5 Interaction Surface for Compacted Clayey Soils

As illustrated in Figure 6-12, the effect of combined saturation and plasticity indices on the electrical resistivity responses of compacted clay is illustrated. When the degree of saturation of the soil is below 30% and the plasticity index of the soil is below 30 according to the interaction surface, the resistance is very large. As the plasticity indices increase within the same range of saturation, the surface resistivity of the soil gradually decreases. In contrast, when the degree of saturation is increased, the resistivity decreases sharply due to the level of saturation. Additionally, it was also found that soil resistivity was very low when the degree of saturation was increased to 60% and above. In this particular case, the interaction surface between degree of saturation, plasticity index, and electrical resistivity can be found parallel to the surface.
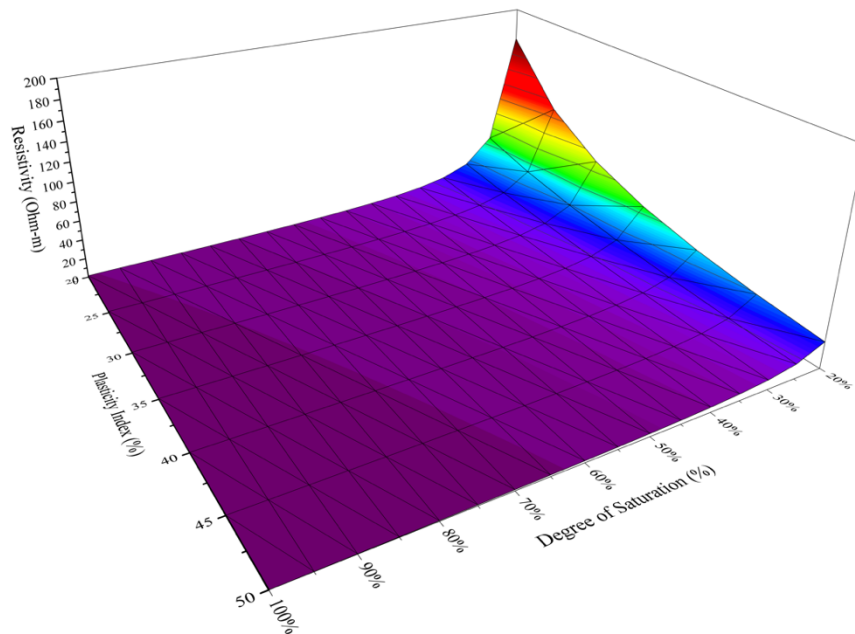
Figure 6-12 Surface interaction diagram for clayey soil

6.3.6 Resistivity vs Degree of Saturation for compacted clays

Variation of electrical resistivity and degree of saturation chart was developed at various plasticity indices. Using the developed MLR the degree of saturation and electrical resistivity was calculated. In the laboratory plasticity index of the clayey soil sample can be easily measured and thus it can be used to measure the degree of saturation of the soil using the filed electrical resistivity. The estimated relationship between the resistivity and plasticity indices are presented in Figure 6-13.
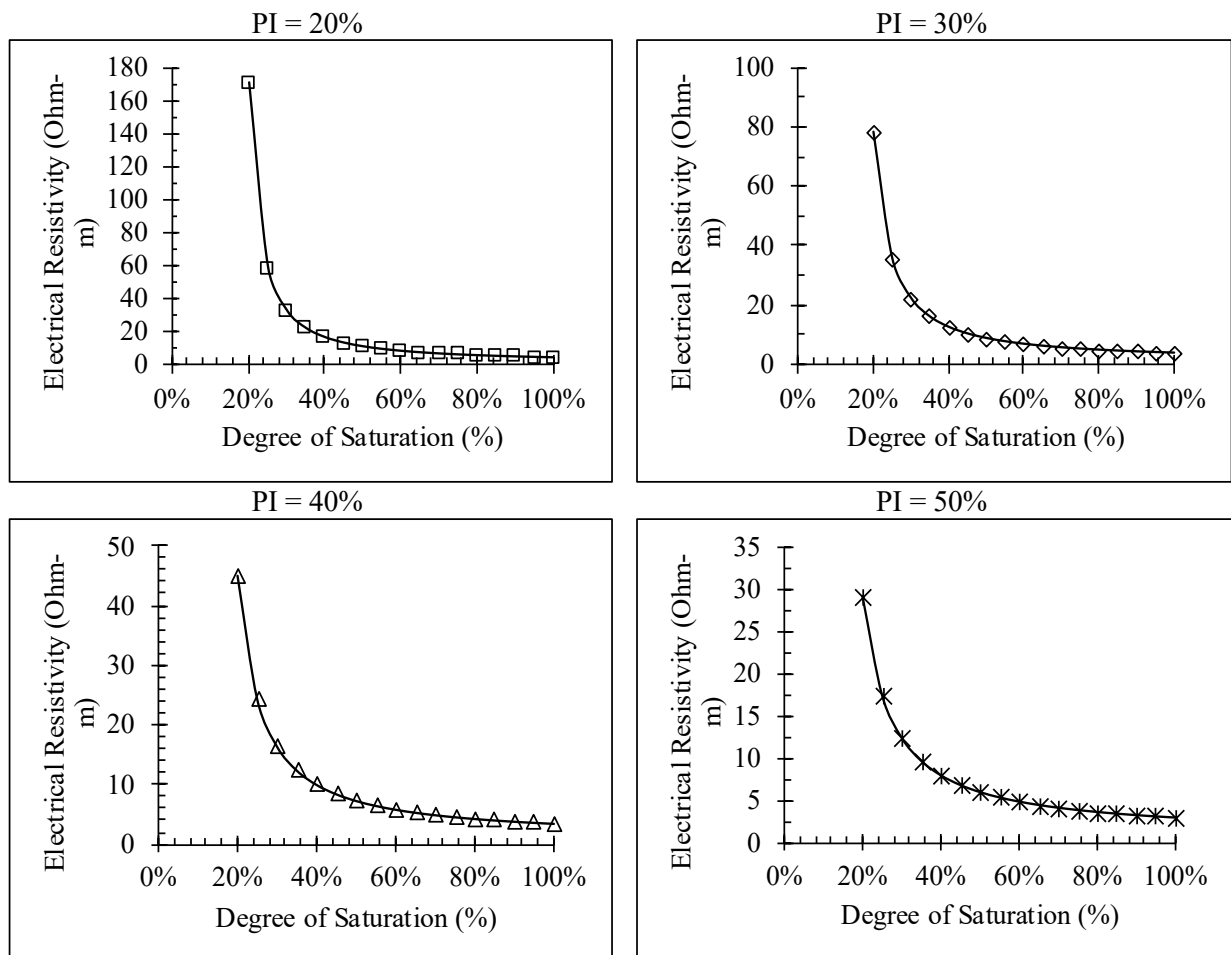
Figure 6-13 Changes in resistivity with degree of saturation at different plasticity indices

6.3.7 Field Validation of the Model

Field validation was done by using the field soil electrical resistivity value. From the electrical resistivity survey, the using the developed equation the degree of saturation was calculated. The estimated degree of saturation was then compared with the actual examined value. The comparison between the estimated and calculated value is given in Figure 6-14. From the figure the maximum variation was observes as 9.5% in degree of saturation value.
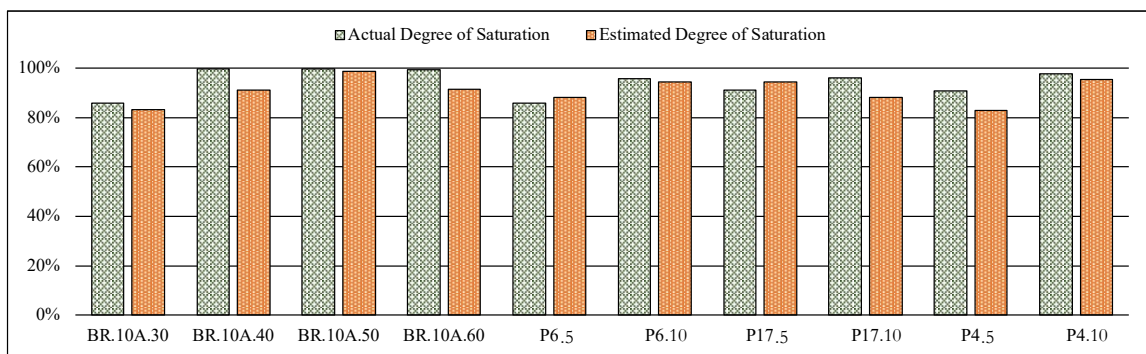
Figure 6-14 Actual value vs. predicted value

6.4 MLR Model of Compacted Sandy Soil

A soil sample whose particle size is greater than 0.075 mm is used for modeling in this section if it contains more than 50% particles of that size.

6.4.1 Scatter plot and correlations among variables (Sandy Soil)

All values of the different parameters are scatter plotted against each other in Figure 6-15. The Figure 6-15 depicts that there is a clear relationship between the degree of saturation and electrical resistivity of sandy soil. Scatter plotted values of two prediction variables shown that

there is no certain relationship between the degree of saturation and percent of sandy soil present in soil.
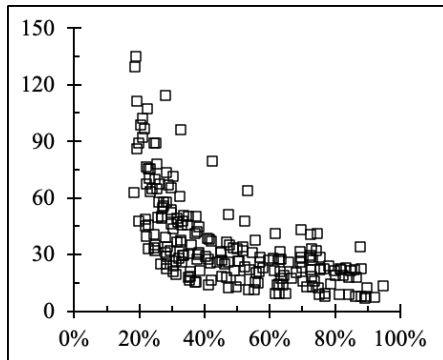
Resistivity

DoS
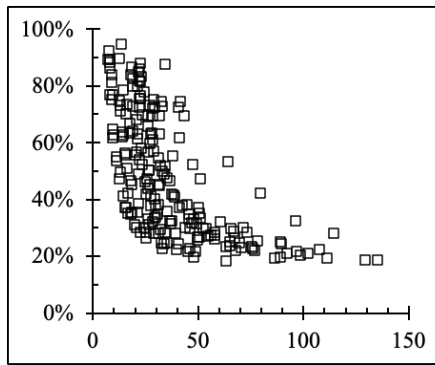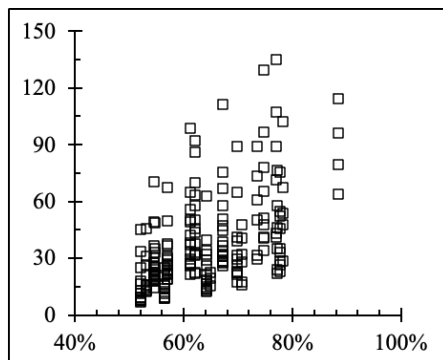
Resistivity

Sand (%)
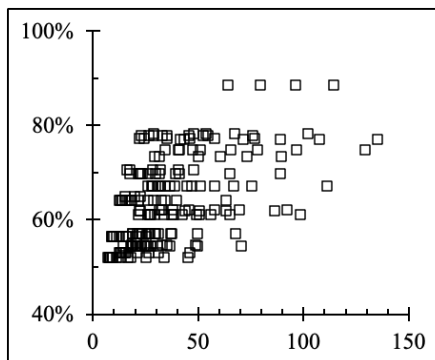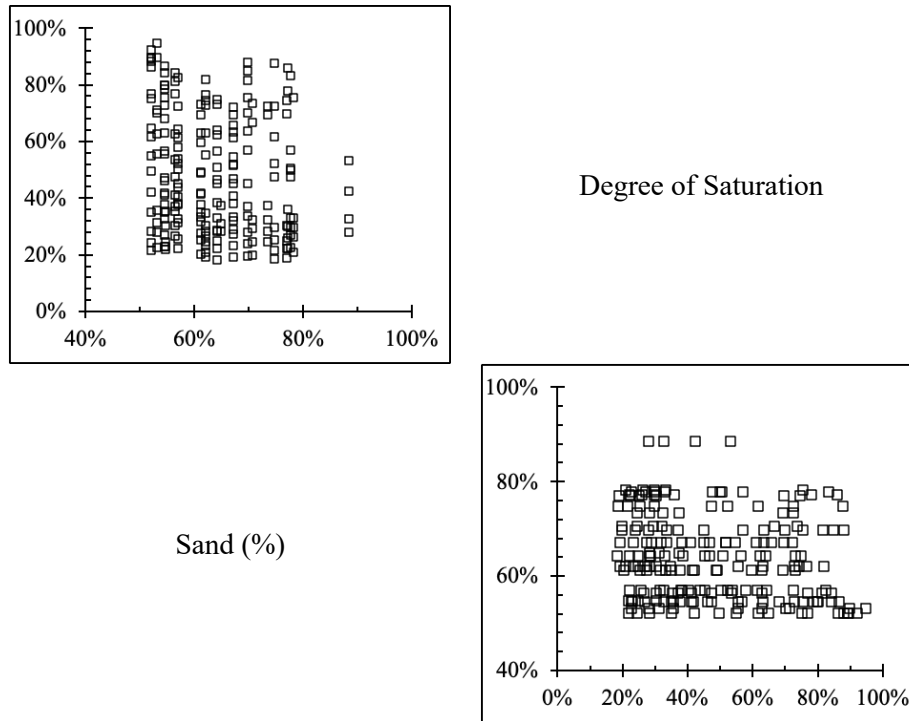
Figure 6-15 Scatterplot among variables (Sandy Soil)

Apart from scattering plotted graphs, correlation analysis was also conducted among the variables to understand the effect of each parameter on the response variable (Table 6-4). Correlation analysis showed that degree of saturation is strongly correlated with resistivity ($r = -0.65$). The relationship between electrical resistivity and sand fraction was not found strong enough. The relationship between the two predictor variables was also determined. The coefficient was found as -0.18, which indicated that there is no multicollinearity among the predictor variables.

Table 6-4 Correlations among predictor and response variables (sandy soil)

	Resistivity	Moisture	% Sand
Resistivity	1.00	-0.61	0.55
Moisture	-0.61	1.00	-0.33
% Sand	0.55	-0.33	1.00

6.4.2 Development of Preliminary Model (Sandy Soil)

To correlate electrical resistivity of soil with degree of saturation and plasticity index, a preliminary multiple linear regression model was developed. The model is as follows:

$$(R_{sand})_i = \beta_0 + \beta_1(MC)_i + \beta_2(SF)_i + \varepsilon_i$$

Where, R = Resistivity of soil, MC = moisture content and SF = sand fraction of the soil, $\beta_0, \beta_1, \beta_2$ are regression parameters, ε_i is random error, and I = 1, 2, 3, ……. n observations. In terms of the physical meaning of regression parameters, it can be said that a regression parameter denotes the variation in the mean response per unit increase of a predictor variable when the other independent variables in the model remain constant. A least squares regression method was used to estimate the regression parameter in this study. Throughout the study, all of the predictor variables are of a quantitative nature.

A correlation analysis was conducted to observe the relationship between the variables. In addition to measuring the strength of the linear relationship between the response and the predictor variables, the correlation coefficient was also used. The summary of coefficient and analysis of variance (ANOVA) from R-studio is presented in Table 6-5. Moisture content has a negative impact on the resistivity measurement of the soil whereas, the sand fraction has positive coefficient in the measurement of resistivity, i.e., an increase in sand fraction of the soil will increase the resistivity response value. The preliminary fitted multiple linear regression equation can therefore be presented as below:

$$R = -8.866 - 65.417 \times (MC) + 120.658 \times (SF)$$

Table 6-5 Preliminary model parameters (Sandy soil)

	Coefficient	Std. Error	t Value	Pr(>|t|)	VIF
Intercept	-2.549	10.535	-0.242	0.809	
Saturation	-159.370	17.361	-9.180	<2e-16	1.119
Sand Fraction	106.480	14.126	7.538	<2e-16	1.119

Preliminary model ANOVA (Sandy soil)

Residual Standard Error	R2	Adjusted R2	F-Statistics	p-Value
17.43	0.5043	0.4995	104.3	2.2e-16

Using ANOVA, the R^2 and adjusted R^2 were found to be 0.60, meaning that the preliminary model can explain 60% of the variation of resistivity. This was determined by the very small p-value associated with the residuals.

6.4.2.1 Verification of Preliminary model

It is now time to verify that the assumptions of the multiple linear regression model are correct. It is important for the model to satisfy the following key criteria: constant error variance, normality of variance, outliers, and multicollinearity among predictor variables (Stevens, 1996; Kutner et al 2005; Huda 2011). Based on the results of the current research, graphical plots and statistical tests were used to diagnose the model assumptions.

6.4.2.1.1 Constant Error variance

The Figure 6-16 shows the residuals vs the fitted values of the preliminary model that will be used to detect the heteroscedasticity. When the residuals are plotted against the fitted values, they need to be randomly distributed without any trend. Furthermore, if residuals are plotted against fitted values, there should not be any trend in residuals. The objective of this criterion is to ensure that in a multiple linear regression model, the constant error variance is met. If any shape appears in the plotting, it indicates that there is a non-constant variance present. It is likely that in

such cases, regression may not be able to predict the response variable correctly. In such cases, variables can be transformed to allow regression to predict the response variable correctly. The figure presented here indicated that there might be heteroscedasticity present in the preliminary model. The trend can be seen to be curvilinear in nature. This was followed by a student-oriented Breusch-Pagan test done in RStudio after more analysis. This p-value from the test is 7.406e-5, which is higher than a = 0.05, showing that residuals are homoscedastic at a = 0.05. Based on these findings, the null hypothesis must be rejected since the residuals are not homoscedastic at a = 0.05.
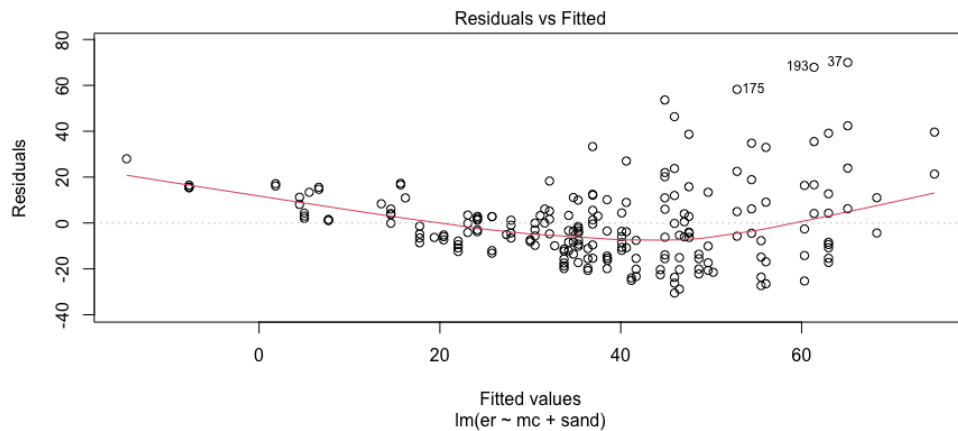
Figure 6-16 Preliminary model residuals vs fitted values plot (sandy soil)

6.4.2.1.2 Normality

A regression model with a multiple linear component should produce a distribution of residual errors that would be considered normal. In order to determine the normality of the residuals, a normal probability plot can be used. The fact that the plot is moderately linear indicates that the residuals are normally distributed. Figure 6-17 shows the plot of the normal probability for the preliminary model based on multiple linear regressions.

.
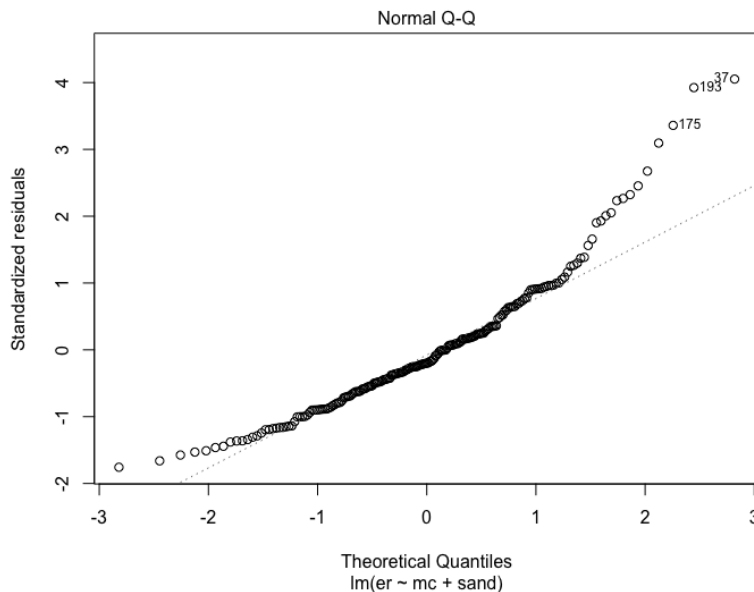
Figure 6-17 Preliminary model normal probability plot (sandy soil)

This plot shows a long tail to the right, and a short tail to the left as can be seen from the graph. This indicates that the distribution of the residuals might not follow a normal distribution. RStudio was used to carry out the Shapiro-Wilk normality test in order to further verify the normality assumption. In this study, a p-value was estimated at 1.084e-8, which is small compared to the null hypothesis of 0.05. Based on the findings, the null hypothesis was rejected indicating that residuals were not normally distributed at 0.05.

6.4.3 Transformation of Variables (Sandy Soil)

Having found that the preliminary model did not satisfy the constant error variance and normality assumptions, a transformation of the response variable was carried out. For the purpose of determining the optimum transformation variable for the response, the Box-Cox plot method was used in Rstudio. In the Figure 6-18, it can be seen that the optimum value for the transformation, which is the power of the variable, is 0. In the final model, however, it was decided

to use the log10 of the response variable. Model that was thus constructed had the following form:
as follows:

$$(R_{sand}{}')_i = \beta_0 + \beta_1 (MC)_i + \beta_2 (SF)_i + \varepsilon_i$$

Where, $R_{sand}{}' = \log(R_{sand})$
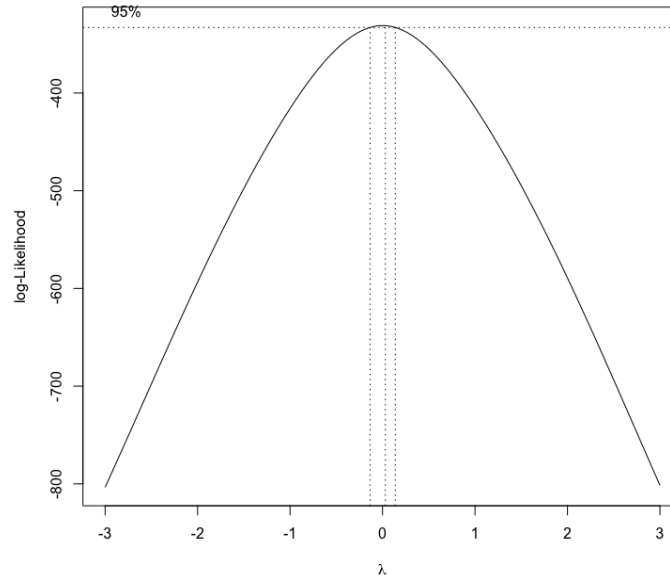
Figure 6-18 Box-Cox plot (sandy soil) for response variable

The transformed model was then subjected to multiple linear regression. A summary of the

analysis of variance (ANOVA) for the final model as well as the parameter estimates are presented

in Table 6-6. As expected, the coefficients of correlation follow the expected sign conventions. In

the case of the ANOVA summary, it can be seen that the adjusted R^2 was satisfactory and

acceptable. It can also be seen that the residual p-value was also very low. As a result, one can

conclude that the final fit MLR equation looks something like this:

$$\log(Resistivity_{sand}) = -0.18240 + \frac{0.35196}{\sqrt{MC}} + 1.22523 \times (SF)$$

Table 6-6 Final model parameters (sandy soil)

	Coefficient	Std. Error	T Value	Pr(>|t|)	VIF
Intercept	-0.18240	0.08642	-2.111	0.036	
Moisture	0.35196	0.02437	14.443	<2e-16	1.0135
Sand Fraction	1.22523	0.12738	9.619	<2e-16	1.0135

Final model ANOVA

Residual Standard Error	R^2	Adjusted R^2	F-Statistics	p-Value
0.1586	0.6736	0.6704	211.5	< 2.2e-16

The next step is to check if the model assumptions of the MLR model are correct.

6.4.3.1 Verification of Final Model

6.4.3.1.1 Constant Error variance

The residuals vs fitted values plot for the final multiple linear regression model is shown in Figure 6-19.
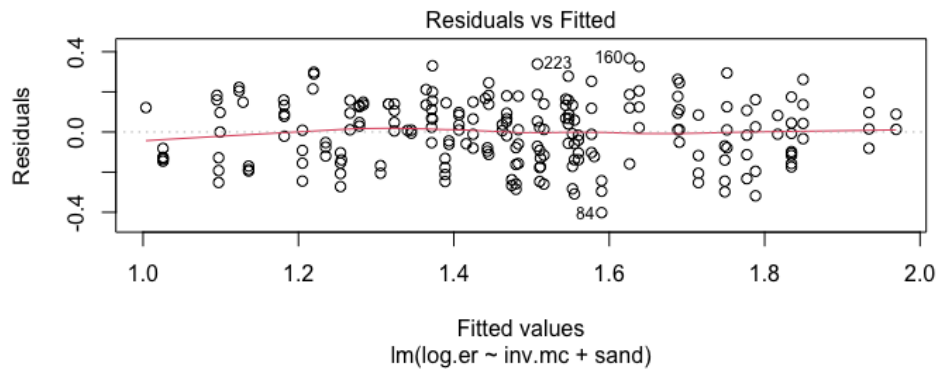
Figure 6-19 Final model residuals vs. fitted values plot (sandy soil)

The plot of the data does not show a curvilinear trend or funnel shape. It appears that the residual values are randomly dispersed. In addition to this analysis, the studentized Breusch-Pagan test was also conducted in RStudio for further analysis. In this particular case, the p-value for the

test was 0.1413, which is greater than the threshold value of a = 0.01. In other words, the null hypothesis cannot be rejected by the test, which indicates that the residuals are homoscedastic at the threshold of a = 0.01. It is expected that the final model will satisfy the constant error variance assumption.

6.4.3.1.2 Normality

The normal probability plot for the final multiple linear regression model is presented in Figure 6-20.
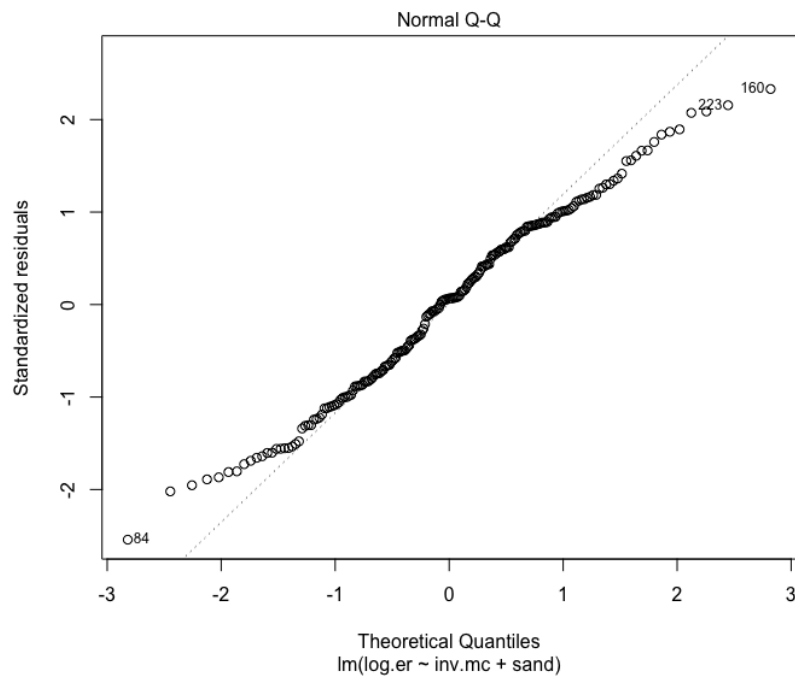
Figure 6-20 Final model normal probability plot (sandy soil)

From the plot, it is evident that there are short tails on both sides. The Shapiro-Wilk normality test was carried out in RStudio to further validate the normality assumption. According to the test, a p-value of 0.06081 was calculated, which is the same as a = 0.01. It can be concluded then, that the null hypothesis cannot be rejected since the residuals are normally distributed at a = 0.01.

6.4.3.1.3 <u>Outlier Test</u>

In RStudio, the outliers were checked using several standard tests, if any were found. An outlier was identified through use of the Bonferroni outlier test. In order to find out whether the outliers have an impact on the final model, DFITS, DFBETAS, and Cook's Distance were implemented. Cook's Distance was compared using F-statistics and a = 0.05 resulting in an F-statistic of 3 for this set of data. Moreover, it is suggested that Di exceeding 0.5 should also be investigated, since it may have an influence (Faysal, 2017).

On the basis of the Bonferroni outlier test, none of the observations were flagged as potential outliers. There were no observations that did not fit the assumptions as determined by DFFITS, DFBETAS, as well as Cook's Distance Test.

6.4.3.1.4 <u>Multicollinearity</u>

According to the VIF in figure, it appears that all of the VIFs in the figure are within the suggested range. Therefore, there is no evidence of serious multicollinearity among the predictor variables.

6.4.3.1.5 <u>Backward Elimination</u>

It is important to note that the backward elimination method starts with all the variables in the model that will act as predictors. Subsequently, it removes insignificant variables incrementally from the model. When none of the insignificant variables remain in the model at the end of the analysis, the analysis is completed. Using this method, all the predictor variables were significant at the significance level of 0.01, and no variables were removed from the analysis

6.4.3.1.6 <u>Stepwise Regression</u>

A stepwise regression method makes use of both backward selection algorithms as well as forward selection algorithms. In the stepwise regression model, we begin with the most significant

predictor variable. The regression is then carried out and the parameters considered are calculated accordingly. As additional variables are added incrementally, they are added according to their significance. As the procedure is repeated until the model with the best parameter parameters is obtained, the process is repeated. It is performed with the help of the F-statistic test in order to determine the statistical significance of data (Kutner et al., 2005). According to this method, the inclusion of two predictor variables helped form the best model.

6.4.4 Validation of the Final Model (Sandy Soil)

It was decided to evaluate the predictive capacity of the resistivity model for compacted soil specimens by using the experimental results obtained from soil samples designated as sandy soils. The objective of comparing the model with new data sets was to evaluate how well it can be applied to different types of clayey soils. Testing of electrical resistivity was conducted at varying degrees of saturation, and the resulting observations were corrected for a temperature of 15.5 degrees Celsius. The Figure 6-21compares the experimental value and predicts value of resistivity.
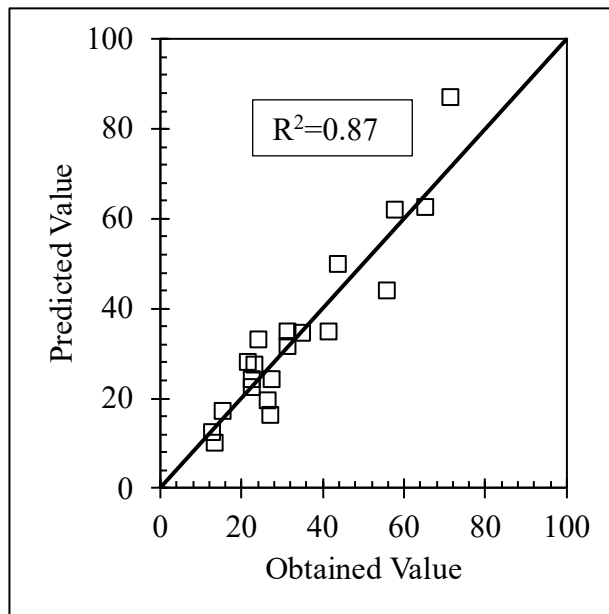
Figure 6-21 Comparison of estimated resistivity with experimental observations (sandy soil)

6.4.5 Interaction Surface for Compacted Sandy Soils

The combined effect of moisture content and sand fraction of sandy soils on the electrical resistivity responses shown in Figure 6-22 are determined from the developed multiple linear regression model. Similar to clayey soil samples, when the moisture content was less than 20% and sand content is higher than 80%, the resistivity was found very high. Resistivity was found decreasing with the increasing moisture content at a fixed sand content. When the sand content is high the decreasing rate is high whereas, at lower sand content the decreasing rate of resistivity with the increasing moisture content was found low. The interaction surface was found parallel to the surface when the moisture content is higher than 30% and sand content was lower then 70%.
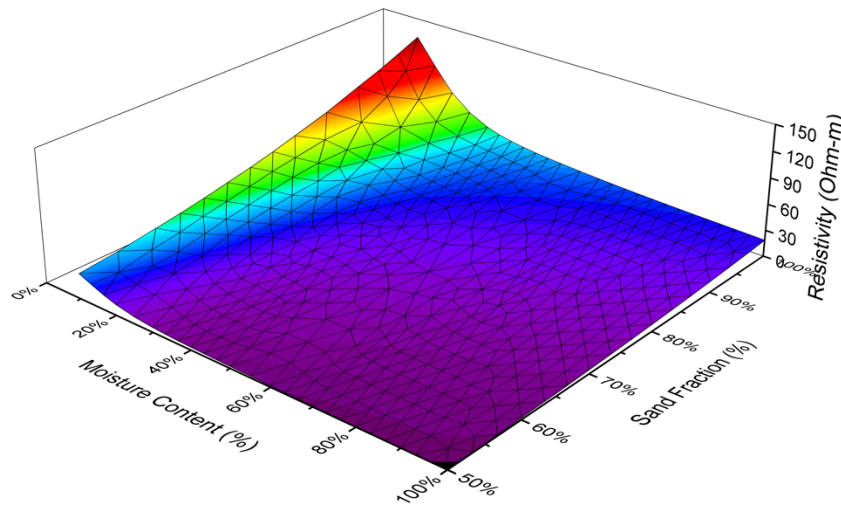
Figure 6-22 Interaction surface correlating resistivity with moisture content and sand fraction for sandy soils

6.4.6 Resistivity vs Degree of Saturation for compacted clays

The variation of resistivity with the increasing moisture content at different sand fraction was determined. The resistivity value at various moisture content was determined using the developed MLR model. Presence of sand fraction was also taken into consideration while developing the variation chart of resistivity. At higher sand fraction contained soil, the resistivity

was found higher compared to the lower sand fraction contained compacted soil sample. Resistivity value decreases very rapidly when the moisture content was increased up to 20%. After that, the rate of decreasing is low in all sandy soil samples. The variation of resistivity with the combined effect of moisture content and sand content is presented in Figure 6-23.
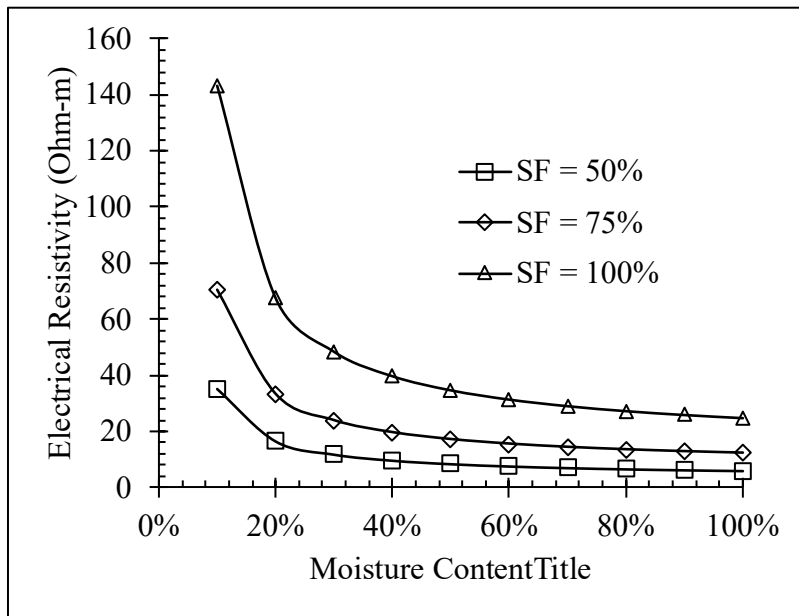
Figure 6-23 Variation of resistivity with the changing moisture content at various sand fraction

CHAPTER 7 CONCLUSIONS AND FUTURE RECOMMENDATIONS

7.1 Introduction

An electrical resistivity imaging survey (ERI) can be successfully used to obtain a continuous subsurface profile of a particular location. However, the use of this promising geophysical approach in geotechnical engineering has yet to be fully explored. Since the changes in soil properties will affect the soil resistivity, the response of the soil to the changes is complicated and hard to interpret. Thus, for a field survey only qualitative information can be derived from resistivity imaging with the aid of resistivity imaging. A study was conducted on various soil samples in order to make electrical resistivity imaging research useful in the engineering field. In this study, the aim was to evaluate the geotechnical properties of the soil through the results of the electrical resistivity testing. To conclude, a statistical model has been developed which can be used to predict soil properties on the field.

7.2 Summary and Conclusions

1. The soil samples for this experimental program were collected from Fort Worth, Beaumont, Corpus Christi, and El-paso based on their geological formations.

2. Total of 30 sites were selected in these four different districts and 88 soil samples were collected, including 25 sandy soil samples and 63 clayey soil samples. Among the clayey soil samples, 44 can be classified as low plastic clay and 19 can be classified as high plastic clay according to the USCS classification.

3. In the selected locations, soil boring was conducted from 10 ft to 90 ft depth using a truck-mounted Texas cone penetration (TCP) auger. During the soil investigation, TCP blow counts

of the subsoil were recorded at regular intervals. Samples of disturbed and undisturbed soil were collected throughout the investigation.

4. Field electrical resistivity measurements were performed on the same day as boring in the investigated areas using the Super Sting R8/IP multichannel system manufactured by Advanced Geosciences Inc. (AGI), Austin, TX. Resistivity profiles were examined using Earth-Imager 2D software.

5. Based on the field study of resistivity values for different types of soil, a resisrivity chart has been developed. The resistivity value of highly plastic clay was recorded to be the lowest.

6. The variation in vertical field electrical resistivity of the boring location was plotted against the TCP value for different soil types. There was a linear relationship observed between the electrical resistivity and the soil TCP blow counts. The coefficient of correlation was found to be 0.8 for sandy soils and 0.59 for clayey soils.

7. To identify the changes in electrical resistivity with changing soil conditions, laboratory experiments were developed with soils of varying geotechnical properties. In total, 1,002 electrical resistivity tests were conducted on soil samples collected for this study. All values of resistivity were calibrated to a standard temperature of 15.5 degrees C.

8. Soil fabric and mineralogy study was conducted in the laboratory with the help of scanning electron microscope and energy dispersive X-ray spectroscopy. Particle shape and pore space of clayey soils and sandy soils were investigated.

9. Electrical resistivity was plotted against the soil properties to evaluate the impact of liquid limit, plastic limit, fine content, activity, pore water conductivity, cation exchange capacity and specific surface area on electrical resistivity response of soil. An overall downward trend

was observed at different saturation level when the resistivity was plotted against these parameters.

10. Soluble sulfate content of the soil particle was measured by following Tex-145 method to evaluate the impact of sulfate content on electrical resistivity at different degree of saturation. Electrical resistivity was found to be decreasing with the increasing soluble sulfate content at different saturation level.

11. In order to explain the changes of resistivity with geotechnical parameters, i.e., moisture content, unit weight, void ratio, volumetric moisture content, degree of saturation., soil samples were categorized into six categories based on their liquid limit higher than 50, between 35 and 50, and lower than 35, and plastic limit higher than 25 and lower than 25.

12. When soil samples were plotted against moisture content, a downward exponential trend was observed. The rate of change of resistivity was not the same for all categories of soil. Soil with higher activity (PI/% clay) shows comparatively lesser changes in resistivity with increasing moisture content. However, the resistivity was found decreasing at a slower rate at moisture content higher than 25% for all types of soils.

13. Soil electrical resistivity was also plotted against dry unit weight and void ratio to examine the change of resistivity with the changes of unit weight. While resistivity shows a downward trend with unit weight, electrical resistivity shows an upward trend when plotted against void ratio.

14. Correlation equation was developed for the changes of electrical resistivity with volumetric moisture content and degree of saturation for all categories of soil. At lower degree of saturation, the resistivity of soils was found decreasing rapidly, however, when the degree of saturation of soil is 40%, the decrease in resistivity was found very lower.

15. For the development of multiple linear regression (MLR) model, degree of saturation and plasticity index were selected as two most important parameters influencing resistivity. It was observed that the other clay properties such as liquid limit, clay content, CEC, SSA and pore water conductivity were correlated with plasticity index. Therefore, only PI was considered as independent variable representing clay parameters.

16. Multiple linear regression equation was developed for compacted clayey soil to explain the changes of resistivity with the soil parameters.

$$\frac{1}{\sqrt{Resistivity}} = 0.3936782 + 0.5572772 \times \log(\text{Dos}) + 0.0036228 \times \text{PI}$$

17. Sandy samples were also evaluated with the changes of electrical resistivity with their soil properties i.e., sand content, unit weight, moisture content, degree of saturation, void ratio.

18. Multiple linear regression model was prepared for sandy soil sample, to easily explain the changes of geotechnical parameter of soil with help of electrical resistivity.

$$\log(Resistivity_{sand}) = -0.18240 + \frac{0.35196}{\sqrt{MC}} + 1.22523 \times (SF)$$

19. Undisturbed soil samples were also collected from the field and tests were conducted in the laboratory to evaluate their geotechnical parameter with the electrical resistivity. The results were compared with previous literature.

20. Different compactive energies were applied to soil samples for compacting and the variation in resistivity was observed for each application. The changes in resistivity occur differently on the dry side of the compaction curve and on the wet side.

21. An observation was made of the variation of the resistance as a function of the uniaxial compression force. From these results, a graph of unconfined compressive strength against resistivity was developed. Using the resistivity value as a measuring tool can indicate the maximum moisture content at which the soil can achieve its maximum compressive strength, however, this method overestimates the compressive strength.

7.3 Recommendations for Future Studies

1. Field results can be incorporated into the estimation of SPT-N and resistivity, thereby improving the relationship between the two. The moisture content of clayey soils can be taken into consideration.

2. By incorporating the field resistivity value for different types of soils into the soil resistivity chart, this can help improve the soil resistivity chart. It would be beneficial if pore water conductivity was taken into consideration for the improvement of the chart.

3. The anisotropic factor can be taken into account by utilizing different resistivity measuring instruments in the laboratory.

4. In this study, only a dipole dipole array was used. Different types of arrays can be used to determine the electrical resistivity of soil at any location.

5. The soil can also be tested using alternative currents with different frequencies instead of direct current, which would allow measuring the soil's resistance response.

6. As part of the current study, a statistical model was developed. However, analysis can be conducted using artificial neural networks to correlate more soil geotechnical properties with electrical resistivity

7. By studying the electrical resistivity of soil profiles on a laboratory scale, it will be possible to determine how moisture propagates through the soil and in which direction. In addition, electrical resistivity can be used to measure changes in the soil in relation to the season.

8. In order to correlate soil strength properties with electrical resistance, soil resistivity can be incorporated during the triaxial test.

9. The relationship between SWCC and resistivity can be investigated in the future considering their correlation with volumetric moisture content

REFERENCES

1. Abidin, M. H. Z., Saad, R., Wijeyesekera, D. C., Ahmad, F., Baharuddin, M. F. T., Tajudin, S. A. A., & Madun, A. (2017). The influences of basic physical properties of clayey silt and silty sand on its laboratory electrical resistivity value in loose and dense conditions. *Sains Malaysiana*, *46*(10), 1959–1969. https://doi.org/10.17576/jsm-2017-4610-35

2. Abu-Hassanein, Z. S., Benson, C. H., & Blotz, L. R. (1996). Electrical Resistivity of Compacted Clays. *Journal of Geotechnical Engineering*, *122*(5), 397–406. https://doi.org/10.1061/(ASCE)0733-9410(1996)122:5(397)

3. AGI. (2009). *EarthImager 2D*. *512*, 139.

4. Aizebeokhai, A. P. (2010). 2D and 3D geoelectrical resistivity imaging: Theory and field design. *Scientific Research and Essays*, *5*(23), 3592–3605.

5. Alam, M. J. Bin. (2017). *Evaluation of Plant Root On The Performance Of Evapotranspiration (Et) Cover System* (Issue October). The university of Texas at Arlington.

6. Alsharari, B., Olenko, A., & Abuel-Naga, H. (2020). Modeling of electrical resistivity of soil based on geotechnical properties. *Expert Systems with Applications*, *141*. https://doi.org/10.1016/j.eswa.2019.112966

7. Amadi, A., & Omotayo, T. (2017). *The nomenclature of geotechnical error traps as a theoretical framework for assessing financial risk in transportation infrastructure projects*. https://doi.org/http://usir.salford.ac.uk/id/eprint/43913

8. Amato, M., Lapenna, V., Rossi, R., & Bitella, G. (2012). Multi-electrode Resistivity Imaging. In S. Mancuso (Ed.), *Measuring Roots: An Updated Approach* (pp. 189–211). Springer Berlin Heidelberg. https://doi.org/10.1007/978-3-642-22067-8_11

9. Ameratunga, J., Sivakugan, N., & Das, B. M. (2016). *Correlations of Soil and Rock Properties in Geotechnical Engineering*. http://www.springer.com/series/13410

10. Archie, G. E. (1942). The Electrical Resistivity Log as an Aid in Determining Some Reservoir Characteristics. *Transactions of the AIME*, *146*(01), 54–62. https://doi.org/10.2118/942054-G

11. Argyroudis, S., Mitoulis, S., Winter, M. G., & Kaynia, A. M. (2018). Fragility of critical transportation infrastructure systems subjected to geo-hazards. *Proceedings 16th European*

Conference on Earthquake Engineering, 1–12.

12. Arjwech, R. (2011). *Electrical resistivity imaging for unknown bridge foundation depth determination*.

13. Arjwech, Rungroj, & Everett, M. E. (2015). Application of 2D electrical resistivity tomography to engineering projects: Three case studies. *Songklanakarin Journal of Science and Technology*, *37*(6), 675–681.

14. ASTM G187-18. (n.d.). Standard Test Method for Measurement of Soil Resistivity Using the Two-Electrode Soil Box Method. In *ASTM Book of Standards* (Issue Reapproved, pp. 1–5). https://doi.org/10.1520/G0187-18

15. Barker, R. D. (1989). Depth of investigation of collinear symmetrical four-electrode arrays. *Geophysics*, *54*(8), 1031–1037. https://doi.org/10.1190/1.1442728

16. Baynes, F. J. (2010). Sources of geotechnical risk. *Quarterly Journal of Engineering Geology and Hydrogeology*, *43*(3), 321–331. https://doi.org/10.1144/1470-9236/08-003

17. Bell, F. G., & Culshaw, M. G. (1998). Some geohazards caused by soil mineralogy, chemistry and microfabric: A review. *Geological Society Engineering Geology Special Publication*, *15*, 427–441. https://doi.org/10.1144/GSL.ENG.1998.015.01.43

18. Bery, A. A., & Saad, R. (2012). *Tropical Clayey Sand Soil ' s Behaviour Analysis and Its Empirical Correlations via Geophysics Electrical Resistivity Method and Engineering Soil Characterizations*. *2012*(February), 111–116.

19. Binley, A., Cassiani, G., Middleton, R., & Winship, P. (2002). Vadose zone flow model parameterisation using cross-borehole radar and resistivity imaging. *Journal of Hydrology*, *267*(3–4), 147–159. https://doi.org/10.1016/S0022-1694(02)00146-4

20. Binley, A., & Kemna, A. (2005). DC Resistivity and Induced Polarization Methods. *Hydrogeophysics*, 129–156. https://doi.org/10.1007/1-4020-3102-5_5

21. Boeckmann, A. Z., & Loehr, J. E. (2016). Influence of Geotechnical Investigation and Subsurface Conditions on Claims, Change Orders, and Overruns. In *Influence of Geotechnical Investigation and Subsurface Conditions on Claims, Change Orders, and Overruns*. Transportation Research Board. https://doi.org/10.17226/21926

22. Bottraud, J. C. ., Bornand, M. ., & Servat, E. (1986). Measurement of soil resistivity as applied to soil survey. *Science Du Sol (France)*, *4*, 279–294.

23. Bowles, J. E. (1988). *FOUNDATION ANALYSIS AND DESIGN. FOURTH EDITION*.

1004.

24. Braga, A. C. O., Malagutti F°_, W., Dourado, J. C., & Chang, H. K. (1999). Correlation of Electrical Resistivity and Induced Polarization Data with Geotechnical Survey Standard Penetration Test Measurements. *Journal of Environmental and Engineering Geophysics*, *4*(2), 123–130. https://doi.org/10.4133/jeeg4.2.123

25. Brunet, P., Clément, R., & Bouvier, C. (2010). Monitoring soil water content and deficit using Electrical Resistivity Tomography (ERT) - A case study in the Cevennes area, France. *Journal of Hydrology*, *380*(1–2), 146–153. https://doi.org/10.1016/j.jhydrol.2009.10.032

26. Bryson, L. S. (2005). Evaluation of Geotechnical Parameters using Electrical Resistivity Measurements. *Earthquake Engineering and Soil Dynamics*, *740*, 1–11.

27. Bryson, L. S., & Bathe, A. (2009). Determination of selected geotechnical properties of soil using electrical conductivity testing. *Geotechnical Testing Journal*, *32*(3), 252–261. https://doi.org/10.1520/gtj101632

28. Campbell, R. B., Bower, C. A., & Richards, L. A. (1949). Change of Electrical Conductivity With Temperature and the Relation of Osmotic Pressure to Electrical Conductivity and Ion Concentration for Soil Extracts. *Soil Science Society of America Journal*, *13*(C), 66–69. https://doi.org/10.2136/sssaj1949.036159950013000c0010x

29. Chen, H., & Lee, C. F. (2004). Geohazards of slope mass movement and its prevention in Hong Kong. *Engineering Geology*, *76*(1–2), 3–25. https://doi.org/10.1016/j.enggeo.2004.06.003

30. Cosenza, P., Marmet, E., Rejiba, F., Jun Cui, Y., Tabbagh, A., & Charlery, Y. (2006). Correlations between geotechnical and electrical data: A case study at Garchy in France. *Journal of Applied Geophysics*, *60*(3–4), 165–178. https://doi.org/10.1016/j.jappgeo.2006.02.003

31. Creedy, G. D. (2006). *Risk Factors Leading To Cost Overrun in the Delivery of Highway Construction Projects*. Queensland University of Technology.

32. Datsios, Z. G., Mikropoulos, P. N., & Karakousis, I. (2017). Laboratory characterization and modeling of DC electrical resistivity of sandy soil with variable water resistivity and content. *IEEE Transactions on Dielectrics and Electrical Insulation*, *24*(5), 3063–3072. https://doi.org/10.1109/TDEI.2017.006583

33. Everett, M. (2013). *Near-surface applied geophysics*.

34. FARRAR, D. M., & COLEMAN, J. D. (1967). THE CORRELATION OF SURFACE AREA WITH OTHER PROPERTIES OF NINETEEN BRITISH CLAY SOILS. *Journal of Soil Science*, *18*(1), 118–124. https://doi.org/10.1111/j.1365-2389.1967.tb01493.x

35. Faysal, M. (2017). STRUCTURAL COMPETENCY AND ENVIRONMENTAL SOUNDNESS OF THE RECYCLED BASE MATERIALS IN NORTH TEXAS. *Progress in Physical Geography*, *14*(7), 450. https://doi.org/10.1177/0309133309346882

36. FHWA. (2015). Soil Nail Walls Reference Manual. *Geotechnical Engineering Circular NO. 7 - Soil Nail Walls Reference Manual*, *132085*, 425.

37. Friedman, S. P. (2005). Soil properties influencing apparent electrical conductivity: A review. *Computers and Electronics in Agriculture*, *46*(1-3 SPEC. ISS.), 45–70. https://doi.org/10.1016/j.compag.2004.11.001

38. Fukue, M., Minato, T., Horibe, H., & Taya, N. (1999). The micro-structures of clay given by resistivity measurements. *Engineering Geology*, *54*(1–2), 43–53. https://doi.org/10.1016/S0013-7952(99)00060-5

39. Giao, P. H., Chung, S. G., Kim, D. Y., & Tanaka, H. (2003). Electric imaging and laboratory resistivity testing for geotechnical investigation of Pusan clay deposits. *Journal of Applied Geophysics*, *52*(4), 157–175. https://doi.org/10.1016/S0926-9851(03)00002-8

40. Gingine, V., Dias, A. S., & Cardoso, R. (2016). Compaction Control of Clayey Soils Using Electrical Resistivity Charts. *Procedia Engineering*, *143*(Ictg), 803–810. https://doi.org/10.1016/j.proeng.2016.06.130

41. Groves, P., Cascante, G., Dundas, D., & Chatterji, P. K. (2011). Use of geophysical methods for soil profile evaluation. *Canadian Geotechnical Journal*, *48*(9), 1364–1377. https://doi.org/10.1139/t11-044

42. Gunn, D. A., Chambers, J. E., Uhlemann, S., Wilkinson, P. B., Meldrum, P. I., Dijkstra, T. A., Haslam, E., Kirkham, M., Wragg, J., Holyoake, S., Hughes, P. N., Hen-Jones, R., & Glendinning, S. (2015). Moisture monitoring in clay embankments using electrical resistivity tomography. *Construction and Building Materials*, *92*, 82–94. https://doi.org/10.1016/j.conbuildmat.2014.06.007

43. Hatta, K. A., & Syed Osman, S. B. A. (2015). Correlation of Electrical Resistivity and SPT-N Value from Standard Penetration Test (SPT) of Sandy Soil. *Applied Mechanics and*

Materials, *785*, 702–706. https://doi.org/10.4028/www.scientific.net/amm.785.702

44. Hesse, A., Jolivet, A., & Tabbagh, A. (1986). New prospects in shallow depth electrical surveying for archaeological and pedological applications. *Geophysics*, *51*(3), 585–594. https://doi.org/10.1190/1.1442113

45. Hirsch, M., Bentley, L. R., & Dietrich, P. (2008). A comparison of electrical resistivity, ground penetrating radar and seismic refraction results at a river terrace site. *Journal of Environmental and Engineering Geophysics*, *13*(4), 325–333. https://doi.org/10.2113/JEEG13.4.325

46. Hisyam, J., & Osman, S. B. S. (2017). The Correlation between Resistivity and Soil Properties as an Alternative to Soil Investigation. *Indian Journal of Science and Technology*, *10*(6), 1–5. https://doi.org/10.17485/ijst/2017/v10i6/111205

47. Holtz, R. D., & Kovacs, W. D. (1981). *AN INTRODUCTION TO GEOTECHNICAL ENGINEERING*.

48. Hossain, J. (2012). *Geohazard Potential of Rainfall Induced Slope Failure* (Issue November). The University of Texas at Arlington.

49. Hossain, M. I. (2017). *Non-Destructive Evaluation of Soil Moisture Evapotraspiration Cover System* (Issue December).

50. Hossain, S., Dharmateja, M., & Hossain, J. (2010). Assessment of geo-hazard potential and site investigations using Resistivity Imaging. *International Journal of Environmental Technology and Management*, *13*(2), 116–129. https://doi.org/10.1504/IJETM.2010.034297

51. Hossain, S., Kibria, G., & Khan, S. (2019). *Site investigation using resistivity imaging*. CRC Press/Balkema.

52. Huda, S. (2011). *A NON-INVASIVE ASSESMENT OF MOISTURE CONTENT OF MUNICIPAL SOLID WASTE IN A LANDFILL USING RESISTIVITY IMAGING*. *13*(128), 234.

53. Hunt, R. E. (2005). Geotechnical Engineering Investigation Handbook. In *Angewandte Chemie International Edition, 6(11), 951–952.* CRC Press. https://doi.org/10.1201/9781420039153

54. Jackson, P. D., Smith, D. T., & Stanford, P. N. (1978). Resistivity-porosity-particle shape relationships for marine sands. *GEOPHYSICS*, *43*(6), 1250–1268.

https://doi.org/10.1190/1.1440891

55. Kalinski, R. J. (1992). Surface geoelectrics for characterizing ground water protective layers and compacted soil liners. In *ETD collection for University of Nebraska - Lincoln*. https://digitalcommons.unl.edu/dissertations/AAI9314404

56. Kalinski, R., & Kelly, W. (1993). Estimating Water Content of Soils from Electrical Resistivity. *Geotechnical Testing Journal*, *16*(3), 323. https://doi.org/10.1520/gtj10053j

57. Kaufman, A. A., & Hoekstra, P. (2001). *Electromagnetic Soundings*.

58. Kibria, G. (2014). *Evaluation of Physico-Mechanical Properties of Clayey Soils Using Electrical Resistivity Imaging Technique.* *8*(May), 44. https://doi.org/10.1192/bjp.205.1.76a

59. KIBRIA, G. (2014). *EVALUATION OF PHYSICO-MECHANICAL PROPERTIES OF CLAYEY SOILS USING ELECTRICAL RESISTIVITY IMAGING TECHNIQUE* (Vol. 2014, Issue May). The University of Texas at Arlington.

60. Kibria, G., & Hossain, M. S. (2015). Investigation of degree of saturation in landfill liners using electrical resistivity imaging. *Waste Management*, *39*, 197–204. https://doi.org/10.1016/j.wasman.2015.02.015

61. Kim, J. H., Yoon, H.-K., & Lee, J.-S. (2011). Void Ratio Estimation of Soft Soils Using Electrical Resistivity Cone Probe. *Journal of Geotechnical and Geoenvironmental Engineering*, *137*(1), 86–93. https://doi.org/10.1061/(asce)gt.1943-5606.0000405

62. Kouchaki, B. M., Bernhardt-Barry, M. L., Wood, C. M., & Moody, T. (2019). A Laboratory investigation of factors influencing the electrical resistivity of different soil types. *Geotechnical Testing Journal*, *42*(4), 829–853. https://doi.org/10.1520/GTJ20170364

63. Kulhawy, F. H., & Mayne, P. W. (1990). *Manual on Estimating Soil Properties on Foundation Design*.

64. Kutner, M., Nachtsheim, C., Neter, J., & Li, W. (2005). *Applied linear statistical models*.

65. Kwader, T. (1985). Estimating Aquifer Permeability from Formation Resistivity Factors. *Ground Water*, *23*(6), 762–766. https://doi.org/10.1111/j.1745-6584.1985.tb01955.x

66. Lamotte, M., Bruand, A., Dabas, M., Donfack, P., Gabalda, G., Hesse, A., Humbel, F. X., & Robain, H. (1994). *Distribution d'un horizon à forte cohésion au sein d'une couverture de sol aride du Nord-Cameroun: apport d'une prospection électrique (Distribution of*

hardpan in soil cover of arid zones. Data from a geoelectrical survey in northern Cameroon).

67. Landviser. (2001). *Theory of Four-Electrode Resistivity/Conductivity Method*. *5263*, 4.

68. Leung, Y. F., Liu, W., Lei, Y., & Hsu, S. C. (2018). Quantifying cost-effectiveness of subsurface strata exploration in excavation projects through geostatistics and spatial tessellation. *Automation in Construction*, *90*(February), 243–252. https://doi.org/10.1016/j.autcon.2018.02.032

69. Liu, S., Chen, L., & Han, L. (2008). Study on electrical resistivity related parameters of contaminated soils. *Geotechnical Engineering for Disaster Mitigation and Rehabilitation - Proceedings of the 2nd International Conference GEDMAR08*, 695–701. https://doi.org/10.1007/978-3-540-79846-0_88

70. Loehr, J. E., Lutenegger, A., Rosenblad, B. L., & Boeckmann, A. (2016). *Geotechnical Site Characterization*. https://doi.org/FHWA-NHI-16-072

71. Loke, M. H. (2004). Tutorial: 2-D and 3-D Electrical Imaging Surveys, 2004 Revised Edition. *Tutorial : 2-D and 3-D Electrical Imaging Surveys*, *July*, 136.

72. Loke M. H. (2015). 2-D and 3-D Electrical Imaging Surveys. *Tutorial*, *May*, 51–52.

73. Long, M., Limacher, R., Donohue, S., L'Heureux, J. S., Solberg, I. L., Rønning, J. S., O'Connor, P., Sauvin, G., Rømoen, M., & Lecomte, I. (2012). Relationship between electrical resistivity and basic geotechnical parameters for marine clays. *Canadian Geotechnical Journal*, *49*(10), 1158–1168. https://doi.org/10.1139/T2012-080

74. Manzur, S. R. (2013). *Hydraulic Performance Evaluation of Different Recirculation*. *May*, 1–222.

75. Matsui, T., Park, S. G., Park, M. K., & Matsuura, S. (2000). *Relationship Between Electrical Resistivity And Physical Properties Of Rocks*. OnePetro.

76. Mayne, P. W., Christopher, B. R., & DeJong, J. (2002). Manual on subsurface investigations. In *Field Hydrogeology* (Issue 132031, pp. 63–77). National Highway Institute. https://doi.org/10.1201/b11056-6

77. McCarter, W. J. (1984). The electrical resistivity characteristics of compacted clays. *Geotechnique*, *34*(2), 263–267. https://doi.org/10.1680/geot.1984.34.2.263

78. Meigh, A. (2013). *Cone penetration testing: methods and interpretation*.

79. Miracapillo, C., & Morel-Seytoux, H. (2015). Preliminary Field Tests to Determine the

Soil Water Content Using Resistivity Measurements. *Procedia Environmental Sciences*, *25*, 158–165. https://doi.org/10.1016/j.proenv.2015.04.022

80. Mitchell, J., & Soga, K. (2005). *Fundamentals of soil behavior*.

81. Mojid, M. A., & Cho, H. (2006). Estimating the fully developed diffuse double layer thickness from the bulk electrical conductivity in clay. *Applied Clay Science*, *33*(3–4), 278–286. https://doi.org/10.1016/j.clay.2006.06.002

82. Munoz-Castelblanco, J., Pereira, J.-M., Delage, P., & Yu Jun, C. (2012). The influence of changes in water content on the electrical resistivity of a natural unsaturated loess.

83. Niederleithinger, E., Weller, A., & Lewis, R. (2013). *Evaluation of Geophysical Techniques for Dike Inspection*. 703–703. https://doi.org/10.4133/sageep2013-058.1

84. Oh, S., & Sun, C. G. (2008). Combined analysis of electrical resistivity and geotechnical SPT blow counts for the safety assessment of fill dam. *Environmental Geology*, *54*(1), 31–42. https://doi.org/10.1007/s00254-007-0790-y

85. Oh, T. M., Cho, G. C., & Lee, C. (2014). Effect of soil mineralogy and pore-water chemistry on the electrical resistivity of saturated soils. *Journal of Geotechnical and Geoenvironmental Engineering*, *140*(11), 1–5. https://doi.org/10.1061/(ASCE)GT.1943-5606.0001175

86. Ozcep, F., Tezel, O., & Asci, M. (2009). *Correlation between electrical resistivity and soil-water content : Istanbul and Golcuk. May 2014*.

87. Palacky, G. J. (1987). Clay mapping using electromagnetic methods. *First Break*, *5*(8). https://doi.org/10.3997/1365-2397.1987015

88. Phan, V. T. A., Hsiao, D. H., & Nguyen, P. T. L. (2016). Effects of fines contents on engineering properties of sand-fines mixtures. *Procedia Engineering*, *142*, 213–220. https://doi.org/10.1016/j.proeng.2016.02.034

89. Pozdnyakov, A. I., Pozdnyakova, L. A., & Karpachevskii, L. O. (2006). Relationship between water tension and electrical resistivity in soils. *Eurasian Soil Science*, *39*(S1), S78–S83. https://doi.org/10.1134/s1064229306130138

90. Pozdnyakova, L. (1999). *ELECTRICAL PROPERTIES OF SOILS. June*.

91. Revil, A., Coperey, A., Shao, Z., Florsch, N., Fabricius, I. L., Deng, Y., Delsman, J. R., Pauw, P. S., Karaoulis, M., de Louw, P. G. B. B., van Baaren, E. S., Dabekaussen, W., Menkovic, A., & Gunnink, J. L. (2017). Complex conductivity of soils. *Water Resources*

Research, *53*(8), 7121–7147. https://doi.org/10.1002/2017WR020655

92. Revil, A., Darot, M., & Pezard, P. A. (1996). From surface electrical properties to spontaneous potentials in porous media. *Surveys in Geophysics 1996 17:3*, *17*(3), 331–346. https://doi.org/10.1007/BF01904047

93. Rezaei, S., Shooshpasha, I., & Rezaei, H. (2018). Empirical Correlation between Geotechnical and Geophysical Parameters in a Landslide Zone (Case Study: Nargeschal Landslide). *Earth Sciences Research Journal*, *22*(3), 195–204. https://doi.org/10.15446/esrj.v22n3.69491

94. Rhoades, J., Chanduvi, F., & Lesch, S. (1999). *Soil salinity assessment: Methods and interpretation of electrical conductivity measurements*.

95. Rhoades, J. D., & van Schilfgaarde, J. (1976). An Electrical Conductivity Probe for Determining Soil Salinity. *Soil Science Society of America Journal*, *40*(5), 647–651. https://doi.org/10.2136/SSSAJ1976.03615995004000050016X

96. Rinaldi, V. A., & Cuestas, G. A. (2002). Ohmic conductivity of a compacted silty clay. *Journal of Geotechnical and Geoenvironmental Engineering*, *128*(10), 824–835. https://doi.org/10.1061/(ASCE)1090-0241(2002)128:10(824)

97. Robinson, D. A., Jones, S. B., Wraith, J. M., Or, D., & Friedman, S. P. (2003). A review of advances in dielectric and electrical conductivity measurement in soils using time domain reflectometry. *Pubs.Geoscienceworld.Org*.

98. Samouëlian, A., Cousin, I., Tabbagh, A., Bruand, A., & Richard, G. (2005). Electrical resistivity survey in soil science: a review. *Soil and Tillage Research*, *83*(2), 173–193. https://doi.org/10.1016/j.still.2004.10.004

99. Samouëlian, Anatja;, Cousin, I., Richard, G., Tabbagh, A., & Bruand, A. (2003). Electrical resistivity imaging for detecting soil cracking at the centimetric scale. *Soil Science Society of America Journal*, *67*(5), 1319–1326.

100. Santamarina, J., Klein, K., & Fam, M. (2001). *Soils and waves*.

101. Schwartz, B. F., Schreiber, M. E., Pooler, P. S., & Rimstidt, J. D. (2008). Calibrating Access-tube Time Domain Reflectometry Soil Water Measurements in Deep Heterogeneous Soils. *Soil Science Society of America Journal*, *72*(4), 917–930. https://doi.org/10.2136/sssaj2007.0208

102. Semenov, A. S. (1980). *Electroexploration with method of natural electrical field (self-*

potential).

103. Sew, I., Engineering, I. C.-I. S. on G., & 2000, undefined. (2000). Planning of subsurface investigation and interpretation of test results for geotechnical design. *Gnpgroup.Com.My*, 22–23.

104. Shah, P. H., & Singh, D. N. (2005). Generalized archie's law for estimation of soil electrical conductivity. *Journal of ASTM International*, *2*(5), 145–164. https://doi.org/10.1520/JAI13087

105. Shevnin, V., Mousatov, A., Ryjov, A., & Delgado-rodriquez, O. (2007). Estimation of clay content in soil based on resistivity modelling and laboratory measurements. *Geophysical Prospecting*, *55*(2), 265–275. https://doi.org/10.1111/j.1365-2478.2007.00599.x

106. Shrestha, P. P., & Neupane, K. P. (2020). Identification of Geotechnical-Related Problems Impacting Cost, Schedule, and Claims on Bridge Construction Projects. *Journal of Legal Affairs and Dispute Resolution in Engineering and Construction*, *12*(2), 1–9. https://doi.org/10.1061/(ASCE)LA.1943-4170.0000375

107. Singha, K., & Gorelick, S. M. (2006). Effects of spatially variable resolution on field-scale estimates of tracer concentration from electrical inversions using Archie's law. *Geophysics*, *71*(3). https://doi.org/10.1190/1.2194900

108. Skempton, A. W. (1984). The Colloidal "Activity" of Clays. In *SELECTED PAPERS ON SOIL MECHANICS* (pp. 60–64). Thomas Telford Publishing. https://doi.org/10.1680/sposm.02050.0009

109. Sreedeep, S., Reshma, A. C., & Singh, D. N. (2004). Measuring soil electrical resistivity using a resistivity box and a resistivity probe. *Geotechnical Testing Journal*, *27*(4), 411–415. https://doi.org/10.1520/gtj11199

110. Stevens, J. (2012). *Applied multivariate statistics for the social sciences*.

111. Sudha, K., Israil, M., Mittal, S., & Rai, J. (2009). Soil characterization using electrical resistivity tomography and geotechnical investigations. *Journal of Applied Geophysics*, *67*(1), 74–79. https://doi.org/10.1016/j.jappgeo.2008.09.012

112. Tomeh, A. A., Alyateem, S., Malik, H., & Malone, B. (2006). Geophysical Surveying and Data Simulation Application to Geotechnical Investigations: A Cost Effective Approach for Developing Economical Foundation Engineering Design Criteria. *GeoCongress 2006: Geotechnical Engineering in the Information Technology Age*, *2006*, 1–6.

https://doi.org/10.1061/40803(187)98

113. Tonks, D., Gallagher, E., & Geol, I. N. E. (2017). Grounds for concern: Geotechnical issues from some recent construction cases. *Proceedings of the Institution of Civil Engineers: Forensic Engineering*, *170*(4), 157–164. https://doi.org/10.1680/jfoen.17.00008

114. Vipulanandan, C., Puppala, A. J., Jao, M., Kim, M. S., Vasudevan, H., Kumar, P., & Mo, Y. L. (2008). *Correlation of Texas Cone Penetrometer Test Values and Shear Strength of Texas Soils: Technical Report*. *August 2006*.

115. Voutou, B., Stefanaki, E., & Giannakopoulos, K. (2008). Electron Microscopy : The Basics. *Physics of Advanced Materials Winter School*, 1–11.

116. Yang, J.-S. (2002). *Three-dimensional complex resistivity analysis for clay characterization in hydrogeologic study* [University of California, Berkeley)].

117. Yoon, G. L., Oh, M. H., & Park, J. B. (2002). Laboratory study of landfill leachate effect on resistivity in unsaturated soil using cone penetrometer. *Environmental Geology*, *43*(1–2), 18–28. https://doi.org/10.1007/s00254-002-0649-1

118. Yoon, Gil Lim, & Park, J. B. (2001). Sensitivity of leachate and fine contents on electrical resistivity variations of sandy soils. *Journal of Hazardous Materials*, *84*(2–3), 147–161. https://doi.org/10.1016/S0304-3894(01)00197-2

119. Zha, F., Liu, S., Du, Y., Cui, K., & Xu, L. (2010). Characterization of Compacted Loess by Electrical Resistivity Method. *Journal of Chemical Information and Modeling*, *53*(9), 1689–1699. https://doi.org/10.1017/CBO9781107415324.004

120. Zhou, Q., Shimada, J., Research, A. S.-W. R., & 2001, undefined. (2001). Three-dimensional spatial and temporal monitoring of soil water content using electrical resistivity tomography. *Wiley Online Library*, *37*(2), 273–285. https://doi.org/10.1029/2000WR900284

APPENDIX

BORING NUMBER P1
PAGE 1 OF 1

LOGO

The University of Texas at Arlington
416 Yates Stress
76010

CLIENT _____	**PROJECT NAME** _____
PROJECT NUMBER _First Visit_	**PROJECT LOCATION** _Beaumont_
DATE STARTED _10/13/19_ **COMPLETED** _10/13/19_	**GROUND ELEVATION** _____ **HOLE SIZE** _inches_
DRILLING CONTRACTOR _____	**GROUND WATER LEVELS:**
DRILLING METHOD _____	**AT TIME OF DRILLING** ---
LOGGED BY _____ **CHECKED BY** _____	**AT END OF DRILLING** ---
NOTES _____	**AFTER DRILLING** ---

DEPTH (ft)	GRAPHIC LOG	MATERIAL DESCRIPTION	SAMPLE TYPE NUMBER	RECOVERY % (RQD)	BLOW COUNTS (N VALUE)	POCKET PEN. (tsf)	DRY UNIT WT. (pcf)	MOISTURE CONTENT (%)	ATTERBERG LIMITS			FINES CONTENT (%)
									LIQUID LIMIT	PLASTIC LIMIT	PLASTICITY INDEX	
0												
		(SC) Gray to Brown; Sandy Clay	SS		8-11-3 (14)							
5		(CL) Brown to Dark Brown; Clay; Moist										
		(CH) Brown; Clay	SPT		2-2-2 (4)							
			ST									
10		(CH) Brown; Clay; Moist										
			SPT		1-2-2 (4)							

Bottom of borehole at 11.5 feet.

LOGO

The University of Texas at Arlington
416 Yates Stress
76010

CLIENT _____

PROJECT NAME _____

PROJECT NUMBER First Visit

PROJECT LOCATION Beaumont

DATE STARTED 10/14/19   COMPLETED 10/14/19

GROUND ELEVATION _____   HOLE SIZE inches

DRILLING CONTRACTOR _____

GROUND WATER LEVELS:

DRILLING METHOD _____

AT TIME OF DRILLING ---

LOGGED BY _____ CHECKED BY _____

AT END OF DRILLING ---

NOTES _____

AFTER DRILLING ---

DEPTH (ft)	GRAPHIC LOG	MATERIAL DESCRIPTION	SAMPLE TYPE NUMBER	RECOVERY % (RQD)	BLOW COUNTS (N VALUE)	POCKET PEN. (tsf)	DRY UNIT WT. (pcf)	MOISTURE CONTENT (%)	LIQUID LIMIT	PLASTIC LIMIT	PLASTICITY INDEX	FINES CONTENT (%)
0												
		(CL) Light Brown, gray; Silty Clay; Moist;	ST									
		(CL-CH) Brown to Light Brown; Clay with sand;	ST									
5		(CH) Brown to Dark Brown; Clay;	SPT		1-0-1 (1)							
			ST									
		(CH) Brown to Dark Brown; Clay; Moist	ST									
10			SPT		2-1-3 (4)							

Bottom of borehole at 11.5 feet.

GEOTECH BH COLUMNS - GINT STD US LAB.GDT - 4/3/20 01:46 - C:\USERS\MXA0516\ONEDRIVE - UNIVERSITY OF TEXAS AT ARLINGTON\LAB DOCS\RESISTIVITY IMAGING\TEST RESULTS\SITE RESISTIVITY RESULT\BEAUMONT\P1\BORELOG P1\BORELOG INFO.GPJ

BORING NUMBER P6

LOGO

The University of Texas at Arlington
416 Yates Stress
76010

CLIENT _____

PROJECT NUMBER _First Visit_

DATE STARTED _10/15/19_   COMPLETED _10/15/19_

DRILLING CONTRACTOR _____

DRILLING METHOD _____

LOGGED BY _____ CHECKED BY _____

NOTES _____

PROJECT NAME _____

PROJECT LOCATION _Beaumont_

GROUND ELEVATION _____ HOLE SIZE _inches_

GROUND WATER LEVELS:

AT TIME OF DRILLING _—_

AT END OF DRILLING _—_

AFTER DRILLING _—_

DEPTH (ft)	GRAPHIC LOG	MATERIAL DESCRIPTION	SAMPLE TYPE NUMBER	RECOVERY % (RQD)	BLOW COUNTS (N VALUE)	POCKET PEN. (tsf)	DRY UNIT WT. (pcf)	MOISTURE CONTENT (%)	ATTERBERG LIMITS			FINES CONTENT (%)
									LIQUID LIMIT	PLASTIC LIMIT	PLASTICITY INDEX	
0												
		(CL) Brown; Silty Clay;	ST									
5		(CL) Brown; Clay	ST									
		(CH) Brown; Clay	SPT		2-2-4 (6)							
			ST									
10		(CH) Dark Brown; Clay										
					1-1-2 (3)							

Bottom of borehole at 11.5 feet.

205

LOGO

The University of Texas at Arlington
416 Yates Stress
76010

CLIENT _____

PROJECT NAME _____

PROJECT NUMBER _First Visit_

PROJECT LOCATION _Beaumont_

DATE STARTED _10/14/19_   COMPLETED _10/14/19_

GROUND ELEVATION _____   HOLE SIZE _inches_

DRILLING CONTRACTOR _____

GROUND WATER LEVELS:

DRILLING METHOD _____

AT TIME OF DRILLING —

LOGGED BY _____   CHECKED BY _____

AT END OF DRILLING —

NOTES _____

AFTER DRILLING —

DEPTH (ft)	GRAPHIC LOG	MATERIAL DESCRIPTION	SAMPLE TYPE NUMBER	RECOVERY % (RQD)	BLOW COUNTS (N VALUE)	POCKET PEN. (tsf)	DRY UNIT WT. (pcf)	MOISTURE CONTENT (%)	ATTERBERG LIMITS			FINES CONTENT (%)
									LIQUID LIMIT	PLASTIC LIMIT	PLASTICITY INDEX	
0												
		(CL) Gray to Light gray; Slighly moist; Silty Sand with clay; sand seam	SS		11-9-6 (15)							
		(CL) Gray; Sandy silty clay;										
5		(CL-CH) Gray to brown; Silty Clay	SPT		1-2-4 (6)							
			ST									
		(CL-CH) Gray to brown; silty clay										
10			SPT		2-1-2 (3)							

Bottom of borehole at 11.5 feet.

GEOTECH BH COLUMNS - GINT STD US LAB.GDT - 4/3/20 01:47 - C:\USERS\MJX\0516\ONEDRIVE - UNIVERSITY OF TEXAS AT ARLINGTON\LAB DOCS\RESISTIVITY IMAGING\TEST RESULTS\SITE RESISTIVITY RESULT\BEAUMONT\P17\BORELOG_P17\BORELOG INFO.GPJ

LOGO

The University of Texas at Arlington
416 Yates Stress
76010

CLIENT SWIS Lab

PROJECT NAME Md Asif Akhtar

PROJECT NUMBER

PROJECT LOCATION Beaumont

DATE STARTED 12/12/19 **COMPLETED** 12/13/19

GROUND ELEVATION **HOLE SIZE** inches

DRILLING CONTRACTOR

GROUND WATER LEVELS:

DRILLING METHOD Wash Boring

▽ **AT TIME OF DRILLING** 6.50 ft

LOGGED BY **CHECKED BY**

AT END OF DRILLING ---

NOTES Wet Rotary set @ 8 ft due to Ground Water Table found at 6.5 ft

AFTER DRILLING ---

DEPTH (ft)	GRAPHIC LOG	MATERIAL DESCRIPTION	SAMPLE TYPE NUMBER	RECOVERY % (RQD)	BLOW COUNTS (N VALUE)	POCKET PEN. (tsf)	DRY UNIT WT. (pcf)	MOISTURE CONTENT (%)	LIQUID LIMIT	PLASTIC LIMIT	PLASTICITY INDEX	FINES CONTENT (%)
0												
		(CL) Silty Clay; Dark Brown; Moist	ST	88								
5		(CH) Clay; Dark Brown to Light Brown; Moist	ST	89								
		(CH) Very soft clay; Light brown to light grey; Moist	SPT		1-1-1 (2)							
			ST	89								
		(CH) Very soft clay; Light brown to light grey; Moist	ST	79								
10		(CL) Slightly Silty Clay; Light brown with some orange and gray; Moist	SPT		6-8-6 (14)							
		(CL) Slightly Silty Clay; Light brown with some orange and gray; Moist	ST	58								
15			SPT		4-5-9 (14)							
		(SW-SC) Clayey Sand; Reddish-brown; Moist	ST	46								
20			SPT		7-12-9 (21)							
		(CL) Silty Clay; Light brown with some orange; Moist and Soft	ST	88								
25			SPT		6-8-8 (16)							
		(CL) Silty Clay; Light brown with some orange; Moist and Soft	ST	100								
30			SPT		6-6-8 (14)							
		(CL) Slightly Silty Clay; Light brown with some orange; Moist	ST	92								
35												

(Continued Next Page)

GEOTECH BH COLUMNS - GINT STD US LAB.GDT - 12/17/19 15:29 - C:\USERS\PUBLIC\DOCUMENTS\BENTLEY\GINT\PROJECTS\GINT STD US LAB.GPJ

LOGO

The University of Texas at Arlington
416 Yates Stress
76010

CLIENT _____

PROJECT NUMBER _____

DATE STARTED 12/12/19   **COMPLETED** 12/13/19

DRILLING CONTRACTOR _____

DRILLING METHOD Wash Boring

LOGGED BY _____ **CHECKED BY** _____

NOTES _____

PROJECT NAME Beaumont Site Investigation with Electrical Resisitivity

PROJECT LOCATION Beaumont (SH 96 and SH69 Intersection)

GROUND ELEVATION _____ **HOLE SIZE** inches

GROUND WATER LEVELS:

AT TIME OF DRILLING ---

AT END OF DRILLING ---

AFTER DRILLING ---

DEPTH (ft)	GRAPHIC LOG	MATERIAL DESCRIPTION	SAMPLE TYPE NUMBER	RECOVERY % (RQD)	BLOW COUNTS (N VALUE)	POCKET PEN. (tsf)	DRY UNIT WT. (pcf)	MOISTURE CONTENT (%)	LIQUID LIMIT	PLASTIC LIMIT	PLASTICITY INDEX	FINES CONTENT (%)
0												
		Dark Brown; Sandy Clay; Organics				1.0						
						1.0						
		Dark Brown; Clay				1.0						
5					0-0-1 (1)	0						
						0						
						.5						
10					0-0-1 (1)							
15					4-8-8 (16)	1.0						
		Gray to Brown; Sandy Clay										
20					5-7-7 (14)	2.0						
		Gray, Brown, Tan; Sandy Clay with White seams			3-5-5 (10)							
25												
30					5-5-5 (10)	2.0						
35												

(Continued Next Page)

FOR ACADEMIC USE ONLY

GEOTECH BH COLUMNS - GINT STD US LAB.GDT - 12/18/19 12:18 - C:\USERS\PUBLIC\DOCUMENTS\BENTLEY\GINT\PROJECTS\GINT STD US LAB.GPJ

208
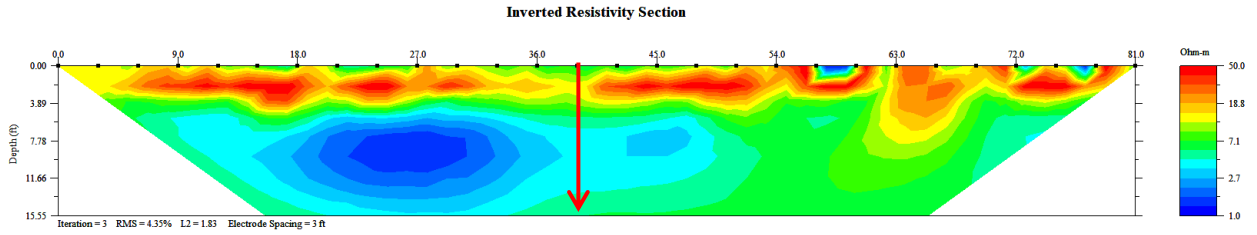
Resistivity profile for B-P1
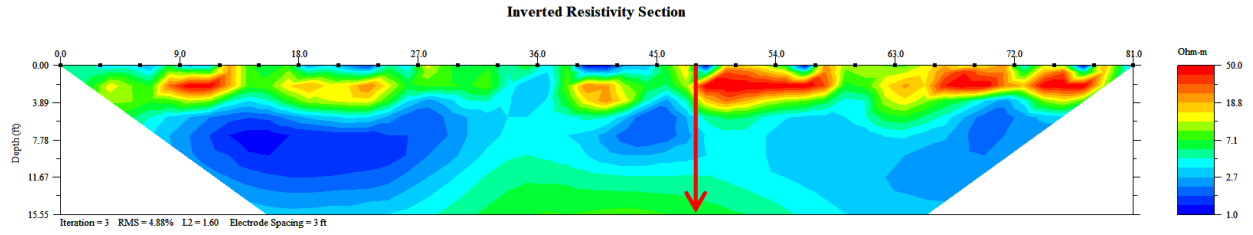
Resistivity profile for B-P4
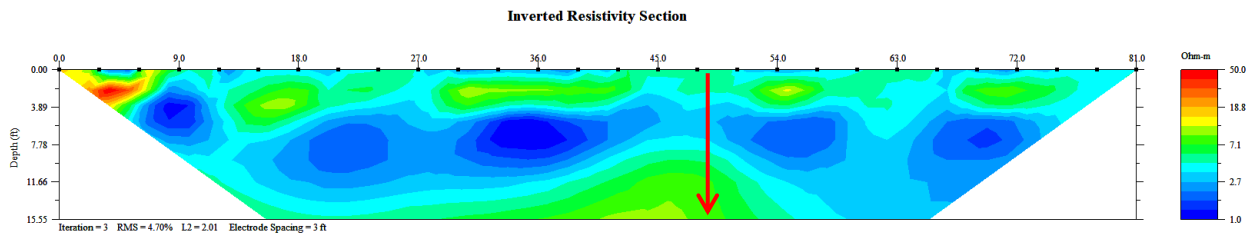
Resistivity profile for B-P6

Resistivity profile for B-P17

Inverted Resistivity Section

Resistivity profile for B-BR6A

Inverted Resistivity Section

Resistivity profile for B-BR10A

Inverted Resistivity Section

Resistivity profile for C-BR202

Inverted Resistivity Section

Resistivity profile for C-BR201

Inverted Resistivity Section
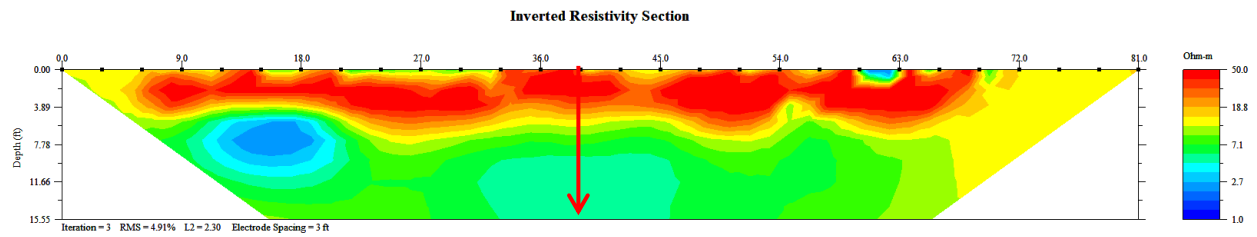
Resistivity profile for C-RW215 & C-RW214
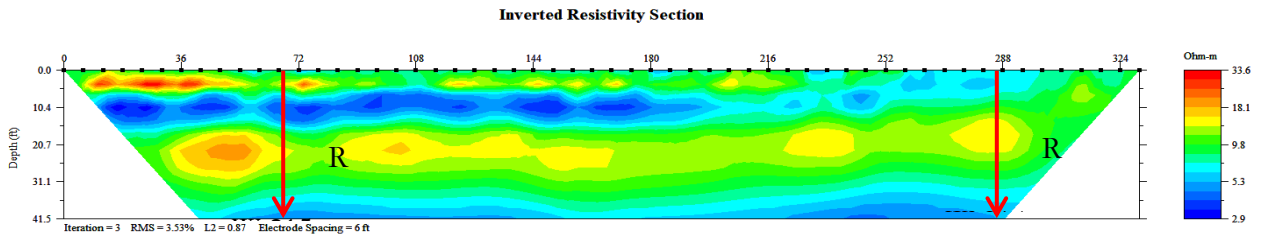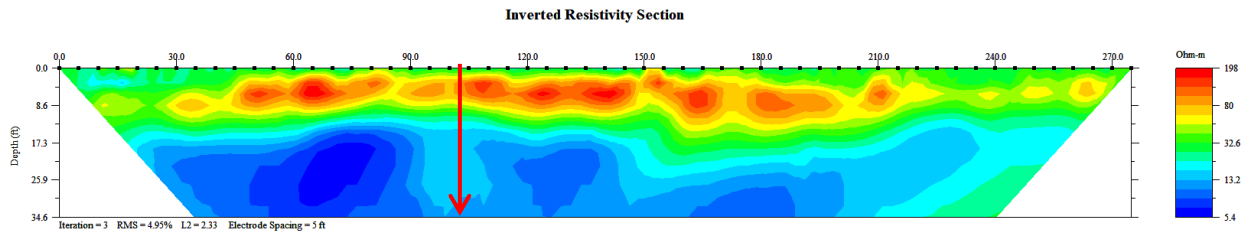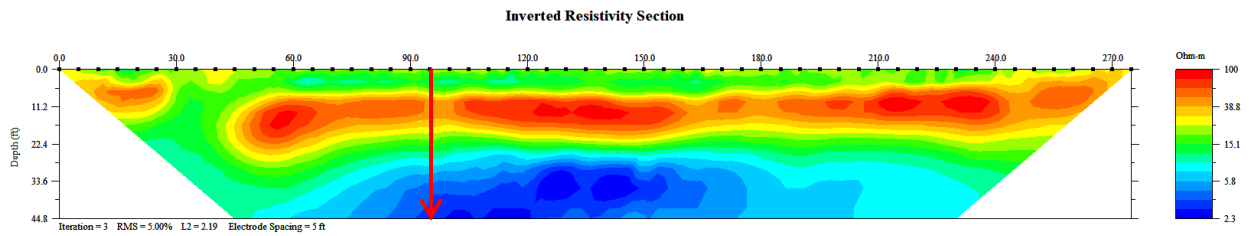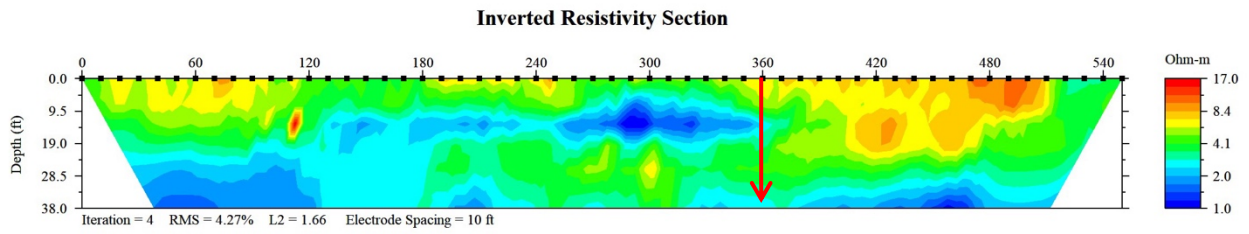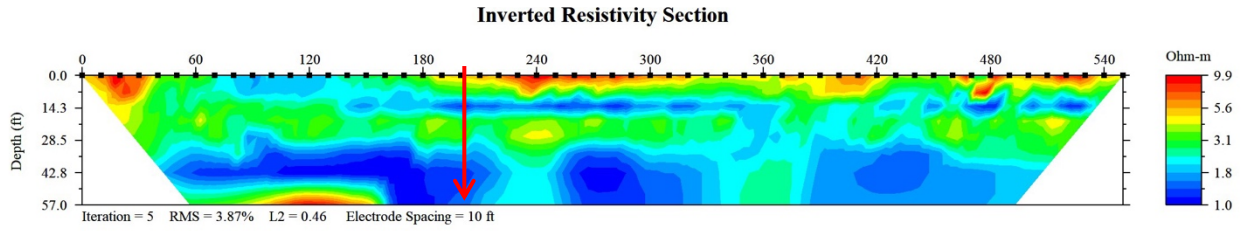
Experimental values for clayey soil

Plas. Index	Deg. Sat. (%)	Elec. Res. (Ohm-m)	Plas. Index	Deg. Sat. (%)	Elec. Res. (Ohm-m)	Plas. Index	Deg. Sat. (%)	Elec. Res. (Ohm-m)
28.10	0.22	32.52	36.10	0.71	3.67	32.00	0.94	4.64
28.10	0.29	16.91	36.10	0.80	3.28	22.80	0.24	36.40
28.10	0.32	14.44	36.10	0.88	3.14	22.80	0.29	21.75
28.10	0.42	8.49	36.10	0.91	3.03	22.80	0.32	18.17
28.10	0.55	5.98	33.60	0.36	14.22	22.80	0.34	16.03
28.10	0.53	6.36	33.60	0.42	10.14	22.80	0.42	13.87
28.10	0.61	5.11	33.60	0.51	7.58	22.80	0.47	11.60
28.10	0.72	4.28	33.60	0.62	5.61	22.80	0.57	9.58
28.10	0.81	3.94	33.60	0.51	6.16	22.80	0.68	8.22
28.10	0.75	4.31	33.60	0.69	4.14	22.80	0.58	9.88
28.10	0.84	3.92	33.60	0.74	3.85	22.80	0.77	7.74
28.10	0.90	3.83	33.60	0.80	3.67	22.80	0.82	7.43
28.10	0.93	3.74	33.60	0.69	4.24	22.80	0.89	6.87
36.10	0.34	12.96	33.60	0.80	3.76	22.80	0.82	7.42
36.10	0.40	9.01	33.60	0.85	3.57	22.80	0.85	7.43
36.10	0.47	6.99	33.60	0.88	3.50	22.80	0.87	7.52
36.10	0.56	5.25	34.30	0.35	12.69	22.80	0.90	7.37
36.10	0.52	5.77	34.30	0.41	8.39	26.10	0.27	46.37
36.10	0.61	4.50	34.30	0.53	5.40	26.10	0.28	40.84
36.10	0.73	3.54	34.30	0.55	5.18	26.10	0.40	16.01
36.10	0.78	3.24	34.30	0.53	5.32	26.10	0.49	11.60
28.20	0.24	58.78	34.30	0.61	4.20	26.10	0.53	10.38
28.20	0.36	15.08	34.30	0.70	3.46	26.10	0.69	7.94
28.20	0.45	9.06	34.30	0.83	2.94	26.10	0.52	7.60
28.20	0.59	5.63	34.30	0.70	3.28	26.10	0.65	6.68
28.20	0.53	5.19	34.30	0.77	3.00	26.10	0.77	5.94
28.20	0.66	3.78	34.30	0.84	2.87	26.10	0.85	5.63
28.20	0.85	2.96	34.30	0.87	2.80	26.10	0.74	6.37
28.20	0.75	3.22	33.00	0.25	45.08	26.10	0.86	5.76
28.20	0.88	2.87	33.00	0.29	23.65	26.10	0.91	5.48
28.20	0.95	2.74	33.00	0.36	13.52	26.10	0.96	5.19
30.20	0.26	31.82	33.00	0.42	8.72	31.30	0.21	62.51
30.20	0.37	12.82	33.00	0.50	6.07	31.30	0.23	45.42
30.20	0.43	11.60	33.00	0.61	4.44	31.30	0.26	35.79
30.20	0.55	7.24	33.00	0.54	4.60	31.30	0.41	11.31
30.20	0.66	5.60	33.00	0.63	3.58	31.30	0.49	8.57
30.20	0.59	5.98	33.00	0.75	3.00	31.30	0.53	7.62
30.20	0.73	4.76	33.00	0.86	2.67	31.30	0.63	6.46
30.20	0.89	3.88	33.00	0.73	3.24	31.30	0.55	6.45
30.20	0.84	4.19	33.00	1.01	2.41	31.30	0.63	5.80

Plas. Index	Deg. Sat. (%)	Elec. Res. (Ohm-m)	Plas. Index	Deg. Sat. (%)	Elec. Res. (Ohm-m)	Plas. Index	Deg. Sat. (%)	Elec. Res. (Ohm-m)
30.20	0.91	4.08	33.00	0.92	2.61	31.30	0.73	5.14
30.20	0.95	3.88	33.00	1.11	2.33	31.30	0.81	4.82
29.40	0.23	49.48				31.30	0.76	5.71
29.40	0.26	32.68	34.36	0.25	32.10	31.30	0.81	5.28
29.40	0.35	12.39	34.36	0.37	9.50	31.30	0.84	5.25
29.40	0.45	7.25	34.36	0.45	7.01	31.30	0.86	5.17
29.40	0.53	5.82	34.36	0.52	5.54	19.00	0.22	30.68
29.40	0.59	4.98	34.36	0.60	4.55	19.00	0.24	26.45
29.40	0.54	5.03	34.36	0.52	4.92	19.00	0.28	20.33
29.40	0.64	3.95	34.36	0.64	3.90	19.00	0.51	12.37
29.40	0.74	3.40	34.36	0.73	3.44	19.00	0.54	11.29
29.40	0.80	3.08	34.36	0.82	3.00	19.00	0.59	10.70
29.40	0.69	4.07	34.36	0.76	3.44	19.00	0.66	10.06
29.40	0.84	3.26	34.36	0.84	3.17	19.00	0.68	11.03
29.40	0.96	3.09	34.36	0.89	3.06	19.00	0.76	10.27
29.40	1.13	2.79	34.36	0.91	3.02	19.00	0.82	9.75
34.50	0.42	9.38	16.50	0.25	67.04	19.00	0.87	9.67
34.50	0.49	7.12	16.50	0.29	34.11	19.00	0.78	10.94
34.50	0.56	5.75	16.50	0.34	21.77	19.00	0.84	10.38
34.50	0.66	4.92	16.50	0.48	8.23	19.00	0.89	10.53
34.50	0.60	4.95	25.24	0.22	45.09	19.00	0.89	10.14
34.50	0.71	4.03	25.24	0.25	29.57	18.00	0.26	52.57
34.50	0.84	3.50	25.24	0.28	23.82	18.00	0.35	31.49
34.50	0.90	3.42	25.24	0.37	12.56	18.00	0.48	19.10
34.50	0.80	3.51	25.24	0.44	9.49	18.00	0.56	14.93
34.50	0.88	3.27	25.24	0.52	7.39	18.00	0.53	17.58
34.50	0.93	3.07	25.24	0.60	6.23	18.00	0.67	13.14
34.50	0.95	3.11	25.24	0.46	8.42	18.00	0.82	11.46
21.00	0.19	65.04	25.24	0.52	7.30	18.00	0.71	14.82
21.00	0.22	39.80	25.24	0.63	5.91	18.00	0.87	12.89
21.00	0.26	26.05	25.24	0.73	5.08	21.20	0.24	56.08
21.00	0.31	17.90	25.24	0.73	6.20	21.20	0.28	36.26
21.00	0.42	11.06	25.24	0.81	5.56	21.20	0.34	19.36
21.00	0.47	9.38	25.24	0.85	5.33	21.20	0.45	11.74
21.00	0.59	7.01	25.24	0.86	5.31	21.20	0.55	9.14
21.00	0.67	6.06	29.90	0.18	40.58	21.20	0.58	8.20
21.00	0.59	6.27	29.90	0.20	28.63	21.20	0.74	6.80
21.00	0.66	5.58	29.90	0.22	26.15	21.20	0.84	6.32
21.00	0.76	5.16	29.90	0.37	10.96	21.20	0.70	7.05
21.00	0.84	4.83	29.90	0.47	6.92	21.20	0.84	6.31
21.00	0.77	5.02	29.90	0.59	5.57	21.20	0.94	5.85
21.00	0.85	4.81	29.90	0.61	5.51	20.90	0.24	62.66

Plas. Index	Deg. Sat. (%)	Elec. Res. (Ohm-m)	Plas. Index	Deg. Sat. (%)	Elec. Res. (Ohm-m)	Plas. Index	Deg. Sat. (%)	Elec. Res. (Ohm-m)
21.00	0.88	4.71	29.90	0.69	4.39	20.90	0.29	29.39
21.00	0.89	4.65	29.90	0.77	4.17	20.90	0.30	18.52
29.90	0.80	4.02	20.60	0.58	6.68	20.90	0.40	12.49
29.90	0.81	4.01	20.60	0.67	6.11	20.90	0.47	9.55
29.90	0.80	4.53	20.60	0.74	5.67	20.90	0.57	7.53
29.90	0.83	4.42	20.60	0.79	5.28	20.90	0.54	6.91
29.90	0.85	4.33	20.60	0.76	6.35	20.90	0.70	5.75
27.70	0.19	46.91	20.60	0.88	5.74	20.90	0.78	5.31
27.70	0.23	31.06	20.60	0.90	5.68	20.90	0.78	4.79
27.70	0.26	22.54	40.16	0.47	8.93	20.90	0.89	4.47
27.70	0.30	17.65	40.16	0.54	6.53	20.90	0.95	4.25
27.70	0.40	10.83	40.16	0.63	5.50	22.30	0.22	45.90
27.70	0.50	8.79	40.16	0.57	5.93	22.30	0.26	30.39
27.70	0.59	6.74	40.16	0.67	4.62	22.30	0.38	10.91
27.70	0.66	5.64	40.16	0.81	3.84	22.30	0.49	8.67
27.70	0.62	5.42	40.16	0.84	3.67	22.30	0.59	7.60
27.70	0.68	5.16	40.16	0.77	4.21	22.30	0.57	6.40
27.70	0.74	4.80	40.16	0.87	3.86	22.30	0.73	5.40
27.70	0.83	4.49	40.16	0.90	3.64	22.30	0.87	4.87
27.70	0.91	4.17	28.04	0.22	50.69	22.30	0.74	5.22
27.70	0.84	4.56	28.04	0.26	33.47	22.30	0.91	4.74
27.70	0.93	4.38	28.04	0.32	25.59	22.30	1.01	4.58
27.70	0.95	4.27	28.04	0.37	15.89	23.00	0.27	63.32
24.50	0.22	47.71	28.04	0.34	23.82	23.00	0.33	31.21
24.50	0.26	29.85	28.04	0.41	18.12	23.00	0.38	17.08
24.50	0.30	20.65	28.04	0.49	15.39	23.00	0.51	9.83
24.50	0.34	16.43	28.04	0.57	13.71	23.00	0.63	7.46
24.50	0.42	11.49	28.04	0.54	17.03	23.00	0.54	6.74
24.50	0.54	8.40	21.20	0.20	32.97	23.00	0.69	5.84
24.50	0.64	6.91	21.20	0.25	18.14	23.00	0.85	5.17
24.50	0.66	6.48	21.20	0.30	14.62	23.00	0.74	5.53
24.50	0.75	5.78	21.20	0.36	11.06	23.00	0.91	4.90
24.50	0.90	5.20	21.20	0.44	12.14	23.00	1.06	4.48
24.50	0.87	5.80	21.20	0.56	8.34	25.30	0.23	61.76
24.50	0.92	5.68	21.20	0.68	6.80	25.30	0.26	34.24
20.60	0.19	35.86	21.20	0.78	6.14	25.30	0.30	23.45
20.60	0.22	23.62	21.20	0.74	6.33	25.30	0.37	16.39
20.60	0.26	17.12	21.20	0.86	5.79	25.30	0.47	11.75
20.60	0.31	13.33	21.20	0.90	5.83	25.30	0.55	9.71
20.60	0.38	10.73	21.20	0.84	7.50	25.30	0.62	8.34
20.60	0.44	9.00	21.20	0.91	7.03	25.30	0.56	7.66
20.60	0.52	7.23	22.10	0.23	30.46	25.30	0.68	8.86

Plas. Index	Deg. Sat. (%)	Elec. Res. (Ohm-m)	Plas. Index	Deg. Sat. (%)	Elec. Res. (Ohm-m)	Plas. Index	Deg. Sat. (%)	Elec. Res. (Ohm-m)
20.60	0.58	6.35	22.10	0.29	16.47	25.30	0.77	7.54
22.10	0.36	13.19	19.60	0.66	14.50	25.30	0.88	7.09
22.10	0.44	9.89	19.60	0.75	13.05	25.30	0.77	9.13
22.10	0.44	10.42	19.60	0.82	11.96	25.30	0.83	8.62
22.10	0.54	8.16	19.60	0.69	15.31	25.30	0.86	8.53
22.10	0.66	6.83	19.60	0.83	13.30	26.20	0.21	75.63
22.10	0.79	6.24	22.50	0.19	44.52	26.20	0.25	45.16
22.10	0.68	7.39	22.50	0.23	31.53	26.20	0.29	28.56
22.10	0.82	6.81	22.50	0.28	21.67	26.20	0.37	20.46
22.10	0.90	6.49	22.50	0.35	16.07	26.20	0.45	14.02
22.10	0.79	8.52	22.50	0.44	20.47	26.20	0.59	11.28
22.10	0.85	7.45	22.50	0.50	17.29	26.20	0.59	11.96
19.60	0.20	34.12	22.50	0.56	15.58	26.20	0.71	10.24
19.60	0.25	26.41	22.50	0.70	13.54	26.20	0.78	9.38
19.60	0.28	23.56	22.50	0.64	14.05	26.20	0.87	8.84
19.60	0.35	16.62	22.50	0.72	13.04	26.20	0.75	11.16
19.60	0.33	26.62	22.50	0.83	11.51	26.20	0.83	10.52
19.60	0.39	21.65	22.50	0.68	14.44	30.30	0.28	39.34
19.60	0.50	15.80	33.90	0.28	33.57	30.30	0.32	25.35
19.60	0.60	12.94	33.90	0.33	19.40	30.30	0.38	20.17
19.60	0.49	16.08	33.90	0.39	12.64	30.30	0.46	15.15
19.60	0.56	14.18	33.90	0.50	7.81	30.30	0.53	12.50
19.60	0.65	12.62	33.90	0.60	6.12	30.30	0.62	10.45
19.60	0.68	12.06	33.90	0.58	6.57	30.30	0.62	10.67
33.90	0.68	5.34	30.00	0.37	11.25	30.30	0.75	9.73
33.90	0.77	4.70	30.00	0.45	8.70	22.40	0.22	76.56
33.90	0.88	4.27	30.00	0.51	7.40	22.40	0.26	43.81
33.90	0.76	4.85	30.00	0.59	6.04	22.40	0.29	29.83
33.90	0.82	4.53	30.00	0.61	6.11	22.40	0.37	19.12
33.90	0.85	4.40	30.00	0.73	5.17	22.40	0.45	14.22
33.90	0.89	4.28	30.00	0.79	4.73	22.40	0.52	12.36
23.60	0.25	58.83	30.00	0.85	4.47	22.40	0.59	10.66
23.60	0.30	32.34	30.00	0.74	4.83	22.40	0.62	10.89
23.60	0.33	25.18	30.00	0.82	4.59	22.40	0.68	10.51
23.60	0.37	19.69	30.00	0.88	4.33	22.40	0.80	9.29
23.60	0.43	13.25	30.00	0.89	4.36	22.40	0.90	8.64
23.60	0.48	11.66	32.00	0.25	34.85	22.40	0.81	9.71
23.60	0.54	10.09	32.00	0.31	18.53	22.40	0.88	10.09
23.60	0.65	8.46	32.00	0.40	10.89	22.50	0.23	56.57
23.60	0.63	9.42	32.00	0.50	7.71	22.50	0.25	40.56
23.60	0.71	8.45	32.00	0.56	6.29	22.50	0.30	26.75
23.60	0.76	8.00	32.00	0.66	5.28	22.50	0.43	15.65

Plas. Index	Deg. Sat. (%)	Elec. Res. (Ohm-m)	Plas. Index	Deg. Sat. (%)	Elec. Res. (Ohm-m)	Plas. Index	Deg. Sat. (%)	Elec. Res. (Ohm-m)
23.60	0.84	7.67	32.00	0.59	6.36	22.50	0.51	12.52
23.60	0.78	8.36	32.00	0.74	5.23	22.50	0.58	10.86
23.60	0.84	8.32	32.00	0.85	4.55	22.50	0.67	9.43
23.60	0.88	7.98	32.00	0.88	4.44	22.50	0.71	9.72
23.60	0.90	8.26	32.00	0.80	5.06	22.50	0.81	8.69
30.00	0.31	25.34	32.00	0.87	4.80	22.50	0.84	8.31
30.00	0.36	17.96	32.00	0.92	4.51	22.50	0.85	8.94
26.30	0.22	48.64	26.30	0.73	7.59	28.50	0.32	34.94
26.30	0.27	29.20	26.30	0.81	7.30	19.70	0.27	37.67
26.30	0.30	23.22	26.30	0.88	6.41	19.70	0.35	22.17
26.30	0.46	12.28	26.30	0.88	6.82	19.70	0.39	18.98
26.30	0.51	11.09	26.30	0.92	7.09	19.70	0.56	12.92
26.30	0.55	9.90	28.50	0.24	52.01	19.70	0.59	12.15
26.30	0.65	8.30	28.50	0.27	43.01	19.70	0.61	12.30
19.70	0.67	11.88	19.70	0.74	12.24	16.50	0.18	2.33
19.70	0.72	12.46	19.70	0.74	12.09	40.16	1.13	76.56

Experimental values for sandy soil

Sand%	MC (%)	Res. (Ohm-m)	Sand%	MC (%)	Res. (Ohm-m)	Sand%	MC (%)	Res. (Ohm-m)
0.62	0.11	92.30	0.78	0.11	54.54	0.77	0.20	41.29
0.62	0.11	69.70	0.78	0.11	52.17	0.71	0.11	47.80
0.62	0.11	57.92	0.78	0.11	45.76	0.71	0.11	40.66
0.62	0.11	45.74	0.78	0.20	35.00	0.71	0.11	31.92
0.62	0.20	37.67	0.78	0.20	33.08	0.71	0.11	28.23
0.62	0.20	31.59	0.78	0.20	28.57	0.71	0.20	17.25
0.62	0.30	32.96	0.78	0.20	26.42	0.71	0.20	16.15
0.62	0.30	32.29	0.78	0.30	22.77	0.77	0.12	76.70
0.53	0.12	45.88	0.62	0.10	86.20	0.77	0.12	57.71
0.53	0.12	31.21	0.62	0.10	63.34	0.77	0.12	46.14
0.53	0.12	26.49	0.62	0.10	50.37	0.77	0.12	35.03
0.53	0.12	21.18	0.62	0.10	43.58	0.77	0.22	24.04
0.53	0.21	15.22	0.62	0.21	22.61	0.77	0.22	21.83
0.53	0.21	14.45	0.62	0.21	21.84	0.73	0.13	89.26
0.53	0.21	13.05	0.77	0.09	135.08	0.73	0.13	73.35
0.53	0.31	15.72	0.77	0.09	107.48	0.73	0.13	60.61
0.53	0.31	12.56	0.77	0.09	89.01	0.73	0.13	50.00
0.53	0.43	13.35	0.77	0.09	71.31	0.73	0.22	31.57
0.78	0.11	75.70	0.77	0.20	43.19	0.73	0.22	29.45

Sand%	MC (%)	Res. (Ohm-m)	Sand%	MC (%)	Res. (Ohm-m)	Sand%	MC (%)	Res. (Ohm-m)
0.55	0.11	48.63	0.52	0.22	9.13	0.70	0.10	89.01
0.55	0.11	34.99	0.52	0.30	9.31	0.70	0.10	65.12
0.55	0.11	24.08	0.52	0.30	8.04	0.70	0.10	39.13
0.55	0.11	18.60	0.52	0.30	7.01	0.70	0.10	29.53
0.55	0.13	33.04	0.52	0.38	8.79	0.70	0.16	41.15
0.65	0.13	22.26	0.52	0.38	7.86	0.70	0.16	31.39
0.65	0.13	19.72	0.52	0.38	7.94	0.70	0.16	26.13
0.65	0.13	15.43	0.52	0.38	7.76	0.70	0.16	17.64
0.78	0.11	102.11	0.52	0.38	7.59	0.70	0.21	23.15
0.78	0.11	67.23	0.56	0.13	25.23	0.70	0.21	22.27
0.78	0.11	53.59	0.56	0.13	20.80	0.70	0.24	22.35
0.78	0.11	47.59	0.56	0.13	16.65	0.70	0.24	21.49
0.78	0.19	28.73	0.56	0.13	15.65	0.70	0.28	22.31
0.52	0.11	45.26	0.56	0.22	14.15	0.64	0.10	63.04
0.52	0.11	33.78	0.56	0.22	12.59	0.64	0.10	39.58
0.52	0.11	25.13	0.56	0.22	11.15	0.64	0.10	32.32
0.52	0.11	18.05	0.56	0.22	9.59	0.64	0.10	28.99
0.52	0.22	16.36	0.56	0.31	9.25	0.64	0.15	34.12
0.52	0.22	12.99	0.56	0.31	8.89	0.64	0.15	26.27
0.52	0.22	11.22	0.56	0.31	8.74	0.64	0.15	21.53
0.64	0.15	18.36	0.61	0.16	21.53	0.67	0.15	30.97
0.64	0.20	18.08	0.61	0.19	50.41	0.67	0.18	44.48
0.64	0.20	16.28	0.61	0.19	37.34	0.67	0.18	36.47
0.64	0.20	15.03	0.61	0.19	33.75	0.67	0.18	34.20
0.64	0.20	13.87	0.61	0.19	27.40	0.67	0.18	28.16
0.64	0.25	13.75	0.61	0.24	27.05	0.67	0.21	31.91
0.64	0.25	12.59	0.61	0.24	26.27	0.67	0.21	30.97
0.64	0.29	13.08	0.61	0.29	27.12	0.67	0.21	27.67
0.61	0.11	98.50	0.67	0.10	111.09	0.67	0.21	26.10
0.61	0.11	65.02	0.67	0.10	75.36	0.67	0.27	28.55
0.61	0.11	55.82	0.67	0.10	57.82	0.67	0.27	28.52
0.61	0.11	29.33	0.67	0.10	47.09	0.75	0.10	129.27
0.61	0.16	49.01	0.67	0.15	66.88	0.75	0.10	96.86
0.61	0.16	42.42	0.67	0.15	50.88	0.75	0.10	78.04
0.61	0.16	38.28	0.67	0.15	38.68	0.75	0.10	65.50
0.75	0.19	51.05	0.75	0.19	40.98	0.75	0.29	34.28
0.75	0.19	47.57	0.75	0.25	40.48	0.57	0.11	67.62
0.57	0.11	49.59	0.57	0.19	23.49	0.55	0.12	36.43
0.57	0.11	36.80	0.57	0.19	21.31	0.55	0.12	27.31
0.57	0.11	29.83	0.57	0.22	26.55	0.55	0.16	30.47
0.57	0.15	37.53	0.57	0.22	22.95	0.55	0.16	27.56
0.57	0.15	30.90	0.57	0.22	18.94	0.55	0.16	24.83
0.57	0.15	25.90	0.57	0.28	21.90	0.55	0.16	20.79

Sand%	MC (%)	Res. (Ohm-m)	Sand%	MC (%)	Res. (Ohm-m)	Sand%	MC (%)	Res. (Ohm-m)
0.57	0.15	22.09	0.57	0.33	18.93	0.55	0.20	25.37
0.57	0.19	29.07	0.55	0.12	70.23	0.55	0.20	25.78
0.57	0.19	26.89	0.55	0.12	49.41	0.55	0.20	20.34
0.55	0.20	21.17	0.55	0.31	22.19	0.89	0.11	96.02
0.55	0.26	20.66	0.55	0.31	21.30	0.89	0.15	79.32
0.55	0.26	18.67	0.55	0.34	18.97	0.89	0.15	63.96
0.55	0.26	14.48	0.55	0.34	17.97	0.55	0.26	18.18

BIOGRAPHY

Md Asif Akhtar was born in Dhaka, Bangladesh, on December 12, 1991. He graduated with a Bachelor of Science in Civil Engineering from Bangladesh University of Engineering and Technology in July 2014. He worked in an industrial job in Bangladesh for four years. He joined the University of Texas at Arlington as a Ph.D. student in June 2018. Mr. Akhtar had the opportunity to work as a research assistant in the SWIS laboratory under the supervision of Dr. Hossain. He actively participated as a group leader in ISWA-SWIS Winter school 2019 and 2020. She was awarded "Outstanding Civil Engineering Ph.D. Student" in recognition of academic excellence in Civil Engineering in the 2019-20 and 2020-21 sessions.

Mr. Akhtar's research interest includes geophysical testing, electrical properties of soil, non-destructive soil testing methods, Mechanically Stabilized Earth (MSE) wall, and geotechnical aspects of Municipal solid waste (MSW). Currently, he is working on the project of development and implementation of advanced geophysical tools for geotechnical analysis funded by TxDOT.